POLITECNICO DI MILANO
Scuola di Ingegneria Industriale e dell'Informazione

Dipartimento di Chimica, Materiali e Ingegneria Chimica "Giulio Natta"
Corso di Laurea Magistrale in Ingegneria Chimica

A pharmacokinetic-pharmacodynamic model for remifentanil administration in anesthesia

Supervisor: prof. Davide MANCA

Master degree thesis of:

Adriana SAVOCA, 837204

Cristina VERGANI, 832889

Academic Year 2015 – 2016

Contents

Figures

Tables

Acronyms

ADME	Absorption, Distribution, Metabolism, and Excretion
AGP	Alpha-1-acid GlycoProtein
AIC	Akaike Information Criterion
AP	Arterial Pressure
ATP	Adenosine Triphosphate
AUC	Area Under Curve
BIS	Bispectral Index
BMI	Body Mass Index
CPB	CardioPulmonary Bypass
CSF	CerebroSpinal Fluid
CSTR	Continuously Stirred Tank Reactor
DAP	Diastolic Arterial Pressure
E	Effect
ECG	ElectroCardioGraphy
EEG	ElectroEncephaloGram
FDA	Food and Drug Administration
GICS	Gastro-Intestinal Circulatory System
GL	Gastric Lumen
HO	Highly perfused Organs
HR	Heart Rate
IAE	Integral of the Absolute Error
ICU	Intensive Care Unit
ISE	Integral of Squared Error

LIL	Large Intestinal Lumen
MAP	Mean Arterial Pressure
ODE	Ordinary Differential Equation
OLT	Orthopic Liver Transplantation
PD	PharmacoDynamics
PDE	Partial Differential Equation
PFR	Plug Flow Reactor
PK	PharmacoKinetics
PT	Poorly perfused Tissues
QSP	Quantitative Systems Pharmacology
R&D	Research and Development
RA	Remifentanil Acid
RR	Respiratory Rate
SAE	Sum of Absolute Errors
SAP	Systolic Arterial Pressure
SIL	Small Intestinal Lumen
SSE	Sum of Squared Error
TCI	Target Controlled Infusion
TIVA	Total Intravenous Anesthesia
UK	United Kingdom
USA	United States of America
WHO	World Health Organization

Symbols

BM	Body Mass	[kg]
BSA	Body Surface Area	[m^2]
C	Drug Concentration	[ng/mL]
CL	Clearance	[mL/min]
CO	Cardiac Output	[L/min]
Eff	Efficiency	-
F	Material Flux	[ng/mL/min]
Fr	Fraction	-
h	Height	[cm] or [m]
IV	Intra Venous dose	[ng/min]
K	Mass transfer coefficient	[min^{-1}]
M	Body mass	[kg]
PO	Drug orally administered	[ng/min]
Q	Plasmatic fraction of blood	[mL/min]
R	Protein binding	-
ρ	Density	[g/mL]
t	Time	[min]
$t_{1/2}\beta$	Half-time elimination	[min]
$t_{1/2}k_{e0}$	Half-life for equilibration	[min]
V	Volume	[cm^3] or [mL]
$V_{d,ss}$	Steady state volume of distribution	[L/kg]

Abstract

Today, anesthesiologists' role is extremely difficult, as there is neither a precise definition of the anesthetic state nor a standard measurement to evaluate analgesia. Furthermore, the optimal analgesic dose must both grant safe conditions and account for the patient features. Therefore, pharmacokinetic-pharmacodynamic (PK-PD) models are growing in importance. Among analgesic opioids used in anesthesia, remifentanil features a short-range action.

Our target is the development of a PK-PD model for remifentanil administration in anesthesia. The reference work is the physiologically-based (PB) PK model of Abbiati *et al.* (2016). Detailed literature investigations led us to neglect two metabolic pathways (*i.e.* kidneys and liver) that are not involved in remifentanil elimination. To predict the PK at high doses we suggest a protein binding mechanism and a dose-elimination dependence. We propose an Arrhenius-type correlation between the elimination rate constants and body temperature. PD models are usually developed to correlate plasma concentration and the corresponding hemodynamic effects, but they do not describe the physiological delay between plasma concentration and effect. To overcome this problem we added an *effect-site compartment*. The resulting PK-PD model is used to study different regimens and the gender/weight influence. Finally, we compare our model and the three-compartment PK-PD model, the most used in the literature.

Our model shows better results, being closer to the real metabolic processes. It is also successful in predicting the PK at high doses but the mechanism behind remains unknown. We also validate the temperature dependence model. Adding the *effect-site compartment*, we get an accurate prediction of the hemodynamic effects in all the anesthesia phases, and achieve an improvement in the PK prediction respect to the classical PK-PD model.

We demonstrate that our model is a suitable tool for the selection of optimal dose regimen, which is still an open issue in anesthesia. As it is able to discriminate among patients, it can be a starting point for the use of personalized formulae to overcome inter-individual variability.

Estratto

Il ruolo dell'anestesista è estremamente difficile, poiché non esiste una definizione precisa dello stato anestetico, nè misure standard dell'azione analgesica. La dose ottimale di analgesico deve garantire condizioni sicure e tener conto delle caratteristiche fisiche dei pazienti. In questo contesto diventano importanti i modelli farmacocinetici-farmacodinamici (PK-PD). Tra gli oppioidi analgesici usati in anestesia abbiamo scelto il remifentanil per il suo rapido *onset* e *offset*.

Scopo di questo lavoro è costruire un modello PK-PD per la somministrazione del remifentanil in anestesia. Il punto di partenza è il modello PK su base fisiologica di Abbiati *et al.* (2016). In accordo con la letteratura, abbiamo trascurato due vie metaboliche non coinvolte nell'eliminazione del farmaco. Per predire la PK ad alte dosi abbiamo proposto una dipendenza del legame proteico e dell'eliminazione dalla dose. Abbiamo poi ipotizzato una relazione di tipo Arrhenius tra le costanti di eliminazione e la temperatura corporea. Abbiamo sviluppato modelli PD per legare la concentrazione plasmatica ai corrispondenti effetti emodinamici, che però non rappresentavano il *delay* che esiste tra concentrazione ed effetto. Il problema è stato superato integrando un *effect-site compartment*. Il modello PK-PD è stato usato per studiare l'effetto di diverse dosi e posologie e del sesso/massa. Infine, abbiamo confrontato il nostro modello e il modello tri-compartimentale PK-PD, il più diffuso.

Essendo più vicino al reale processo metabolico, il nostro modello ha prodotto risultati migliori. Anche se il meccanismo dietro il *trend* dei dati per alte dosi rimane non chiaro, il modello riesce a descriverli. Il modello che propone la dipendenza dalla temperatura è stato convalidato. Con l'aggiunta dell'*effect-site compartment* il modello riesce a predire gli effetti emodinamici durante l'intera anestesia. Rispetto al modello classico, il nostro comporta un avanzamento nella predizione della PK.

Il modello proposto è un valido strumento per la scelta della dose ottimale. Inoltre, essendo sensitivo alle caratteristiche fisiche, può essere un punto di partenza per approfondire terapie individualizzate.

1. INTRODUCTION

1.1 Research context and objectives of the thesis

The development of quantitative computer modeling of biological systems and the study of drugs pharmacokinetics and pharmacodynamics is today of growing importance to biomedical research.

This is confirmed by the 2011 publication of a white paper by NIH (National Health Institute, USA) concerning the institution of a new discipline: **Quantitative Systems Pharmacology** (Leil and Ermakov, 2015).

QSP consists of the integration of two disciplines:

(i) Systems biology, aimed at studying the relationship between genes and biologically active molecules in order to develop qualitative models of these systems;
(ii) Quantitative pharmacology, focused on computer-aided modeling and simulation to increase the understanding of the pharmacokinetics and pharmacodynamics of drugs.

In the past, the approach to drug discovery was based on the empirical evidences from nature. This approach was renamed 'Pharmacognosy' by a German scientist, C.A. Seydler, who used the word 'pharmakognosie' for the first time in 1815 in his book titled "*Analecta pharmacognostica*", by merging two Greek words: "*pharmakon*" (φάρμακον), which means drug and "*gignosco*" (γιγνώσκω) which means acquiring knowledge.

This approach originates in Egypt and India: medicines were recorded in the Egyptian papyrus about 1500 BC and later in the Indian "Ajur veda" (meaning "Science of Life"). Later, Ancient Rome also promoted the development of drug discovery: in about 77 AD, Dioscorides, a Greek military physician and pharmacognosist of Nero's army, recorded about 600 kinds of crude drugs in his book "De materia medica". This book played an important role in the pharmacology and botany of crude drugs in the 15th century. Pliny the Elder (23-79 AD), contemporary of Dioscorides, gave a brief account in his "Hystoria" of nearly 1000 species of plants, most of which could be used as medicines. Throughout the Middle Age, European physicians referred to the Arab works "De Re Medica" by John Mesue (850 AD), "Canon Medicinae" by Avicenna (980-1037), and "Liber Magnae Collectionis Simplicum Alimentorum Et Medicamentorum" by Ibn Baitar (1197-1248), in which over 1000 medicinal plants were described. In 18th century, in his work *Species Plantarium* (1753), Linnaeus (1707-1788) provided a brief description and classification of the species described until then. Later, early 19th century was a turning point in the knowledge and use of medicinal plants. The discovery and isolation of alkaloids from poppy (1806), ipecacuanha (1817), strychnos (1817), quinine (1820), pomegranate

(1878), and other plants, then the isolation of glycosides, marked the beginning of scientific pharmacy. With the improvement of the chemistry, other substances from medicinal plants were also discovered such as hormones and vitamins (Petrovska, 2012).

Since the middle of the last century, due to the advances in biochemical and medical sciences, drug discovery has evolved from the empirical approach to a new hypothesis-driven and mechanism-based approach. This has led to two apparently contrasting effects that can be detected starting from the '60s: an increase of the percentage of new drug applications approved by FDA (Food and Drug Administration, USA) (Fig.1 A) and, at the same time, a decline in the productivity of drugs (Fig. 1 B).

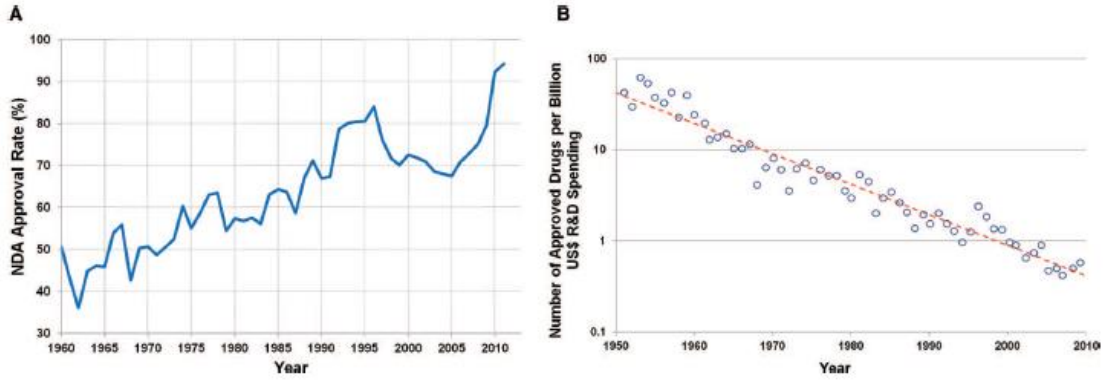

Figure 1 - (A) Rate of approval for FDAs since 1960 (US Food and Drug Administration, 2013), (B) Number of approved drugs for every billion US dollars spent on R&D (Scannel et al., 2012).

This second effect of the modern approach is due to the difficulty of finding new therapeutic targets and to the increase in the costs associated with the discovery and the development of new drugs. This is a typical consequence of any new industry: in order to limit this effect, it is necessary to find strategies that allow increasing the probability of commercial success of the product, and at the same time decrease the development costs (Leil and Bertz, 2014).

Computer-aided modeling is the appropriate solution for both these goals. In fact, computer simulations enable to test a very high number of situations *in silico*: this means that it is possible to establish the probability of failure of a drug without performing real clinical tests, which are highly expensive. Another important and related advantage is that it is possible to predict the effects of multiple therapeutic interventions in combination, whose testing in the clinic would be in most cases economically and practically unfeasible.

Moreover, QSP models are based on the understanding of the biological pathways, the disease processes, and the drug mechanisms of action. Therefore, they are effective tools for integration of biological knowledge and formulation of pharmacological hypotheses, can aid in pre-clinical and clinical experiments design, and they can provide

a support for a better insight on the interaction between drugs and biological systems, which is essential in the target identification stage.

For all these reasons, it is possible to claim that QSP allows facing the growing challenges in efficiency and productivity for Research & Development (R&D) of drugs. Given this, it is worth discussing the reasons why the pharmaceutical industry has been slow to integrate computer-aided modeling, compared to other fields, such as aerospace or electronics. The common perception that biology is too complex to be described with mathematical equations has played an important role, but mostly a lack of adequate graduate training programs for pharmaceutical modeling and simulation scientists and the lack of support from governments funding agencies for academic research have slowed the process down (Leil and Bertz, 2014).

QSP tools consist of pharmacokinetic and pharmacodynamic models. While pharmacokinetics describes the rate of the processes of a drug inside the body, in particular absorption, distribution, metabolism and excretion (ADME processes), pharmacodynamics describes the relation between the plasma and/or tissue concentration of the drug and the magnitude of the pharmacological effect.

The development of a QSP model for the prediction of pharmacokinetics and pharmacodynamics should undergo a rigorous stepwise process, with three main steps that can be summarized as follows:

1) Gather the knowledge about physiological processes that will be incorporated in the model and definition of the aim of the model targets;
2) Collection of clinical and non-clinical data and development of the system of mathematical equations that will describe the processes and the compartments of the model;
3) The model identification by means of relevant data belonging to the target patient population.

This problem needs therefore to be faced with a modeling approach, which is an engineering skill. Pharmacokinetic and pharmacodynamic analyses require the ability to build a compartmental and possibly physiologically-based model of the human body which will then be adapted to a specific drug, by considering its physiochemical characteristics.

Within this particular context, the chemical engineer can play an important role, because of the experience and skills in modeling. Actually, the equations that are used to study the evolution of the drug in the organs and tissues are analogous to the material balances that chemical engineers use to model the pieces of equipment of chemical plants. Organs and tissues can be considered as they are or lumped into compartments, which can be modeled as perfectly mixed or plug flow reactors,

depending on the specific features of the organs and tissues. Therefore, these compartments become the control volumes of the material balances of the drug. The drug transport processes inside the human body through the tissues can be described as diffusion processes or convective motion, which can be modeled by means of relations such as Fick's law. Mass transfer processes are a typical study topic of chemical engineering.

The main purpose of this thesis is to build a pharmacokinetic-pharmacodynamic model specific for an analgesic opioid called remifentanil and suitable for the induction and maintenance of anesthesia. In this particular field, this model can be a powerful tool, especially to investigate the range of dosage that prevents the occurring of the typical adverse effects related to opioids. The problems related to anesthesia and the potential adverse effects of remifentanil will be discussed in details in Paragraphs 1.3 and 1.4.

The reference article of our thesis is Abbiati *et al.* (2016), whose physiologically-based pharmacokinetic model equations have been modified in order to make the model more suitable for remifentanil, with a special focus on the specific features related to its distribution in the human body, the elimination pathways, and the dependence of the elimination on factors such as the body temperature and the administered dose.

Once the pharmacokinetic model is validated, the thesis focuses on pharmacodynamic models to link the concentration of remifentanil in the blood to its pharmacological effect in terms of heart rate, systolic arterial pressure, and mean arterial pressure. The choice of considering only hemodynamic changes comes from both the acknowledgement of the relevance that these effects have for opioids and the availability of experimental data in the literature.

Finally, a combined model is developed by linking the pharmacokinetic and pharmacodynamic models by means of a virtual compartment defined as the 'Effect-site compartment'. After validation, this combined model is used for *in silico* simulations of patients with peculiar characteristics, in order to investigate the effect of factors such as gender and body mass on the pharmacokinetics and pharmacodynamics of remifentanil, and for investigations on the dose (regimen) selection.

Paragraph 1.2 presents a general insight of ADME processes and drug pharmacodynamics. A special focus on remifentanil is then given in Paragraph 1.4, to explain the reasons why it was chosen as reference drug for our research activity.

1.2 Pharmacokinetics and pharmacodynamics

The administration of a drug to a patient is an activity that involves several questions, such as the dose selection and the choice of the suitable treatment among similar drugs. In order to make the right choice, it is extremely important to understand the pharmacokinetics and the pharmacodynamics of the drug.

Pharmacokinetics (PK) is the study of the *motion* of drugs into, within, and out of the body, and involves the processes of absorption, distribution, metabolism, and excretion (ADME processes).

On the other hand, the pharmacodynamics (PD) studies the biochemical and physiological effects of the drugs and the mechanisms of their interactions, including receptor binding, post-receptor effects, and chemical interactions. Fig. 2 provides an idea of how these two aspects interact.

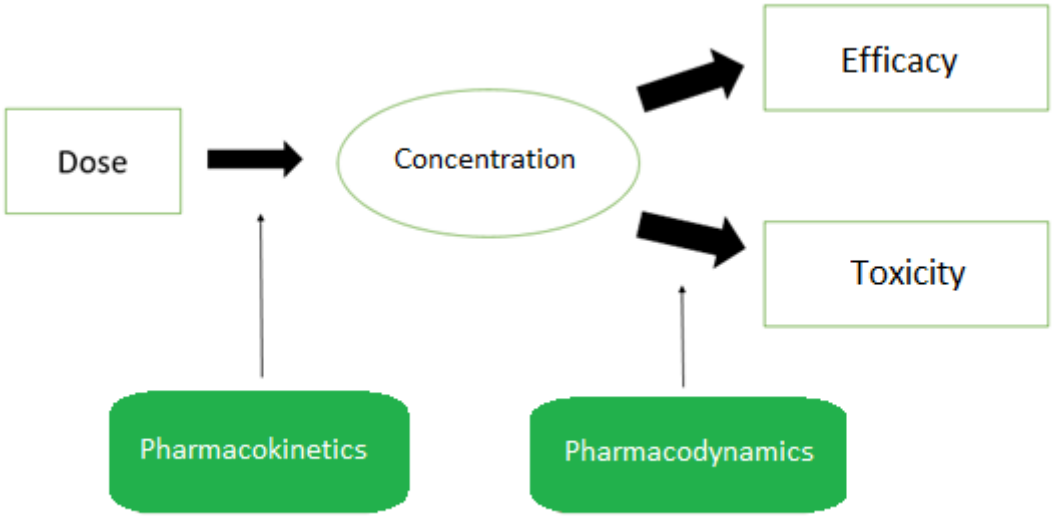

Figure 2 - Schematic representation of the interaction between the pharmacokinetics and the pharmacodynamics of a drug. PK analyses provide the concentration profile associated to the selected dose that can be used for PD analyses, which provide the effect profile, used to define the efficacy and the toxicity of the drug. Adapted from Merck Manual, 1982.

By combining pharmacokinetics and pharmacodynamics, it is possible to explain the relationship between the dose and the response of a drug. In fact, the pharmacological response depends on the drug binding to its target, while the concentration of the drug at the receptor site that affects the pharmacological effect depends on the administered dose.

1.2.1 Pharmacokinetics

Pharmacokinetics can be described as the study of the action of the body on a drug, therefore it concerns the description of the mechanisms of absorption, bioavailability, distribution, metabolism, and excretion.

The mechanism of absorption is related to the drug physiochemical properties, formulation and way of administration. It is possible to have different ways of administration: oral, parenteral, topical, and by inhalation. In order to be absorbed, a drug must be in solution or, in the case of a solid drug, it has to be able to disintegrate and disaggregate. If the drug is not administered by intravenous infusion, it has to cross a significant number of semi-permeable cell membranes in order to reach the systemic circulation. The bimolecular lipid layer of a membrane defines its permeability characteristics.

Drugs may cross the membranes through passive diffusion, facilitated passive diffusion, or active transport. Fig. 3 shows a schematization of these three different mechanisms.

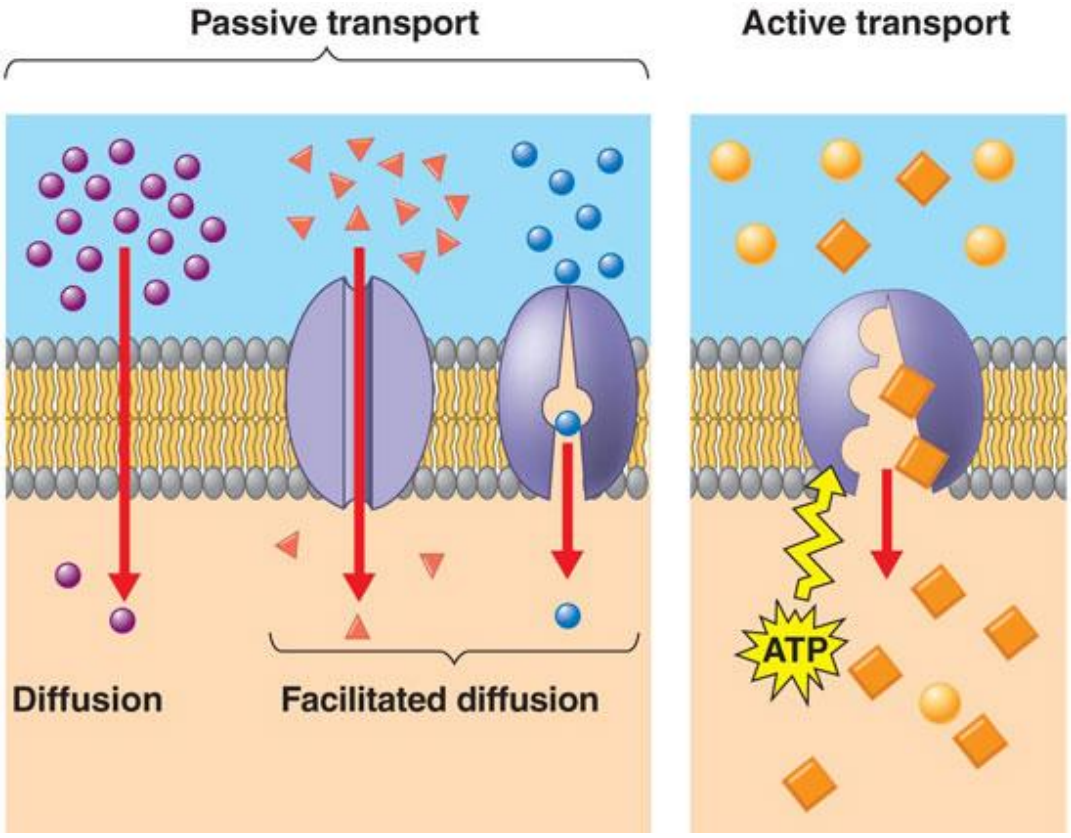

Figure 3 - Schematization of three mechanisms of transport: passive transport (left), facilitated transport (middle), and active transport (right). In the first case the transport occurs because of the drug concentration gradient across two regions. In the second case a carrier molecule facilitates the transport. The last case is a selective process that occurs with the expenditure of an ATP molecule. Taken from Merck Manual, 1982.

In case of passive diffusion, the drug molecule diffuses across the cell membrane passing from a region where its concentration is high to one where is low. The diffusion rate is directly proportional to the gradient of concentration between these areas, but it also depends on other features, such as the molecule's lipid solubility, size, degree of ionization, and area of absorptive surface of the cell. For instance, lipid soluble molecules and small-size molecules will diffuse more rapidly. Also, drugs that exist in a unionized form in aqueous solution are usually lipid soluble and, as a consequence, are able to diffuse more easily. The proportion of unionized molecules is defined by the environmental pH and the acid dissociation constant of the drug, known as pKa.

In general, molecules with low lipid solubility cross the membrane more rapidly than expected. This can be related to the mechanism of facilitated passive diffusion. In this case, the membrane features a carrier molecule that combines reversibly with the substrate molecule. The complex carrier-substrate diffuses rapidly across the membrane, releasing the drug on the other side. Therefore, the membrane allows the transit of substrates with a specific molecular configuration and the transport is limited by the availability of carriers.

Eventually, active transport is a selective process that requires an energy expenditure, by consumption of one or more ATP molecules that represent the “energy of the cell”. This mechanism allows carrying out transport in the direction along which the concentration gradient increases.

It is interesting to underline that these mechanisms are very similar to the transport mechanisms in which industrial membranes are involved.

The bioavailability represents the extent and the rate at which the drug or its metabolite(s) enter the systemic circulation to reach the site of action. It is largely affected by specific features of the drug, which for instance may depend on its design.

In case of intravenous administration, the drug directly enters the systemic circulation and therefore it has only to be distributed to the tissues or organs of interest. If the drug is administered by other means (*e.g.*, oral administration), it has first to reach the systemic circulation and then be distributed to the different tissues and organs. In the particular case of orally administered drugs, the bioavailability is low. The reason is related to the fact that they have to pass through the intestinal wall and then through the liver that are both common sites of the first phase of metabolism. As a result, some drugs can be metabolized before reaching an adequate plasma concentration.

Another reason for low bioavailability may be an insufficient time for the absorption of the drug in the Gastro-Intestinal tract. In addition, age, sex, physical activity, genetic phenotype, stress, and disorders can affect the bioavailability.

Bioavailability can be assessed through the determination of the area under the plasma concentration versus time curve, known as AUC, shown in Fig. 4. It is directly proportional to the total amount of unchanged drug that reaches the systemic circulation.

Plasma drug concentration increases with the extent of absorption. The maximum peak is reached when the drug rate of elimination is equal to the one of absorption. The time at which the peak of plasma concentration occurs is the most widely-used general index of absorption rate: the slower the absorption, the later the peak.

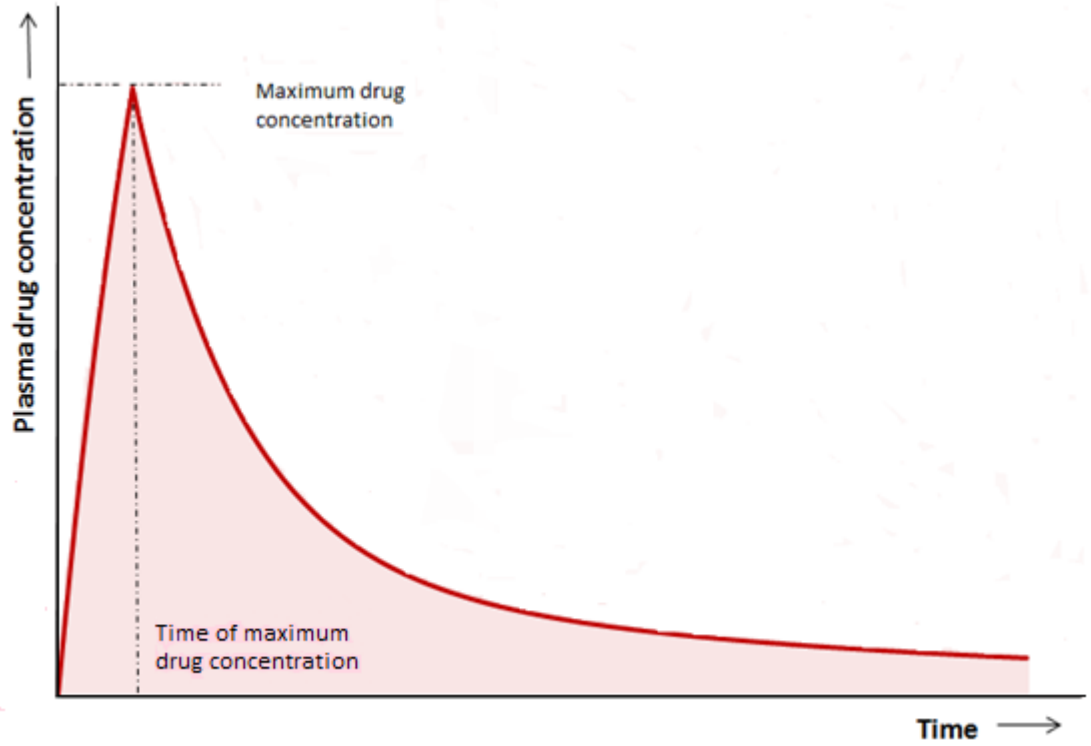

Figure 4 - Representation of the AUC (Area Under Curve), that in the figure is the colored area. AUC is directly proportional to the total amount of unchanged drug that reaches the systemic circulation. The figure is adapted from Merck Manual, 1982.

Once the drug has entered the systemic circulation, it is distributed to the different organs and tissues. In general, distribution is not homogeneous because it depends on the blood perfusion, tissue binding, local pH, and the permeability of the cell membranes. The entry rate of a drug into a tissue mainly depends on the rate of the blood flow to the tissue, but it is also related to the tissue mass and the partition characteristics between blood and tissue. The distribution equilibrium between blood and tissue is reached faster in more vascularized areas, if the diffusion across the membrane is not the limiting step.

The extent of the drug distribution in the body is related to the degree of plasma protein and/or tissue binding. The drug is transported by blood as free or reversibly/irreversibly bound to blood components (*e.g.*, blood cells) or proteins. The most important plasma proteins that can interact with drugs are albumin, α1-acid glycoprotein, and lipoproteins.

Only the unbound fraction of drugs is available for passive diffusion out of blood vessels to tissues or organs where it shows its pharmacological effect. The unbound drug concentration in systemic circulation determines the drug concentration at the active sites.

The accumulation of drugs in tissues and organs can prolong the action of the drug because they can release the accumulated drug as plasma drug concentration decreases.

Metabolism and excretion occur simultaneously with distribution, which makes the process dynamic and complex.

The drug metabolism is the biochemical modification of pharmaceutical substances, mainly due to enzymes. In general, drug metabolism converts lipophilic chemical compounds into excreted hydrophilic products. Fig. 5 shows a schematization of the action of enzymes.

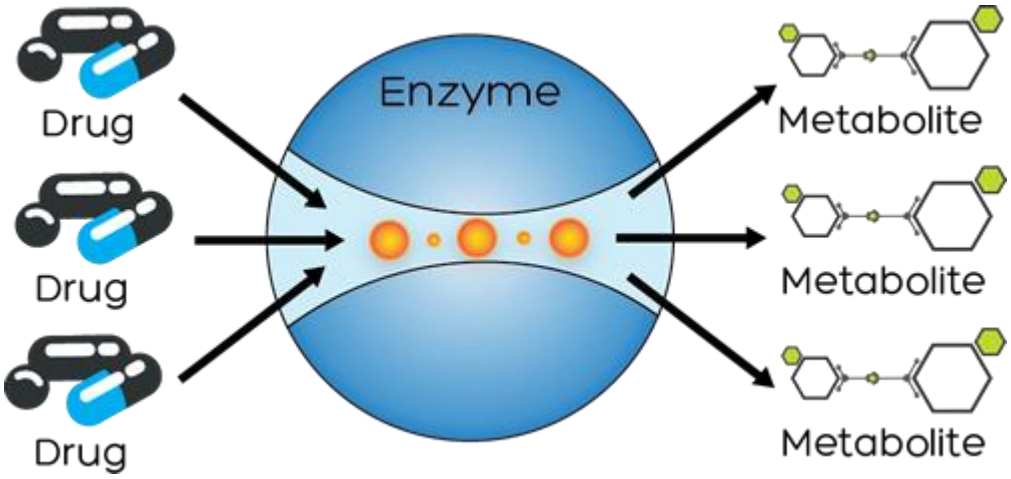

Figure 5 - General schematization of enzymes drug metabolism. Taken from Merck Manual, 1982.

The rate of metabolism determines the duration and the intensity of the pharmacological effect of the drug. The metabolism can be described as a set of metabolic pathways that modify the chemical structure of the molecule. These pathways are bio-transformations characterized by different reactions.

Drug metabolism is divided into three phases. In the first one, enzymes introduce reactive or polar groups into the drug. This first phase may be characterized by reactions of oxidation, reduction, hydrolysis, cyclization, and decyclization. These modified compounds are then conjugated to polar compounds in the second phase. The sites where conjugation reactions occur are: carboxyl (-COOH), hydroxyl (OH), amino ($-NH_2$), and sulfydryl (-SH) groups. These reactions are catalyzed by transferase enzymes.

The products of these reactions have a higher molecular weight and tend to be less active than their precursors, unlike phase one reactions, which often produce active metabolites. In the last phase, the resulting complex can be either further processed or recognized by efflux transporters and excreted of cells.

Regardless the excretion, it is possible to consider the kidneys as the main organs for the excretion of water-soluble substances. The biliary system contributes to the excretion depending on the amount of drug that is not reabsorbed by the Gastro-Intestinal tract. In general, the contribution of intestine, saliva, and lungs to excretion is small, except for particular cases as the exhalation of volatile anesthetics or for specific mammals who spit large amounts of saliva (*e.g.*, horses).

Fig. 6 shows the typical path of metabolism and excretion of a drug.

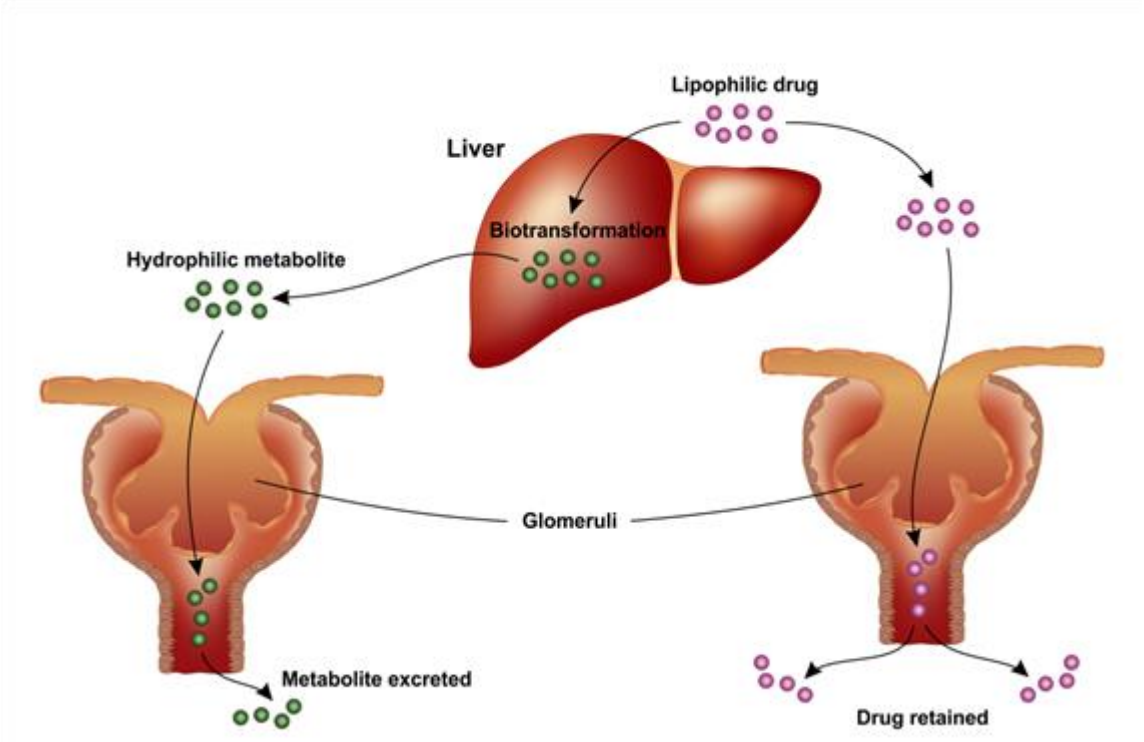

Figure 6 - Typical metabolic pathway of a lipophilic drug inside the human body. The drug is first metabolized by the liver and then it reaches the kidneys where it is eliminated. Taken from Merck Manual, 1982.

1.2.2 Pharmacodynamics

Pharmacodynamics studies how drugs affect the human body and allows describing the receptor binding, the post-receptor effects, and the chemical interactions between drugs and receptors.

The pharmacodynamics of a drug can be affected by differences in the body mass, the gender or the race, physiologic changes due to disorders (*e.g.*, genetic mutations, malnutrition, Parkinson disease, and diabetes), aging, or the interaction with other drugs. In particular, aging can alter the receptor binding or the post-receptor response sensitivity, while the interaction among drugs results in competition for receptor binding sites and/or alteration of the post-receptor response.

In our opinion, it is worth lingering briefly on the mechanisms of action of drugs and the role of receptors in those mechanisms.

In fact, drugs have to interact with receptors in order to act effectively. Receptors are macromolecules involved in chemical signaling between and within cells and can be located on the cell membrane or inside the cytoplasm. The activated receptors will then directly or indirectly regulate cellular biochemical processes.

In general, the molecules that bind a receptor are called ligands and can activate or inhibit a receptor. Each ligand can interact with multiple receptor subtypes and bind to particular regions of a receptor called “recognition sites”. The interaction between the ligand and the receptor is influenced by external factors as well as by intracellular regulatory mechanisms, for instance the density of receptors.

Receptors are selective and this selectivity represents the degree to which a drug acts on a given site respect to other sites. The degree of interaction between the molecule of a drug and the receptor depends on the probability that the molecule occupies a receptor at any instant and on the intrinsic efficacy that represents the degree to which a ligand activates a receptor and leads to the cellular response. These characteristics mainly depend on the chemical structure of the drug. Fig. 7 shows a simple schematization of the interaction between the drug and its receptor.

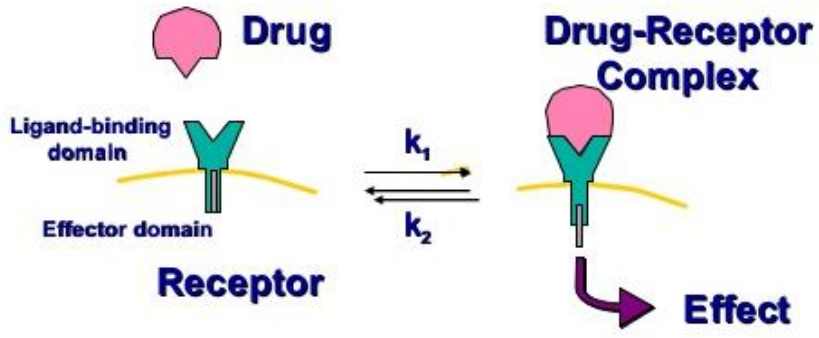

Figure 7 - Interaction between a drug and its specific receptor. The pharmacological effect is explicated through this interaction. Taken from Merck Manual, 1982.

The pharmacological effect also depends on the residence time of the drug, which is the period of time that the complex drug-receptor persists. The lifetime of this complex is influenced by dynamic processes that control the rate of association of the drug with the receptor and of dissociation of the drug from the receptor.

The physiologic functions are regulated by the simultaneous action of several receptors, activated or not by a drug or by other types of molecules, and there are a number of steps between the initial molecular drug-receptor interaction and ultimate tissue or organ response.

As previously explained, a drug can either activate or inhibit the receptor. If the receptor is activated by the drug, this is called agonist, conversely it is called antagonist.

Agonists activate the receptors in order to obtain the desired response. Conventional agonists increase the proportion of activated receptors, while inverse agonists stabilize the receptor in its inactive confirmation and act similarly to competitive antagonists. In fact, antagonists prevent the activation of the receptor. For instance, they can increase the cellular function by substituting the activity of a substance that normally decreases that function.

Antagonists can be classified as reversible or irreversible: reversible antagonists can rapidly dissociate from their receptors, while the irreversible antagonists form a stable, permanent, or nearly permanent chemical bond with the receptors.

In case both agonists and antagonists are present, the mechanism of interaction may be competitive or non-competitive. If it is competitive, the binding of an antagonist to the receptor prevents the binding of an agonist with the same receptor and vice versa, while in the non-competitive mechanism, the agonist and the antagonist can be bound simultaneously. In this second case, the binding of the antagonist reduces or prevents the action of the agonist. Fig. 8 represents the different possible mechanisms of interaction between a drug and its specific receptor.

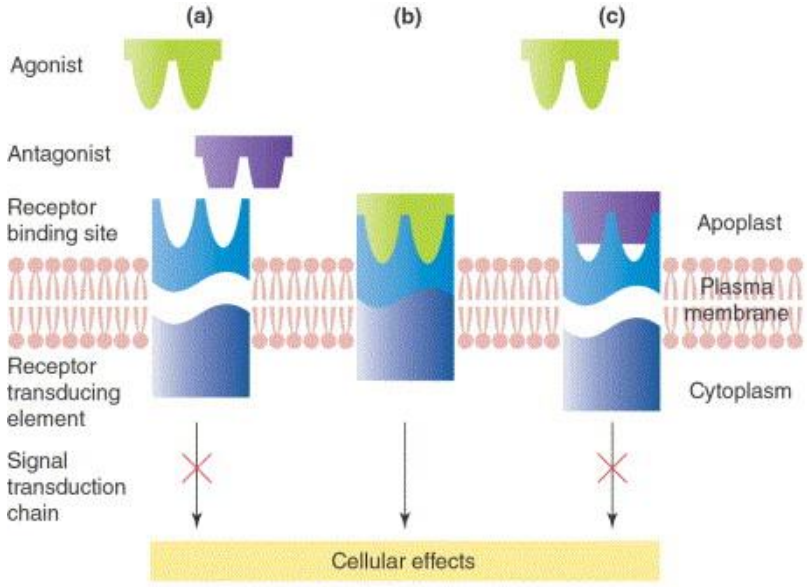

Figure 8 - Mechanisms of action of both agonists and antagonists. Taken from Merck Manual, 1982.

There are drugs that produce effects without altering the cellular function and without binding to a receptor. This kind of drugs act through a series of chemical reactions and interactions, depending on the type of drug and on its effect. However, this thesis will not cover these issues.

It is now clear what the ways in which a drug can explicate its effects are.

In pharmacodynamics, it is also important to understand the relation between the dose and the effect of a drug. In general, the concentration of the drug at the site of action controls the pharmacological action. However, the response to the concentration may be rather complex and it is usually nonlinear.

A clear explanation of what pharmacokinetics and pharmacodynamics are is essential in order to understand the steps that follow.

1.3 Analgesics and anesthesiology

General anesthesia is a reversible state that includes unconsciousness, amnesia, analgesia, and akinesia, with concomitant stability of the cardio-respiratory and autonomic systems. In order to reach the proper anesthetic state for surgery, analgesics are considered fundamental pharmacological components.

Analgesics can also be called pain medicines. In fact, their main application is in the relief of pain. The difference between anesthetics and analgesics is in the mechanism of action: analgesics act without blocking the conduction of nerve impulses, altering sensory perception, or affecting consciousness, which is instead what anesthetics do. In fact, they can be classified either as anti-inflammatory drugs, which alleviate pain by

reducing local inflammatory responses, or as opioids, which act on the brain by reducing the number of pain signals sent by the nervous system and the brain's reaction to them.

Given this, it is easy to understand that analgesia is an important aspect of a balanced anesthesia. However, anesthesiologists have multiple inconsistent definitions of the anesthetic state and do not have standard measurements to assess it and evaluate analgesia. As the role of the anesthesiologists has become more and more complex, it is important to provide them with effective tools that allow inducing anesthesia safely and maintaining the patients' vital functions before, during, and after surgery.

In this respect, a PK-PD model can be greatly helpful. In fact, *in silico* simulations would be highly useful for the analysis of the response to different dosages of the analgesic and the assessment of the dosage range that prevents adverse effects (*e.g.*, hypotension and bradycardia).

Opioids are the most widely used analgesics in the induction and maintenance of anesthesia. The term "opioid" has been adopted as a general classification of those agents that share chemical structures, sites of action, and mechanism of action with morphine (see Fig. 9), and with endogenous opioid substances inside the human body.

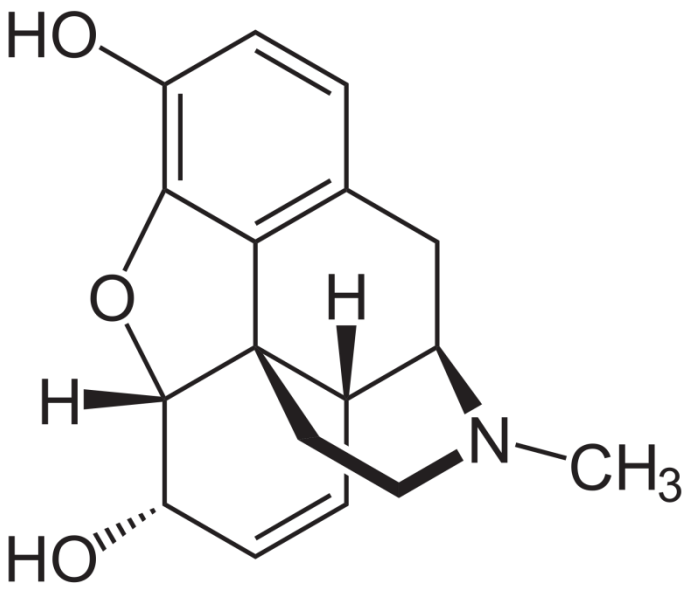

Figure 9 - Chemical structure of morphine.

Opium is a powder that can be obtained from the dried juice of the poppy *Papaver somniferum*. In the XIX century, opium extract was found to contain more than 20 distinct complex organic bases, called alkaloids. Among them, it is possible to find morphine, codeine, and papaverine that replace the crude opium extracts in therapeutics. In the '50s of last century, several new morphine-like drugs were

developed. In those years, the number of compounds available for pain relief increased, but there was limited information about their mechanism and their sites of action.

Opioid analgesics are also known as narcotic drugs because they may induce sleep. They can be used either during anesthesia or to alleviate short- or long-term pains. Opioid drugs are also useful in the treatment of general postoperative, severe pain, and other specific uses.

Analgesic opioids can act as agonists or antagonists. They work by binding to opioid receptors located in the brain, spinal cord, and other areas of the human body. By doing so, they are able to reduce the intensity of the message of pain that is sent to the brain, with the result of reducing the perception of pain.

1.4 Remifentanil

1.4.1 Introduction and physiochemical characteristics

The importance of the role of the opioid analgesics in anesthesia and the relevance that a PK-PD model would have in this field were discussed in Paragraph 1.3. It is now interesting to understand what are the criteria of selection and the differences in the components of the analgesic opioids family.

At the end of the '90s new trends in anesthesia have led to the development of increased potency, reduced cardiovascular toxicity, and short acting agents. This was reflected by the introduction of fentanyl, sufentanil and alfentanil in anesthesia (Glass *et al., 1999*).

All these opioids are more potent than their *older* counterparts, such as morphine. Moreover, they do not cause histamine release and produce fewer cardiovascular changes. However, those drugs still had a considerably long context-sensitive half-time, so the need for a truly short-acting drug remained.

Within this frame, remifentanil was approved by FDA in 1996. It was developed and designed purposely to provide a rapid and predictable offset of action, resulting in a potent and short-acting synthetic opioid analgesic drug. Table 1 reports the main pharmacokinetic parameters of remifentanil, alfentanil, and fentanyl.

Table 1 - Comparison of some of the most important pharmacokinetic parameters of three drugs belonging to the fentanyl family: alfentanil, fentanyl, and remifentanil. Values from Glass et al. (1999).

Parameters	*Alfentanil*	*Fentanyl*	*Remifentanil*
$V_{d,ss}$[L/kg]	0.25-0.75	3-5	0.3-0.4
$t_{1/2}\beta$ [min]	60-120	180-300	8-20
$t_{1/2}k_{e0}$ [min]	0.6-1.2	0.6-1.2	1-1.5

$V_{d,ss}$ is the steady-state volume of distribution of the drug and reflects the actual blood and tissue volume into which a drug is distributed. Remifentanil has a smaller volume of distribution than fentanyl, and a comparable one respect to alfentanil. This means that remifentanil is an improvement respect to fentanyl from the point of view of distribution.

$t_{1/2}\beta$ is the half-time elimination defined as the time required for the drug concentration in the plasma to decrease of the 50% during the metabolic phase, corresponding to the time required to degrade/eliminate 50% of the drug from the body after an intravenous (IV) bolus. This parameter proves remifentanil to be a shorter-acting agent compared to both fentanyl and alfentanil.

$t_{1/2}k_{e0}$ is the half-life for equilibration, defined as the time-lag before concentration changes in plasma are reflected in the effect-site compartment (see Paragraph 4.1), which represents the drug site of action. This produces a delay in both onset and offset of pharmacodynamic effect when infusion rates are changed (Hill, 2004). Even if this parameter is higher for remifentanil, it is worth observing that the difference is not numerically significant. Therefore, it is still possible to consider remifentanil as a rapid equilibrating drug.

From the chemical point of view, remifentanil is a piperidine derivative, a 3-(4-methoxycarbonyl4[(Loxopropyl)phenylamino]-L-piperidine) propanoic acid, methyl ester (Fig. 10). It is supplied in its hydrochloride form, as a white lyophilized powder. The synthesis of this molecule is based on the substitution with alchil-esther bonds on the piperidine ring, because these groups are susceptible to inactivation in presence of the *aspecific* esterases in the blood and in the tissues, resulting in a very rapid metabolism of the drug, and therefore a reduction in the offset time, which is the feature that distinguishes remifentanil from other drugs of the fentanyl family (Glass *et al., 1999*).

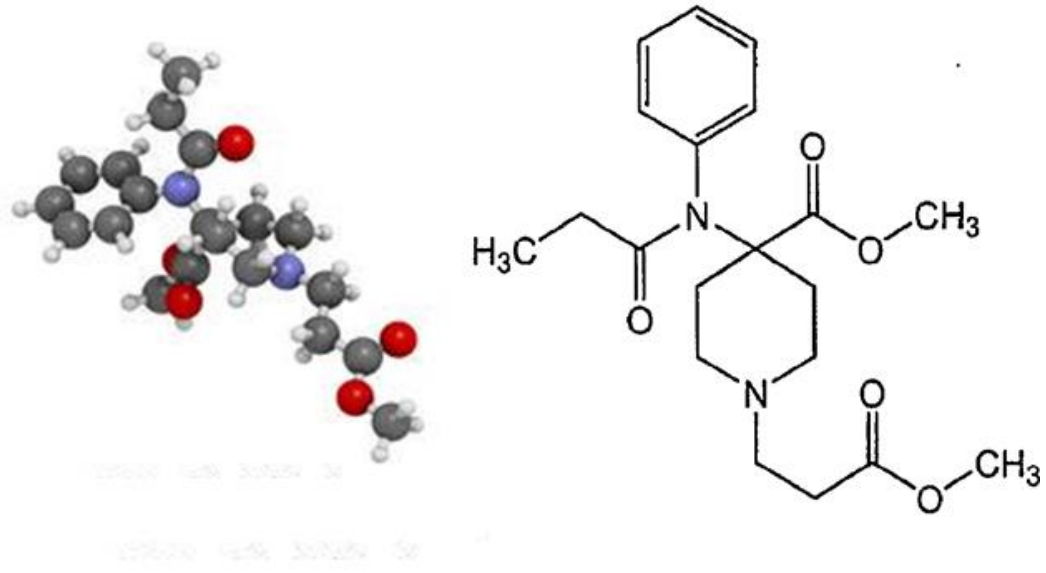

Figure 10 - Chemical structure of remifentanil. (Left) The atoms are represented as spheres. White spheres are hydrogen, grey are carbon, blue are nitrogen, and red are oxygen.

1.4.2 Mechanism of action

Remifentanil is widely applied in the induction and maintenance of general anesthesia, since it is able to suppress the perception of pain and calm the emotional response to it. In fact, opioid binding studies demonstrate that remifentanil has strong affinity with μ-opioid receptors and less with the δ and k receptors (Glass *et al.*, 1999). These receptors explicate an analgesic action, but at different levels:

(i) μ receptors are responsible for analgesia (sovraspinal mechanism, see explanation below) and its main undesired effects (miosis, respiratory depression, reduction of the gastro-intestinal activity, euphoria);
(ii) k receptors are also responsible for analgesia (at the spinal level, see explanation below) and may cause miosis, respiratory depression, and dysphoria. However, they produce less adverse effects and do not contribute to provoking dependence;
(iii) δ receptors are more important in the periphery because they affect and reduce the intestinal transit and depress the immune system, but may also have a minor contribution to analgesia.

μ receptors explicate their action with the sovraspinal mechanism: they are linked to the G proteins, a family of biologic receptors, and inhibit the enzyme adenylate-cyclase, causing the closure of the calcium channels and as a consequence a lower release of neurotransmitters. In this case, the result is the modulation of the pain perception signal.

At the post-synaptic level (spinal mechanism), receptors activate the potassium channels and therefore cause hyper-polarization of the cellular membranes, with consequent modulation of the action potential. The analgesic effect is thus explicated by

inhibiting the nociceptive information pathway, which in simpler terms is the transmission of the pain signal (Al-Hasani and Brucas, 2011).

1.4.3 Pharmacokinetics of remifentanil

As previously mentioned, the peculiar configuration of remifentanil makes it susceptible to metabolism by *aspecific* esterases in blood and tissues. In vitro studies in blood and in vivo studies in dogs demonstrated rapid and extensive metabolism of this compound by ester hydrolysis, which lasts 3.8-8.3 min (Stiller *et al.*, 1995). Several studies describing the pharmacokinetics of remifentanil have been performed in humans. In the initial assessment, remifentanil demonstrated a rapid onset, small volume of distribution, rapid distribution, and clearance.

The rapid onset of remifentanil is demonstrated by its short half-time for equilibration $t_{1/2}k_{e0}$ between plasma and its effect-site compartment (see Table 1).

This short $t_{1/2}k_{e0}$, together with its rapid redistribution, results in a time to peak drug effect of 1.5 min after an IV bolus (Egan *et al.* (1993); Glass *et al.* (1993)). This rapid onset and offset of remifentanil and, thus, minimal latency between dose administration and observed effect should translate into an opioid that is very easy to titrate in clinical practice.

The esterase–based metabolism of remifentanil makes its pharmacokinetics independent of end-organ failure. The pharmacokinetics of remifentanil resulted in fact unaltered in patients with documented hepatic or renal failure. More on this will be discussed in Chapter 2.

The primary metabolite of remifentanil is remifentanil-acid (GI90291, *aka* RA) (Fig. 11). RA is eliminated through the kidneys and therefore accumulates in patients with renal failure, who have a predicted creatinine clearance lower than 10 ml min^{-1}. However, because of the very low potency of the metabolite, simulations indicate that even after a 24h infusion, the metabolite will not reach clinically significant concentrations. Therefore, there will be no relevant pharmacological effects. Hoke *et al.* (1997) demonstrated that RA is much less potent, about 1/4600 times, than remifentanil as μ-opioid agonist in dogs and it is possible to assume the same potency ratio in men.

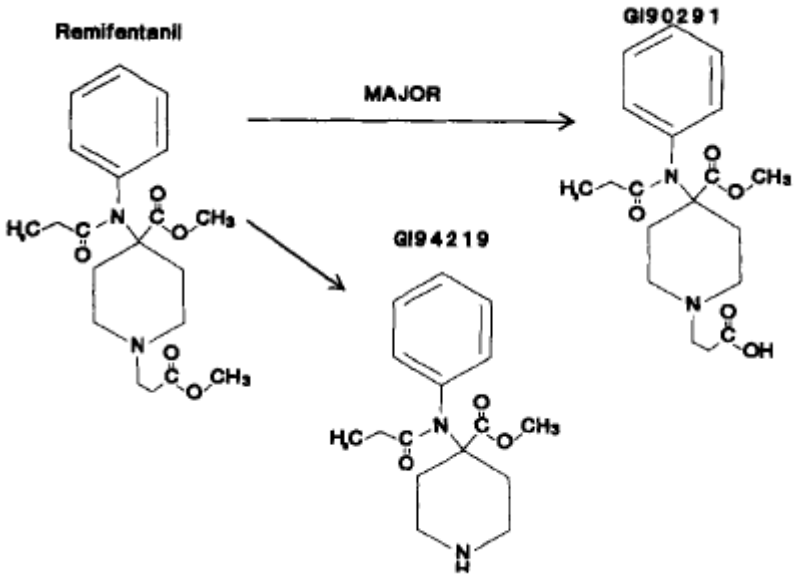

Figure 11 - Metabolic pathway of remifentanil. The main metabolite is GI90291 (RA), which is produced by hydrolysis reactions. Taken from Glass et al. (1999).

As far as 'special' categories of patients are concerned, studies have demonstrated that in pediatric patients, aged 2-12 years, the pharmacokinetics of remifentanil is very similar to that reported in adults (Minto *et al.*, 1997). Instead, in the elderly the onset of drug effect is slower and they showed to be more sensitive to remifentanil and other μ-opioid receptor agonists. In addition, they showed a smaller volume of distribution and a slightly lower clearance. The net result of these differences is that dosing should be decreased with increasing age (Davis *et al.*, 1995).

The current formulation of remifentanil contains glycine. The epidural administration of glycine in dogs has produced agitation, pain, dysfunction, and inability to coordinate inferior arts ("Agenzia Italiana del Farmaco"). Therefore, remifentanil is not administered epidurally: work in humans has been with IV administration only.

1.4.4 Pharmacodynamics of remifentanil

The potency of an opioid is often quoted in terms of morphine equivalents, which usually refers to its potency after a single bolus administration. However, opioids are administered either as a single dose or an infusion and because of this there will be differences in drug disposition and, as a consequence, in the resulting potency.

Ideally, the potency of an opioid is determined by its ability to provide pain relief, but since pain relief is very subjective, a number of other measures of opioid effect have been used to determine the relative potencies.

Remifentanil produces dose-dependent increases in analgesic effect. Based on its ability to provide analgesia in volunteers after a single bolus dose administration, remifentanil

is 20-30 times more potent than alfentanil (Egan *et al.*, 1996). Like alfentanil, increasing analgesic potency is linked with an increasing respiratory depression (Glass *et al.*, 1999). The following subsections report the effects produced by remifentanil.

Hemodynamic effects

In doses up to 2 μg/kg remifentanil produces minimal alterations of systemic blood pressure and heart rate: the reduction of the blood pressure is between 10 and 40%, with a mild decrease of heart rate (Glass *et al.*, 1993). Occasionally, greater decreases in blood pressure may occur in presence of other drugs and are largely due to marked bradycardia, which can be prevented by pretreating patients with glycopyrrolate (Sebel *et al*., 1995).

Respiratory effects

In absence of any external stimulation, a remifentanil infusion rate of 0.05–0.1 μg kg^{-1} min^{-1} results in 50% depression of minute ventilation in presence of 8% inspired CO_2 (the measure and registration of the partial pressure of CO_2 in the inspired air, defined capnography, can be used to monitor the cardiovascular and respiratory functions of patients) in volunteers (James *et al.*, 1992). Obviously, the degree of respiratory depression that results from any dose of remifentanil depends not only on the administered dose, but also on multiple factors such as age, general medical condition, presence of pain, and other stimuli. However, the primary advantage of remifentanil over other μ-opioids having similar undesired effects is that it can be administered during anesthesia, when ventilation is controlled, at doses that result in marked respiratory depression and profound analgesia, but allow having an adequate spontaneous ventilation within 10 min from the end of the infusion. Similarly, if respiratory depression is noted in a patient who is breathing spontaneously during remifentanil administration, reducing or terminating the infusion will rapidly (usually within 3 min) restore adequate ventilation. If required, remifentanil's respiratory depressant effect can be reversed by naloxone (Amin *et al.*, 1995).

This is why remifentanil must not be administered where there is lack of a suitable technology that allows preventing dangerous situations and accidents.

Effects on the Nervous Central system

Remifentanil causes a dose-dependent suppression of the electroencephalogram (EEG). Seizures have not been reported during the administration of remifentanil to humans. Its effects on cerebral blood flow, intracranial pressure, and cerebral metabolic rate seem similar to those of other μ-opioids. Remifentanil was used successfully in patients with mildly increased intracranial pressure presenting for surgery (Warner *et al.*, 1996).

Muscle rigidity

Like other opioids, remifentanil causes a dose-dependent increase in the incidence and severity of muscle rigidity. Since the onset of effect is very rapid, rigidity is more likely to be observed compared with fentanil and sufentanil. When compared at equipotent doses, the incidence and severity of rigidity is similar between remifentanil and alfentanil. Doses lower than 2 µg/kg administered over 1 min have not been reported to cause rigidity. As a result, the initial dose of remifentanil should not exceed 1 µg/kg over 1 min (Glass *et al.*, 1993).

1.4.5 Clinical uses and dosage

For the induction of anesthesia, remifentanil is supplied in combination with a general anesthetic such as propofol, thiopental, or isoflurane. These anesthetics are also called "hypnotic agents" because they induce the unconsciousness state and the mechanism of action is still unclear in most of the cases.

It can be administered with a rate infusion between 0.5 and 1 µg/kg/min, that can be preceded by an initial single bolus of 1 µg/kg (over 30 s to 1 min). Table 2 reports the recommended doses of remifentanil in combination with other drugs used during anesthesia.

Bolus injection is not necessary in case of endotracheal intubation occurring after 8-10 min from the start of the drug infusion. After endotracheal intubation the rate infusion should be reduced, in the range of 0.05-2 µg/kg min, depending on the anesthetic technology used, as indicated in Table 2.

Table 2 - Recommended doses of some important drugs in anesthesiology. Source: Injection Prescribing Information by Mylan.

Induction of anesthesia:	*IV infusion dose [µg/kg/min]*	*Dose range [µg/kg min]*
Remifentanil	0.5-1 (not for less than 30 seconds)	-
Maintenance of anesthesia:		
Nitrogen oxide (66%)	0.4	0.1-2
Isoflurane (initial dose 0.5 MAC)	0.25	0.05-2
Propofol (initial dose 100 [µg/kg min])	0.25	0.05-2

For postoperative analgesia, remifentanil should be initially administered by continuous infusion at a rate of 0.1 µg/kg/min. The infusion rate may be adjusted every 5 min in 0.025 µg/kg/min increments to balance the patient's level of analgesia and respiratory rate. Rates greater than 0.2 µg/kg/min are generally associated with respiratory

depression, that corresponds to a respiratory rate (RR) less than 8 breaths/min, while the usual respiratory rate is 12-16 breaths/min. In addition, bolus doses should be avoided because of a high incidence of apnea, muscle rigidity, and bradycardia.

Because of these peculiar features, the importance of remifentanil has grown in the last years, which is confirmed by the high number of publications in which remifentanil is the reference drug (see Chapter 2). For this reason, remifentanil has been chosen for this thesis work. Chapter 2 and 3 will discuss and explain the different phases that have led to the PK-PD model for remifentanil.

2. PHARMACOKINETICS

2.1 Pharmacokinetics modeling: focus on Physiologically Based Pharmacokinetics models

As discussed in Chapter 1, mathematical models are growing in importance for the study of the pharmacokinetics of drugs and in general in the pharmaceutical industry.

These models are mainly used to describe the dynamic evolution of drug concentration in plasma, tissues, and organs. Usually, these models are compartmental. Even if the literature reports one- and two-compartment models (Dershwitz *et al.* (1996); Minto *et al.* (1997); Egan *et al.* (1998); Pitsiu *et al.* (2004); Sam *et al.* (2009)), the classical PK model has at least a central compartment that represents plasma and two peripheral compartments (Jones and Rowland-Yeo, 2013). The flows between the peripheral compartments and the central compartment are described by rate constants. Of the peripheral compartments, one usually represents the tissues that are highly perfused by blood and therefore is defined as the 'Rapidly equilibrating compartment', while the other represents the tissues that are poorly perfused and therefore is defined as the 'Slowly equilibrating compartment' (Miller *et al.*, 2014). Fig. 12 shows a schematic representation of a classical three-compartment model.

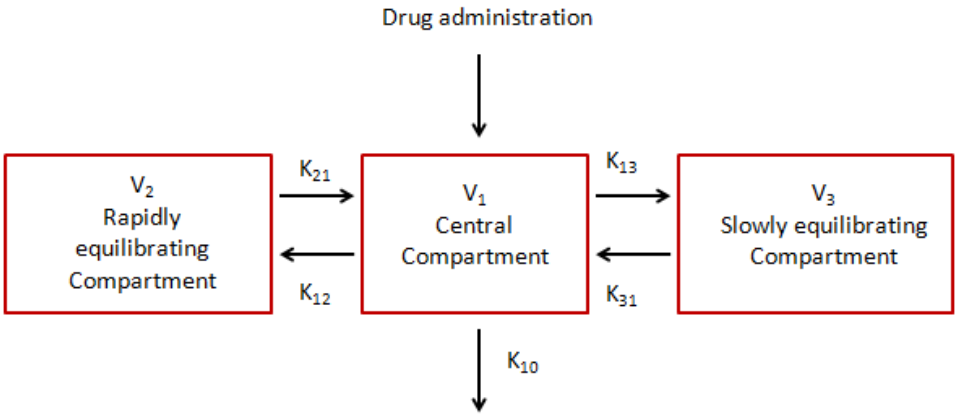

Figure 12 - Classical three-compartment pharmacokinetic model. The central compartment represents the plasma, while the side compartments represent the highly perfused organs/tissues (Rapidly equilibrating Compartment) and poorly perfused organs/tissues (Slowly equilibrating Compartment).

The parameters of three-compartment PK models, which are the rate constants that regulate the flows entering and exiting the compartments, do not have any physiological meaning. However, they can be transformed into more intuitive parameters, such as the volume of distribution and the clearance that can also be used to evaluate the half-time

life of the drug (see Paragraph 1.4 for further details on these parameters). Demographic and physiologic variables (*e.g.*, the body weight, the metabolic function) are sometimes used as covariates in PK models, as it is known that they can affect the profile of the drug concentration in time. The main features of the three-compartment model will be discussed in more details in Paragraph 5.1.

Physiologically-Based Pharmacokinetic models (PBPK) are the result of a special branch of pharmacokinetics: in fact, these models reconcile the physiology and anatomy of the animal or human body with the biochemistry of the study drug. The compartments of PBPK models actually correspond to anatomic parts of mammals that is to say specific organs and tissues, and the blood circulation complies with the basic physiology, while the drug transportation is due to blood, other physiological flows, or diffusion.

The embryonic development of PBPK models occurred in between ‘20s and ‘40s. In '20s Haggard (1924) quantitatively described the introduction of ethyl ether into the body, during the first few breaths. He wrote an equation to describe the relation between the inhaled ether and the concentration of ether in blood, although at that time the tools to solve this equation were not available. The recognized ‘father’ of PBPK models is Teorell (1937), who provided for the first time a physiological model for drug distribution. Again, he did not have the tools to solve the problem (Reddy *et al.*, 2005). A schematic representation of the work of Teorell is reported in Fig. 13.

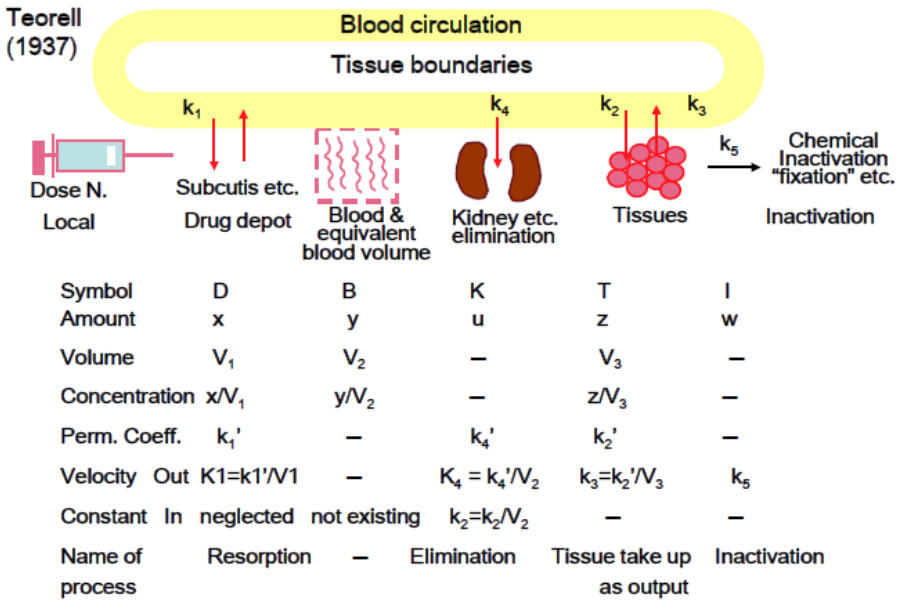

Figure 13 - Representation of Teorell's model (1937). Taken from Reddy et al. (2005).

Later, in the '60s and '70s, PBPK modeling evolved and maturated in the chemotherapeutic area, mainly due to the efforts of investigators with expertise in chemical engineering process design and control. In particular, Bischoff and Dedrick can be distinguished for their pioneering publications: respectively, "Drug distribution in Mammals" (1967) and "Animal scale-up" (1973).

However, the application of PBPK models in the pharmaceutical industry has been limited until recently, because of the mathematical complexity of the models and the need for a large number of parameters required as inputs to the models. This has not prevented the number of publications involving PBPK modeling from increasing significantly in last years, thus spreading this approach across the scientific community. One of the results is that a large number of commercial platforms, which integrate these methodologies have been introduced, such as the Simcyp Population-Based Simulator (Simcyp, Sheffield, UK), GastroPlus (Simulations Plus, Lancaster, CA), PKSIM (Bayer Technology Services, Leverkusen, Germany) (Reddy *et al.*, 2005).

Reassuming, PBPK models describe the concentration-time evolution in specific tissues or organs and in the plasma or blood, following mainly intravenous or oral administration. When the concentration of a therapeutic target is highly related to a chemical efficiency or toxicity, PBPK models may be quite useful, being especially suited to explore and understand the effects of the inter- and intra-individual variability in pharmacokinetics. In addition, they allow studying the drug concentration in the target organs and assessing the effects of the variation of the dose regimen on them.

In general, PBPK simulations provide a tool that is nearer to a full prediction of drug disposition for new therapeutic targets and can help in the selection of the best drug candidates. This is the reason why PBPK is currently used at all levels of the drug discovery and development process and has some relevant advantages compared to the classical PK models.

2.2 Abbiati et al. (2016) PBPK model

Most of the authors in literature used a classical three-compartment model to study the pharmacokinetics of remifentanil (Glass *et al.* (1993); Dershwitz *et al.* (1996); Egan *et al.* (1996); Minto *et al.* (1997); Pitsiu *et al.* (2004); Sam *et al.* (2008)). The reference work of our thesis is instead the Physiologically-Based Pharmacokinetic (PBPK) model developed by Abbiati *et al.* (2016), in order to exploit some of the advantages explained in Paragraph 2.1.

In fact, the main improvement of this kind of model is that it allows taking into account both the anatomical and physiological consistencies with the mammalian/human body. This means that PBPK models can produce a realistic representation. In order to do that, it is necessary to evaluate a few adaptive parameters, such as the physiological

constants that are computed depending on some specific features of the patient, such as the body weight. For the sake of clarity, this thesis focuses on the human body only, although few modifications can be applied to the proposed models to adapt to other species of mammals.

Fig. 14 shows the general structure of the model.

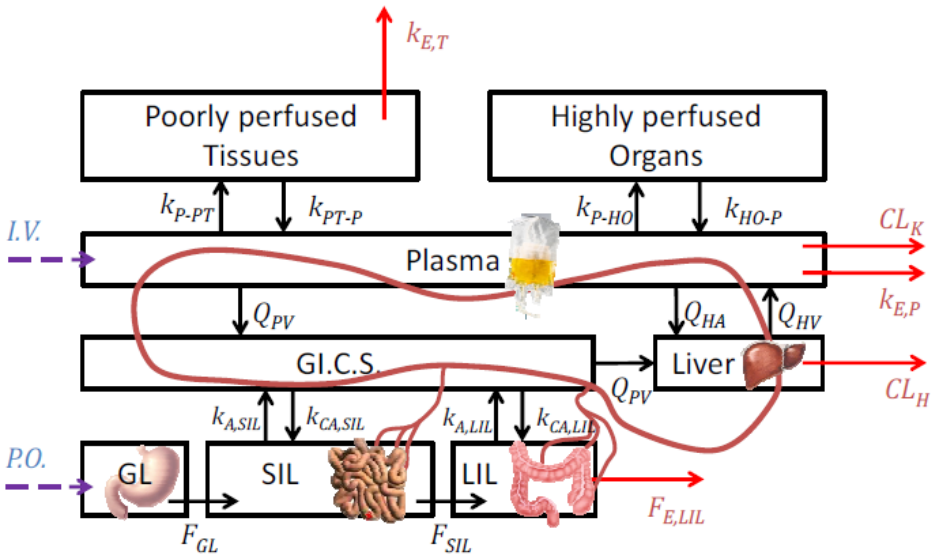

Figure 14 - Representation of Abbiati et al. (2016) model composed of eight compartments: GL (Gastric Lumen), SIL (Small Intestinal Lumen), LIL (Large Intestinal Lumen), GICS (Gastro-Intestinal Circulatory System), Liver, Plasma, PT (Poorly Perfused Tissues) and HO (Highly Perfused Organs). In addition, the material flows between the different compartments are represented with black arrows. Red arrows show the elimination paths and purple dashed arrows the possible administration paths. Taken from Abbiati et al. (2016).

It is possible to distinguish between lumped compartments and single organs. One of the most important regions of the model, for both role and for dimension, is the Gastro-Intestinal tract. This region is divided into four compartments: the Gastric Lumen (GL), the Small Intestinal Lumen (SIL), the Large Intestinal Lumen (LIL), and the Gastro-Intestinal Circulatory System (GICS). The first three compartments (GL, SIL, and LIL) represent respectively the stomach and the main parts of the intestine that are the most important sites of absorption in case of orally-administered drugs (P.O., *i.e. per os*). The fluxes that describe the path of an orally-administered drug in this region are shown in Fig. 14 as $F_{GL,}\, F_{SIL}, F_{E,LIL}$. They are defined as the ratio between the concentration of the drug and the residence time of it in the corresponding lumen ($F_i = {}^{C_i}/_{\tau_i}$). $F_{E,LIL}$ represents the elimination via feces. Mass transfer in the Gastro-Intestinal tract can proceed in both directions, depending on the developed gradient and on the mass transfer coefficients $K_{A,SIL}$ and $K_{A,LIL}$, used to consider the diffusion from the intestinal lumens towards outside, and $K_{CA,SIL}$ and $K_{CA,LIL}$, for the counter-diffusion. The mass

transfer through the gastric barrier can be neglected due to the high resistance of the stomach wall and the shorter residence times of the drug in this section.

GICS belongs to the Gastro-Intestinal region, but it can be considered as part of the section of the model that describes the drug circulation in the body, together with the Plasma Compartment and the hepatic vein. In fact, GICS consists of the blood vessels that go from the intestine to the liver and for this reason it can be considered as a particular section of the circulatory system. The most important GICS vessels are the portal vein that goes from the Gastro-Intestinal tract to the liver and the mesenteric artery that supplies the Gastro-Intestinal tract. The microcirculatory gastro-intestinal vessels are part of this compartment, too. Q_{PV} is the characteristic flow rate of the portal vein.

Liver (H) is considered as a single compartment. It is the metabolic center of the human body and in fact, the majority of the drugs is metabolized here. CL_H is the hepatic clearance, a parameter that provides information about the metabolic activity of the liver. It is defined as the volume of blood that is purified from the drug per unit of time. After exiting the liver, the blood enters the hepatic vein that represents another part of the systemic circulation. The volumetric flux that flows inside this vessel is Q_{HV}.

The drug is therefore transported by blood, which in this model is identified with a specific compartment that is the Plasma compartment, and reaches all the tissues and the organs of the body. In case of intravenous administrations (IV), the drug directly enters the Plasma compartment. It is important to underline that in this model Plasma is not identified with blood, but only with its liquid fraction that is the plasma. All the corpuscular components of the blood (*i.e.* erythrocytes, leukocytes, and platelets) are not considered, since the drug active principle is present only in plasma. The volume of the plasma is about 54% of the total volume of blood in humans.

With this respect, it is important to take into account the protein binding phenomenon that is represented by parameter R in the equations. In fact, a fraction of the drug that enters the systemic circulation may bind to the plasma proteins and therefore is transported neither to tissues nor to organs. Protein binding is an intrinsic characteristic of the drug and can affect its distribution process, as only the remaining unbound fraction interacts with the receptors and produces pharmacological effects. This topic will be discussed in details in Paragraph 2.7.

Four parameters allow defining the drug transport by means of the Plasma compartment: Q_{PV} and Q_{HA} indicate the fraction of plasma that circulates respectively in the portal vein (from GICS to Liver) and in the hepatic artery (from Liver to the rest of the body). K_{P-PT} is the term related to the transport phenomena from Plasma to Poorly Perfused Tissues. K_{P-HO} is the term that accounts for the transport phenomena from Plasma to Highly Perfused Organs. K_{PT-P} and K_{HO-P} are counterparts of K_{P-PT} and

K_{P-HO} respectively, and therefore represent the counter-diffusion terms of the drug transport from tissues and organs to Plasma. Poorly Perfused Tissues (PT) and Highly Perfused Organs (HO) represent two other compartments. These compartments lump tissues and organs that are not considered individually. The Poorly Perfused Tissues compartment is composed of tissues that are not significantly perfused by blood, as for example bones, muscles, and skin. The Highly Perfused Organs compartment lumps organs that are significantly perfused by blood, as for example lungs, brain, and kidneys.

Now, it is possible to analyze the metabolism and excretion regions of the human body. Liver and intestine are not the only organs that play an important role in the metabolism and excretion of a drug. In the model there are three additional terms related to the metabolism, elimination, and excretion processes. $K_{E,P}$ accounts for the direct metabolism of the drug that occurs in the Plasma and it is a mass transfer coefficient. CL_K quantifies the drug filtered by kidneys and excreted by urine. $K_{E,T}$ accounts for the metabolic reactions that occur in the compartment of Poorly Perfused Tissues.

The clearances of the liver and the kidneys (CL_H and CL_K) are evaluated as the product of the total volumetric flow rate of plasma that reaches the organs and their efficiency ($CL_i = Q_i \cdot Eff_i$).

The flow rates can vary from patient to patient, because they will depend on the specific body features (*e.g.*, body mass), while the efficiency of the organs is a generic value. It is interesting to underline that CL_K is not applied to the Highly Perfused Organs compartment to which the kidneys belong, but it is applied to the plasma compartment because its value is referred to the plasmatic drug concentration.

Therefore, the total number of compartments of this model is eight. The drug evolution in these compartments can be simulated by solving a system of eight ordinary differential equations (ODEs), with suitable initial conditions, where each equation represents the molar balance of the drug in a specific compartment. The solution in fact provides the dynamic concentration profiles of the drug in the compartments. The ODEs system is reported in the following.

Gastric Lumen:

$$\frac{dC_{GL}(t)}{dt} = \frac{PO(t)}{V_{GL}} - F_{GL}(t) \tag{1}$$

Small Intestinal Lumen:

$$\frac{dC_{SIL}(t)}{dt} = -C_{SIL}(t) \cdot K_{A,SIL} + F_{GL}(t) \cdot \frac{V_{GL}}{V_{SIL}} - F_{SIL}(t) + C_{GICS}(t) \cdot (1 - R) \cdot K_{CA,SIL} \cdot \frac{V_{GICS}}{V_{SIL}} \tag{2}$$

Large Intestinal Lumen:

$$\frac{dC_{LIL}(t)}{dt} = -C_{LIL}(t) \cdot K_{A,LIL} + F_{SIL}(t) \cdot \frac{V_{SIL}}{V_{LIL}} - F_{E,LIL}(t) + C_{GICS}(t) \cdot (1-R) \cdot K_{CA,LIL} \cdot \frac{V_{GICS}}{V_{LIL}} \quad (3)$$

Plasma Compartment:

$$\frac{dC_P(t)}{dt} = -C_P(t) \cdot \left(K_{P-PT} \cdot (1-R) + K_{P-HO} \cdot (1-R) + \frac{Q_{HA}}{V_P} + \frac{Q_{PV}}{V_P}\right) + C_P(t) \cdot K_{PT-P} \cdot \frac{V_{PT}}{V_P} + C_L(t) \cdot \frac{Q_{HV}}{V_P} + C_{HO}(t) \cdot K_{HO-P} \cdot \frac{V_{HO}}{V_P} - C_P(t) \cdot (1-R) \cdot K_{E,P} - C_P(t) \cdot \frac{CL_K}{V_P} + \frac{IV(t)}{V_P} \quad (4)$$

Poorly Perfused Tissues Compartment:

$$\frac{dC_{PT}(t)}{dt} = -C_{PT}(t) \cdot \left(K_{PT-P} + K_{E,T}\right) + C_P(t) \cdot (1-R) \cdot K_{P-PT} \cdot \frac{V_P}{V_{PT}} \quad (5)$$

Gastro-Intestinal Circulatory System:

$$\frac{dC_{GICS}(t)}{dt} = -C_{GICS}(t) \cdot \left(\frac{Q_{PV}}{V_{GICS}} + (1-R) \cdot K_{CA,SIL} + (1-R) \cdot K_{CA,LIL}\right) + C_{SIL}(t) \cdot K_{A,SIL} \cdot \frac{V_{SIL}}{V_{GICS}} + C_{LIL}(t) \cdot K_{A,LIL} \cdot \frac{V_{LIL}}{V_{GICS}} + C_P(t) \cdot \frac{Q_{PV}}{V_{GICS}} \quad (6)$$

Liver:

$$\frac{dC_L(t)}{dt} = -C_L(t) \cdot \left(\frac{Q_{HV}}{V_L} + \frac{CL_H}{V_L}\right) + C_P(t) \cdot \frac{Q_{HA}}{V_L} + C_{GICS}(t) \cdot \frac{Q_{PV}}{V_L} \quad (7)$$

Highly Perfused Organs Compartment:

$$\frac{dC_{HO}(t)}{dt} = -C_{HO}(t) \cdot K_{HO-P} + C_P(t) \cdot (1-R) \cdot K_{P-HO} \cdot \frac{V_P}{V_{HO}} \quad (8)$$

The sign convention is assumed positive for the fluxes entering the compartments and negative for the fluxes exiting the compartments.

Mass transport phenomena are very important to reach a realistic description of the paths of the drug inside the human body. Mass transport can occur by means of two different phenomena: simple mass transfer or via blood circulation. In the first case, the mass transfer flux is equal to the concentration of the considered compartment multiplied by the corresponding mass transfer coefficient. In the second case, the mass transfer flux is equal to the volumetric flux that flows inside the channel of interest multiplied by the relative concentration.

Equations 1 and 4 contain the terms related to the drug way of administration. $PO(t)$ is the dose for an orally-administered drug, while $IV(t)$ is the dose in case of intravenous administration. These terms represent the amount of drug that is administered to the patient, expressed as mass over unit of time (*e.g.*, [μg/min]).

With reference to Equations 2 and 3, which describe the drug concentration in the SIL and LIL compartments, one could object that the intestinal lumen should not be treated as a continuously stirred tank reactor (CSTR), but rather as a plug flow reactor (PFR). The reason is that the intestine is a longitudinal duct, therefore these two equations should be modified to better describe the movement of an oral bolus in this region. However, by doing so, there would be two independent variables to describe the evolution in time and space and the system would become a partial differential equation (PDE) system. A possible strategy to solve this problem is to discretize spatially the PDEs as a series of perfectly mixed sub-compartments. By doing so, one would obtain a set of ODEs instead of a PDE and the number of equations would depend on the adopted discretization step.

Equations (1-8) allow describing the path of a drug in the different compartments. However, to get a complete insight of what happens inside the human body, it is also important to consider the ways of elimination and excretion of a drug. To this purpose, five more equations are required.

$$\frac{dA_{E,LIL}}{dt} = \frac{C_{LIL}(t)}{t_{LIL}} \cdot V_{LIL} \tag{9}$$

$$\frac{dA_{E,P}(t)}{dt} = C_P(t) \cdot (1 - R) \cdot K_{E,P} \cdot V_P \tag{10}$$

$$\frac{dA_{E,T}(t)}{dt} = C_T(t) \cdot K_{E,T} \cdot V_T \tag{11}$$

$$\frac{dA_H(t)}{dt} = C_L(t) \cdot CL_H \tag{12}$$

$$\frac{dA_K(t)}{dt} = C_P(t) \cdot CL_K \tag{13}$$

The terms A_i of Equations (9-13) represent the total amount of drug, expressed in [ng], that is eliminated through the different pathways of the different compartments or organs of interest. Equation 9 is related to the Large Intestinal Lumen (LIL), therefore it represents the elimination of the drug via feces. Equations 10 and 11 refer to the metabolism that occurs in plasma and tissues respectively, mainly due to enzymes. The role of the metabolism of remifentanil by enzymes will be further discussed in Paragraph 2.7. Equation 12 is related to the metabolism accomplished by the liver, while Equation 13 is related to the drug elimination by kidneys.

Equations (9-13) are not part of the ODE system, but are used in order to obtain some information for a complete view of the problem.

In the equations there are 28 parameters that can be divided into 3 categories: (i) individualized parameters, (ii) assigned parameters, (iii) degrees of freedom (see also Table 3).

Table 3 - Parameters of the model that can be categorized into: individualized, assigned, or degrees of freedom.

Symbol	*Units*	*Description*	*Type*
Q_{HA}	mL/min	Volumetric flux of Hepatic Artery	Individualized
Q_{HV}	mL/min	Volumetric flux of Hepatic Vein	Individualized
Q_K	mL/min	Volumetric flux of Cardiac output to Kidneys	Individualized
Q_{PV}	mL/min	Volumetric flux of Portal Vein	Individualized
V_{GICS}	cm^3	Volume of GICS compartment	Individualized
V_{GL}	cm^3	Volume of GL compartment	Individualized
V_{HO}	cm^3	Volume of HO compartment	Individualized
V_L	cm^3	Volume of Liver compartment	Individualized
V_{LIL}	cm^3	Volume of LIL compartment	Individualized
V_P	cm^3	Volume of Plasma compartment	Individualized
V_{PT}	cm^3	Volume of PT compartment	Individualized
V_{SIL}	cm^3	Volume of SIL compartment	Individualized
R	-	Protein binding	Assigned
t_{GL}	min	GL residence time	Assigned
t_{LIL}	min	LIL residence time	Assigned
t_{SIL}	min	SIL residence time	Assigned
Eff_H	-	Efficiency of elimination of liver	Degree of freedom
Eff_K	-	Efficiency of elimination of kidneys	Degree of freedom
$K_{A,LIL}$	min^{-1}	Mass transfer coefficient from LIL to GICS	Degree of freedom
$K_{A,SIL}$	min^{-1}	Mass transfer coefficient from SIL to GICS	Degree of freedom
$K_{CA,LIL}$	min^{-1}	Mass transfer coefficient from GICS to LIL	Degree of freedom
$K_{CA,SIL}$	min^{-1}	Mass transfer coefficient from GICS to SIL	Degree of

			freedom
$K_{E,P}$	min^{-1}	Constant of elimination of Plasma	Degree of freedom
$K_{E,T}$	min^{-1}	Constant of elimination of Tissues	Degree of freedom
K_{HO-P}	min^{-1}	Mass transfer coefficient from HO to Plasma	Degree of freedom
K_{P-HO}	min^{-1}	Mass transfer coefficient from Plasma to HO	Degree of freedom
K_{P-PT}	min^{-1}	Mass transfer coefficient from Plasma to PT	Degree of freedom
K_{PT-P}	min^{-1}	Mass transfer coefficient from PT to Plasma	Degree of freedom

It is possible to adopt different approaches to calculate, assign, and fit the parameters listed in Table 3, depending on the class to which they belong.

Individualized parameters may be calculated through specific correlations available in the literature (Brown *et al.*, 1997). In general, these correlations mainly depend on two features of the patient: sex and weight. The presence of these parameters allows personalizing the model, so that it better suits a patient. In fact, it is intuitive that the mass and gender of a patient can play an important role in the dose prescription and affect the dynamic evolution of the drug in the body. This topic will be further discussed in Paragraph 4.7.

Different correlations are available for the evaluation of these parameters. First of all, it is possible to quantify the total cardiac output (CO), which is an important piece of information because it affects the flow rates directed to tissues and organs.

Two different correlations are considered for the CO evaluation in Abbiati *et al.* (2016), depending on the demographic data information available. These correlations and in general correlations used to compute different individualized parameters are based on either the body mass (BM) or the body surface area (BSA). BM is the weight of the patient expressed in [kg], while BSA represents the surface of the human body, expressed in [m^2]. For clinical purposes, BSA is a better index to express the metabolic mass than BM because it is less affected by abnormal adipose mass. There are different correlations that can be used to calculate the BSA that depend on the weight and the height of the patient, for instance Mosteller (1987) formula (Equation 14).

$$BSA = \frac{h \cdot BM}{3600} \tag{14}$$

Where h is the height in [cm], and BM the body mass in [kg].

As previously mentioned, CO may be computed using correlations based on either BSA or BM. If BSA is available, the correlation applied is (Cowles *et al.*, 2002):

$$CO = 3.5 \cdot BSA \tag{15}$$

while if the body mass (BM) is known, it is possible to use (Linsted and Schaeffer, 2002):

$$CO = 0.084 \cdot BM \tag{16}$$

Knowing the value of CO, it is possible to evaluate the flow rates of blood vessels. The correlations used to find the different flow rates depend on the gender. The ones used to calculate the volumetric flow rates of different blood vessels for males are:

$$Q_{PV} = 0.19 \cdot CO \tag{17a}$$

$$Q_{HA} = 0.06 \cdot CO \tag{18a}$$

$$Q_{HV} = 0.25 \cdot CO \tag{19a}$$

$$Q_{K} = 0.19 \cdot CO \tag{20a}$$

The ones for females are:

$$Q_{PV} = 0.21 \cdot CO \tag{17b}$$

$$Q_{HA} = 0.06 \cdot CO \tag{18b}$$

$$Q_{HV} = 0.27 \cdot CO \tag{19b}$$

$$Q_{K} = 0.17 \cdot CO \tag{20b}$$

In case of a group of patients composed of females and males, it is possible to use averaged coefficients (Williams and Leggett, 1989). All these flow rates are then multiplied by 0.54 in order to account only for the plasmatic flow rate.

In order to evaluate the volumes of the different compartments, it is necessary to know the organ/tissue body mass fraction and their density, indicated respectively with Fr_{BMi} and ρ_i:

$$V = \sum_i \frac{BM \cdot \mathrm{Fr_{BMi}}}{\mathrm{\rho_i}} \tag{21}$$

where i refers to:

- Poorly Perfused Organs, as fat, bones, heart, muscles
- Highly Perfused Organs, as brain, kidneys, spleen
- Liver
- Gastro-Intestinal Circulatory System
- Plasma

- The compartments that belong to the Gastro-Intestinal tract, *i.e.* the Gastric Lumen, the Small Intestinal Lumen, and the Large Intestinal Lumen.

It is interesting to underline that lungs are not included in the Highly Perfused Organs because of their nature. They are indeed highly vascularized, but they have a very low density when they are expanded, therefore it is very difficult to find a reliable value of their volume. Sexual organs are neglected too, because in the literature there is no information available and they are negligible in terms of volume respect to other organs. Table 4 reports the values of the body mass fraction and the density of the different organs and tissues.

Table 4 - Body mass fraction and density of different organs and tissues (Brown et al., 1997).

Organ/Tissue	Fr_{BM}	*Density [g/ml]*
Blood	0.079	1.06
Bones (cortex)	0.143	1.6
Brain	0.02	1.035
Fat	0.214	0.913
GICS	0.0001766	1
Heart	0.005	1.03
Kidneys	0.004	1.05
Liver	0.026	1
Muscles	0.4	1.041
Skin	0.037	1.3
Spleen	0.00026	1.05

It is necessary to underline that there is no formula available in the literature for GICS. For this reason, Abbiati *et al.*, (2016) proposed a way to evaluate its volume. The main component of GICS is the portal vein, therefore by computing the volume of this vessel, it is possible to have an approximate estimate of the volume of GICS. A cylindrical geometry and an average length and diameter, of 1.1 and 5.8 cm, respectively, are employed to evaluate the volume of the portal vein. The body mass fraction is calculated by assuming the BM of a generic patient of 80 kg. Since the portal vein is not the only component of the GICS, despite being the main one, this value is overestimated by 35%. Once the GICS volume is known, it is possible to evaluate the body mass fraction of GICS as follows:

$$Fr_{BM,GICS} = \frac{V_{PV}}{BM \cdot 1000} = 0.0001766 \qquad (22)$$

The assigned parameters are not individualized because of the lack of correlations based on specific features of the patient in the literature. However, it is possible to either determine these parameters experimentally or find them in the literature. For this reason, they are assumed constant and equal to a specific value. The only parameter known with sufficient accuracy from the literature is the fraction of drug bound to plasma proteins that is 70% (Egan *et al.*, 1998).

The degrees of freedom of the model do not have a direct correspondence with physiological aspects and can only be determined numerically. Indeed, they are evaluated by means of a nonlinear regression procedure that minimizes an objective function, for instance the sum of the squared errors (SSE) or the sum of the absolute values of the errors (SAE), where the error is the difference between the experimental data of the drug concentration in blood/plasma and the predicted concentration of the model. It is important to underline that the concentration of the drug in blood is the only data available in the literature. In fact, when a human being is involved in an experimental activity, the blood concentration is the only pharmacokinetic parameter that can be measured. The measures of the concentration of the drug in other sites, as tissues or organs, are possible through biopsies in humans, but these techniques are invasive and allow analyzing only a very small part of the considered tissue. In addition, biopsies cannot be iterated to obtain a profile of the drug concentration in the site of interest.

The optimization technique is a nonlinear regression based on a constrained and multidimensional optimization algorithm, in order to maintain the values of the different degrees of freedom within proper ranges. These intervals are defined according to hypotheses based on the physics of the problem.

The model presented above is a generic model that can be simplified considering specific cases. The drug studied by Abbiati *et al.* (2016) is remifentanil. Its specific features allow reducing the number of equations that have to be solved. First of all, remifentanil is only administered by intravenous infusion (see Chapter 1), therefore it is possible to neglect the Gastro-Intestinal tract, as discussed above. However, it is necessary to consider the counter diffusion from the Gastro-Intestinal Circulatory System to the gastro-intestinal region, which remains unchanged in Equation 6.

Remifentanil is a lipophilic molecule and therefore its diffusion across the cellular membranes is facilitated, which promotes the distribution process. Moreover, remifentanil is metabolized by *aspecific* esterases in plasma and tissues, such as muscles and poorly perfused organs. This topic will be further discussed in Paragraph 2.3. According to Abbiati *et al.* (2016), $K_{E,P}$ and $K_{E,T}$ are therefore more important than CL_H and CL_K as routes of elimination of the drug.

Fig. 15 shows the reduced structure of the model for remifentanil.

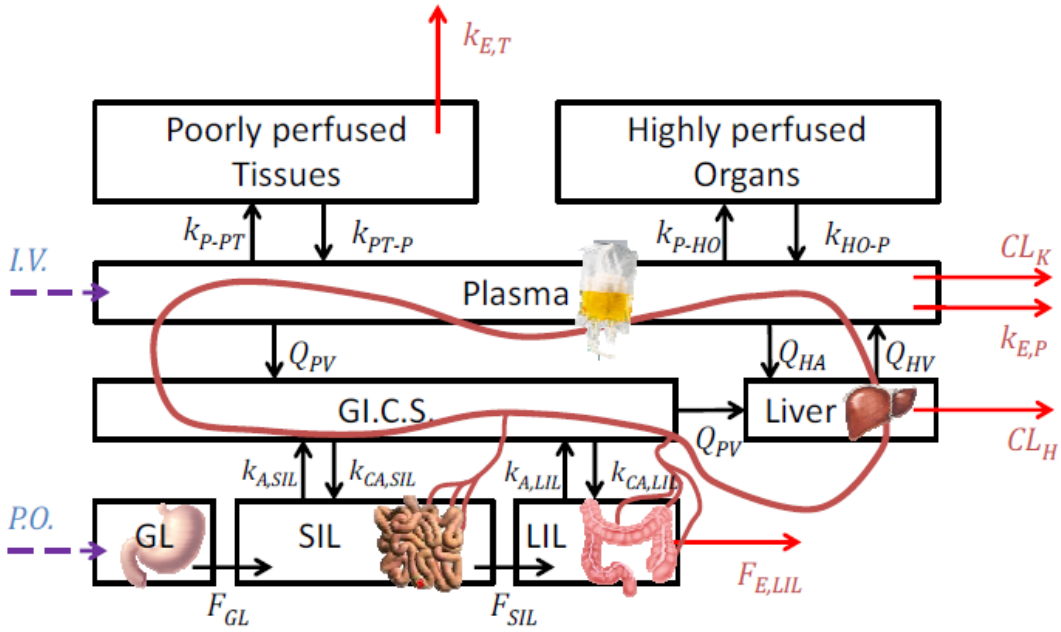

Figure 15 - Schematic representation of the minimized model for remifentanil. GL, LIL, and SIL are neglected because remifentanil is an intravenous administered drug. Taken from Abbiati et al. (2016).

As shown in Fig. 15, the number of compartments considered for the specific case of remifentanil, and in general for all of the intravenous administered drugs, is five. This implies a reduction of the number of ODEs that are necessary to describe the dynamic evolution of the concentration of the drug in the human body. The number of degrees of freedom decreases as well, from 12 to 8. The number of individualized parameters is also reduced, because the volumes of the compartments belonging to the Gastro-Intestinal tract are not interesting in this case. Only the number of the assigned parameters remains unchanged.

2.3 Six-parameter PK model

The model presented by Abbiati *et al.* (2016) has been modified in this thesis to make it more suitable for remifentanil and capable to represent what happens to this particular drug inside the human body. The final goal is to correlate the dose of remifentanil to its pharmacological effect. In order to understand how the model had to be modified, we sought advice from the scientific literature, with a special focus on the metabolic processes and the drug elimination pathways.

Dahaba *et al.* (1999) compared the recovery parameters of Total Intravenous Anesthesia (TIVA) with remifentanil and propofol, and hemodynamic responses to pre-operative events, in a group of end-stage renal-failure patients and a control group of healthy patients. They concluded that, despite the heavy renal dysfunction and associated biochemical/physiological deficiencies of those patients, the TIVA recovery with remifentanil and propofol is not affected at all.

In a different and more specific study, Dahaba *et al.* (2002) aimed at evaluating the pharmacokinetics of remifentanil in a group of end-stage renal-failure patients in comparison with a group of healthy patients. They found a significant alteration in the pharmacokinetics but they remarked that this difference could not be due to a lower degradation as remifentanil metabolism is esterase-based and therefore independent of the kidneys status. However, their role cannot be completely neglected since the kidneys are important in the degradation of remifentanil acid (RA), *i.e.* its main metabolite, which has a very reduced potency compared to the drug (see Chapter 1). They attributed this PK difference to different factors that will be deepened in Paragraph 2.6.

On the other hand, Hoke *et al.* (1997) were interested in verifying that remifentanil is independent on renal function and therefore compared two groups of volunteers, where one was composed of renal-failure patients. According to their results, there was no difference in the pharmacokinetics of the two groups. The difference between their results and Dahaba's ones may be attributed to different rates of infusion between the studies, a different number of patients, and different times for the hemodialysis.

Pitsiu *et al.* (2004) assessed the PK of remifentanil and RA, as part of an open-label safety study, which means that both the researchers and the patients knew the treatment that was being administered, in intensive care unit (ICU) patients with varying (from normal to severe) degrees of renal impairment. They found that RA accumulates in patients with moderate/severe renal impairment. However, eventually no prolongation of μ-opioid effects was observed.

Des Breen *et al.* (2004) performed a similar study and found that there was no evidence of increased offset time with increased duration of exposure to remifentanil in either group.

According to these findings, it is possible to claim that remifentanil metabolism is not affected by any degree of renal dysfunction.

As mentioned above, the majority of the drugs is metabolized by the liver. Several literature papers assessed the liver role in the remifentanil metabolism.

Navapurkar *et al.* (1998) investigated the pharmacokinetics of remifentanil in patients undergoing Orthopic Liver Transplantation (OLT, the previous liver is removed and the transplant is placed at that location in the body of the recipient). This means that they studied the pharmacokinetics of the drug in presence and in absence of the liver. The pharmacokinetics resulted to be different in these conditions. However, they remarked that the differences should not to be attributed to the liver role in the metabolism but rather to other factors, which will be discussed in more details in Paragraph 2.6.

Dershwitz *et al.* (1996) drew similar conclusions. They studied the pharmacokinetics of remifentanil in patients affected by severe liver disease compared to healthy patients.

The result emerging from the literature is that remifentanil is metabolized only by *aspecific* esterases present in blood and tissues. This means that neither the liver nor the kidneys take part to the elimination of remifentanil. In fact, since organ dysfunction and the duration of drug infusion usually affect the offset of the effects of traditional opioids, this organ-independent metabolism of remifentanil makes it ideal for the treatment of patients with hepatic and renal dysfunction. This peculiar characteristic of remifentanil also makes it the most short-acting agent in the fentanyl drugs family.

In our opinion and according to the scientific literature, both plasma and tissue eliminations should be considered as the only two degradation pathways. As a result, Equations 9, 12, and 13 can be neglected. Fig. 16 shows the neglected elimination pathways. Consequently, the parameters to be determined get reduced from 8 to 6. To distinguish the original model from Abbiati *et al.* (2016) and our model, from now on the two will be called respectively 8P model and 6P model, depending on the number of parameters.

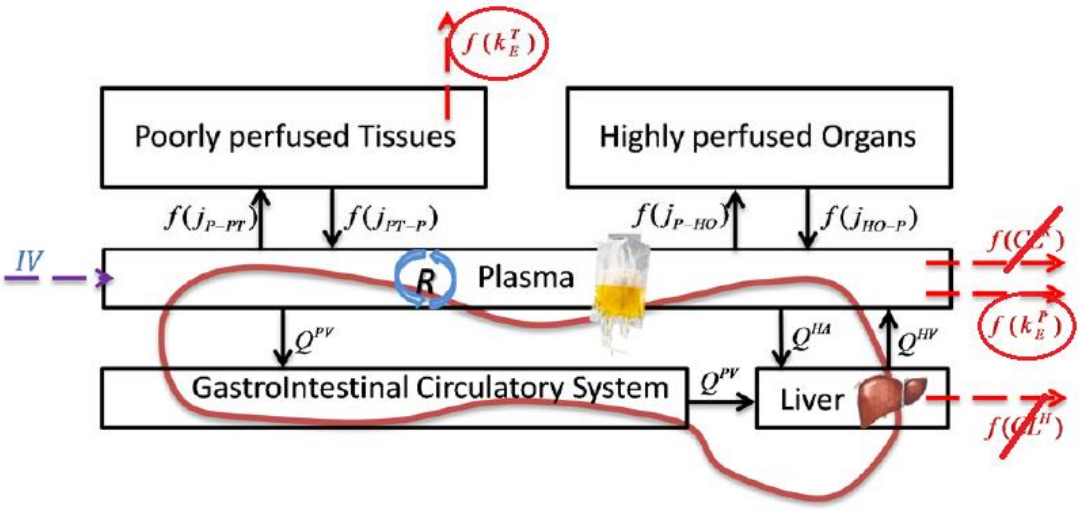

Figure 16 - Schematization of the six-parameter model. The hepatic and renal clearances can be neglected. Adapted from Abbiati et al. (2016).

The six parameters are identified by means of a constrained optimization procedure, using Matlab function *Fmincon*. The objective function to be minimized is the normalized absolute error between the predicted blood concentration and the measured blood concentration:

$$f_{obj} = \sum_{i=1}^{N_s} \sum_{j=1}^{N_p} \sum_{k=1}^{N_m} \left(\frac{\left| C_{i,j,l}^{exp} - C_{i,j,l}^{mod} \right|}{N_m} \right) \tag{23}$$

where N_s is the number of case-studies, N_p is the number of patients of the *k-th* case-study and N_m is the number of measures (measured blood/plasma concentrations).
The parameters of the model are identified from the experimental data available in Dahaba *et al.* (2002). Table 5 lists the initial estimates, which are the values of the parameters of the model of Abbiati *et al.* (2016), and the final values for the parameters, resulting from the optimization procedure.

Table 5 - From the left: lower bounds for the constrained optimization, initial values of the model parameters, upper bounds for the constrained optimization, final optimized values derived from the parameter identification procedure.

Parameters	*Lower bounds*	*Initial values*	*Upper bounds*	*Optimized values*
K_{PT-P}	0.1	0.279	0.5	0.332
K_{P-PT}	0.3	0.479	0.7	0.538
K_{P-HO}	0.4	0.662	1	0.751
K_{HO-P}	0.02	0.044	0.07	0.0461
$K_{E,P}$	1.5	1.732	2	1.779
$K_{E,T}$	0.01	0.063	0.1	0.0678

It is worth observing that the parameters did not change dramatically, as expected. Paragraph 2.4 compares qualitatively and quantitatively the results of the 8P model and of the 6P model.

2.4 Model validation and comparison with Abbiati et al. (2016) work

2.4.1 Case-study 1: Egan et al. (1996)

In order to characterize the remifentanil pharmacokinetics, Egan *et al.* (1996) studied ten adult male volunteers, who received different doses from 1 to 8 µg/kg/min with an infusion of 20 min. Although the results show a significant inter-individual variability, the volunteers were between 18 and 40 years old, and within 15% of their ideal body weight. Fig. 17 shows the results of the simulations of the ten volunteers with Abbiati *et al.* (2016) model (on the left, based on 8 adaptive parameters) and our 6P model (on the right).

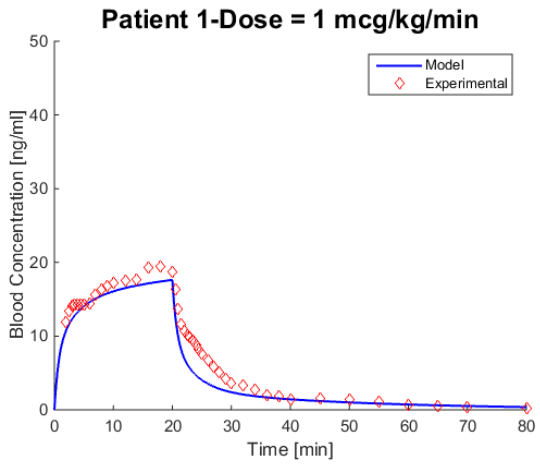
Patient 1-Dose = 1 mcg/kg/min
Model
Experimental
Blood Concentration [ng/ml]
Time [min]

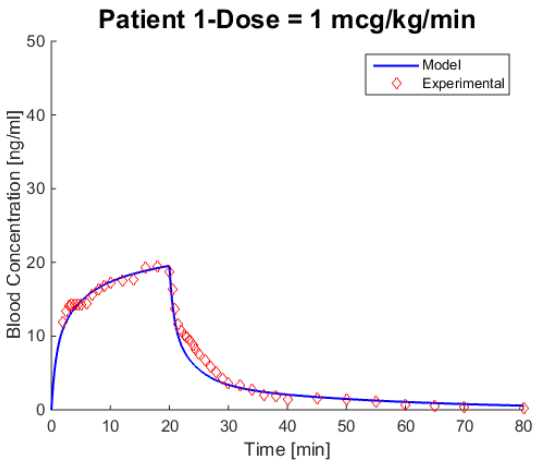
Patient 1-Dose = 1 mcg/kg/min
Model
Experimental
Blood Concentration [ng/ml]
Time [min]

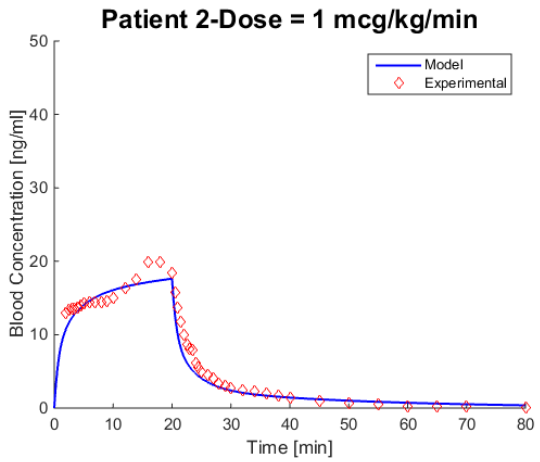
Patient 2-Dose = 1 mcg/kg/min
Model
Experimental
Blood Concentration [ng/ml]
Time [min]

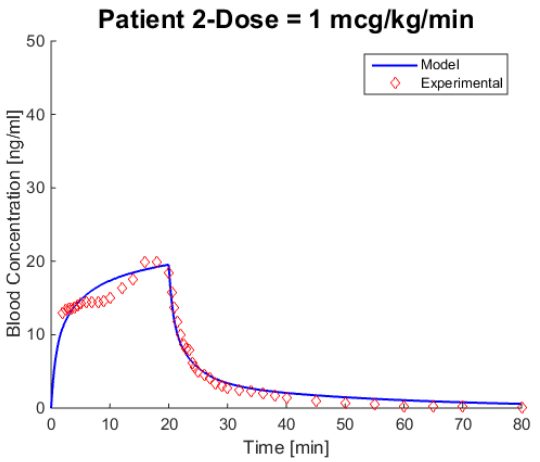
Patient 2-Dose = 1 mcg/kg/min
Model
Experimental
Blood Concentration [ng/ml]
Time [min]

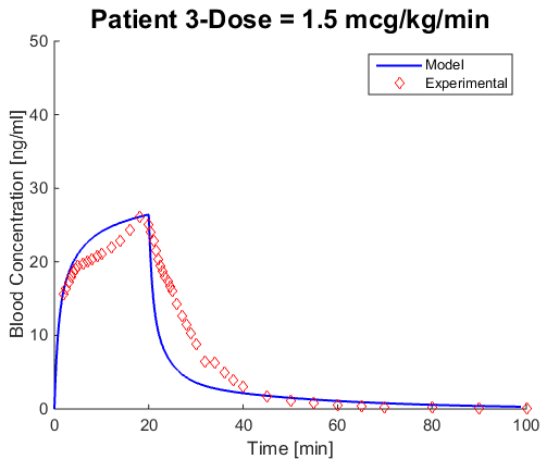
Patient 3-Dose = 1.5 mcg/kg/min
Model
Experimental
Blood Concentration [ng/ml]
Time [min]

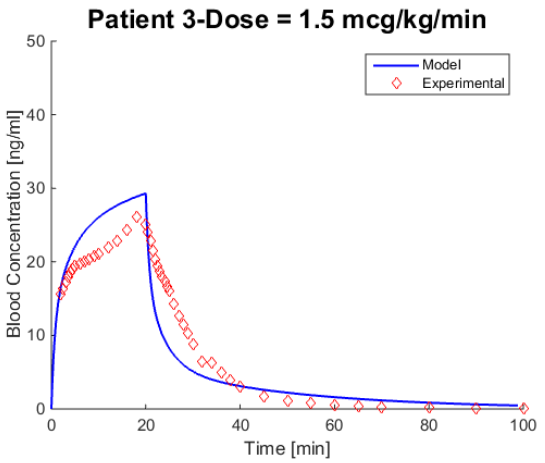
Patient 3-Dose = 1.5 mcg/kg/min
Model
Experimental
Blood Concentration [ng/ml]
Time [min]

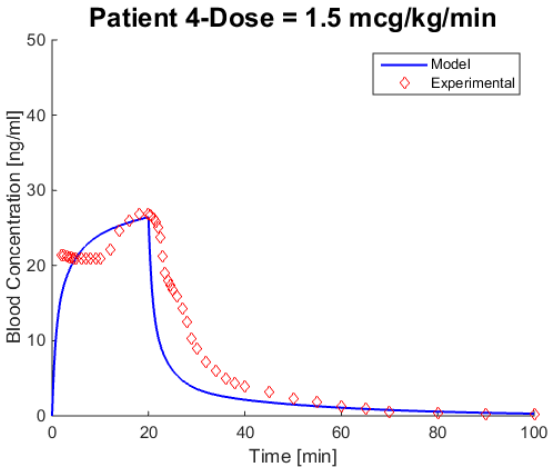
Patient 4-Dose = 1.5 mcg/kg/min
Model
Experimental
Blood Concentration [ng/ml]
Time [min]

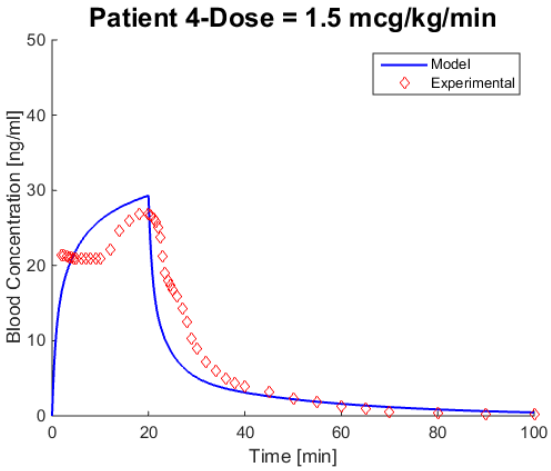
Patient 4-Dose = 1.5 mcg/kg/min
Model
Experimental
Blood Concentration [ng/ml]
Time [min]

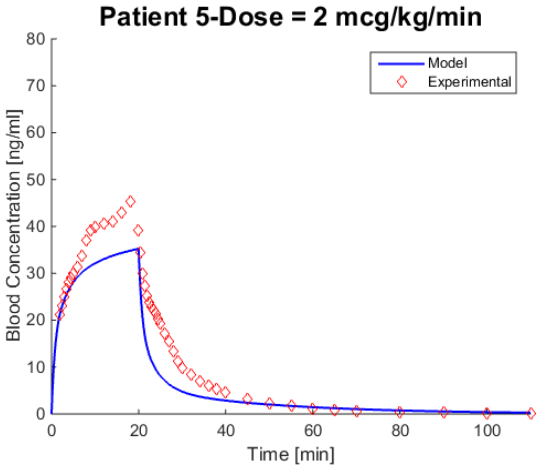
Patient 5-Dose = 2 mcg/kg/min
Model
Experimental
Blood Concentration [ng/ml]
Time [min]

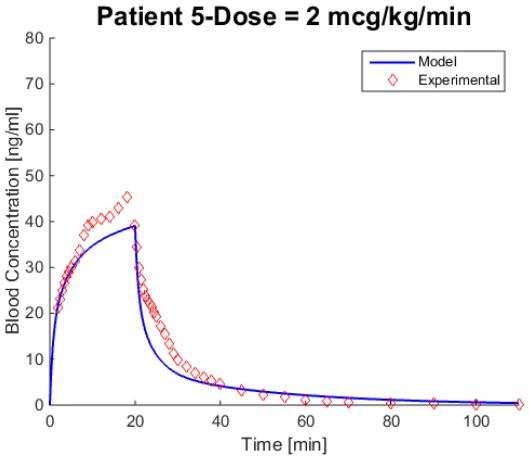
Patient 5-Dose = 2 mcg/kg/min
Model
Experimental
Blood Concentration [ng/ml]
Time [min]

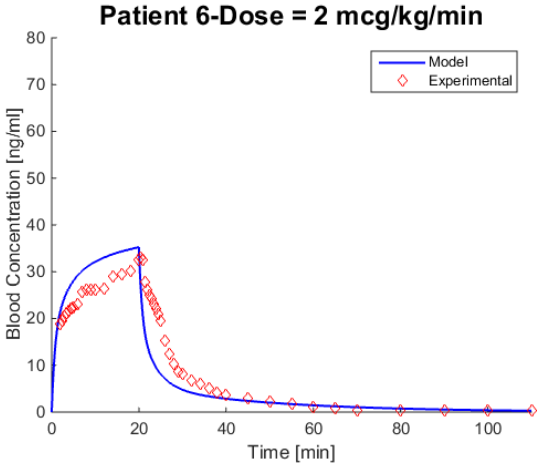
Patient 6-Dose = 2 mcg/kg/min
Model
Experimental
Blood Concentration [ng/ml]
Time [min]

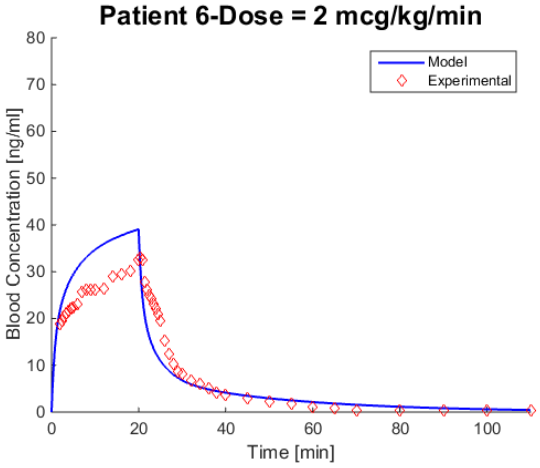
Patient 6-Dose = 2 mcg/kg/min
Model
Experimental
Blood Concentration [ng/ml]
Time [min]

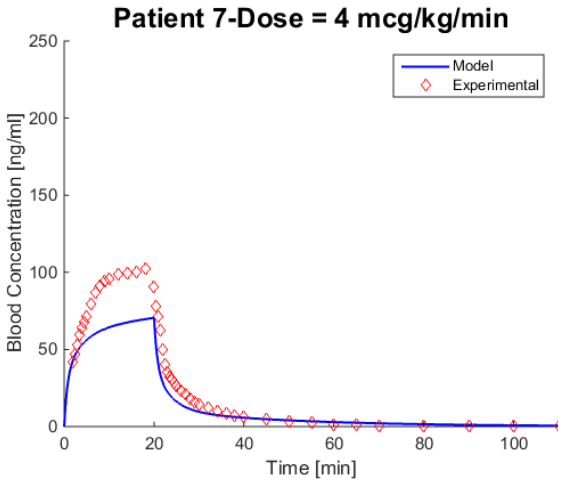
Patient 7-Dose = 4 mcg/kg/min
Model
Experimental
Blood Concentration [ng/ml]
Time [min]
0
50
100
150
200
250
0
20
40
60
80
100

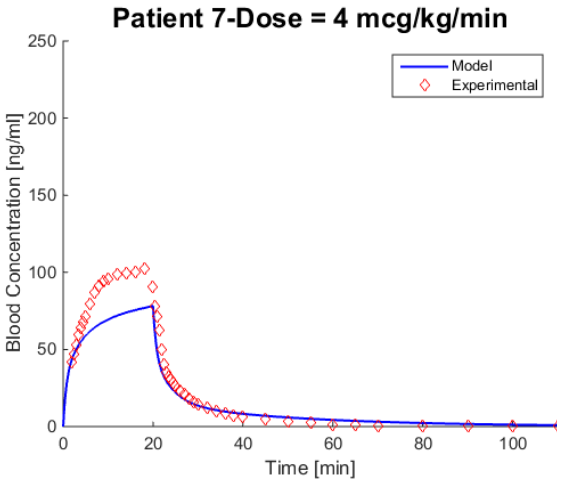
Patient 7-Dose = 4 mcg/kg/min
Model
Experimental
Blood Concentration [ng/ml]
Time [min]
0
50
100
150
200
250
0
20
40
60
80
100

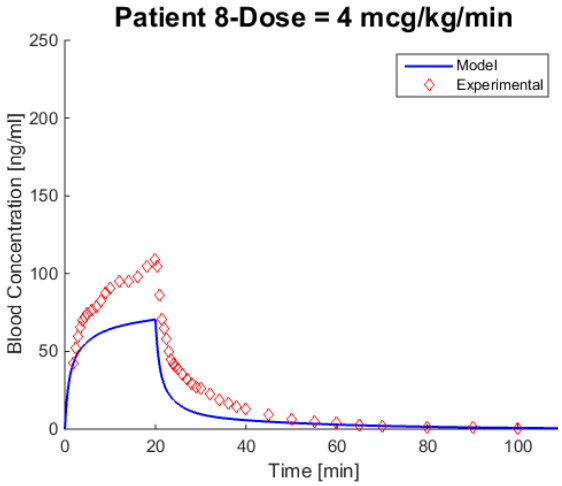
Patient 8-Dose = 4 mcg/kg/min
Model
Experimental
Blood Concentration [ng/ml]
Time [min]
0
50
100
150
200
250
0
20
40
60
80
100

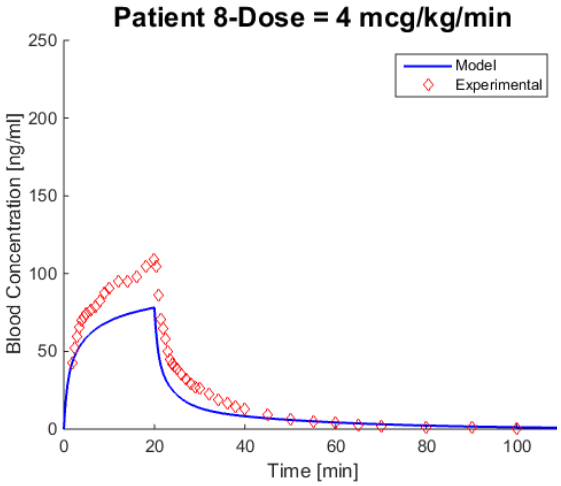
Patient 8-Dose = 4 mcg/kg/min
Model
Experimental
Blood Concentration [ng/ml]
Time [min]
0
50
100
150
200
250
0
20
40
60
80
100

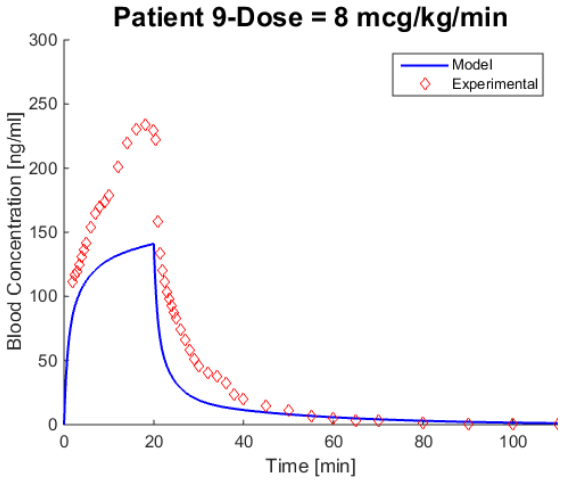
Patient 9-Dose = 8 mcg/kg/min
Model
Experimental
Blood Concentration [ng/ml]
Time [min]
0
50
100
150
200
250
300
0
20
40
60
80
100

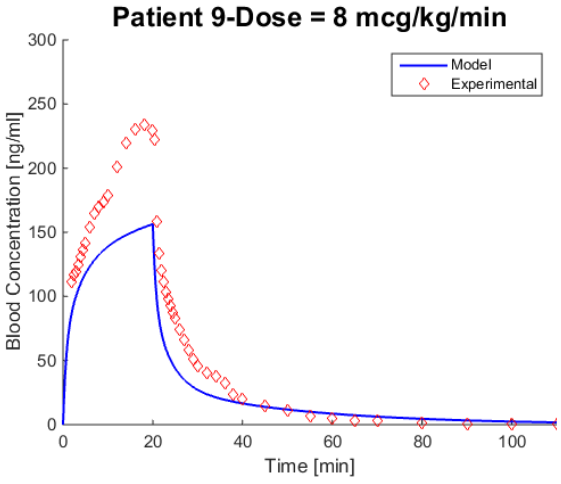
Patient 9-Dose = 8 mcg/kg/min
Model
Experimental
Blood Concentration [ng/ml]
Time [min]
0
50
100
150
200
250
300
0
20
40
60
80
100

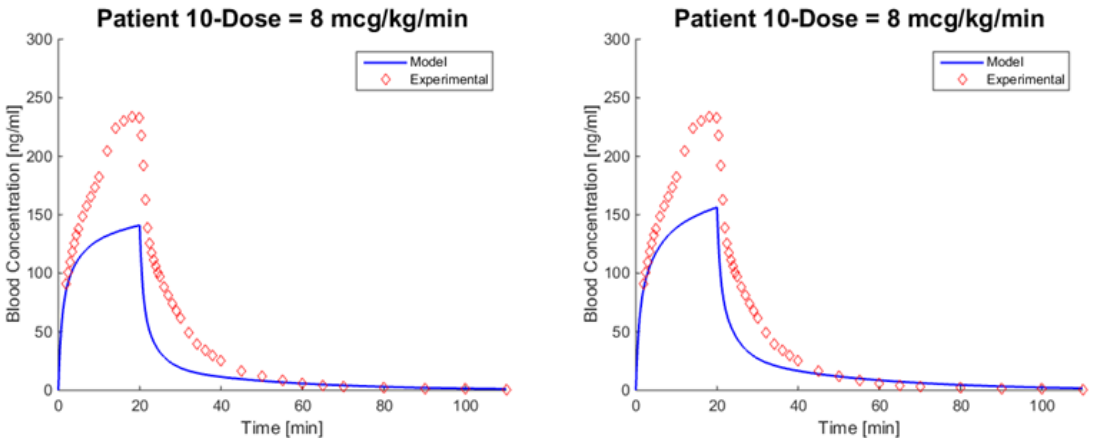

Figure 17 - Experimental data (red) from Egan et al. (1996). Ten volunteers were administered increasing doses of remifentanil with a 20 min infusion. The left portion shows the results of the 8P model (blue) from Abbiati et al. (2016), whilst the right portion the results of the 6P model (blue). It is possible to see that moderately better results are obtained with the 6P model.

It is worth observing that the performance of both models is satisfactory for small doses, but it degrades as the dose increases. Paragraph 2.7 will discuss in more details this critical point.

The rate of absorption determines the level of the maximum peak in the plasma and the required time to reach it. When any drug is administered to a patient, the plasma concentration is determined by the equilibrium between absorption and elimination, in fact the variation of the plasma concentration at any time results from the difference of the rates of the two processes. This means that the maximum peak is obtained when the two fluxes are equal. Moreover, the importance of the peak concentration is related to the therapeutic window, which defines the range of doses that produce therapeutic response without causing any significant undesired effect in the patients, as the therapeutic window can be defined between the maximum safe concentration and the minimum effective concentration. For this reason, the peak concentration, C_{Max}, is a very important pharmacokinetic parameter.

It is useful to define some parameters that allow comparing the two models quantitatively.

First, because of the importance of C_{Max}, it is interesting to evaluate the percentage relative error between the peak concentration of the experimental data and the peak concentration of the model:

$$\Delta C_{max}\,\% = \frac{C_{max,mod} - C_{max,exp}}{C_{max,exp}} \cdot 100 \tag{24}$$

Table 6A reports the values of $\Delta C_{max}\%$ for the two models.

Table 6A - Comparison of $\Delta C_{max}\%$ values for the patients of Egan et al. (1996). Left column, $\Delta C_{max}\%$ values for the 8P model of Abbiati et al. (2016). Right column, $\Delta C_{max}\%$ values for the 6P model.

Patient	*Infusion dose [µg/kg/min]*	*8P model*	*6P model*
1	1	9.45	0.35
2	1	11.70	2.06
3	1.5	2.10	8.60
4	1.5	4.40	11.37
5	2	20.30	14.60
6	2	6.74	18.40
7	4	36.10	29.40
8	4	37.70	30.90
9	8	39.90	33.30
10	8	39.90	33.30

It is worth observing that both models exhibit a satisfactory precision in the C_{Max} prediction for doses lower than 4 µg/kg/min, but it is possible to appreciate that the 6P model is moderately better in predicting the peak concentration, except for patients 3,4, and 6.

Indeed, the measured blood concentrations of these three patients are characterized by an abnormal and peculiar trend (Fig. 17) that can be attributed to inter-individual variability or possible errors in the measurement procedure, and this might be the reason why the 6P model fails to predict the peak concentration with better results for these three patients.

Another important pharmacokinetic parameter is the area under the curve (AUC), which measures the drug amount that reaches the systemic circulation after drug administration, and is directly proportional to the amount of drug that was absorbed. The validity of the model can be assessed by evaluating the relative error between the AUC of the experimental data and the AUC of the model:

$$\Delta AUC = \frac{AUC_{mod} - AUC_{exp}}{AUC_{exp}} \cdot 100 \qquad (25)$$

Table 6B lists the results.

Table 6B - Comparison of ΔAUC values for the patients of Egan et al. (1996). Left column, ΔAUC values for the 8P model of Abbiati et al. (2016). Right column, ΔAUC values for the 6P model.

Patient	Infusion dose [µg/kg/min]	8P model	6P model
1	1	9.85	4.33
2	1	2.18	12.54
3	1.5	5.02	9.75
4	1.5	16.79	3.56
5	2	20.80	8.02
6	2	1.06	17.01
7	4	25.39	13.64
8	4	34.26	23.65
9	8	34.90	24.40
10	8	38.15	28.15

In practice, AUC is calculated by means of the trapezoidal rule and therefore it is strongly affected by the peculiarity of the trend due to the inter-individual variability. Since our goal was to compare the performance of the two models, the conclusion is that AUC is probably not the most appropriate and reliable parameter for our goals.

Consequently, it is possible to evaluate other parameters.

The sum of the absolute errors (SAE) between the predicted concentrations and the measured concentrations was calculated as follows:

$$SAE = \sum_{i=1}^{N_p} \sum_{j=1}^{N_m} \frac{|C_{i,j}^{mod} - C_{i,j}^{exp}|}{N_m} \tag{26}$$

Where N_m is the number of measured values of the study, N_p is the number of patients of the *k-th* case-study.

The integral of the absolute error (IAE) was evaluated as follows:

$$IAE = \int_{t0}^{tf} \left| C_{mod} - C_{exp} \right| dt \tag{27}$$

As for the AUC (Equation 25), the integral was evaluated by means of the trapezoidal rule, but differently from the AUC, the integral allows to quantify the deviation of the model from the measured blood concentrations for the whole duration of the infusion. The IAE is usually applied in Process control of chemical plants (Stephanopoulos, 1984) as a performance index.

These parameters are more reliable respect to the sum of the squared error (SSE) and the integral of the squared error (ISE), as SSE and ISE are less recommended in case of small/large errors. Moreover, SAE and IAE are suggested in case of errors of the same order of magnitude.

Tables 6C and 6D list the values of these parameters for the two considered models.

Table 6C - Comparison of SAE values for the patients of Egan et al. (1996). Left column, SAE values for the 8P model of Abbiati et al. (2016). Right column, SAE values for the 6P model.

Patient	Infusion dose [µg/kg/min]	8P model	6P model
1	1	0.83	0.56
2	1	0.92	0.87
3	1.5	2.00	2.00
4	1.5	1.58	1.53
5	2	2.16	1.54
6	2	2.34	2.39
7	4	7.62	6.30
8	4	8.05	6.38
9	8	16.27	13.60
10	8	13.66	11.46

Table 6D - Comparison of IAE values for the patients of Egan et al. (1996). Left column, IAE values for the 8P model of Abbiati et al. (2016). Right column, IAE values for the 6P model.

Patient	Infusion dose [µg/kg/min]	8P model	6P model
1	1	42.11	27.90
2	1	45.09	42.16
3	1.5	77.59	77.59
4	1.5	86.34	83.80
5	2	140.32	99.53
6	2	133.41	135.93
7	4	400.67	330.54
8	4	522.81	414.43
9	8	1005.52	839.37
10	8	525.8	432.94

SAE and IAE confirm the results obtained by the evaluation of $\Delta C_{max}\%$. In fact, the 6P model appears to provide a moderate improvement in the prediction of the measured concentrations.

However, it is important to compare the performance of the two models for different dose regimens and different patient conditions.

2.4.2 Case-study 2: Westmoreland et al. (1993)

Westmoreland *et al.* (1993) performed an open-label, escalating dose pharmacokinetic study on 24 patients undergoing impatient (meaning that the patient is staying overnight or longer after the surgery is completed, for care or observation) surgery, who were divided into four groups. They were administered single boluses of 2, 5, 15, and 30 µg/kg over 1 min. Each patient included in the study had normal clinical laboratory test results.

Figure 18 shows the performance of the two models.

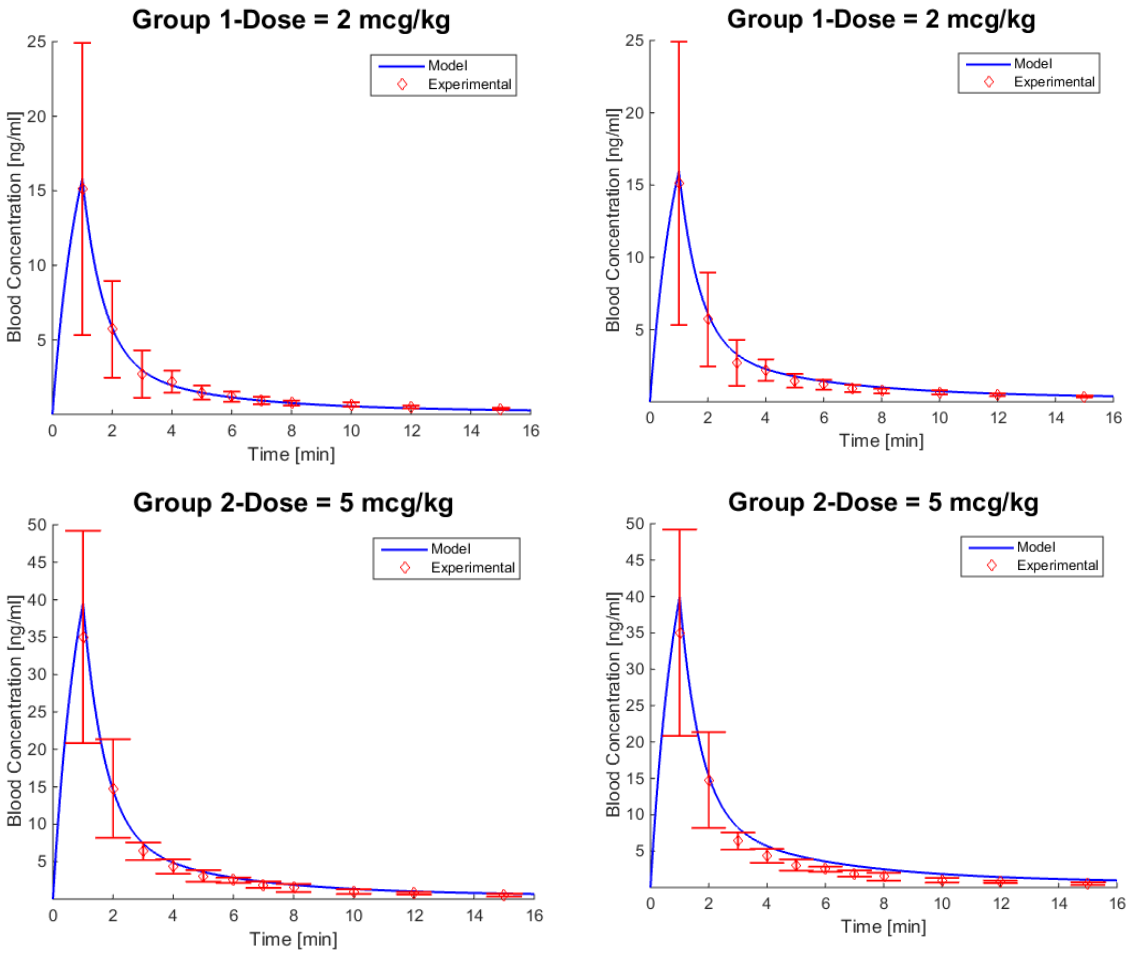

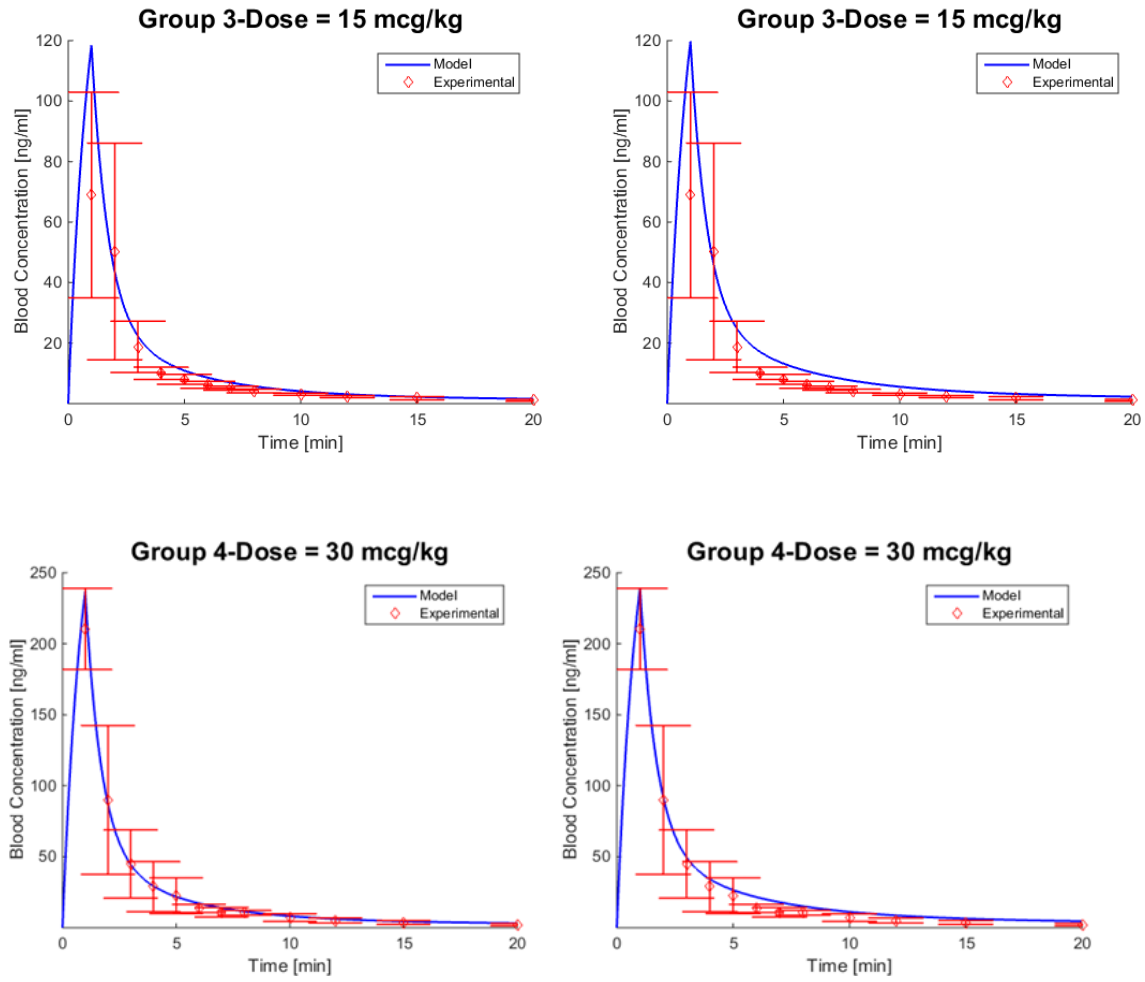

Figure 18 - Experimental data (red) from Westmoreland et al. (1993). Four groups of patients were administered with four boluses over 60 s. On the left the results of the 8P model (blue) from Abbiati et al. (2016), on the right the results of the 6P model (blue).

As in the previous case, it is possible to analyze the values of $\Delta C_{max}\%$, SAE, and IAE for this case-study, in order to compare the predictive ability of the two models. Tables 7A, 7B, and 7C list the values of such parameters.

Table 7A - Comparison of $\Delta C_{Max}\%$ values for the patients of study of Westmoreland et al. (1993). Left column, $\Delta C_{Max}\%$ values for the 8P model of Abbiati et al. (2016). Right column, $\Delta C_{Max}\%$ values for the 6P model.

Group	*Bolus dose [µg/kg]*	*8P model*	*6P model*
1	2	4.51	5.66
2	5	12.81	14.05
3	15	71.84	73.74
4	30	12.55	13.79

Table 7B - Comparison of SAE values for the patients of study of Westmoreland et al. (1993). Left column, SAE values for the 8P model of Abbiati et al. (2016). Right column, SAE values for the 6P model.

Group	Bolus dose [μg/kg]	8P model	6P model
1	2	0.13	0.24
2	5	0.59	1.03
3	15	4.29	5.31
4	30	2.49	4.62

Table 7C - Comparison of IAE values for the patients of study of Westmoreland et al. (1993). Left column, IAE values for the 8P model of Abbiati et al. (2016). Right column, IAE values for the 6P model.

Group	Bolus dose [μg/kg]	8P model	6P model
1	2	1.42	2.90
2	5	7.13	14.09
3	15	52.40	70.12
4	30	31.60	68.66

It is possible to observe that Abbiati *et al.* (2016) model (*i.e.* 8P model) produced moderately better results, although both the simulated curves are close to the central values of the measured blood concentrations and belong to the standard deviation bands. Moreover, the difference in the values of the performance indexes is not relevant.

It is also important to underline that the 6P model has the advantage of a better representation of reality, therefore it is probable that it will provide better results if applied to other cases of study. It is interesting to notice that both models fail to describe the experimental data of Group 3. It is reasonable to assume a possible gross error in the experimental measurements or some missing details in the paper on the lumped patients of that group.

2.4.3 Case-study 3: Pitsiu et al. (2004)

Pitsiu *et al.* (2004) assessed the pharmacokinetics of remifentanil and RA on 40 Intensive Care Unit (ICU) adults, with increasing degrees of renal impairment, from normal/mildly to moderate/severe. They were divided into four groups depending on the degree of renal impairment. Remifentanil was infused for 72 h at a rate of 6-9 μg/kg/h. In the simulations, an averaged infusion dose of 7.5 μg/kg/h was employed. Figure 19 shows the results of simulations compared to experimental data of single patients belonging to the four groups. Unfortunately, only averaged demographic data were available, which did not allow personalizing the simulations at a higher extent.

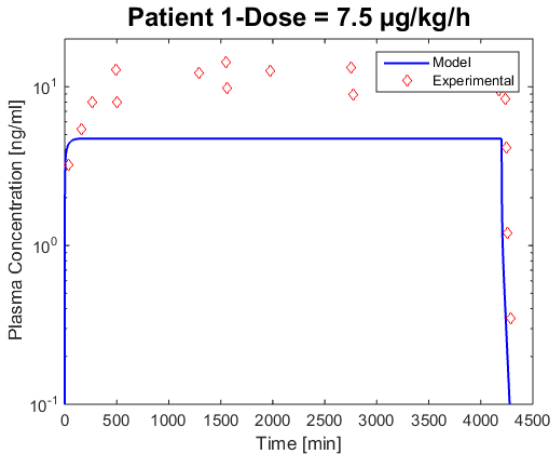
Patient 1-Dose = 7.5 µg/kg/h
Model
Experimental
Plasma Concentration [ng/ml]
Time [min]

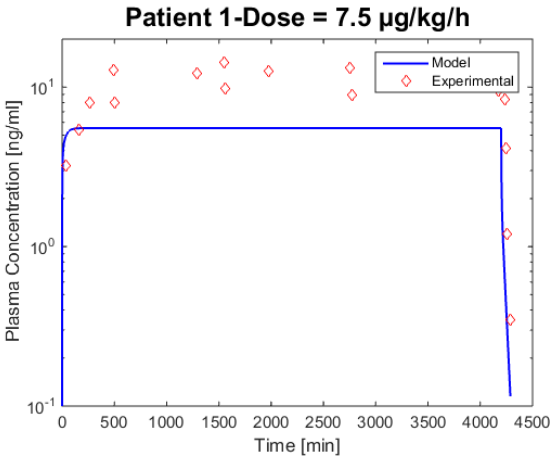
Patient 1-Dose = 7.5 µg/kg/h
Model
Experimental
Plasma Concentration [ng/ml]
Time [min]

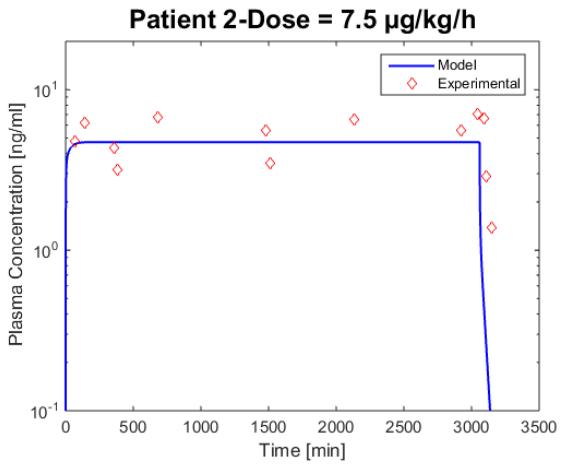
Patient 2-Dose = 7.5 µg/kg/h
Model
Experimental
Plasma Concentration [ng/ml]
Time [min]

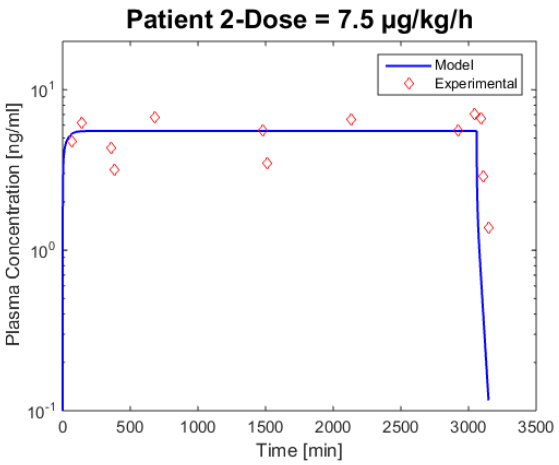
Patient 2-Dose = 7.5 µg/kg/h
Model
Experimental
Plasma Concentration [ng/ml]
Time [min]

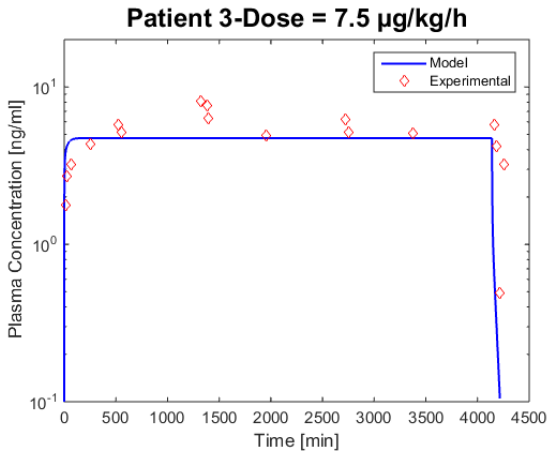
Patient 3-Dose = 7.5 µg/kg/h
Model
Experimental
Plasma Concentration [ng/ml]
Time [min]

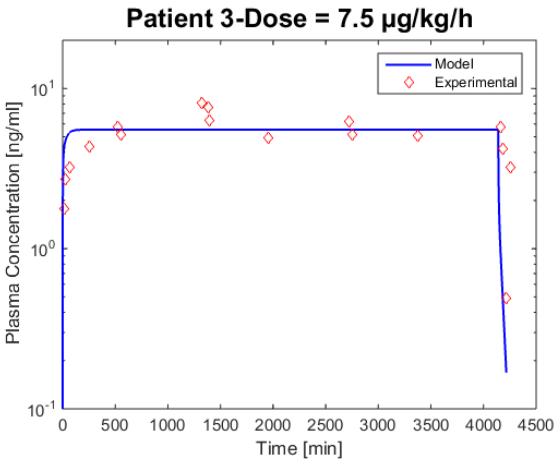
Patient 3-Dose = 7.5 µg/kg/h
Model
Experimental
Plasma Concentration [ng/ml]
Time [min]

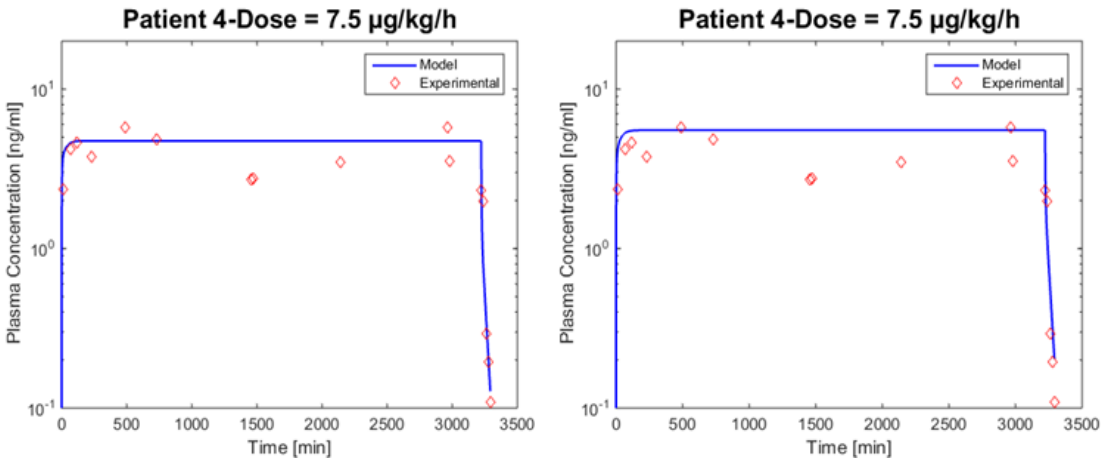

Figure 19 - Experimental data of four patients administered with a dose of 6-9 µg/kg/h for 72 h (Pitsiu et al., 2004). Left side, results of the 8P model (blue) of Abbiati et al. (2016). Right side, results of the 6P model (blue). It is possible to observe that the 6P model produces moderately better results.

Tables 8A and 8B report the results in terms of SAE and IAE, as the maximum concentration value is not interesting for this specific study because of the long duration of the infusion.

Table 8A - Comparison of SAE values for the patients of study of Pitsiu et al. (2004). Left column, SAE values for the 8P model of Abbiati et al. (2016). Right column, SAE values for the 6P model.

Patient	*Infusion dose [µg/ kg/ min]*	*8P model*	*6P model*
1	7.5	4.87	4.31
2	7.5	1.75	1.56
3	7.5	1.75	1.11
4	7.5	0.95	1.30

Table 8B - Comparison of IAE values for the patients of study of Pitsiu et al. (2004). Left column, IAE values for the 8P model of Abbiati et al. (2016). Right column, IAE values for the 6P model.

Patient	*Infusion dose [µg/ kg/ min]*	*8P model*	*6P model*
1	7.5	82.13	72.30
2	7.5	22.04	19.40
3	7.5	28.50	18.64
4	7.5	14.46	19.81

The high values of SAE and IAE for the first patient can be attributed to the fact that an averaged dose was employed for the simulation of the groups. Probably, this particular patient was subjected to a smaller infusion dose.

Again, the 6P model shows moderately better results, except for Patient 4. However, the values of SAE and IAE are not significantly different, and it is fair to observe that the measured concentrations data for Patient 4 are rather scattered and this may affect the evaluation of the performance indexes.

2.4.4 Case-study 4: Glass et al. (1993)

Glass *et al.* (1993) investigated the pharmacokinetics of remifentanil in 30 volunteers, aged 18 to 40, all of them within 15% their ideal body weight. They received a single bolus of 2 µg/kg for 1 min.

The experimental data shown in Figure 20 are averaged over those 30 patients and the large standard deviation band of the first experimental measure demonstrates a strong inter-individual variability.

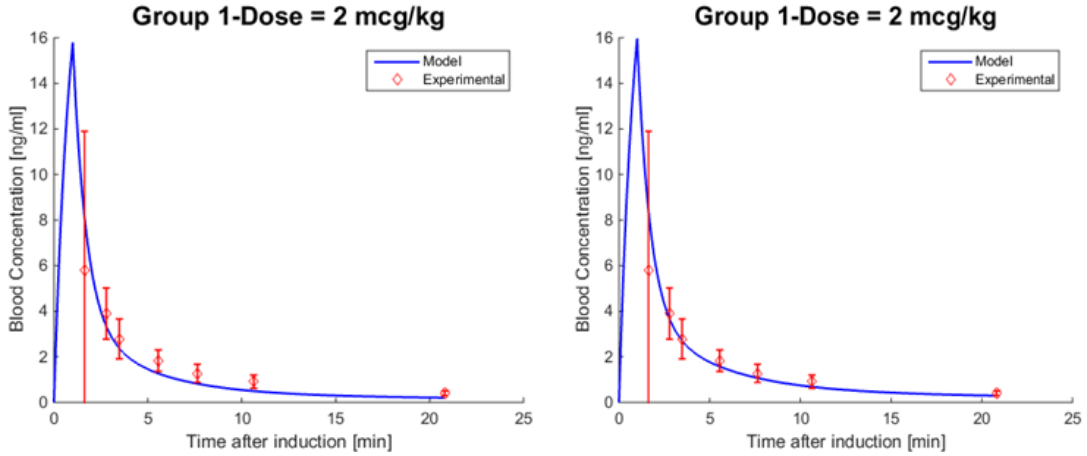

Figure 20 - Experimental data (red) of 30 volunteers administered with a single bolus for 60 s (Glass et al., 1993). Left side, the results of the 8P model (blue) of Abbiati et al. (2016). Right side, results from the 6P model (blue). It is possible to see that the 6P model produces moderately better results.

Again, it is possible to evaluate the values of SAE and IAE in order to compare the two models (Tables 9A and 9B).

Table 9A - Comparison of SAE values for the patients of study of Glass et al. (1993). Left column, SAE values for the 8P model of Abbiati et al. (2016). Right column, SAE values for the 6P model.

Group	*Bolus dose [µg/kg/min]*	*8P model*	*6P model*
1	2	0.701	0.201

Table 9B - Comparison of IAE values for the patients of study of Glass et al. (1993). Left column, values for the Abbiati et al. (2016) model. Right column, values for the 6P model.

Group	*Bolus dose [µg/kg/min]*	*8P model*	*6P model*
1	2	3.646	2.338

Glass *et al.* (1993) started the blood sampling after 2 min since the start of the infusion, therefore no information about the maximum experimental concentration is available in the paper. For this reason, it is not possible to calculate the values of $\Delta C_{Max}\%$.

Consistently with the results obtained in the previous studies (except for Westmoreland *et al.*, 1993), both SAE and IAE show a moderate improvement in the prediction of the 6P model. In addition, Fig. 20 shows that the 6P model curve falls within the standard deviation bands in a better way than the 8P model of Abbiati *et al*. (2016).

2.4.5 Conclusions

In general, both 8P and 6P models show a reliable precision in the prediction of the experimental data, within the clinical dosage range. The clear deviation of the model from the experimental values of the blood/plasma concentrations in case of high doses (Case-study 1) will be further discussed in Paragraph 2.6, in which a possible solution is suggested. Finally, it is possible to conclude that the 6P model does not produce a dramatic improvement but yet a recognizable one, in the prediction of the experimental blood/plasma concentrations of remifentanil, with the additional advantage of being more consistent with the real physiology of the pharmacokinetics of the drug inside the human body.

2.5 Akaike Information Criterion

The Akaike Information Criterion (AIC) is a method that allows comparing the capability of prediction of different models. This criterion was developed in 1971 by the Japanese mathematician Hirotsugu Akaike (Chen *et al.*, 1991).

AIC takes into account both the ability of fitting the experimental data and the complexity of the model:

$$AIC = \sum_{i}^{Np} \frac{N_m \cdot \ln(\frac{SSEt}{N_m})}{N_p} + 2p \tag{28}$$

Where:

$$SSEt = \sum_{i=1}^{Nm} \left(C_{i,exp} - C_{i,mod} \right)^2 \tag{29}$$

Where N_m is the number of measured values, N_p is the number of patients of the *k-th* case-study, and p is the number of parameters of the model. We chose Case-study 1 (Egan *et al.*, 1993) for the evaluation of the AIC since it is the one with the highest number of patients and the largest variation of dose. The number of patients is therefore ten.

According to the general rule of selection of the best candidate model, the one with the lowest AIC value is to be preferred. As shown in Table 10, the 6P model is the best candidate model, even if the difference between the values is not dramatic, consistently with the results obtained (Paragraph 2.4).

Table 10 - AIC values for the two models. It is possible to notice that the value is lower for the 6P model.

AIC – *8P model*	AIC – *6P model*
257.115	242.935

2.6 Limitations of the model

Navapurkar *et al.* (1998) investigated the remifentanil pharmacokinetics in six adult patients undergoing Orthopic Liver Transplantation (OLT, meaning that the liver is transplanted from a donor into its normal position in the body of the recipient). The patients that took part to the study were aged 18 to 60 and were within 25% of their ideal body weight. They did not have any cardiac, pulmonary, or renal disease.

OLT involves three main phases: (i) the dissection or hepatic phase (from the beginning of surgery to the clamping of the hepatic blood supply and venous drainage), (ii) the anhepatic phase (from clamping of the vascular supply to release of the portal vein clamp), (iii) the reperfusion phase, which starts when the portal vein is unclamped. Remifentanil was administered as single bolus of 10 µg/kg for 1 min before the dissection phase and before the anhepatic phase.

The advantage of studying the pharmacokinetics during the OLT is that it provides a good chance to study extra-hepatic metabolism, *i.e.* the metabolic activity carried out by tissues and organs other than the liver.

Fig. 21 shows that the 6P model over-estimates ($\Delta C_{Max}\% = 142$) the experimental data of Patient 1 during the dissection (hepatic) phase. This may lead to think that the model does not correctly describe remifentanil pharmacokinetics, or that it is somehow either case-study- or dose-dependent, although it was validated with data coming from reasonably different clinical studies that imply various conditions.

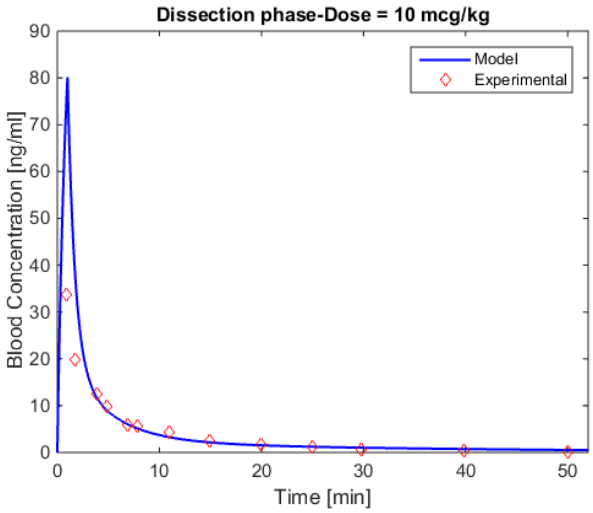

Figure 21 - Comparison between the 6P model (blue) and the experimental data (red) of Patient 1 from Navapurkar et al. (1998). It is evident that the model overestimates the peak of the blood concentration of remifentanil.

Actually, Navapurkar *et al.* (1998) explain that there is a difference between the pharmacokinetics during the dissection (hepatic) and the anhepatic phases, and that this difference can be attributed to a great blood loss and as a consequence fluid replacement in the dissection (hepatic) phase. The result is an effect of hemodilution. In fact, they detected lower blood concentration and an apparent increased clearance in the dissection (hepatic) phase, as shown in Fig. 22, again referred to the same patient.

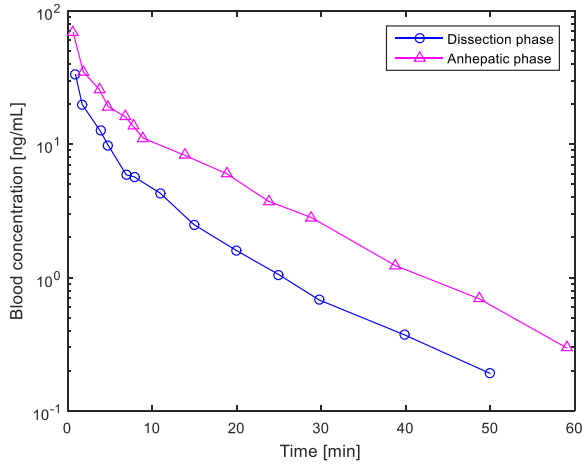

Figure 22 - Measured blood concentrations of Patient 1 during the dissection (hepatic) and anhepatic phases.

This probably means that the model is not able to predict the pharmacokinetics of remifentanil because it cannot predict the hemodilution effect that affects both the remifentanil and its metabolite pharmacokinetics during the dissection phase.

A complementary situation was found by Dahaba *et al.* (1998). They compared the pharmacokinetics and recovery parameters of TIVA (Total Intravenous Anesthesia) in 22 end-stage renal-failure and 22 normal-function patients. The patients were aged 20 to 59 and were within 20% of their ideal body weight. They found that the pharmacokinetics was significantly altered in case of patients with severe renal impairment, as it is possible to observe in Fig. 23 that shows the measured blood concentrations of the two groups averaged over the 22 patients.

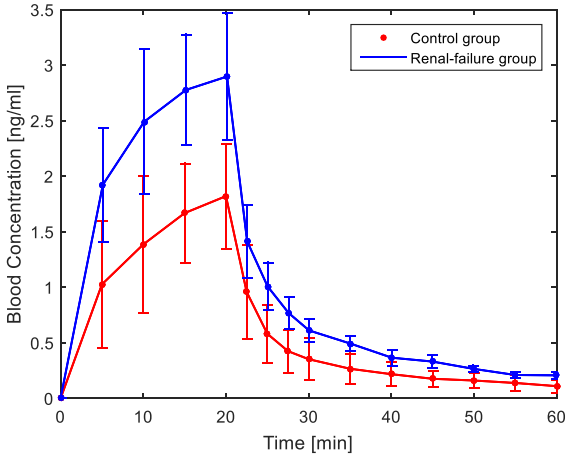

Figure 23 - Measured blood concentrations of healthy (red) and renal-failure (blue) patients from Dahaba et al. (1998). It is possible to detect a difference in the pharmacokinetics between healthy and sick patients.

They attributed this difference to the fact that these patients exhibit fluids depletion and therefore a reduced volume of distribution, because they were recently subject to hemodialysis. Although this pharmacokinetic alteration does not necessarily reflect into a difference in the pharmacological effect of the drug, it cannot be neglected as for the difference in the pharmacokinetics due to the fluid replacement. This is the reason why the model is not able to correctly predict the experimental data in these two cases.

In fact, in this case the model underestimates the experimental data ($\Delta C_{Max}\% = 50$), as it is possible to observe in Fig. 24, contrarily to the previous case, and this is consistent and reasonable as the situation is opposite. Actually, while in the previous case the pharmacokinetics alteration was due to hemodilution, in this case it is due to an effect of fluids volume reduction.

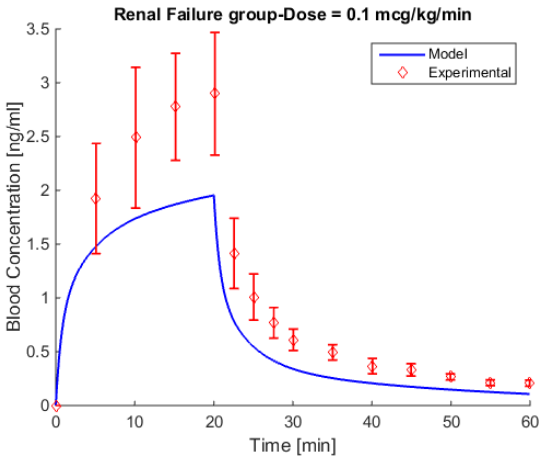

Figure 24 - Comparison between the 6P model and the experimental data of Dahaba et al. (1998). It is evident that the model underestimates the experimental data.

It is possible to conclude that in these special situations/conditions, it would be appropriate to add a correction factor to the plasma volume V_p and to the flow rates of the main veins and arteries to take into account the effects of either fluid dilution or fluid depletion.

2.7 Dose dependence

As mentioned above, the model exhibits a higher deviation from experimental data with the increase of the dose (Fig. 17). This was particularly evident in case study 1 (Egan *et al.,* 1993) since it implies high doses that are actually out of the clinical range, reported in Chapter 1. Fig. 25 shows both the experimental and model trend of the concentration peak respect to the dose. The red diamonds are the experimental concentration peaks reported by Egan *et al.* (1993), while the blue dashed line represents the trend of the 6P model concentration peak *versus* dose.

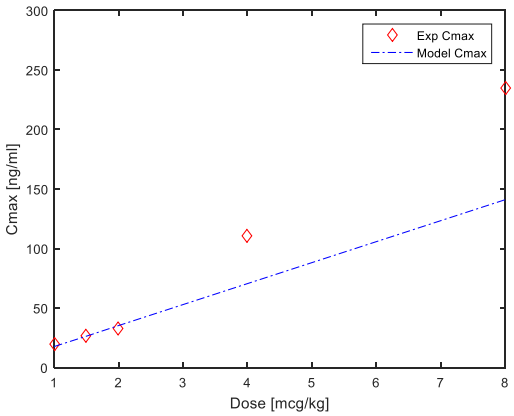

Figure 25 - Trend of the experimental and model maximum concentration of remifentanil for increasing dose (experimental C_{max} (red) from Egan et al., 1993). It is possible to observe a linear trend for doses up to 2 µg/kg. For higher doses the model C_{max} (blue) deviates from the experimental data.

It may seem unusual that the concentration has a linear dependence on the dose, since the 6P model is not linear, but we remark that we are considering only the peak concentration value.

The reason why the model is not able to predict the blood concentration of remifentanil at high doses may be related to a variation of the protein binding phenomenon, which in our model is instead a fixed parameter ($R = 70\%$), or to an effect of saturation of the hydrolysis enzymes, which implies that the elimination rate reaches a *plateau*. In the following, we try to illustrate how these two possible mechanisms can be incorporated in the model, by including in the first case a functional dependence of the parameter R (*i.e.* index of the protein binding) on the administered dose and in the second case a dependence of the elimination rate constants on the dose.

2.7.1 Variation of the protein binding

Remifentanil has a protein binding that is equal to 70% (Egan *et al.*, 1998). The two-third of this drug is bound to alpha-1-acid glycoprotein (AGP). This protein is one the most important plasma proteins in the human body, together with albumin and lipoproteins. These proteins have a number of different functions, whose most important for our modeling purposes is the drug binding.

Initially, albumin was considered the main binding protein, but AGP has become more important even if its plasma concentration is much lower than the albumin one (Tesseromatis *et al.*, 2011).

Alpha-1-acid glycoprotein belongs to the family of glycoproteins. They feature one or more oligosaccharides of different complexity, linked by covalent bonds. It is possible to find these proteins on the external surface of the plasmatic membrane, in the extracellular matrix, and in the blood.

AGP, also known as oromuscoid (ORM), is a single chain composed by 183 amino acids, with two disulfide bridges (Fournier *et al.*, 1999). Its normal plasma concentration is 0.6-1.2 mg/mL, which corresponds to 1-3% of plasma proteins (Tesseromatis *et al.*, 2011). This protein has an unusual high solubility in water and in many other organic solvents. Fig. 26 shows the complexity of the structure of this protein.

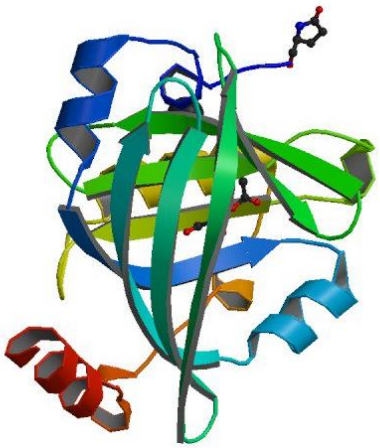

Figure 26 - Structure of alpha-1-acid glycoprotein, taken from Tesseromatis et al. (2011).

AGP is one of the most important acute-phase proteins in humans. Being an acute-phase protein, its serum concentration increases in response to infections, inflammations, and systemic tissue injuries.
Alpha-1-acid glycoprotein is synthesized by the liver, in particular by hepatocytes, but it can also be produced by extra-hepatic cells. The regulation of extra-hepatic AGP gene expression was examined at the end of the last century (Tesseromatis *et al.* (2011)). The hypothesis that an acute phase response could take place in extra-hepatic cells and could be regulated by inflammatory mediators as in hepatocytes is now well admitted. The first evidence of this fact was given by experiments on the active synthesis of AGP by human breast epithelial cells. Nowadays there are evidences of the expression of this protein in different extra-hepatic tissues and organs, as hearth, ileum, stomach, colon, and lung. Therefore, both the normal and the acute-phase production of AGP may take place in hepatic or extra-hepatic cells.

The biological function of AGP is not well known, but a number of physiological activities were discussed in the literature, such as immunomodulating effects (Fournier *et al.* (1999), Tesseromatis *et al.* (2011)). AGP is also able to bind and carry numerous basic

and neutral lipophilic drugs from endogenous and exogenous origin, as also acidic drugs. Both the immunomodulating and binding activities have been demonstrated to be function of the carbohydrate composition (Tesseromatis *et al.* (2011)).

The nature of the drug binding of AGP has been the subject of several studies (Wong et Hsia (1983); Ponganis and Stanski (1985); Gillis et al. (1995)). Its binding capacity mainly depends on the conformational change of the protein, on the polarity of the ligand (the higher the polarity of the molecule that has been binding AGP, the weaker the interaction), on the temperature, and on several other amino acid residues lying at the periphery of the hydrophobic domains of this protein.

The changes in protein plasma levels during acute-phase have a significant impact on the drug binding extent, which cause modifications of the drug action, distribution, disposition, and elimination. If the plasma concentration of this protein changes or increases rapidly, plasma drug concentration and drug effect can be unpredictable. Under these conditions, an estimate of the free drug fraction can be useful. Furthermore, the assessment of the correct AGP levels can influence the proper dosage adjustment, to obtain an optimal therapeutic target.

Therefore, the variation of plasma concentration of AGP, linked to the ability of the protein to bind drugs, may have a great influence on the pharmacokinetics of drugs.

The physical explanation can be related to the fact that in some situations, for instance during surgery, the production of alpha-1-acid glycoprotein increases and a higher drug concentration following a higher dose may lead to an increase of the remifentanil percentage bound to AGP.

If the protein binding increases, a lower drug amount will be available in the plasma. This means that the gradient between plasma and tissues/organs is lower and this will cause an accumulation of the drug in the plasma, due to the decrease of the drug amount that exits blood (which corresponds to the Plasma compartment of the model). This effect can be observed in Figure 25, and may be the reason that makes the experimental maximum concentration higher than the predicted maximum concentration.

According to these hypotheses, the fixed parameter R is substituted by a functional dependence on the administered dose (Equation 30), in analogy with the phenomenon of pore blocking in either catalysts of chemical processes or filter units of industrial processes. In fact, different models of filtration can be used to take into account the decrease of the availability of free pores after some time from the beginning of filtration. According to the theory of intermediate pore blocking, at the beginning each particle blocks a pore. Therefore, after some time, the majority of the pores will be occupied. An exponential function accounts for the depletion of available pores. The

concept that we want to apply is similar but the situation is opposite. In our case, during surgery, we hypothesize that the number of alpha-1-acid glycoproteins increases. When a high dose is administered to a patient, a higher drug amount is available and can bind to these proteins. Consequently, we adopt an exponential function to account for the increase of the percentage of the drug bound to the plasma proteins:

$$R = C \cdot e^{a \cdot dose \cdot infusion\_time} \tag{30}$$

where C and a are suitable constants. By means of a regression procedure, the parameters values are 0.7 for C, and 0.000997 for a. It is interesting to notice that C is equal to the literature value for remifentanil protein binding, so that the exponential function is only a correction factor that takes into account the dose dependence.

Therefore, the final model is:

$$R = 0.7 \cdot e^{0.000997 \cdot dose \cdot infusion\_time} \tag{31}$$

This expression substitutes the assigned parameter R in Equations (4-6), 8, 10.

2.7.2 Saturation of enzymes

The second hypothesized mechanism is an effect of saturation of hydrolysis enzymes. Remifentanil is mainly metabolized by *aspecific* esterases present in blood and tissues. Several enzymes belong to this family: pseudocholinesterase, cholinesterase, thioesterase, and phosphoric monoester/diester hydrolase (Nelson and Cox, 1970). In general, esterases are hydrolysis enzymes that split an ester into an acid and an alcohol in presence of water, as product.

Despite different research activities were designed to understand which are the specific enzymes able to metabolize remifentanil (Selinger *et al*. (1995); Davis *et al.* (1997); Manullang *et al.* (1999); Davis *et al.* (2002)) this piece of information is still unknown. It is possible to find studies that excluded some particular enzymes, such as pseudocholinesterase, also known as butyrylchoinesterase. Davis *et al.* (2002) made in vitro studies on the blood of five different patients with a known deficiency of pseudocholinesterase and demonstrated that the rate of metabolism was not different from the one of a control group. Selinger *et al*. (1995) made other *in vitro* experiments and assessed that the metabolism of remifentanil is not due to pseudocholinesterase, acetylcholinesterase or carbonic anhydrase. Also Davis *et al.* (1997) made in vitro studies that confirmed these results in a previous publication. Also, Manullang *et al.* (1999) presented a case-study that confirmed Davis *et al.* (1997) results.

As mentioned above, another possible explanation of the fact that the model deviates from the experimental data for high doses can be related to the metabolism of the drug. In fact, the model underestimates the experimental data. This could be related to an overestimation of the elimination capability by the enzymes. It is possible that the

enzymes reach a condition of saturation if the dose increases. This would mean that the concentration of the substrate is too high, and they would not able to eliminate it, due to their preservation of the same elimination rate.

The enzymes saturation can be described by the Michaelis-Menten' s theory. This theory explains and models the trend of the rate of a reaction catalyzed by enzymes, in response to the variation of the concentration of the substrate and of the enzymes (Fig. 27). By initially increasing the peak of concentration of the substrate, the rate of the reaction increases until it reaches a "plateau", defined as V_{Max}. This maximum condition is related to the enzymes saturation.

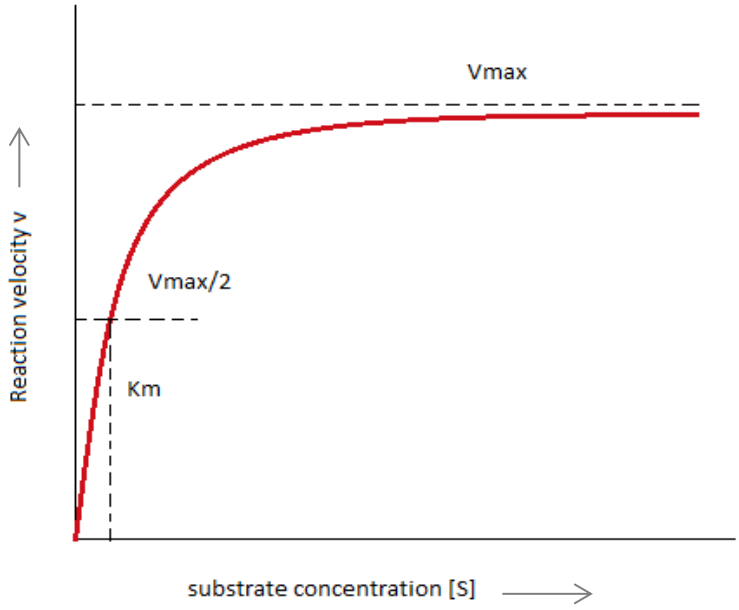

Figure 27 - Trend of the rate of a reaction catalyzed by enzymes, in response to the variation of the substrate and enzymes concentrations. (Source: UW (University of Washington) Departments web server).

Michaelis-Menten kinetics is formulated as follows:

$$E + S \underset{k_{-1}}{\overset{k_1}{\leftrightarrow}} ES \xrightarrow{k_2} E + P$$

$$V = \frac{k_2 \cdot [E]_0 \cdot [S]}{K_m + [S]} \tag{32}$$

Where V is the reaction velocity, $[E]_0$ is the concentration of the enzyme, $[S]$ is the concentration of the substrate and K_m is the so-called Michaelis-Menten constant that can be computed as follows:

$$K_m = \frac{k_{-1} + k_2}{k_1} \tag{33}$$

In order to apply this theory, it is necessary to know the formation and dissociation rate constants k_1, k_2, and k_{-1} of the enzyme-substrate complex. However, these values are related to the specific enzyme that metabolizes the drug. Since this piece of information is still not available in the literature for remifentanil, in our case it is not possible to know these parameters.

Since the saturation of enzymes is a possible explanation of the mismatch between the model and the experimental data for high doses, but it is not possible to use Michaelis-Menten's theory, the strategy adopted is similar to the one used for the implementation of the dependence of the protein binding on the dose. In fact, an exponential model was chosen, also according to graphical data analyses.

The rate constants of elimination in plasma and tissues have been modified, introducing the following equation:

$$k = C \cdot e^{-a \cdot dose \cdot infusion\_time} \tag{34}$$

where C and a are suitable constants.

C is different for either the plasma or the tissues. To compute these values, a nonlinear regression was performed, basing on the knowledge of the experimental values of the concentration peak and the corresponding dose. The value of C is 1.726 for plasma and 0.0546 for tissues. These values correspond to the elimination rate constants of the 6P model. Therefore, as in the previous case, the exponential function is used to correct the model as a function to the administered dose. The value of a is the same for both rate constants, which is consistent with the physics of the problem because the enzymes that metabolize the drug are indeed *aspecific*.

The applied relations are:

$$k_{el,P} = 1.726 \cdot e^{-0.00374 \cdot dose \cdot infusion\_time} \tag{35a}$$

$$k_{el,T} = 0.0546 \cdot e^{-0.00374 \cdot dose \cdot infusion\_time} \tag{35b}$$

Therefore $k_{el,P}$ and $k_{el,T}$substitute the two degrees of freedom $K_{E,P}$ and $K_{E,T}$ in Equations 4, 10 and 5, 11, respectively.

2.7.3 Results and discussion

It is now possible to analyze and compare the results of these two models. The study in which the deviation is more evident is the one of Egan *et al.* (1993) as it is the one that implies high doses, out of the clinical dosage range, as mentioned above.

Fig. 28 shows the results of the model that includes the functional dependency of protein binding on the dose, compared with the results of the 6P model.

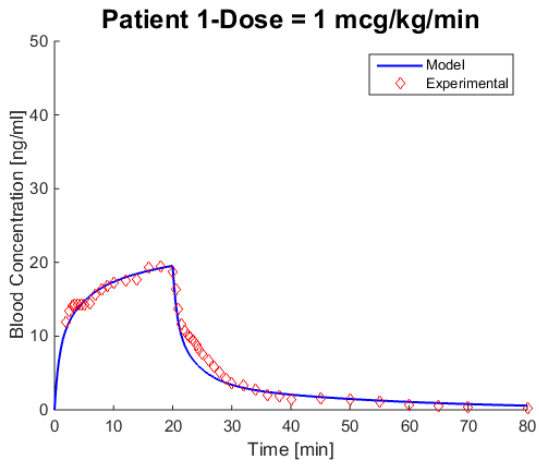
Patient 1-Dose = 1 mcg/kg/min
Model
Experimental
Blood Concentration [ng/ml]
Time [min]

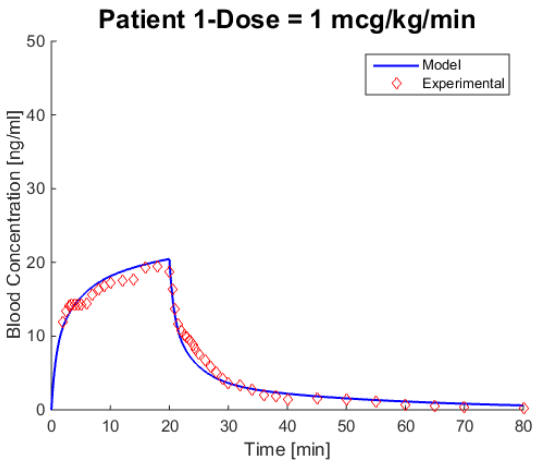
Patient 1-Dose = 1 mcg/kg/min
Model
Experimental
Blood Concentration [ng/ml]
Time [min]

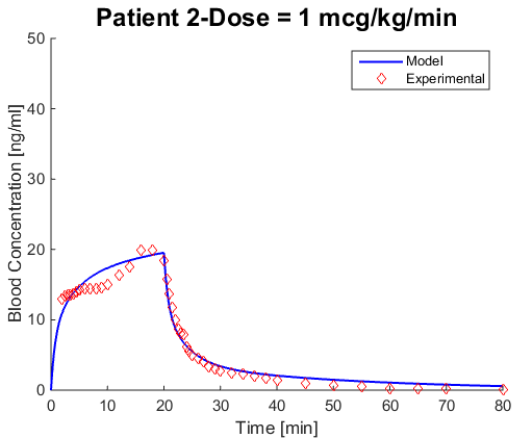
Patient 2-Dose = 1 mcg/kg/min
Model
Experimental
Blood Concentration [ng/ml]
Time [min]

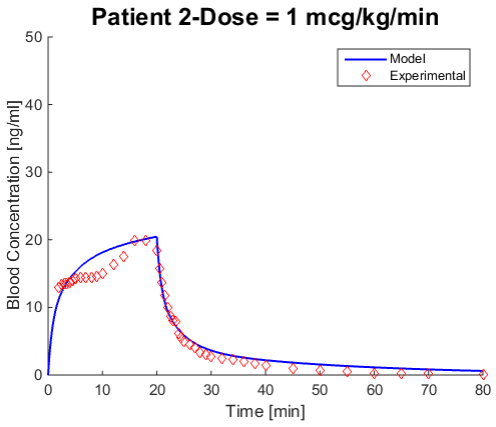
Patient 2-Dose = 1 mcg/kg/min
Model
Experimental
Blood Concentration [ng/ml]
Time [min]

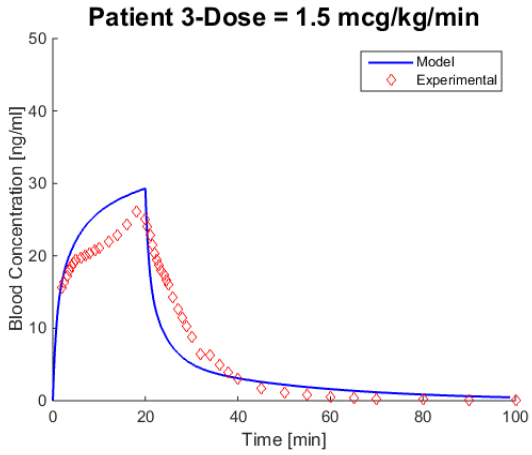
Patient 3-Dose = 1.5 mcg/kg/min
Model
Experimental
Blood Concentration [ng/ml]
Time [min]

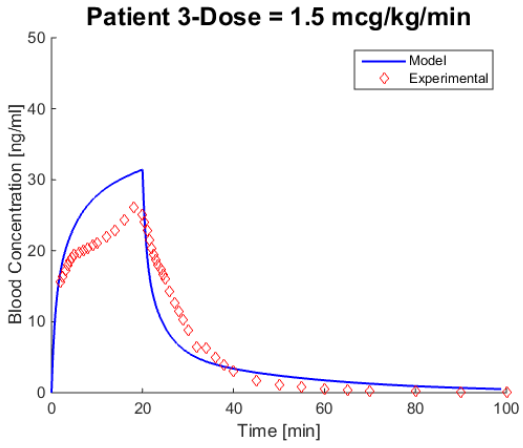
Patient 3-Dose = 1.5 mcg/kg/min
Model
Experimental
Blood Concentration [ng/ml]
Time [min]

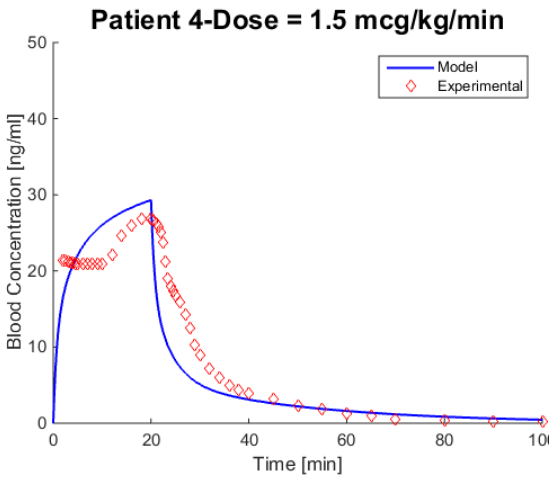
Patient 4-Dose = 1.5 mcg/kg/min
Model
Experimental
Blood Concentration [ng/ml]
Time [min]

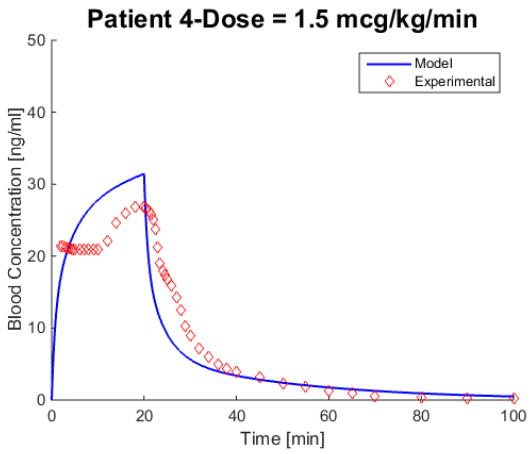
Patient 4-Dose = 1.5 mcg/kg/min
Model
Experimental
Blood Concentration [ng/ml]
Time [min]

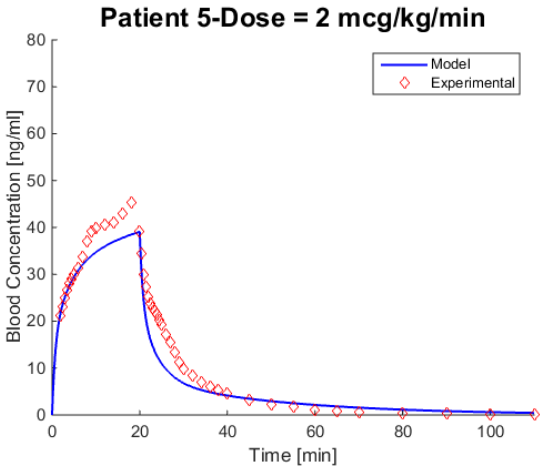
Patient 5-Dose = 2 mcg/kg/min
Model
Experimental
Blood Concentration [ng/ml]
Time [min]

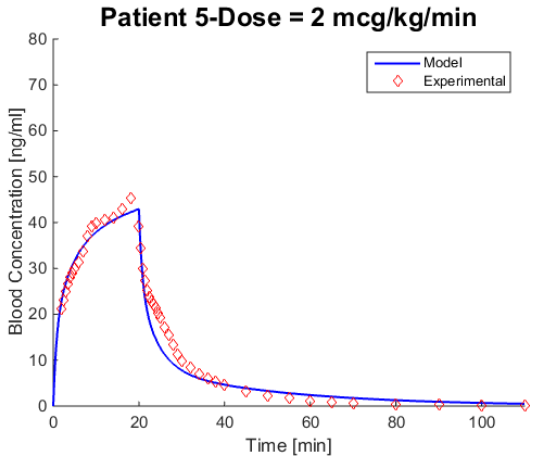
Patient 5-Dose = 2 mcg/kg/min
Model
Experimental
Blood Concentration [ng/ml]
Time [min]

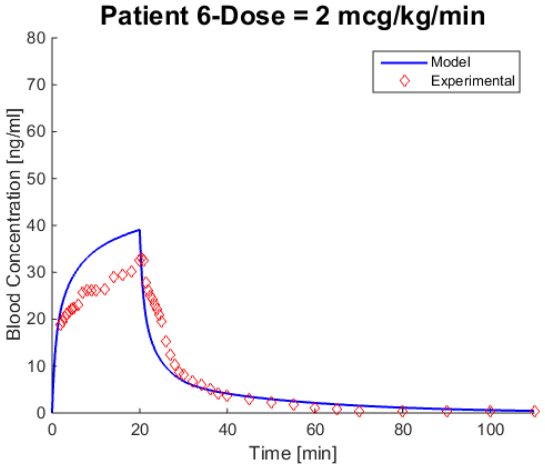
Patient 6-Dose = 2 mcg/kg/min
Model
Experimental
Blood Concentration [ng/ml]
Time [min]

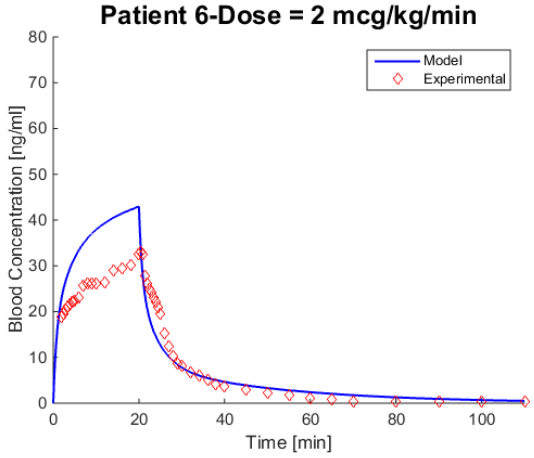
Patient 6-Dose = 2 mcg/kg/min
Model
Experimental
Blood Concentration [ng/ml]
Time [min]

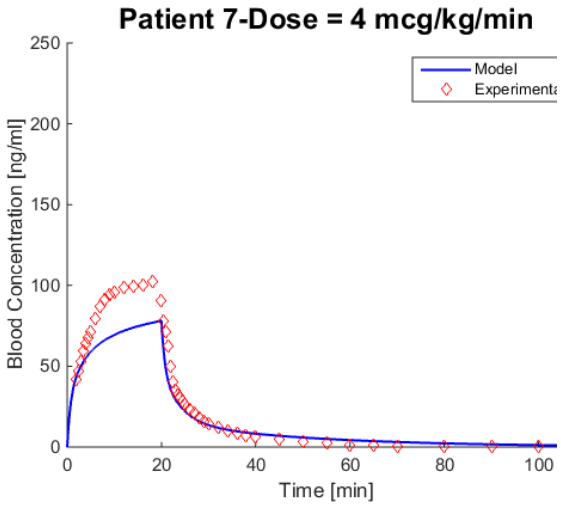
Patient 7-Dose = 4 mcg/kg/min
Model
Experimenta
Blood Concentration [ng/ml]
Time [min]

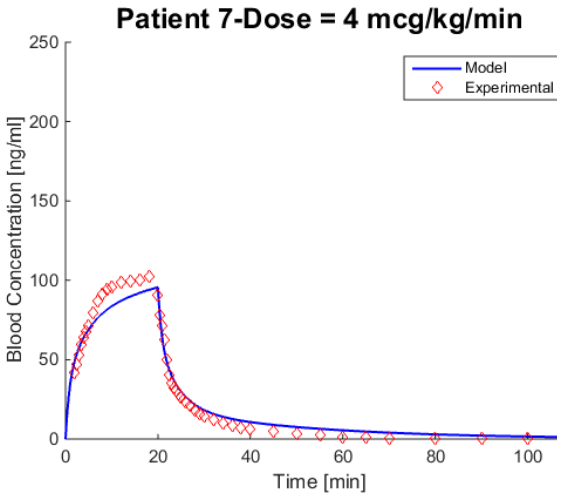
Patient 7-Dose = 4 mcg/kg/min
Model
Experimental
Blood Concentration [ng/ml]
Time [min]

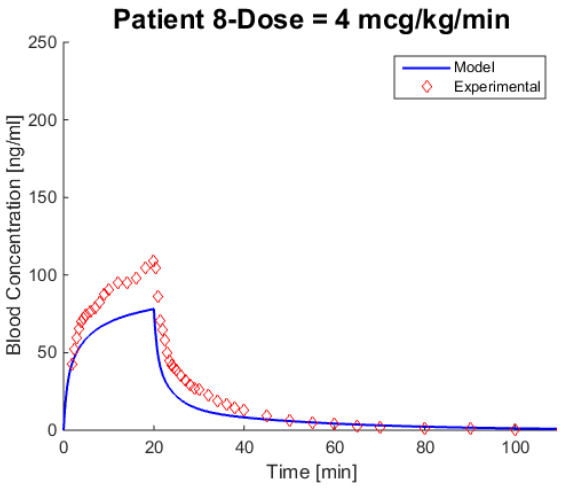
Patient 8-Dose = 4 mcg/kg/min
Model
Experimental
Blood Concentration [ng/ml]
Time [min]

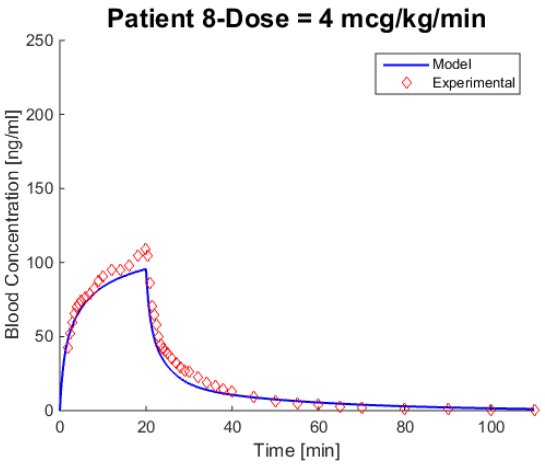
Patient 8-Dose = 4 mcg/kg/min
Model
Experimental
Blood Concentration [ng/ml]
Time [min]

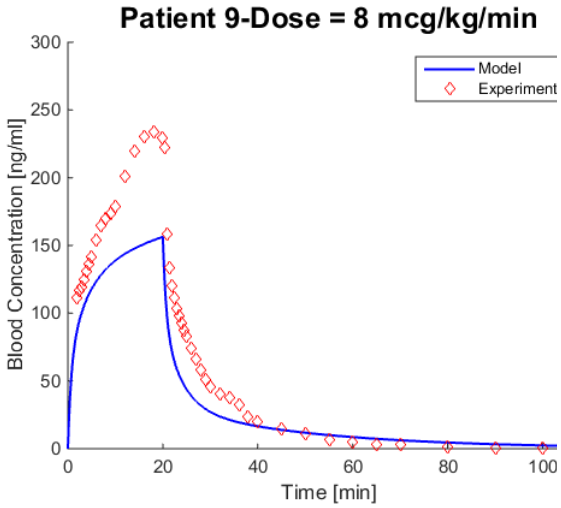
Patient 9-Dose = 8 mcg/kg/min
Model
Experiment
Blood Concentration [ng/ml]
Time [min]

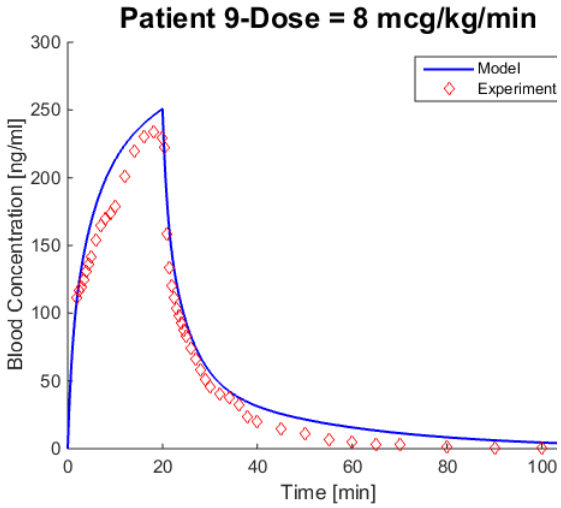
Patient 9-Dose = 8 mcg/kg/min
Model
Experiment
Blood Concentration [ng/ml]
Time [min]

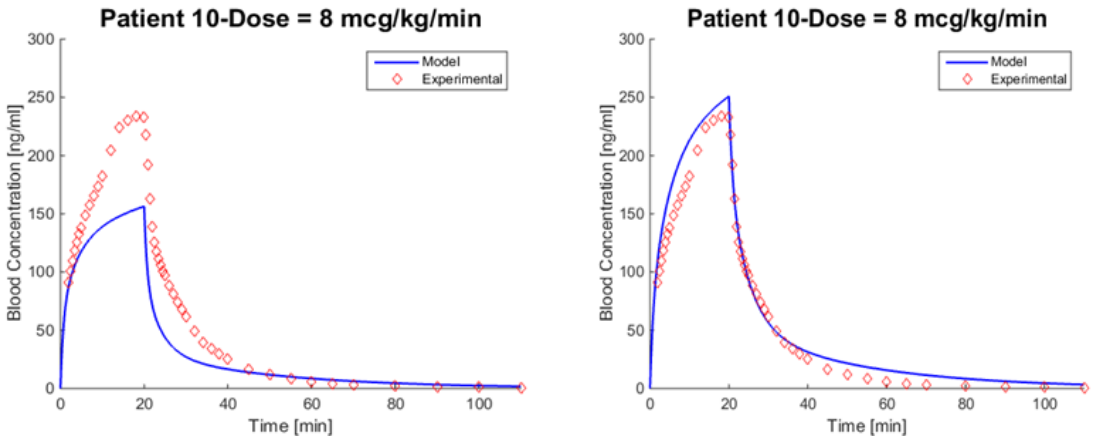

Figure 28 - Experimental data (red) from Egan et al. (1993). The left portion shows the results of the 6P model (blue). The right portion shows the results of the 6P Binding model (blue). It is possible to see that better results are obtained with the 6P Binding model.

It is evident that the introduction of the variation of the protein binding with the dose allows obtaining better results. The ability of prediction of the model is now satisfactory for both low and high doses. It is possible to analyze the performance indexes to demonstrate the improvement of the model.

Tables 11A, 11B, and 11C reports the values of $\Delta C_{Max\%}$, SAE, and IAE respectively.

Table 11A - Comparison of $\Delta C_{Max}\%$ values between the models. Left column, values of the 6P model. Right column, values of the 6P Binding model.

Patient	*Dose [µg/kg/min]*	*6P model*	*6P Binding Model*
1	1	3.60	5.10
2	1	2.06	2.50
3	1.5	11.37	19.00
4	1.5	8.59	16.00
5	2	14.59	6.20
6	2	18.36	30.00
7	4	30.91	15.50
8	4	29.41	13.40
9	8	33.32	7.00
10	8	33.34	6.97

Table 11B - Comparison of IAE values between the models. Left column, values for the 6P model. Right column, values for the 6P Binding model.

Patient	Dose [µg/kg/min]	6P model	6P Binding Model
1	1	27.90	28.65
2	1	42.16	46.62
3	1.5	77.59	81.22
4	1.5	83.80	89.41
5	2	99.53	78.73
6	2	135.93	153.63
7	4	330.54	231.41
8	4	414.43	220.86
9	8	839.37	513.76
10	8	432.94	221.30

Table 11C - Comparison of SAE values between the models. Left column, values for the 6P model. Right column, values for the 6P Binding model.

Patient	Dose [µg/kg/min]	6P model	6P Binding Model
1	1	0.56	0.57
2	1	0.87	0.96
3	1.5	2.00	2.11
4	1.5	1.53	1.63
5	2	1.54	1.21
6	2	2.39	2.71
7	4	6.30	4.46
8	4	6.38	3.42
9	8	13.60	8.50
10	8	11.46	5.91

From the values of these performance indexes, it may seem that the 6P model achieves better results for Patients 3, 4, and 6. However, it has already been discussed that the experimental data trend of these patients is unusual. This may indeed affect the results.

Better performance is obtained by simulating the patients with the 6P model for the lowest dose (1 µg/kg/min), but the values for the protein binding variation model are

still acceptable, considering that this model show a significant improvement for the higher doses (*i.e.* 2, 4, 8 µg/kg/min).

It is now possible to examine the results of the model that takes into account the effect of the enzymes saturation (Fig. 29).

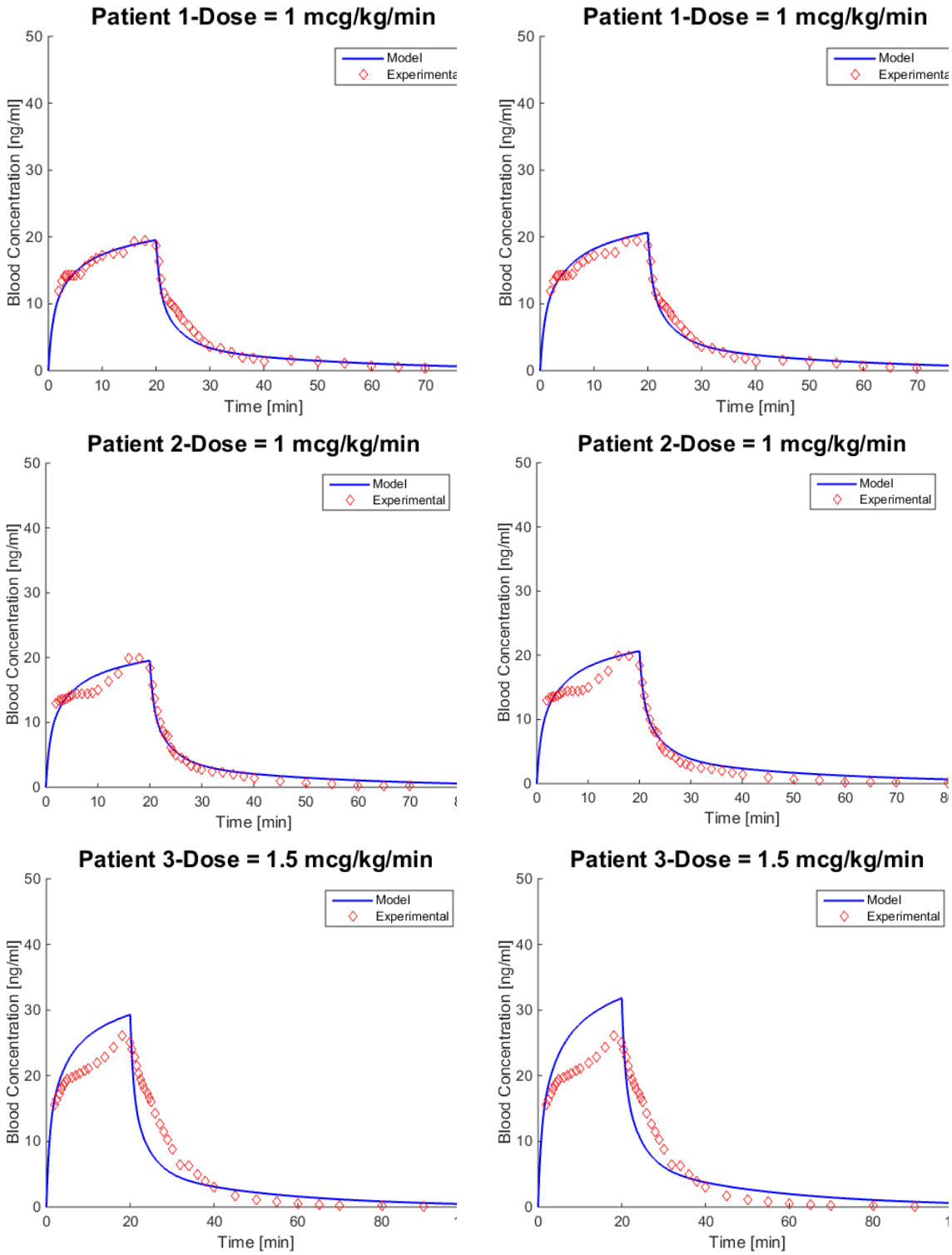

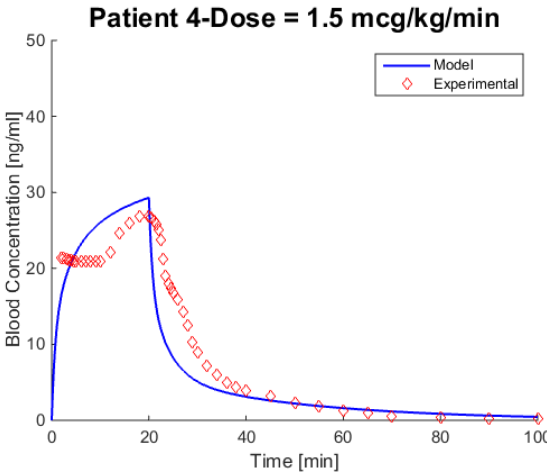
Patient 4-Dose = 1.5 mcg/kg/min
Model
Experimental
Blood Concentration [ng/ml]
Time [min]

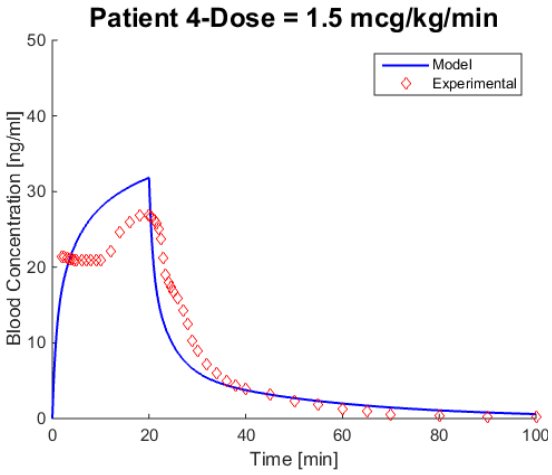
Patient 4-Dose = 1.5 mcg/kg/min
Model
Experimental
Blood Concentration [ng/ml]
Time [min]

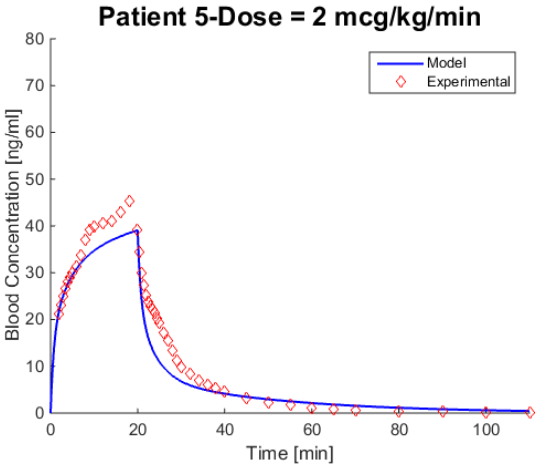
Patient 5-Dose = 2 mcg/kg/min
Model
Experimental
Blood Concentration [ng/ml]
Time [min]

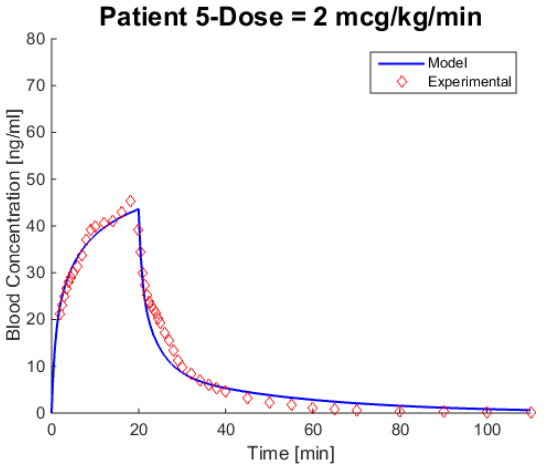
Patient 5-Dose = 2 mcg/kg/min
Model
Experimental
Blood Concentration [ng/ml]
Time [min]

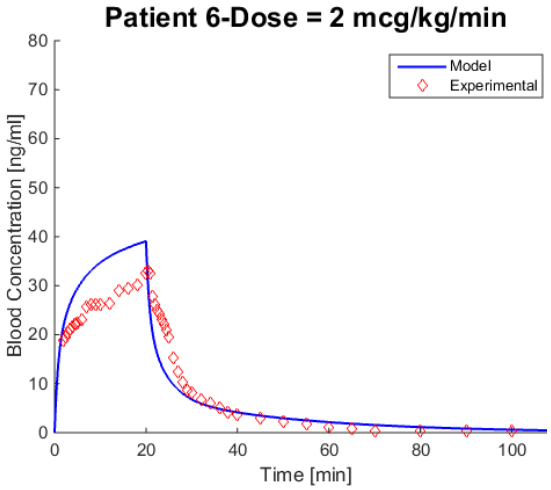
Patient 6-Dose = 2 mcg/kg/min
Model
Experimental
Blood Concentration [ng/ml]
Time [min]

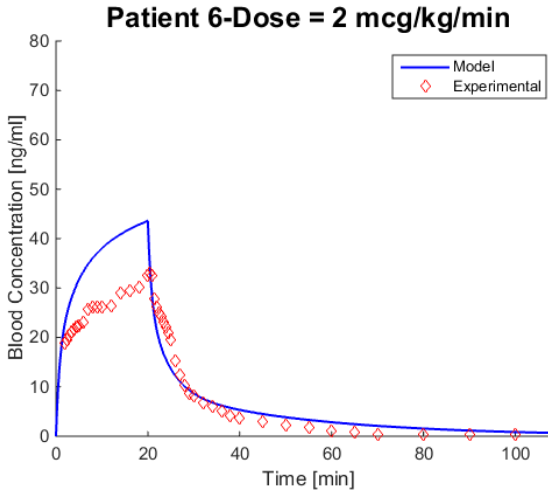
Patient 6-Dose = 2 mcg/kg/min
Model
Experimental
Blood Concentration [ng/ml]
Time [min]

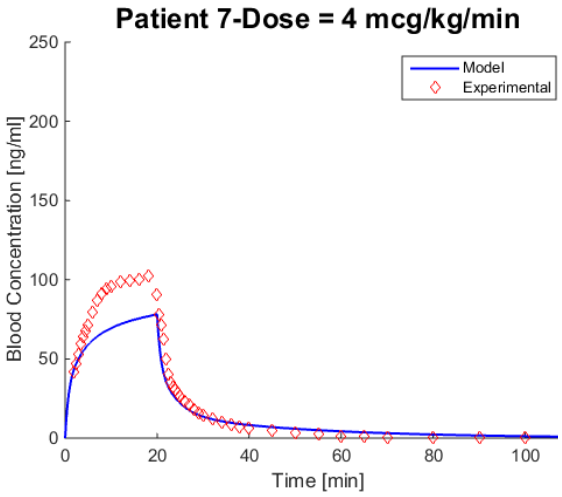
Patient 7-Dose = 4 mcg/kg/min
Model
Experimental
Blood Concentration [ng/ml]
Time [min]
0
50
100
150
200
250
0
20
40
60
80
100

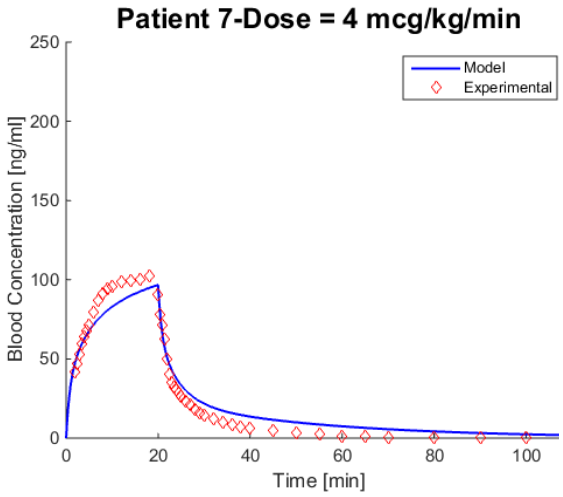
Patient 7-Dose = 4 mcg/kg/min
Model
Experimental
Blood Concentration [ng/ml]
Time [min]
0
50
100
150
200
250
0
20
40
60
80
100

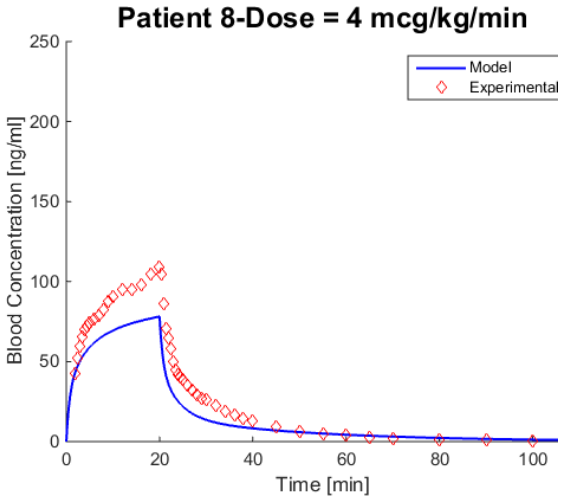
Patient 8-Dose = 4 mcg/kg/min
Model
Experimental
Blood Concentration [ng/ml]
Time [min]
0
50
100
150
200
250
0
20
40
60
80
100

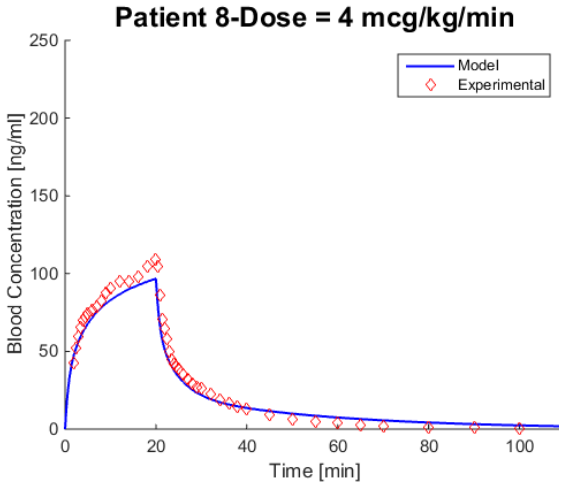
Patient 8-Dose = 4 mcg/kg/min
Model
Experimental
Blood Concentration [ng/ml]
Time [min]
0
50
100
150
200
250
0
20
40
60
80
100

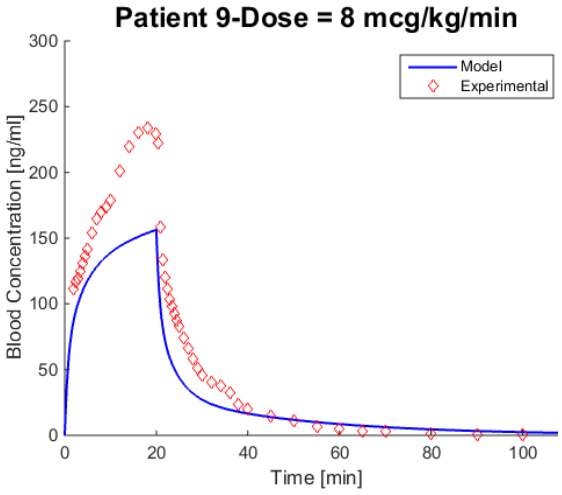
Patient 9-Dose = 8 mcg/kg/min
Model
Experimental
Blood Concentration [ng/ml]
Time [min]
0
50
100
150
200
250
300
0
20
40
60
80
100

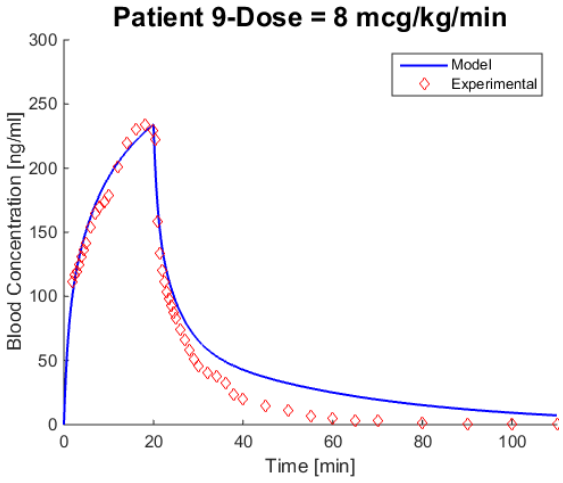
Patient 9-Dose = 8 mcg/kg/min
Model
Experimental
Blood Concentration [ng/ml]
Time [min]
0
50
100
150
200
250
300
0
20
40
60
80
100

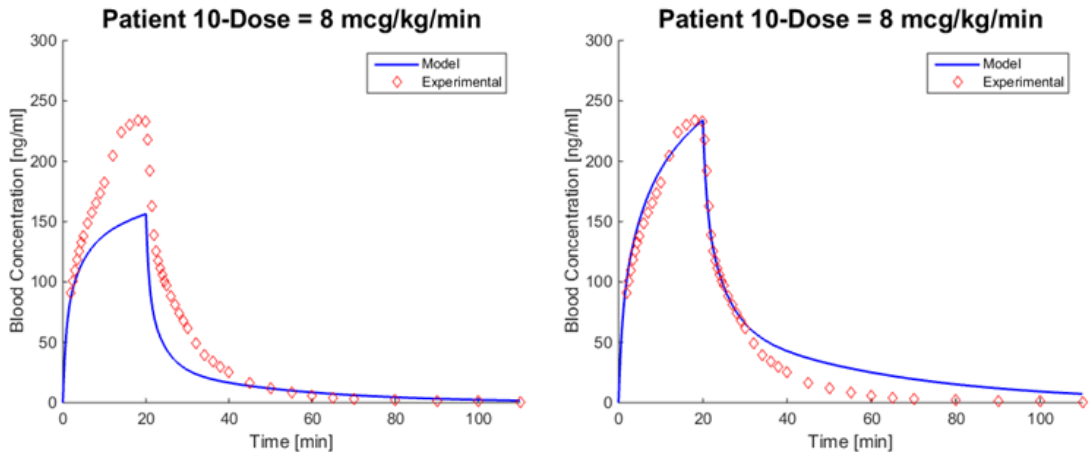

Figure 29 - Experimental data (red) from Egan et al. (1993). The left portion reports the results of the 6P model (blue). The right portion shows the results of the 6P Enzymes mode (blue). It is possible to see that better results are obtained with the 6P Enzymes model.

Again, it is evident that the introduction of the enzymes saturation implies an improvement in the prediction capability of the model. As in the previous case, it is interesting to analyze the performance indexes that show the improvement of the model (see Table 12A, 12B, and 12C).

Table 12A - Comparison of $\Delta C_{Max}\%$ values between the models for Egan et al. (1996). Left column, values of the 6P model. Right column,values of the 6P Enzymes model.

Patient	*Dose [µg/kg/min]*	*6P model*	*6P Enzymes model*
1	1	0.36	6.10
2	1	2.06	3.50
3	1.5	11.37	2.10
4	1.5	8.59	18.00
5	2	14.59	4.70
6	2	18.36	32.0
7	4	30.91	14.50
8	4	29.41	12.30
9	8	33.32	0.14
10	8	33.34	0.16

Table 12B - Comparison of IAE values between the models for Egan et al. (1996). Left column, values of the 6P model. Right column,values of the 6P Enzymes model.

Patient	*Dose [µg/kg/min]*	*6P model*	*6P Enzymes model*
1	1	27.90	31.22
2	1	42.16	51.13
3	1.5	77.59	82.64
4	1.5	83.80	91.42
5	2	99.53	80.74
6	2	135.93	164.63
7	4	330.54	304.95
8	4	414.43	233.07
9	8	839.37	712.60
10	8	432.94	319.63

Table 12C - Comparison of SAE values between the models for Egan et al. (1996). Left column, values of the 6P model. Right column,values of the 6P Enzymes model.

Patient	*Dose [µg/kg/min]*	*6P model*	*6P Enzymes model*
1	1	0.56	0.62
2	1	0.87	1.04
3	1.5	2.00	2.14
4	1.5	1.53	1.66
5	2	1.54	1.24
6	2	2.39	2.90
7	4	6.30	5.85
8	4	6.38	3.61
9	8	13.60	11.60
10	8	11.46	8.45

The considerations made above can be extended to this second model.

After having analyzed the results of the modified models, it may be useful to compare them. Table 13 lists the performance indexes for the two models, in order to make the comparison easier.

Table 13 - Values of the performance indexes. Comparison between the 6P Enzymes and the 6P Binding model.

Patient	*Dose [μg/kg/min]*	$\Delta C_{Max}\%$		IAE		SAE	
		6P Enzymes model	*6P Binding model*	*6P Enzymes model*	*6P Binding model*	*6P Enzymes model*	*6P Binding model*
1	1	6.10	5.10	31.22	28.65	0.62	0.57
2	1	3.50	2.50	51.13	46.62	1.04	0.96
3	1.5	2.10	19.00	82.64	81.22	2.14	2.11
4	1.5	18.00	16.00	91.42	89.41	1.66	1.63
5	2	4.70	6.20	80.74	78.73	1.24	1.21
6	2	32.00	30.00	164.63	153.63	2.90	2.71
7	4	14.50	15.50	304.95	231.41	5.85	4.46
8	4	12.30	13.40	233.07	220.86	3.61	3.42
9	8	0.14	7.00	712.60	513.76	11.60	8.50
10	8	0.16	6.97	319.63	221.30	8.45	5.91

Concerning the $\Delta C_{Max}\%$ values and the higher administered doses, the 6P Enzymes model seems to work better than the 6P Binding model, while for the lower doses the opposite happens. However, both models show acceptable values, except for Patients 3, 4, and 6. This is related to the unusual trend of the experimental data, as it has already been explained. Both SAE and IAE indicate that the 6P Binding model gives better results than the 6P Enzymes model. In fact, the 6P Enzymes model may give a better prediction of the blood concentration peak, but it overestimates the final part of the concentration profile, which is important from the point of view of the pharmacological effect offset.

From a qualitative and quantitative point of view, it is possible to assess that both models produce a consistent improvement in the prediction of the experimental data.

Actually, such high doses are not of interest for anesthesia, since they are out of the recommended range (see Paragraph 1.4), in fact the model does not present equally high deviations from the experimental data in the other case studies.

This is the reason why we did not find studies that focus on this subject in literature. However, it could be interesting to study the mechanism of interaction of remifentanil with enzymes and plasma proteins, to understand how it operates, and whether these modifications of the 6P model efficiently account for it.

2.8 Temperature dependence

Remifentanil is often used in surgeries that present conditions of therapeutic hypothermia. Therapeutic hypothermia is a treatment that lowers the core temperature of a patient under 35.0 °C, to improve its prognosis. There are different degrees of hypothermia, which can lead to adverse physiologic effects, exiting the range of protection of the neuronal structure and function. Hypothermia can be classified according to the degree of cooling and include mild hypothermia (temperature of 32-34 °C), moderate hypothermia (temperature of 30-32 °C) and severe or "deep" hypothermia (below 30 °C). Furthermore, the duration of the therapeutic hypothermia depends on the subject population.

In the following, the general effects of hypothermia on human body are listed, with a special focus on how hypothermia affects drugs pharmacokinetics.

First, it is important to analyze hemodynamic and electrocardiographic changes. Hypothermia affects the myocardial functions, reduces heart rate, but produces an overall increase in the contractility of the heart in sedated patients. Concerning the blood pressure, some patients may experience an increase of it, while others may see no changes (Anderson and Poloyac, 2013).

Mild hypothermia is also associated with abnormal heart rhythms. During cooling, hypothermia causes an increase in plasma norepinephrine levels and the activation of the sympathetic nervous system. This leads to constriction of peripheral vessels and to a subsequent transfer of the blood to centrally located veins in the core compartment of the body. Ultimately, this results in an increase in venous return, which leads to mild sinus tachycardia that means a regular but slow heart rate, less than 50 beats/min or less (Anderson and Poloyac, 2013).

As temperature continues to drop even further below 35 ˚C, the heart rate begins to down till sinus bradycardia (Anderson and Poloyac, 2013). The heart rate will continue to decrease progressively as temperature drops to 33˚C and below.

It is now possible to concentrate on the effect that hypothermia may have on pharmacokinetics. Even if oral administration is not of interest in this work, it is interesting to know that because of the decrease in the blood flow at the site of absorption and the reduction in gastrointestinal motility, hypothermia may lead to a decreased rate and prolonged time to reach maximal concentration for some drugs.

Consequently, the time of onset may be delayed and the magnitude of the pharmacological response diminished (Anderson and Poloyac, 2013).

Concerning drug distribution, hypothermia has mixed effects on protein binding, blood pH, and other factors. Moreover, mild hypothermia also may alter the volume of distribution V_d of the drug (Anderson and Poloyac, 2013). The limited number of published studies to date suggests no significant alteration in drug disposition during mild cooling. However, only a small number of drugs have been evaluated with respect to changes in distribution.

Hypothermia was shown to decrease the metabolic rate by approximately 8% per 1 ˚C drop in body temperature (Anderson and Poloyac, 2013). Similar decreases in oxygen consumption and carbon dioxide production are observed. Similarly, this decrease in metabolic rate arises from a global decrease in the rate of drug metabolism in the liver or in blood and tissues, because metabolic reactions are enzyme-mediated. The rate of these enzyme-mediated reactions is in fact highly temperature sensitive, thus the rate of these reactions is significantly slowed by hypothermia.

Renal or liver elimination will not be analyzed more in depth since they are not significant for remifentanil PK.

Some authors focused on the effect of the core temperature variation on the pharmacokinetics of remifentanil.

Michelsen *et al.* (2001) studied the pharmacokinetics of remifentanil in 68 patients undergoing Cardiopulmonary Bypass (CPB). The purpose of using hypothermia is to provide a degree of organ (and organism) protection and safety margin during CPB. In fact, CPB in conjunction with systemic hypothermia induces lower pump flows, better myocardial protection, less blood trauma, and better organ protection than those achieved by means of a norm-thermic perfusion.

Michelsen *et al.* (2001) proposed different models for the pharmacokinetics (two-compartment and three-compartment models, depending or not on body weight), and the temperature variation during operation. Eventually, they found that the best model was the two-compartment one, with clearances depending on the body weight. They linked the clearance to the temperature by using the following relation:

$$CL_e = e^{\alpha(T-37)} \tag{36}$$

where the temperature varies between 20 and 35°C and α is evaluated by means of suitable nonlinear regression methods. According to their results, the clearance decreases of 6.37% for each degree of temperature.

Russel *et al.* (1997) studied the pharmacokinetics of remifentanil in 16 adult patients undergoing CPB. They collected blood samples during the three surgery phases: (i) pre-

CPB, (ii) hypothermal CPB, (iii) post-CBP (rewarming). They found that the clearance was reduced of about 20% with a decrease of temperature from 35 °C to 28-30 °C, because of the reduction in the enzymes activity.

Michelsen *et al*. (2001) compared their results with Russel *et al.* (1997) and justified the difference by suggesting that Russel *et al.* (1997) did not account for inter-individual variability of patients, because they studied a reduced number of patients.

Davis *et al.* (1999) investigated the pharmacokinetics of remifentanil in 12 children undergoing CBP. The temperature varied in a very narrow range (1.2-2 °C) between pre-bypass and post-bypass phases. They found an increase of 20% in the clearance of the drug in the post-bypass phase.

Sam *et al.* (2009) performed a similar study on 9 infants and children undergoing CBP. Temperature was not found to be a significant factor affecting the clearance. This conclusion was explained by the limited range of temperature variation (33.7-38 °C) and the relatively short duration of the CBP that may have hindered the ability to identify changes in the clearance during bypass (Sam *et al.*, 2009). The differences from the other studies were attributed to different factors related to the operation (hemodilution, temperature variation, *etc*.) and to the physical condition and age of the patients.

It is also interesting to analyze the physiological and biological changes due to the opposite situation, hyperthermia: the increase of the body temperature above normal values. Hyperthermia can be a consequence of exposure to hot environments, fever, exercise, and anesthesia. High environment temperatures can result in heavy sweating and, as a consequence, decreased blood volume, decreased blood pressure, and increased heart rate (Vander *et al.,* 1997). In general, an increase in the body temperature results in an increase of the metabolic rate. In fact, fever is believed to be beneficial because if speeds up the chemical response of the immune system. However, body temperatures higher than 41 °C can be dangerous (Vander *et al.*, 1997).

The interest in the effect of temperature on the drug elimination and the lack of a model for the description of such dependence in the literature led us to investigate this dependence and propose a model to be used for operations involving hypothermia, such as CPB. We did not propose a model for hyperthermia conditions because of the lack in the literature of papers reporting its effects on the pharmacokinetics of remifentanil.

2.8.1 Temperature dependence model

The relevance of hypothermia effects on remifentanil metabolism and clearance led us to include a dependence of the blood and tissues elimination rate constants on body temperature. In fact, remifentanil is metabolized through enzymatic hydrolysis

reactions, therefore we hypothesized the following dependence, by combining the information acquired from the literature and the relation that links the kinetic constants of conventional chemical reactions to temperature (*i.e.* the Arrhenius' law):

$$k_{el,P} = A_1 \cdot e^{(\theta\,(T-37))} \tag{37a}$$

$$k_{el,T} = A_2 \cdot e^{(\theta\,(T-37))} \tag{37b}$$

Where A_1 and A_2 are pre-exponential factors, and θ is a parameter conceptually similar to an activation energy. The exponential function represents a correction that becomes more important as the temperature deviates from the normal core body temperature that is approximately equal to 37 °C. In fact, the initial values for A_1 and A_2 are the elimination constants of the 6P model, derived from the resolution of the nonlinear regression problem (see also Paragraph 2.3).

Since the enzymes that metabolize remifentanil are *aspecific* both in plasma and in tissues, it results reasonable assuming the same value for θ in the two elimination constants, $k_{el,P}$ and $k_{el,T}$. Therefore, the only difference between the rate constants is due to the pre-exponential factors. For the sake of simplicity, from now on the model will be called '6P temperature model'.

The 6P temperature model parameters are therefore the same as the 6P model: K_{PT-P}, K_{P-PT}, K_{P-HO}, K_{HO-P}, which characterize the blood flow-rates through the compartments, with the addition of θ, A_1, and A_1 which determine the importance of the temperature effect on the elimination of remifentanil. The parameters are estimated by means of a nonlinear regression, and with the initial estimates coming from the original 6P model, except for θ. The initial estimate for θ came from Michelsen *et al.* (2001) study, who proposed a similar correlation applied to a three-compartment model.

Two different methods were applied to solve the nonlinear regression problem.

In the first case, the same optimization strategy as for the identification of the 6P model was adopted: the constrained optimization routine of Matlab *Fmincon*. Again, the objective function to be minimized is the sum of the normalized absolute errors between the measured blood concentration and the predicted blood concentration of the drug:

$$f_{obj} = \sum_{i=1}^{N_s} \sum_{j=1}^{N_p} \sum_{k=1}^{N_m} \left(\frac{\left| C_{i,j,l}^{exp} - C_{i,j,l}^{mod} \right|}{N_m} \right) \tag{38}$$

where N_s is the number of case studies, N_p is the number of patients of the *k-th* case-study, and N_m is the number of measures (measured blood/plasma concentrations).

Table 14 reports the initial estimates for the parameters of the model, with the lower and upper bounds.

Table 14 - Initial values of the model parameters. Second column, lower bound of parameters. Fourth column, upper bounds of parameters.

Parameters	*Lower bound*	*Initial value*	*Upper Bound*
K_{PT-P}	0.1	0.332	0.5
K_{P-PT}	0.3	0.538	0.7
K_{P-HO}	0.4	0.751	1
K_{HO-P}	0.02	0.0461	0.07
A_1	1.5	1.779	2
A_2	0.01	0.0678	1
θ	0.001	0.0712	1

The second numerical approach to the problem adopted the Penalty function method. This method allows solving an overall unconstrained problem that at the same time accounts for a number of user-defined constraints. The optimization problem is formulated as follows:

$$\begin{cases} Min(f(x)) \\ h(x) = 0 \\ g(x) > 0 \end{cases}$$

Where $f(x)$ is the objective function of the 6P temperature model, $h(x)$ are the equality constraints, $g(x)$ are the inequality constraints.

According to this method, the objective function $f(x)$ is thus modified to include the constraints:

$$f_{obj} = (\, f(x) + \mu \cdot h^2(x) \; + \eta \cdot \; |min\{0, g(x)\}|) \tag{39}$$

Where μ and η are suitable weights applied to the constraints.

If the equality and inequality constraints are satisfied the second and third term of Equation 39 are null and the objective function becomes the same as the original one. Conversely, the second and/or third terms are positive (in fact the constraints are squared or in absolute value) and as a result the function is *penalized* by being translated vertically upwards.

Our problem does not feature any equality constraints. The upper and lower bounds are therefore rearranged as inequality constraints and included in vector $g(x)$:

$$g(x) = [(k_{PT-P} - k_{PT-P,lower\ bound}); (-k_{PT-P} + k_{PT-P,upper\ bound});$$
$$(k_{P-PT} - k_{P-PT,\ lower\ bound}); (-k_{P-PT} + k_{P-PT,\ upper\ bound});$$
$$(k_{P-HO} - k_{P-HO,\ lower\ bound}); (-k_{P-HO} + k_{P-HO,\ upper\ bound});$$
$$(k_{HO-P} - k_{HO-P,\ lower\ bound}); (-k_{HO-P} + k_{HO-P,\ upper\ bound});$$
$$(A_1 - A_{1,\ lower\ bound}); (-A_1 + A_{1,\ upper\ bound});$$
$$(A_2 - A_{2,\ lower\ bound}); (-A_2 + A_{2,\ upper\ bound});$$
$$(\theta - \theta_{\ lower\ bound}); (-\theta + \theta_{\ upper\ bound})]$$

The weights η are initially set to 1, so that all the constraints have the same relevance in the procedure. However, an in-depth analysis of the specific numerical problem allowed highlighting that k_{T-P} and k_{P-HP} play a major role and therefore their weights were increased. By doing so, the constraints for these two parameters (*i.e.* k_{T-P} and k_{P-HP}) were more important respect to the others.

The objective function was thus rewritten as follows:

$$f_{obj,Penalty} = \sum_{i=1}^{N_s}\sum_{j=1}^{N_p}\sum_{k=1}^{N_m}\left(\frac{\left|C_{i,j,l}^{exp} - C_{i,j,l}^{mod}\right|}{N_m}\right) + \sum_{1}^{Ndf} |\eta \cdot \min(0, g(x))| \qquad (40)$$

where N_s is the number case studies, N_p is the number of patients of the *k-th* patients, N_m is the number of measured blood/plasma concentrations, and N_{df} is the number of degrees of freedom (which is also equal to the number of both lower and upper constraints).

The two optimization procedures produced different values for the parameters of the candidate model. In both cases, the best results were obtained by identifying the parameters using the experimental data of the measured blood concentrations from Michelsen *et al.* (2001) study. Eventually, the identified model was validated using the experimental data from Sam *et al.* (2009) and Davis *et al.* (1999).

Table 15 lists the final values of the parameters deriving from the solution of the optimization problem with the two numerical strategies.

Table 15 - Final values of the model parameters. Left column, values from the application of the penalty function method. Right column, values from the constrained optimization routine.

Parameter	*Penalty function method*	*Constrained optimization*
K_{PT-P}	0.02781	0.1927
K_{P-PT}	0.6997	0.6317
K_{P-HO}	0.9513	0.9976
K_{HO-P}	0.0201	0.02
A_1	1.9048	1.7227
A_2	0.0051	0.0667
θ	0.1546	0.1382

2.8.2 Results and discussion -Case-study 1: Davis et al. (1999)

Davis *et al.* (1999) investigated the pharmacokinetics of remifentanil in 12 children undergoing CPB. Blood was sampled during the pre-bypass and the post-bypass phase. They were administered with a single bolus of 5 µg/kg over 1 min before bypass and the same bolus after bypass. Only averaged experimental data on the blood concentrations are available in the paper. Fig. 30 shows the results of the simulation with the models identified by the two optimization methods, compared with the experimental data.

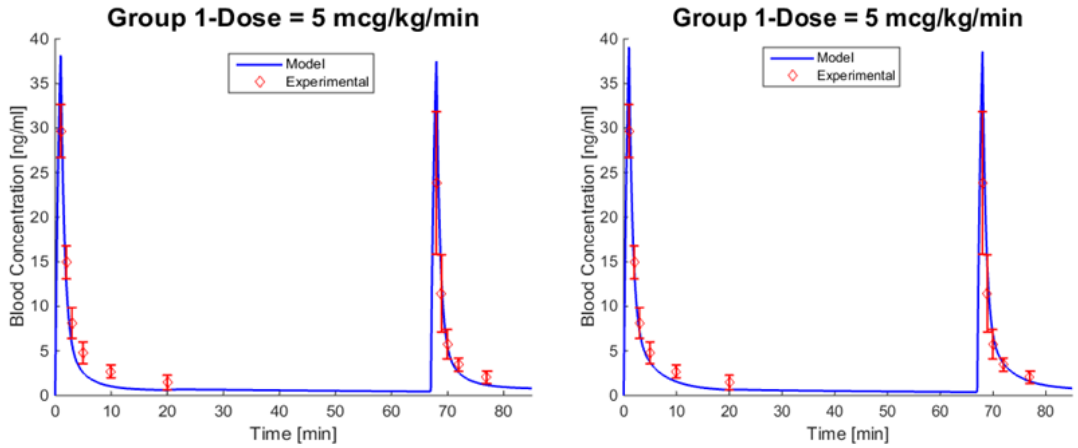

Figure 30 - (Left) Results of the penalty function method. (Right) Results of the constrained optimization. Experimental data (red) of Davis et al. (1999).

Fig. 30 shows the blood concentration-time evolution of remifentanil in the children undergoing CPB, throughout the whole operation. The first peak is due to the first bolus administered before the operation (pre by-pass), while the second peak is due to the second bolus, administered at the end of the operation (post by-pass).

Table 16 reports the values of the performance indexes, *i.e.* $\Delta C_{Max}\%$, SAE, and IAE.

Table 16 - Comparison of $\Delta C_{Max}\%$, SAE, and IAE values between the set of parameters. Left column, values for the penalty function method. Right column, values for the constrained optimization.

Performance index	*Penalty function method*	*Constrained optimization method*
$\Delta C_{Max}\%$	28.61	31.88
SAE	2.91	2.83
IAE	30.2945	28.926

First of all, it is worth observing that both models fail to reproduce the second peak: in fact, there is no appreciable difference between the peaks. In other words, the model is not able to enhance the temperature variation from 35.9 °C (pre-bypass temperature) to 36.7 °C (post-bypass temperature). In the discussion of their results, Davis *et al.* (1999) underline that they obtained different values from those of Russel *et al.* (1997), whose patients were adults. In fact, according to Russel *et al.* (1997), norm-thermic CBP does not affect remifentanil pharmacokinetics, but only hypothermic CBP does. Davis *et al.* (1999) experimental results show that the pharmacokinetics is relevantly affected in norm-thermic conditions, in fact, as it was mentioned, the temperature variation between bypass and post bypass is 0.2-2 °C, which is not high indeed. However, they justify these results with some remarks that are independent of temperature: "*Why there is an effect of CPB on remifentanil clearance in children is unclear. However, the presence of intracardiac shunts and differences in study design (i.e., relative ratio of CPB prime volume to body weight, body temperature control, and analytical assays) may all be contributing factors. Some of these issues can be further addressed. In addition to age, the underlying disease states of the paediatric patients differed from the adults. Patients in our study had CHD, with increased pulmonary to systemic blood flow ratios secondary to their intracardiac shunt, whereas patients in the adult study had normal cardiac anatomy and presumed normal pulmonary-to-systemic blood flow ratios. Because of the lung's metabolic function, changes in pulmonary blood flow may alter a drug's pharmacokinetic profile''.*

The not negligible deviation of the predicted concentrations from the measured data may also be related to these potential causes of alteration of the pharmacokinetics. Moreover, because of the lack of demographic data on the single patients, it is only possible to reproduce the medium trend of the blood concentration-time relationship.

Fig. 31 shows that the model is actually capable of representing the effect of temperature on the pharmacokinetics. In fact, this is a simulation of a virtual patient administered with two boluses at different times, in a situation that is analogous to the one previously analyzed, but at different temperature conditions. The first peak temperature condition is T= 30°C, while the second is T = 40°C.

As expected, as the temperature increases, the drug accumulation in the blood reduces, as the elimination reactions, which are enzyme-catalyzed, run faster. In fact, the first peak concentration is 43.62 ng/mL, while the second one is 34.46 ng/mL. This means that a simulated difference of 10°C of the body temperature corresponds to a difference of about the 25% in peak concentration under the same administered dose, in line with Russel *et al.* (1997) findings.

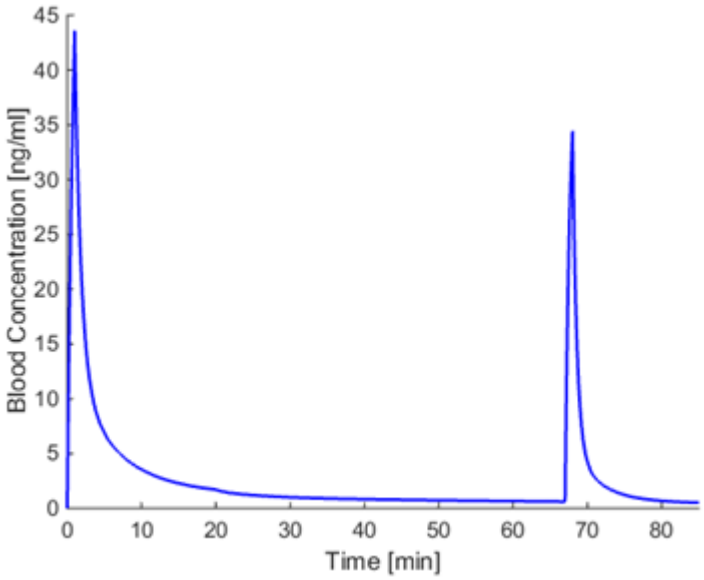

Figure 31 - Simulation of a virtual patient administered with two boluses of remifentanil.

2.8.3 Results and discussion - Case-study 2: Sam et al. (2009)

Similarly, Sam *et al.* (2009) collected the data from nine infants and children undergoing CPB. This study relates to Davis *et al.* (1999) for the limited range of the temperature variation (33.7-38 °C) and the relatively short duration of the CPB that according to Sam *et al.* (2009) may have affected negatively the ability to identify any changes in the clearance during hypothermia. Arterial blood samples were taken prior, during, and post CPB.

They administered a dose of 18 µg/kg as a single bolus over 1 min at the beginning of the pre-CPB phase, a dose of 25 µg/kg immediately before the CPB again over 1 min and a varying infusion dose during all the three phases. The infusion rates were different from patient to patient. Unfortunately, the paper reports only information about the average infusion rates. Table 17 lists the average infusion rates expressed in µg/kg/min:

Table 17 - Average administered infusion rates throughout the three phases of the operation (Sam et al., 2009).

Phase	*Averaged infusion rates [µg/kg/min]*
Pre-bypass	0.264 ± 0.205
During bypass	0.339 ± 0.12
Post-bypass	0.321 ± 0.175

The available experimental data refer to two of the nine patients, this is the reason why Fig. 32 does not report the standard deviation bands of the experimental data. However, averaged demographic data were employed in the simulation, since the paper did not report any piece of information about the single patients. Fig. 32 shows the results and Table 18 lists the $\Delta C_{Max}\%$, SAE and IAE values.

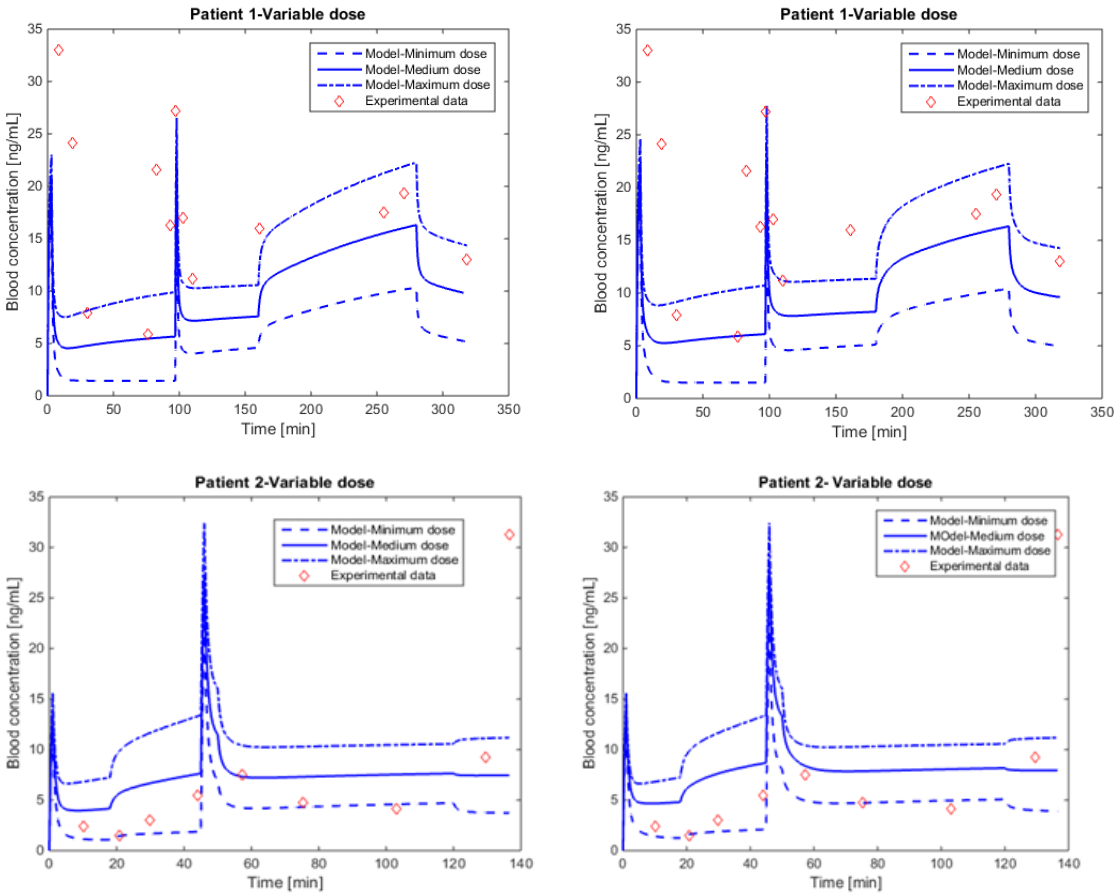

Figure 32 - Experimental data (red) of Patient 1 and 2 from Sam et al. (2009). On the left the penalty function method results, on the right the constrained optimization results.

Table 18 - Comparison of the values of performance indexes between the set of parameters. Left column, values for the penalty function method. Right column, values for the constrained optimization.

Performance index	*Patient*	*Penalty function method*	*Constrained optimization*
$\Delta C_{Max}\%$	1	16,4	19,6
	2	-	-
SAE	1	9,85	9,491
	2	7,35	8,31
IAE	1	112.438	108.341
	2	53.745	62.3129

It was not possible to evaluate $\Delta C_{Max}\%$ for the second patient because of the lack of the experimental maximum concentration.

2.8.4 Conclusions

It is possible to observe that similar acceptable results in the simulation of Davis *et al.* (1999) and Sam *et al*. (2009) patients were obtained, although the two different numerical methods identified different parameter sets. Indeed, the obvious advantage of using the Penalty function method consists in the conversion of the constrained optimization problem to an unconstrained optimization one. In general, unconstrained problems are numerically simpler to solve, as conventional algorithms can be applied. Moreover, if the constrained optimization algorithm is not robust, it is easy to fall into a local minimum, which would mean that the problem has not been optimally solved. In this respect, the Penalty function method results more reliable, even if the drawback of the penalty function method is that the solution to the unconstrained penalized problem is not theoretically/perfectly the exact solution of the original problem.

Because of the lack of experimental data in the literature, it was not possible to proceed further with the analysis of the pharmacokinetics dependence on temperature. However, this model and the suggested *modus operandi* may be a good starting point for further investigations.

3. PHARMACODYNAMICS

3.1 Pharmacodynamic modeling of remifentanil

Pharmacodynamic modeling is based on a quantitative integration of pharmacokinetics, pharmacological systems, and physiological processes. It is an important aspect of pharmacology because it allows understanding the intensity and the time evolution of the drug effects on the body. The application of these models to the analysis of the experimental data grants the quantification and prediction of the drug interaction with the human body. This may be useful for therapeutic purposes.

In the '60s, Gerard Levy was the first to mathematically demonstrate a link between pharmacokinetics and the rate of decline of *in vivo* pharmacological response (Levy, 1964). Starting from this discovery, pharmacodynamics has evolved into a quantitative field that aims to mathematically characterize the time evolution of the drug effects through the modeling of its mechanisms of action.

The main purposes of pharmacodynamic modeling are to (i) integrate known system components and functions, (ii) generate and test alternative hypotheses about the drug mechanisms and the system responses under different conditions, and (iii) estimate system specific parameters that otherwise may be inaccessible. These models are applicable to a wide range of disciplines within the biological sciences including pharmacology and toxicology, wherein there is a critical need to understand and predict desired and adverse responses to a particular drug.

The construction and evaluation of a relevant PD model requires the knowledge of the molecular and cellular mechanisms of pharmacological and toxicological responses, and a range of quantitative experimental data of meaningful biomarkers to understand the target-drug interactions and clinical effects. Proper experimental designs are essential to ensure that sensitive and reproducible data are collected. They should cover a reasonably wide dose/concentration range and have an appropriate study duration. Typically, studies should involve two or three doses to adequately estimate the nonlinear parameters of most pharmacodynamic models with a simultaneous collection of concentration and response data.

The model typology, the nature of the biomarkers, the degree of inter-subject variability, and complexities within dataset are just few considerations when selecting an approach for the development of a PD model. In this work, the collected data take into account a significant variety of patient conditions, to confront with the problem of inter-individual variability and test the prediction capability of the model.

The practical modeling approach is based on few steps. First, it is necessary to define the objectives of the investigation and perform a careful graphical analysis of the

experimental data. By doing so, the selection of appropriate techniques and conditions for the model construction and evaluation will be easier. A good graphical analysis may reduce the number of candidate models and help determining the initial parameter estimates. Despite the progress in computational algorithms, good initial parameter values can reduce the possibility of falling into local minima and be used as a consistency check when compared to final parameters or literature reported values.

After having selected the best model for the reference drug, it is necessary to estimate the parameter values. This is done by means of a nonlinear regression technique. Once the parameters have been evaluated, an external dataset, not used for the identification of the model, allows validating the model and determine if it is generalizable. Indeed, the identified model should reasonably generate new insights and testable hypotheses, and provide guidance for subsequent decisions in drug discovery, development, and pharmacotherapy. These models are extremely useful in anesthesia. In fact, in this field it is important to select the optimal dose in order to avoid undesired side effects, since the dose selection and the pharmacodynamics are strictly related.

There are different models with varying degrees of complexity that can be used to describe the pharmacological effects of drugs, depending on their specific features. From the scientific literature, it emerges that the most suitable model capable to describe the pharmacodynamics of rapidly-equilibrating drugs is the Hill equation (Felmlee *et al*., 2012). Hill's equation assumes that the drug effect (E) is directly proportional to the receptors occupancy and that the plasma drug concentration is in rapid equilibrium with effect site:

$$E = E_0 \pm \frac{E_{max} * C_p}{EC_{50} * C_p} \tag{41}$$

This equation is also known as "E_{max} model" and describes the concentration-effect relationship in terms of a baseline effect, E_0, the maximum possible effect, E_{max}, and the drug concentration that produces half of the maximum effect, EC_{50}.

The model used to describe the remifentanil PD is the full Hill equation (Dershwitz *et al.* (1996); Minto *et al.* (1997); Standing *et al.* (2010)). This equation, also known as the "sigmoid E_{max} model", incorporates a curve fitting parameter γ, which accounts for the steepness of the concentration-effect relationship, which may exhibit nonlinear trends typical of human anatomical and physiological features:

$$E = E_0 \pm \frac{E_{max} * C_p^{\gamma}}{EC_{50}^{\gamma} * C_p^{\gamma}} \tag{42}$$

Initial γ estimates can be determined by assuming a linear slope (m) of the effect versus log-concentration plot:

$$m = \frac{E_{max} * \gamma}{4} \tag{43}$$

This means that the initial value of m depends on the experimental data, making γ strongly dependent on the patient characteristics and study features. However, we recall that this is only a way to compute an initial estimate.

The literature suggests also a modified "sigmoid E_{max} model" (Dershwitz *et al.*,1996; Minto *et al.*, 1997) for remifentanil pharmacodynamics:

$$E = E_0 \pm (E_{max} - E_0) * \frac{C_p^{\gamma}}{EC_{50}^{\gamma} * C_p^{\gamma}} \tag{44}$$

Equation 44 is the starting point of the pharmacodynamic modeling of this thesis. Paragraph 3.2 presents and briefly discusses the main pharmacodynamic effects produced by the remifentanil action.

3.2 Pharmacological effects

Different pharmacodynamic effects can be measured in order to control drugs action. Heart rate, blood pressure (*i.e.* systolic, diastolic, and mean arterial pressure (AP)), minute ventilation, and bispectral index are particularly important for opioids because they allow monitoring the 'depth' of anesthesia, for the reasons discussed in Paragraphs 1.3 and 1.4.

3.2.1 Blood pressure

The cardiovascular system has three types of pressures: hemodynamic, kinetic energy, and hydrostatic. Hemodynamic pressure is the energy imparted to the blood by contraction of the left ventricle of heart. It is preserved by the elastic properties of the blood vessels. Kinetic energy is the energy associated with the motion of the blood inside the arterial system. Hydrostatic energy is the result of the contributions of the gravity and the fluid density. Arterial blood pressure is therefore the sum of these three contributions and is defined as the force exerted by blood per unit area on the arterial wall (McGhee and Bridges, 2002).

Arterial pressure is measured at its peak, which is the systolic arterial pressure (SAP) and at its through that is the diastolic arterial pressure (DAP). Both are expressed in [mmHg]. Table 19 reports the normal ranges for systolic and diastolic pressure.

Table 19 - Ranges for systolic and diastolic pressures. Source: American Heart Association.

Category	*Systolic [mmHg]*	*Diastolic [mmHg]*
Hypotension	<90	<60
Normal	90-119	60-79
Pre hypertension	120-139	80-89
Stage 1 hypertension	140-159	90-99
Stage 2 hypertension	160-179	100-109
Hypertensive urgency	≥ 180	≥ 110
Isolated systolic hypertension	≥ 160	<90

Systemic mean arterial pressure (MAP) is defined as the mean perfusion pressure throughout the cardiac cycle. It is generally closer to DAP because diastole represents about two thirds of the cardiac cycle when the mean heart rate is close to 60 beats/min. This relation is expressed by equation 45, which links SAP, DAP, and MAP.

$$MAP = \frac{(SAP + 2 \cdot DAP)}{3} \tag{45}$$

Blood pressure can be measured by either invasive or noninvasive techniques. Invasive techniques are restricted to hospital settings, while noninvasive techniques are more common and are mainly based on auscultatory and oscillometric techniques (McGhee and Bridges, 2002).

The auscultatory method is the most widely used in clinical activities and is based on a stethoscope and a sphygmomanometer, which consists of an inflatable cuff placed around the upper arm roughly the same vertical height as the heart, attached to a mercury manometer. The mercury manometer measures the height of a column of mercury, giving an absolute result without need for calibration. Consequently, the auscultatory method is not subject to the errors and possible drift of calibration that affect other methods. A cuff of the appropriate size is fitted smoothly, then inflated manually by repeatedly squeezing a rubber bulb until the artery is completely occluded. Listening with the stethoscope to the brachial artery at the antecubital area of the elbow, the examiner slowly releases the pressure in the cuff. When blood just starts to flow in the artery, the turbulent flow creates a pounding. The pressure at which this sound is first heard is the systolic blood pressure. The cuff pressure is further released until no sound can be heard, at the diastolic arterial pressure.

The oscillometric method is based on the observation of oscillations in the sphygmomanometer cuff pressure, which are caused by the oscillations of blood flow. The electronic version of this method is sometimes used in long-term measurements

and general practice. It uses a sphygmomanometer cuff, like the auscultatory method, but with an electronic-pressure sensor (transducer) to observe cuff pressure oscillations, electronics to automatically interpret them, and automatic inflation and deflation of the cuff. The pressure sensor is periodically calibrated to maintain accuracy.

Oscillometric measurements require less skill than the auscultatory technique and may be suitable for use by untrained staff and automated monitoring of patients at home.

In practice the different methods do not produce identical results. An algorithm and experimentally obtained coefficients are used to adjust the oscillometric results to give readings, which best match the auscultatory measures.

3.2.2 Heart rate

The heart rate (HR), or pulse, is the number of times the heart beats per minute. Normal heart rate varies from person to person. The resting heart rate corresponds to the heart that is pumping the lowest amount of blood a person needs when they are not exercising. For a person that is sitting or lying, calm, relaxed, and not ill, the normal heart rate is between 60 and 100 beats per minute (American Heart Association). However, a heart rate lower than 60 beats per minute does not necessarily mean a medical problem because it could be the result of taking particular drugs, as beta blockers, or it could be common for people who get much exercise, such as athletes.

It is necessary to analyze the heart structure in order to deeply understand what a heartbeat is. The heart is a muscle that is composed of four chambers. The upper chambers are called atria, while the lower ones are called ventricles. The right atrium receives oxygen-poor blood from the body and pumps it to the right ventricle, from which it is pumped to the lungs. The left atrium receives oxygen-rich blood from the lungs and pumps it to the left ventricle, from which it is pumped to the body. A natural electrical system causes the heart muscle to contract. Normally the heartbeat starts in the right atrium in a group of special heart cells called sinoatrial node. These cells send out an electrical signal that spreads throughout the heart along electrical pathways. These pathways transmit the signal to the lower chambers of the heart, which causes the heart muscle contraction. Regular electrical signals keep the heart pumping blood to the lungs and to the body. This electrical activity can be monitored in order to measure the heartbeat.

Heart rate can be measured on different parts of the body, such as on the wrists, inside the elbow, on the side of the neck and on the top of the foot. In general, it is measured through the electrocardiogram (ECG) that is a test that checks the electrical activity of the heart by measuring how electrical impulses move through the heart muscle as it contracts and relaxes.

This electrical activity is reported as line tracings on paper, as the ones showed in Fig. 33, which also features the anatomical structure of the heart.

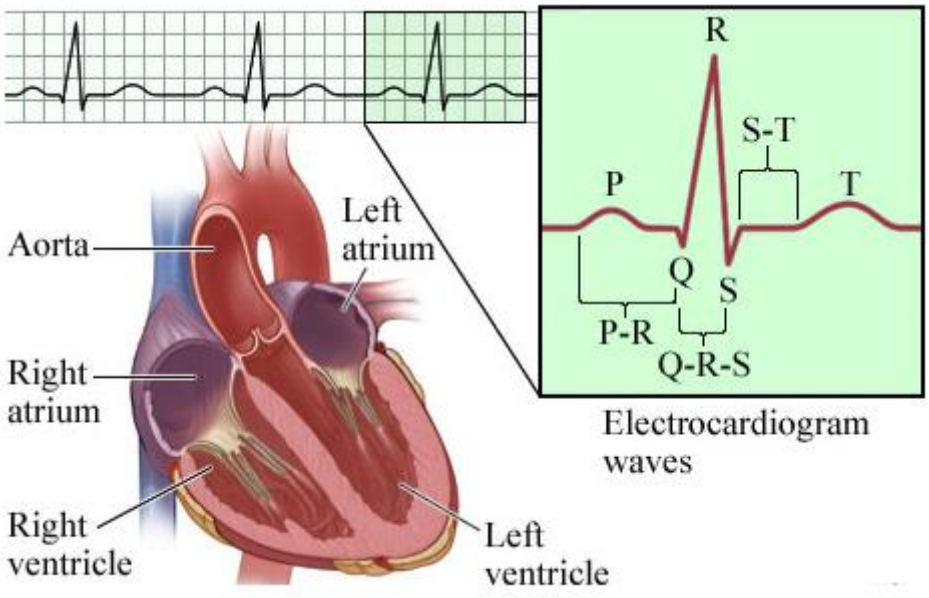

Figure 33 - Generic trend of ECG (top). Heart anatomy (bottom). Taken from the American Heart Association.

The line of an ECG is composed of spikes and dips that are called waves. Figure 33 shows that the line is composed of different parts:

- The P wave is a record of the electrical activity through the upper heart chambers.
- The QRS complex is a record of the movement of electrical impulses through the lower heart chambers.
- The ST segment shows when the ventricle is contracting, but no electricity is flowing through it. It usually appears as a straight line between the QRS complex and the T wave.
- The T wave shows when the ventricles are resetting electrically and preparing for the next muscle contraction.

3.2.3 Minute ventilation

Minute ventilation refers to the amount of air that a person breathes per minute, expressed in liters. This is an important factor anesthesiologists consider when a patient is undergoing surgery. Minute ventilation can vary based on whether or not the patient is stressed, exercising, or participating to other activities. An increase in the ventilation is the result of an increase in a demand for oxygen combined with an increase in the production of carbon dioxide. A decrease is the result of a decrease in oxygen demand and carbon dioxide production. A healthy human body will alter the minute ventilation

in an attempt to maintain physiologic homeostasis. The resting minute ventilation is about 5-8 L/min (Miller and Keane, 2003).

Minute ventilation can be found by multiplying the respiratory rate for the tidal volume or it can be measured through devices as respirometers.

The respiratory rate is the measure of the number of breaths per minute, while the tidal volume is the volume of air a person moves into and out of the lungs during quiet breathing. It is treated in practice as a flow rate.

Respirometers are devices that measure the rate of exchange of oxygen and/or carbon dioxide of a person. If designed to measure the CO_2 release, it consists of a sealed container with the living specimen together with a substance that absorbs the carbon dioxide given off during respiration. If designed to measure the oxygen uptake, a U-tube manometer is used to directly show the pressure difference between the container and the atmosphere.

The literature does not report a sufficient quantity of minute ventilation experimental data related to remifentanil. For this reason, it was not possible to develop a PD model that correlates remifentanil plasma concentration to the correspondent minute ventilation.

3.2.4 Bispectral index

Bispectral index (BIS) is one of the technologies employed by anesthesiologists to manage and control the hypnotic state of the patients. The bispectral index is a statistically based, empirically derived, complex parameter. It is a weighted sum of several electroencephalographic sub-parameters, including a time domain, frequency domain, and high order spectral sub-parameters (Kaul and Barthi, 2002). In fact, it allows analyzing and converting a complex signal like the electroencephalogram (EEG) into a single number. The BIS monitor provides a single dimensionless number that defines the depth of anesthesia of the patient (Kissin, 2000). This number ranges from 0 (equivalent to EEG silence, *i.e.* encephalic death) to 100 (*i.e.* perfectly awaken and responsive person).

A BIS value between 40 and 60 is an appropriate level for general anesthesia (Natick, 1997). When a subject is awake, the cerebral cortex is active and EEG reflects vigorous activity. When asleep or under general anesthesia, the pattern of activity changes. Overall, there is a change from higher-frequency signals to lower-frequency signals, which can be shown by Fourier analysis, and there is a tendency for signal correlation from different parts of the cortex to become more random.

The advantage of BIS, respect to the other effects mentioned above, is that it is a continuous measure, differently from heart rate or arterial pressure. However, as for minute ventilation, the literature does not report a sufficient quantity of experimental

data related to remifentanil. For this reason, it was not possible to develop a PD model that correlates remifentanil plasma concentration to the correspondent bispectral index.

3.3 Modeling approach

As already remarked, remifentanil main application is in the induction and maintenance of general anesthesia. In literature, a remarkable quantity of experimental data on the pharmacologic effects of remifentanil during anesthesia is available (especially hemodynamic effects: Thompson *et al.* (1998); Alexander *et al.* (1999); O'Hare *et al.* (1999); Shajar *et al*. (1999); Hall *et al.* (2000); Maguire *et al.* (2001); Batra *et al.* (2004); Park *et al.* (2011); Lee *et al.* (2012)). In most cases after the induction of anesthesia and the administration of the reference drug, laryngoscopy and tracheal intubation are performed. Laryngoscopy is the endoscopy of the larynx, a part of the throat. It is a medical procedure that allows obtaining a view of the vocal folds and glottis and it may be performed to facilitate tracheal intubation during general anesthesia or for surgical procedures on the larynx or other parts of the upper trachea-bronchial tree. Intubation is a critical moment and it usually causes a cardiovascular stress response. Xue *et al.* (2006) report that there are inconsistent findings on these effects, probably due to differences in study methods, sample sizes, techniques of anesthesia, and intubation.

However, it is interesting to observe that all the experimental data collected show that intubation is rapidly followed by an increase in the heart rate that causes an increase in the blood pressure. According to Shribman *et al.* (1987) this is a sympathoadrenal response to tracheal intubation due to the stimulation of the supraglottic region by tissues tension induced by laryngoscopy. This tension of the supraglottic muscles stimulates the vagal nerve that consequently causes the increase of the adrenaline serum concentration. These explanations are confirmed by Saroj *et al.* (2016), who underline the importance of choosing the optimal dose of analgesic that allows attenuating this response in order to avoid dangerous situations such as ischemia and acute heart failure.

Figure 34 shows an example of the cardiovascular stress response, in terms of arterial pressure and heart rate. The experimental data in Fig. 34 come from Hall *et al.* (2000).

Hall *et al.* (2000) studied 60 female patients, aged 20-65, undergoing laryngoscopy. The patients were lumped into two groups. Group 1 received a bolus of 1 μg/kg for 30 s followed by an infusion of 0.5 μg/(kg min), while Group 2 received a bolus of 0.5 μg/kg for 30 s followed by an infusion of 0.25 μg/(kg min) for the whole duration of the operation.

In Hall *et al.* (2000), intubation is performed 3.5 min after the drug administration beginning (time 0 in Fig. 34). It is worth noticing that the maximum effect occurs 1 min after the intubation, while the stress response disappears in approximately 3 min for SAP and MAP and 2 min for HR.

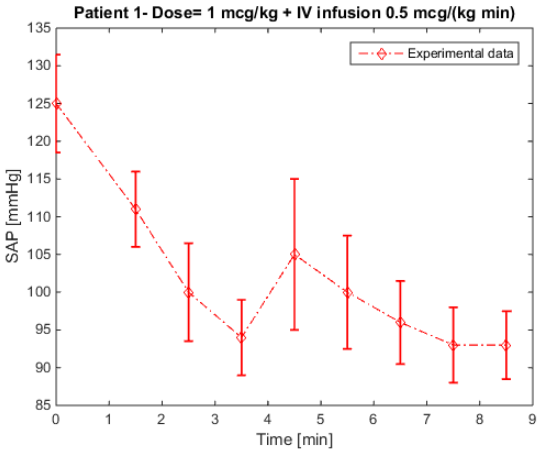

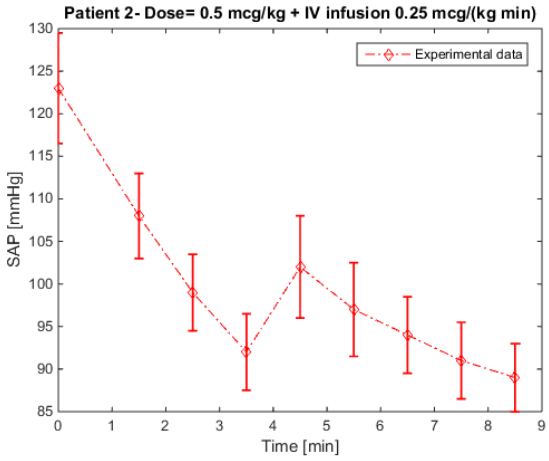

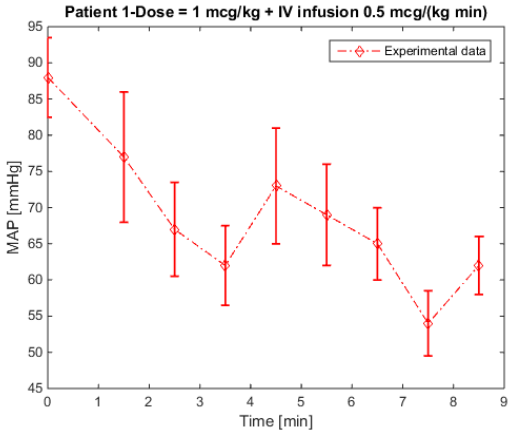

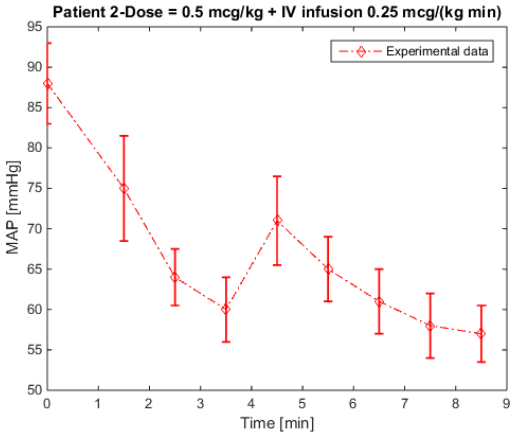

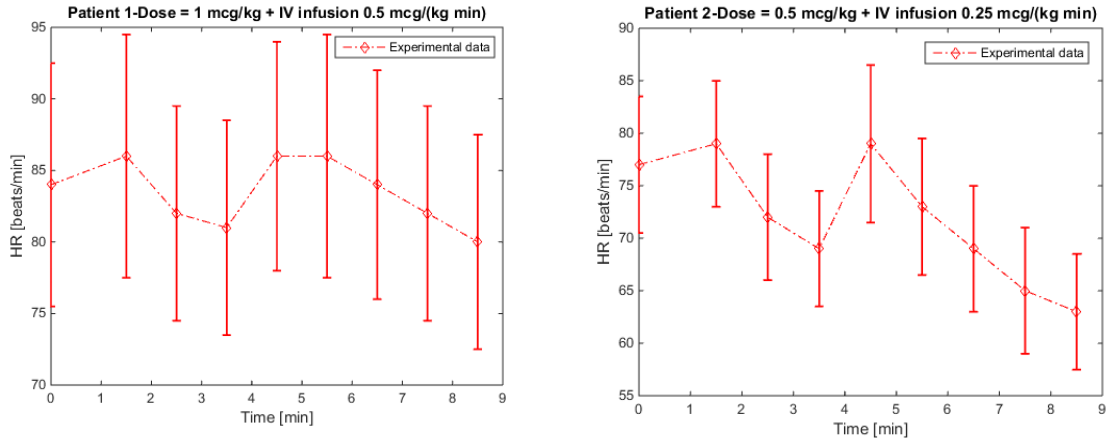

Figure 34 - Experimental data from Hall et al. (2000). (Top) Experimental SAP. (Middle) Experimental MAP. (Bottom) Experimental HR. Standard deviation bars provide a measure of the inter-individual variability. The peak that can be detected at 4.5 min is due to the cardiovascular stress response of the patient to intubation and laryngoscopy.

Two different peaks can be detected in the heart rate trend. The second peak is due to the response to intubation, as for SAP and MAP. In the first minutes, the experimental data show that the heart rate tends to increase before the beginning of the intubation procedure. A decrease would be expected instead, because of the initial administration of remifentanil (Saroj *et al.*, 2016).

According to the literature and to anesthesiologists, the first peak is an *emotional* one. It occurs when the drug has not completely explicated its effect yet and the patient is still awake and worried for the imminent procedure. Because of the nature of this peak, it would be senseless to model it. Therefore, the procedure of parameters identification of the pharmacodynamic model is run neglecting the experimental data referred to this short and preliminary phase, which precedes intubation. Therefore, in this phase the model takes into account only the effect of the drug.

Different studies were examined to collect the experimental data that make viable the identification of a pharmacodynamic model capable to describe the cardiovascular effects of remifentanil. All these considerations are common for the experimental data available. Tables 20A, 20B, and 20C list the required time for the maximum effect. It is possible to observe that it is always approximately 1 min.

Table 20A - Time required to reach the SAP peak.

CASE-STUDY	*Time to reach the peak [min]*
O'Hare et al. (1999) Group 1,2,3	1.00
Lee et al. (2012)	1.00
Park et al. (2011) Group 1,2	0.50
Mean	0.88
Standard deviation	0.25

Table 20B -Time required to reach the MAP peak

CASE-STUDY	*Time to reach the peak [min]*
Batra et al. (2004) Group 1,2	0.98
Alexander et al. (1999) Group 1,2,3	1.00
Hall et al. (2000) Group 1,2	1.00
Thompson et al. (1998)	1.00
Mean	0.9966
Standard deviation	0.0077

Table 20C - Time required to reach the HR peak.

CASE-STUDY	*Time to reach the peak [min]*
Hall et al. (2000) Group 1,2	1.00
Lee et al. (2012)	1.00
Maguire et al. (2001)	1.00
O'Hare et al. (1999) Group 1,2,3	1.00
Park et al. (2011) Group 1,2	0.50
Shajar et al. (1999)	1.00
Mean	0.90
Standard deviation	0.20

Another important feature, which is common to the above mentioned case studies, is the percentage increase of cardiovascular response respect to the value corresponding to the intubation time, *i.e.* the value that precedes the stress response. Tables 21A, 21B, and 21C list the values of the different case studies. The percentage of increase of the effect is quantified as follows:

$$Delta = \frac{|E_{effect} - E_{ini}|}{E_{ini}} * 100 \quad (46)$$

Where E_{effect} is the maximum value that can be achieved as response to laryngoscopy and intubation, while E_{ini} is the value of the effect when the procedure starts.

Table 21A - Percentage of increase for SAP.

CASE-STUDY	*% of increase [-]*
O'Hare *et al.* (1999) - *Group* 1	9.90
O' Hare *et al.* (1999) - *Group* 2	10.20
O' Hare *et al.* (1999) - *Group* 3	17.20
Lee *et al.* (2012)	8.50
Park *et al.* (2011) - *Group* 1	11.60
Mean	11.48
Standard deviation	3.38

Table 21B - Percentage of increase for MAP.

CASE-STUDY	*% of increase [-]*
Batra et al. (2004)	-
Alexender et al. (1999)	-
Hall et al. (2000) - Group 1	17.70
Hall et al. (2000) - Group 2	18.30
Thompson et al. (1998)	18.00
Mean	18.00
Standard deviation	0.30

In Batra *et al*. (2004) and Alexander *et al.* (1999) the increase is not quite evident due to the high doses administered to the patients. This is why the percentage is not reported in Table 21B.

Table 21C - Percentage of increase for HR.

CASE-STUDY	*% of increase [-]*
Hall et al. (2000) - Group 1	6.17
Hall et al. (2000) - Group 2	14.19
Lee et al. (2012)	12.45
Maguire et al. (2001)	20.80
O'Hare et al. (1999) - Group 1	8.05
O'Hare et al. (1999) - Group 2	4.70
O'Hare et al. (1999) - Group 3	1.28
Park et al. (2011) - Group 1	7.58
Park et al. (2011) - Group 2	5.49
Shajar et al. (1999)	6.08
Mean	8.20
Standard deviation	5.00

It is possible to notice that the percentages are sometimes different among patients of the same study. This occurs because such patients received different doses, which induces a different effect of the administered drug. In fact, the higher the dose the lower the effect, and as a consequence, the lower the increase of heart activity. In addition, the dispersion of the percentages of the cases of study is low (see standard deviations in Table 21A, 21B, and 21C).

It is also important to analyze the time at which the effect starts to disappear after the maximum value. Table 22A, 22B, and 22C list the values for the different studies.

Table 22A - Time required for the decrease of SAP.

CASE-STUDY	*Time for the decreasing [min]*
O'Hare et al. (1999) - Group 1, 2, 3	2.00
Lee et al. (2012)	2.00
Park et al. (2011) - Group 1, 2	2.00
Mean	2.00
Standard deviation	0.00

Table 22B - Time required for the decrease of MAP.

CASE-STUDY	*Time for the decreasing [min]*
Batra et al. (2004) - Group 1, 2	-
Alexander et al. (1999) - Group 1, 2, 3	-
Hall et al. (2000) - Group 1, 2	2.50
Thompson et al. (1998)	1.50
Mean	2.00
Standard deviation	0.70

As mentioned above, in Batra *et al.* (2004) and Alexander *et al.* (1999) the peak response to intubation is not so evident to allow identifying the decrease time. This issue is better explained at Paragraph 3.3.1.

Table 22C - Time required for the decrease of HR.

CASE-STUDY	*Time for the decreasing [min]*
Hall *et al. (2000) - Group 1, 2, 3*	2.00
Lee *et al. (2012)*	2.00
Maguire *et al. (2001)*	3.00
O'Hare *et al. (1999)- Group 1, 2, 3*	2.00
Park *et al. (2011) - Group 1, 2*	2.00
Shajar *et al. (1999)*	3.00
Mean	2.20
Standard deviation	0.58

The main consequence of all these considerations is that the 'simple' sigmoidal E_{max} model is not adequate for the description of the collected experimental data, except for the phase that precedes the intubation, as shown in Fig. 35, where the experimental data refer to Group 1 of O'Hare *et al.* (1999).

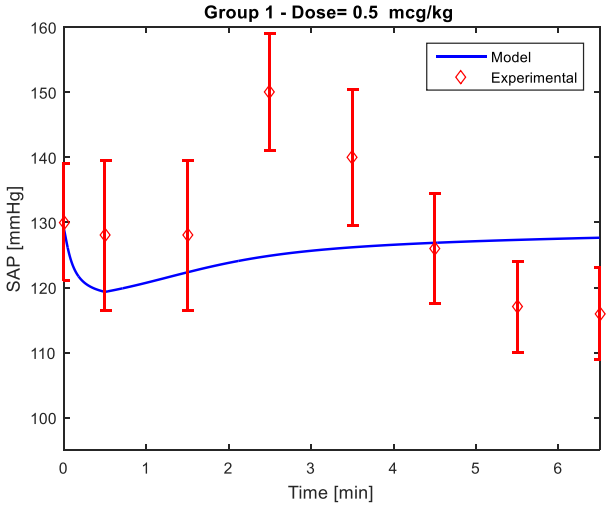

Figure 35 - Comparison between the experimental data (red) of Group 1 of O'Hare et al. (1999) and the simulation with the sigmoidal E_{max} model (blue). The patient received 0.5 µg/kg over 30 s. The model does not represent the stress response to intubation.

Subsections 3.3.1 and 3.3.2 discuss the modeling approach. Because of some differences in the trends of the experimental data, different modeling strategies were used for the heart rate and for the arterial pressure.

3.3.1 MAP and SAP model

Fig. 34 shows that the trend of the experimental data of MAP and SAP can be conceptually divided into three phases. The first phase starts at time 0, which is the time of anesthesia induction and remifentanil administration, and ends when intubation starts.

The duration of this first period depends on the time at which intubation is performed. During this first phase that precedes the intubation, both MAP and SAP can be described by means of the sigmoidal E_{max} model.

The effect of this first phase is described as follows (Minto *et al.*, 1997):

$$E_1 = E_0 - |E_{max} - E_0| \cdot \frac{{C_p}^{\gamma}}{{C_p}^{\gamma} + {EC_{50}}^{\gamma}} \tag{47}$$

Where:

- E_0 is the baseline of the awake patient, which is an assigned parameter;
- E_{max} is the maximum pharmacological effect of the drug;
- C_p is the plasma concentration, derived from the PBPK model (Chapter2);
- γ is a curve fitting parameter;
- EC_{50} is the concentration that corresponds to 50% of the maximum effect.

A second phase can be distinguished with the start of intubation. This phase ends when the maximum response to the procedure is achieved. The duration can be assumed as 1 min, as previously discussed (see Tables 20A and 20B). In this phase, the E_{max} model must be overestimated by adding a term that accounts for the cardiovascular stress response to intubation. Based on the trends of experimental data, this additional term was modeled to reproduce the response of a first-order dynamic system.

The equation that describes the effect in this phase is:

$$E_2 = E_0 - |E_{max} - E_0| \cdot \frac{{C_p}^{\gamma}}{{C_p}^{\gamma} + {EC_{50}}^{\gamma}} + Delta \cdot K_p \cdot \left(1 - e^{-\frac{t-t_{int}}{\tau_1}}\right) \quad (48)$$

Where:

- K_p is the static gain, which represents the maximum effect of the response to intubation;
- t_{int} is the intubation time, which is known and therefore is an assigned parameter;
- τ_1 is the characteristic time of the first order response;
- $Delta$ is an assigned parameter that has been chosen on the basis of the analysis of the experimental data (see Tables 21A and 21B). For sake of simplicity, it is assumed 0.1 for SAP and 0.18 for MAP.

Finally, 1 min after the intubation time, in the last phase, the effect is described by the following equation, which takes into account the reduction of the stress response:

$$E_3 = E_0 - |E_{max} - E_0| \cdot \frac{{C_p}^{\gamma}}{{C_p}^{\gamma} + {EC_{50}}^{\gamma}} Delta \cdot K_p \cdot \left(1 - e^{-\frac{t-t_{int}}{\tau_1}}\right) - Gamma \cdot K_p \cdot \left(1 - e^{-\frac{t-t_{Max}}{\tau_2}}\right) \quad (49)$$

Where:

- t_{Max} is the time of the maximum effect, which is defined as 1 min after the time of the intubation;
- τ_2 is the characteristic time of the reduction of the effect and is defined as $2\tau_1$ on the basis of the experimental data analysis;
- $Gamma$ is an assigned parameter that has been chosen on the basis of the experimental data analysis, as for $Delta$. It is 0.2 for SAP and 0.1 for MAP.

Summarizing, it is possible to distinguish two categories for the parameters: (i) assigned parameters that depend on the study methods and in practice on the choices of the anesthesiologist (t_{int}) or the conditions of the patient (E_0) or graphic analysis ($Delta$, $Gamma$, t_{Max}), (ii) degrees of freedom (E_{max}, γ, EC_{50}, K_p, τ_1).

The degrees of freedom of the model were identified through a parametric nonlinear regression procedure, based on a constrained optimization algorithm. The objective function is defined as the normalized absolute error between the predicted and the measured effects, in terms of MAP and SAP:

$$f_{obj} = \sum_{i=1}^{N_s} \sum_{j=1}^{N_p} \sum_{l=1}^{N_m} \left(\frac{\left| Effect_{i,j,l}^{exp} - Effect_{i,j,l}^{mod} \right|}{N_m} \right) \tag{50}$$

Where N_s is the number of studies, N_p the number of patients of the *k-th case-study*, and N_m the number of measured values of the effect.

The parameters of SAP model were identified with the data from Maguire *et al.* (2001), while the parameters of MAP model were identified with the data from Thompson *et al.* (1998). Tables 23A and 23B list the initial estimates for the parameters of the model along with the lower and upper bounds, defined according to suitable feasibility regions and/or graphical data analysis, and the optimal final values.

Table 23A - Adaptive parameter details of SAP model.

Parameter	*Lower bounds*	*Initial estimates*	*Upper bounds*	*Optimized values*
E_{max}	90	100	120	117.525
γ	1	1	10	1.324
EC_{50}	0.5	2	3	1.319
τ_p	0.6	0.75	1.5	1.402
K_p	110	130	160	121.170

Table 23B - Adaptive parameter details of MAP model.

Parameter	*Lower bounds*	*Initial estimates*	*Upper bounds*	*Optimized values*
E_{max}	40	45	65	52.70
γ	0.5	0.5	10	0.89
EC_{50}	0.1	1.5	2	1.45
τ_p	0.5	1	5	4.80
K_p	55	65	70	56.25

3.3.2 HR model

Starting from the considerations made in Paragraph 3.3.1, it is possible to develop a model to predict the time evolution of the heart rate, under the influence of remifentanil. As mentioned above, the first peak that characterizes the experimental

data (Fig. 34) will not be considered in the deployment of the model, because it could alter the value of the pharmacodynamic parameters. Fig. 36 shows the trend of the experimental data where the measured values that belong to the *emotional* peak, which occurs immediately after the induction of anesthesia and the administration of remifentanil, are removed. Only few points are neglected and not the entire tract before intubation because this phase is important and cannot be neglected, as it is the one that immediately follows remifentanil administration.

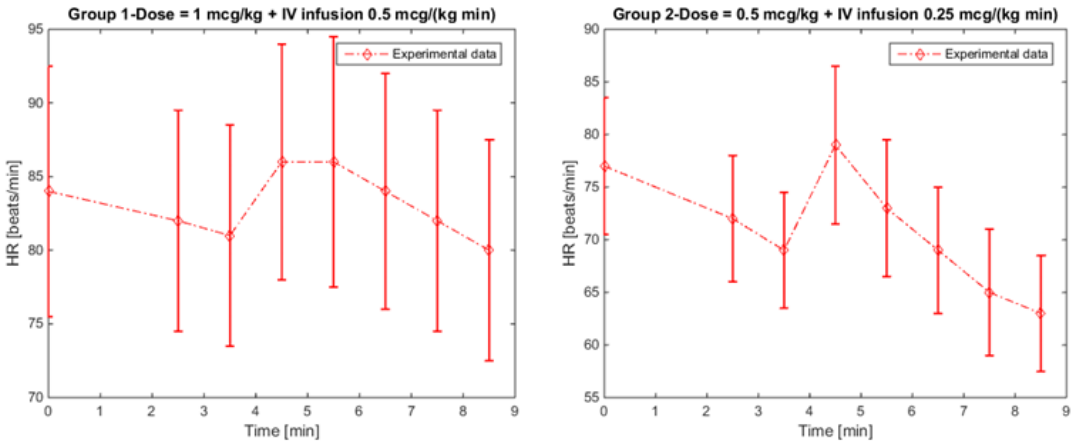

Figure 36 - Experimental HR from Group 1 and 2 of Hall et al. (2000), minus the first peak.

In order to model this behavior, it is necessary to divide the trend into four separate sections. The first part starts from the value of the baseline of the patient that corresponds to time 0, which in general corresponds to the induction of anesthesia and administration of remifentanil. The baseline is the normal value of the patient heart rate, before the beginning of any possible treatment. This first part ends when the intubation starts. The time when this occurs depends on the case-study, but it is always known in the practice. The equation used to describe this first tract is the one proposed by Minto *et al.* (1997), *i.e.* the modified sigmoid E_{max} model:

$$E_1 = E_0 - |E_{max} - E_0| \cdot \frac{C_p^{\gamma}}{EC_{50}^{\gamma} + C_p^{\gamma}} \tag{51}$$

Where the qualitative meaning of these parameters is the same of the one presented in the AP model.

The second tract starts with the beginning of endotracheal intubation and laryngoscopy and ends when the maximum effect is reached. As explained in Paragraph 3.3, this peak is caused by a simpathoadrenal response, produced by the intubation and laryngoscopy procedure. The analysis of experimental data allowed understanding if the time interval needed to reach this maximum is the same for the different case studies reported in the literature. The mean is 0.9 min, with a variance of 0.04 (see also Table 20C). This value

corresponds to 54 s but for the sake of simplicity we assumed that this tract lasts 1 min, which is also the value that characterizes the majority of the case studies.

In order to model this second tract, it is necessary to consider two different effects: the one of the drug and the one caused by the procedure. The mechanism that causes the increment of heart rate, explained in Paragraph 3.1, is quite complex and because of its nature, it would not be meaningful to model it. For this reason, an expression that has a trend similar to the experimental data was adopted. The equation used is the one that describes the dynamic response of a first order system:

$$E_2 = E_0 - |E_{max} - E_0| \cdot \frac{C_p^{\gamma}}{EC_{50}^{\gamma} + C_p^{\gamma}} + Delta \cdot K_p \cdot \left(1 - e^{-\frac{t - t_{int}}{\tau_1}}\right) \quad (52)$$

Where:

- K_p is the static gain as in previous case. The value, to which the model tends, is the maximum effect caused by the laryngoscopy and the endotracheal intubation;
- τ_1 is the time constant of the process, as in SAP and MAP models;
- $Delta$ is an assigned parameter. It is the percentage of increment caused by the procedure. According to literature findings (Shribman *et al.*, 1987), the increment is more or less equal to 10% of the heart rate when the intubation starts. In addition, an analysis of the experimental data confirmed this value (see also Table 21). The mean value is 8%, with a variance of 0.3%. This is the value that was used in this model;
- t_{int} is the time when the intubation starts, which is reported in the different case studies.

The third tract accounts for the reduction of the stress response. Again, an analysis of the experimental data allowed quantifying the time taken to reduce the effect. Table 22C reports the values of the different case studies. The averaged value of the different case studies is 2.2 min, with a variance of 0.3 min. 2.2 min corresponds to 2 min and 12 s, so for sake of simplicity, we assumed that the third tract lasts 2 min that is also the value that characterizes the majority of the studies.

The concavity of the dynamic response of a first order process (*i.e.* similar to the one of a tank that sees its level decreasing) is opposite to the concavity of the experimental data. Fig. 37 shows the trend of the experimental data of Group 1 from O'Hare *et al.* (1999), compared to the trend of the model, considering the first order response of an emptying tank. For this reason, in the case of HR the curve was simply mirrored by changing its sign. In this tract, it is necessary to consider three different terms: the one of the drug, the one of the heart rate increase, and the one of the heart rate decrease.

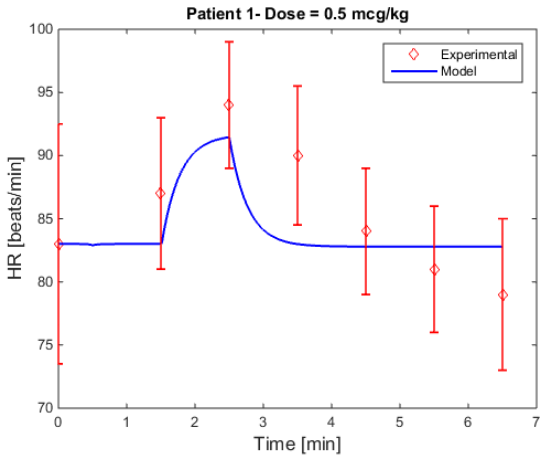

Figure 37 - Experimental data (red) of O'Hare et al. (1999). The blue line is the modified E_{max} model overestimated with the 1st order response. The concavity is opposite respect to the one of the experimental data.

The equation that describes this tract is:

$$E_3 = E_0 - |E_{max} - E_0| \cdot \frac{C_p^{\gamma}}{EC_{50}^{\gamma} + C_p^{\gamma}} + Delta \cdot K_p \cdot \left(1 - e^{-\frac{t-t_{int}}{\tau_1}}\right) + Delta \cdot K_p \cdot \left(1 - e^{\frac{t-t_{Max}}{\tau_2}}\right) \quad (53)$$

Where:

- t_{Max} is the time when the peak occurs that corresponds to 1 min after the beginning of the procedure;
- τ_2 is a characteristic time. It is necessary to assign a dedicated characteristic time because the heart rate decreases more slowly respect to its increase.

Since the curve is only mirrored, the percentage of increase and of decrease of the effect is the same (Equation 53 figures twice the parameter $Delta$). In the last tract it is necessary to add another contribution. Looking at the experimental data, the heart rate tends to return approximately to its normal value after that procedure. Therefore, in this tract four contributions have to be considered, adding this last effect to the previous terms. This term is modeled as a first order system (*e.g.*, emptying of the tank).

The equation that describes this last tract is:

$$E_4 = E_0 - |E_{max} - E_0| \cdot \frac{C_p^{\gamma}}{EC_{50}^{\gamma} + C_p^{\gamma}} + Delta \cdot K_p \cdot \left(1 - e^{-\frac{t-t_{int}}{\tau_1}}\right) + Delta \cdot K_p \cdot \left(1 - e^{\frac{t-t_{Max}}{\tau_2}}\right) + \frac{E_0 - E_{0,norm}}{E_0} \cdot E_{0,norm} \cdot \left(1 - e^{-\frac{t-t_{end}}{\tau_2}}\right) \quad (54)$$

Where:

- $E_{0,norm}$ is the value towards which the experimental value tends in general. For the sake of simplicity, it is assumed equal to the minimum value of the normal heart rate range that is 60 beats/min;
- t_{end} is the time at which the effect induced by the laryngoscopy ends.

Finally, the degrees of freedom that have to be computed through a regression procedure are: E_{max}, γ, EC_{50}, K_p, τ_1 and τ_2. As for $MAP$and SAP, it is possible to distinguish two categories for the parameters: (i) assigned parameters that depend on the study methods and on the choices of the anesthesiologist (t_{int}) or the conditions of the patient (E_0) or graphic analysis ($Delta$, t_{Max}, t_{end}, $E_{0,norm}$), (ii) degrees of freedom (E_{max}, γ, EC_{50}, K_p, τ_1, τ_2).

The objective function used to compute these parameters is:

$$f_{obj} = \sum_{i=1}^{N_s}\sum_{j=1}^{N_p}\sum_{l=1}^{N_m}\left(\frac{\left|Effect_{i,j,l}^{exp} - Effect_{i,j,l}^{mod}\right|}{N_m}\right) \quad (55)$$

Where N_s is the number of case studies, N_p is the number of patients of the *k-th* study, and N_m is the number of experimental data on the effect.

A constrained optimization, using the Matlab function *Fmincon*, was performed.

Table 23C lists both the initial and final values of the parameters together with the upper and lower bounds.

Table 23C - Adaptive parameter details of HR model.

Parameters	*Lower bounds*	*Initial values*	*Upper bounds*	*Optimized values*
E_{max}	60	70	80	68.05
γ	2	6	8	6.98
EC_{50}	1	2	12	10.02
K_p	80	87	100	0.20
τ_1	0.2	0.26667	0.8	95.00
τ_2	2	2.7	6	3.24

An analysis of the experimental data allowed assigning both the initial values and the bounds. It is possible to notice that the considered ranges are wide, because of the inter-variability among patients and because of the differences between the studies, in terms of doses, ways of administration (bolus, infusion, or both) and other surgery

conditions. The experimental data used to identify the pharmacodynamic (PD) model come from Engelhard *et al.* (2004); O'Hare *et al*. (1999).

3.4 Results and discussion – SAP model

3.4.1 Case-study 1: Lee et al. (2012)

Lee *et al.* (2012) studied 90 adult patients, with no statistically significant differences in gender, age, height, or weight. The patients were divided into three groups, which respectively received (i) saline solution, (ii) dexmedetomidine, and (iii) remifentanil (single bolus of 1 µg/kg for 1 min). Aim of the study was to compare the ability of dexmedetomidine and remifentanil in lowering the cardiovascular response due to laryngoscopy and intubation. Fig. 38 shows the results of the PD model compared to the experimental SAP of the third group of patients of the study.

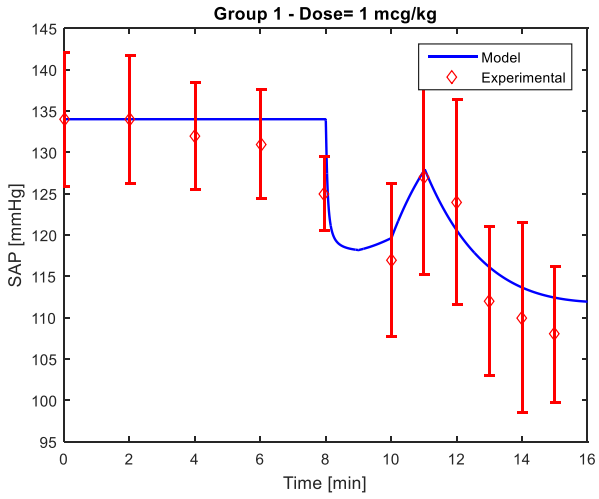

Figure 38 - Comparison between the PD model (blue) and the experimental data (red) of Group 1 from Lee et al. (2012).

It is possible to state that the PD model predicts the experimental SAP with a rather good level of precision. The simulated curve follows the central values of the experimental standard deviations.

It is possible to observe that after the peak of the stress response, the experimental data decrease until they reach a SAP value of 95-119, which is the normal SAP range.

Another important observation is that experimental SAP values start decreasing before the administration of remifentanil, which occurs 8 min after the surgery beginning. The reason may be related either to peculiar conditions of the patients or, to an error about the administration time of the drug.

Similarly to PK, it is here necessary to define some performance indexes in order to evaluate the model accuracy in predicting the hemodynamic effects. As the sigmoidal E_{max} model was modified to account for the cardiovascular stress response to intubation, it is interesting to assess the model capability to reproduce the peak effect by means of the following parameter:

$$\Delta E_{Max}\,\% = \frac{|Maximum\ effect_{\exp} - Maximum\ effect_{mod}|}{Maximum\ effect_{\exp}} \cdot 100 \tag{56}$$

To evaluate the accuracy of the model (see Table 24), the sum of the absolute errors (SAE) between the predicted and measured effects is assumed (and found) appropriate, for the same reasons discussed in Chapter 2.

$$SAE = \frac{\sum_{j=1}^{N_m}\sum_{l=1}^{N_p}\left|Effect_{i,j}^{exp} - Effect_{i,j}^{mod}\right|}{N_m} \tag{57}$$

Where N_p is the number of patients of the *k-th* case-study and N_m is the number of measured values of the effect.

Table 24 - $\Delta E_{Max}\%$ and SAE values for Group 1 of Lee et al. (2012).

$\Delta E_{Max}\%$	SAE
0.720	2.995

3.4.2 Case-study 2: O'Hare et al. (1999)

O'Hare *et al*. (1999) studied the effect of 3 bolus doses of remifentanil on the arterial pressure response to laryngoscopy and tracheal intubation of 3 groups of 20 patients. The three groups were administered increasing doses of remifentanil for 30 s, respectively 0.5, 1 and 1.25 µg/ kg. Fig. 39 shows the SAP comparison between experimental data and simulated curves.

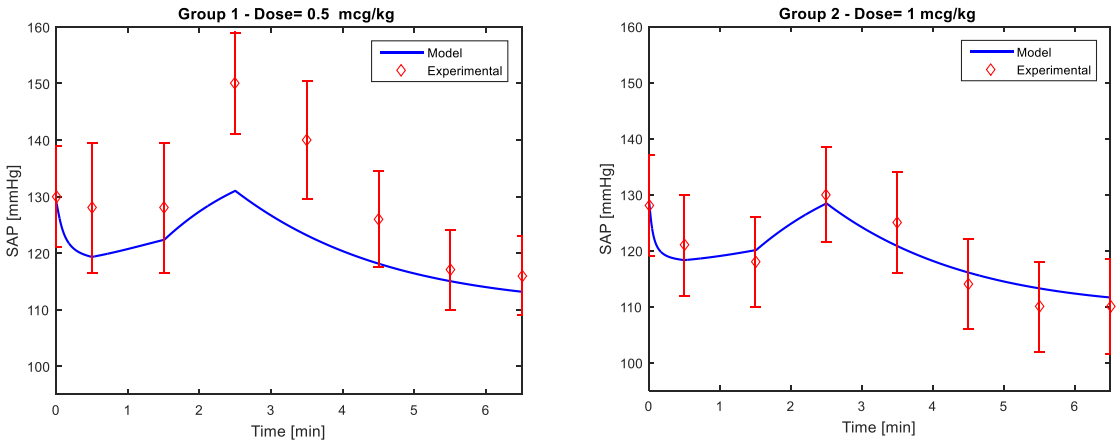

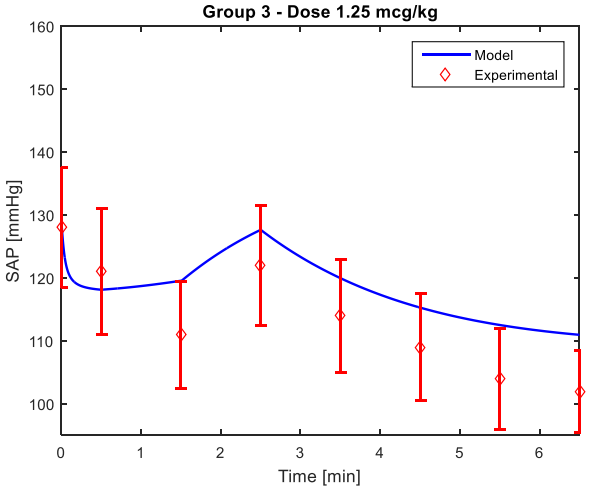

Figure 39 - Comparison between the PD model (blue) and the experimental data (red) of Group 1, 2, and 3 from O'Hare et al. (1999).

The results of the PD model are reasonably good, except for Group 1. The reason may be attributed to the reduced bolus and, therefore, to the low blood concentration of the drug that can affect the results in terms of pharmacologic effect (see Table 25).

Table 25 - $\Delta E_{Max}\%$ and SAE values for Group 1,2, and 3 of O'Hare et al. (1999).

Group	$\Delta E_{Max}\%$	SAE
1	12.650	7.980
2	1.200	2.318
3	4.630	5.976

3.4.3 Case-study 3: Park et al. (2011)

With the aim of finding the optimal dose of remifentanil to mitigate the cardiovascular responses to tracheal intubation, Park *et al.* (2011) administered doses of 0.5 µg/kg/min or 1 µg/kg/min over 30 s to 48 pregnant women with severe pre-eclampsia. This condition is the reason why the baseline is particularly high.

The patients were lumped into two groups. Fig. 40 shows the results of the PD model compared to the measured SAP.

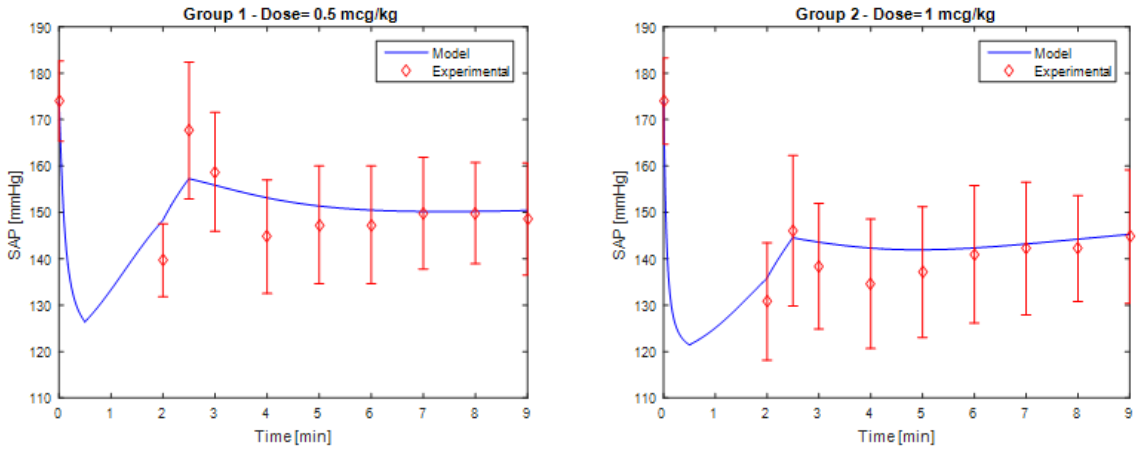

Figure 40 - Comparison between the PD model (blue) and the experimental data (red) of Group 1 and 2 from Park et al. (2011).

The model is capable to predict the peak effect with a rather good precision. In addition, the simulated response follows the central values of the standard deviation band for most of the experimental data.

Table 26 - $\Delta E_{Max}\%$ and SAE values for Group 1 and 2 of Park et al. (2011).

Group	$\Delta E_{Max}\%$	SAE
1	6.170	4.017
2	1.020	2.919

3.4.4 Case-study 4: Nora et al. (2007)

Nora *et al.* (2007) investigated the influence of the dosing regimen of remifentanil on the ability of attenuation of the response to intubation. Even if only three experimental data registered in three representative moments are available, it is still interesting to evaluate the prediction capability of the model. Thirty adult patients were administered 0.3 µg/kg/min of remifentanil as intravenous infusion for the duration of the operation. Fig. 41 shows the results of the simulations of two groups of patients. The difference between Group 1 and Group 2, which respectively represent and lump two groups of 15 patients each, is in the time of the induction of anesthesia. For Group 2 the induction starts 2 min later, as can be observed in Figure 41.

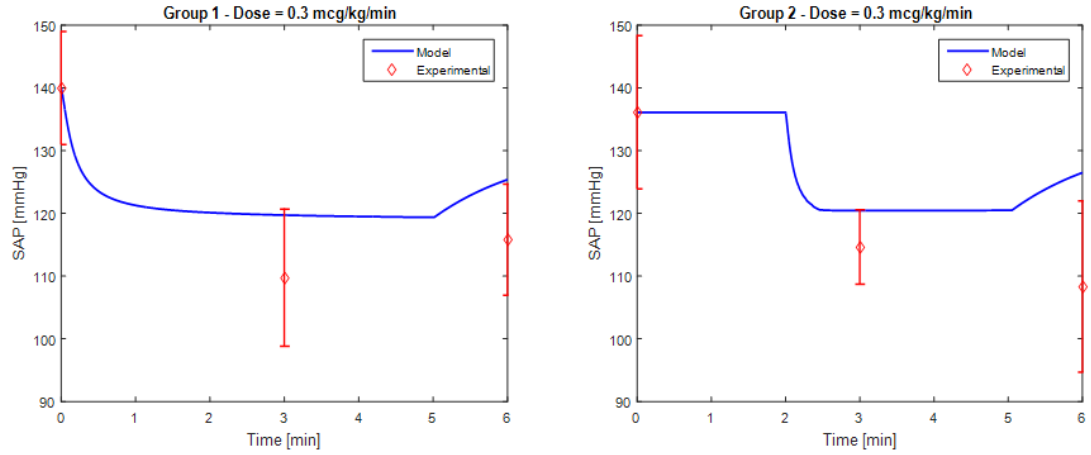

Figure 41 - Comparison between the PD model (blue) and the experimental data (red) of Group 1 and 2 of Nora et al. (2007).

The model produces better results in the first case. However, in both cases the accuracy is acceptable (see also Table 27).

Table 27 - $\Delta E_{Max}\%$ and SAE values for Group 1 and 2 of Nora et al. (2007).

Group	$\Delta E_{Max}\%$	SAE
1	10.430	7.994
2	8.310	6.526

3.4.5 Conclusions

In general, the model is capable to predict the measured SAP with reasonable accuracy for a sufficiently wide range of doses, different dose regimens, and patients in different conditions, which is confirmed by the low values of the SAE of all the case studies. Moreover, the values of $\Delta E_{Max}\%$ are always below 15%, which shows a satisfactory capability in the peak-effect prediction.

Nonetheless, it is worth highlighting that the model was validated for patients with awake baseline in the 135-175 mmHg range. Therefore, it is not recommendable to extrapolate this model to patients with baseline values outside of that range.

3.5 Results and discussion – MAP model

3.5.1 Case-study 1: Hall et al. (2000)

Hall *et al*. (2000) studied 60 female patients, aged 20-65, undergoing laryngoscopy. The patients were lumped in two groups. Group 1 received a bolus dose of 1 µg/kg for 30 s followed by an infusion of 0.5 µg/kg/min, while Group 2 received a bolus dose of 0.5 µg/kg for 30 s followed by an infusion of 0.25 µg/kg/min for the whole duration of the surgery.

Fig. 42 shows the comparison between the simulated PD curve and the experimental data.

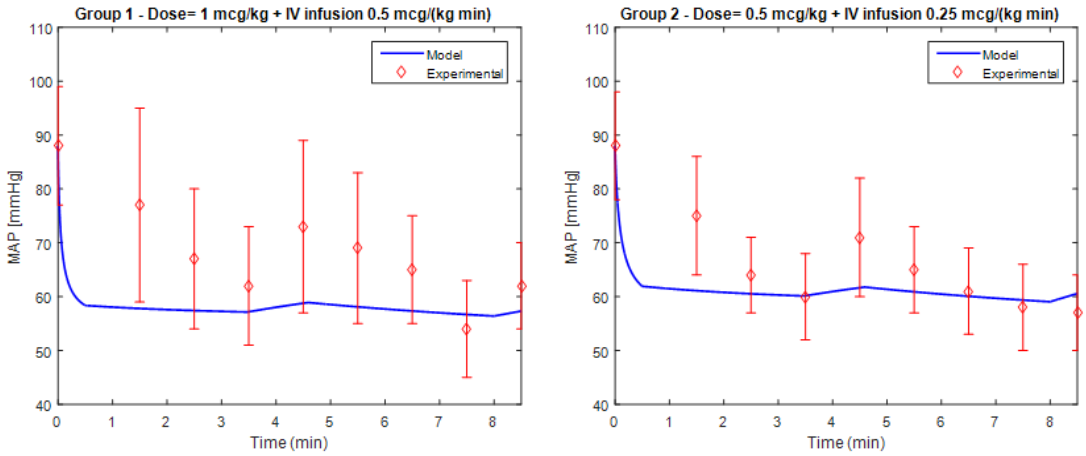

Figure 42 - Comparison between the PD model (blue) and the experimental data (red) of Group 1 and 2 from Hall et al. (2000).

It is worth observing that the model can represent the trend of the experimental data and that the curve always belongs to the standard deviation bands, except for the phase that comes first the intubation procedure (see also Table 28).

Table 28 - $\Delta E_{Max}\%$ and SAE values for Group 1 and 2 of Hall et al*. (2000).*

Group	$\Delta E_{Max}\%$	SAE
1	19.300	8.193
2	13.000	4.095

3.5.2 Case-study 2: Alexander et al. (1999)

Alexander *et al*. (1999) compared the remifentanil capability of tempering the cardiovascular response to intubation by administering three different boluses (3, 4, and 5 μg/kg for 10 s) to 50 patients undergoing laryngoscopy. The patients were divided into 3 groups: the first one consisted of 12 patients, and the other 2 of 19 patients each.

Fig. 43 shows the results of the PD model and the experimental data.

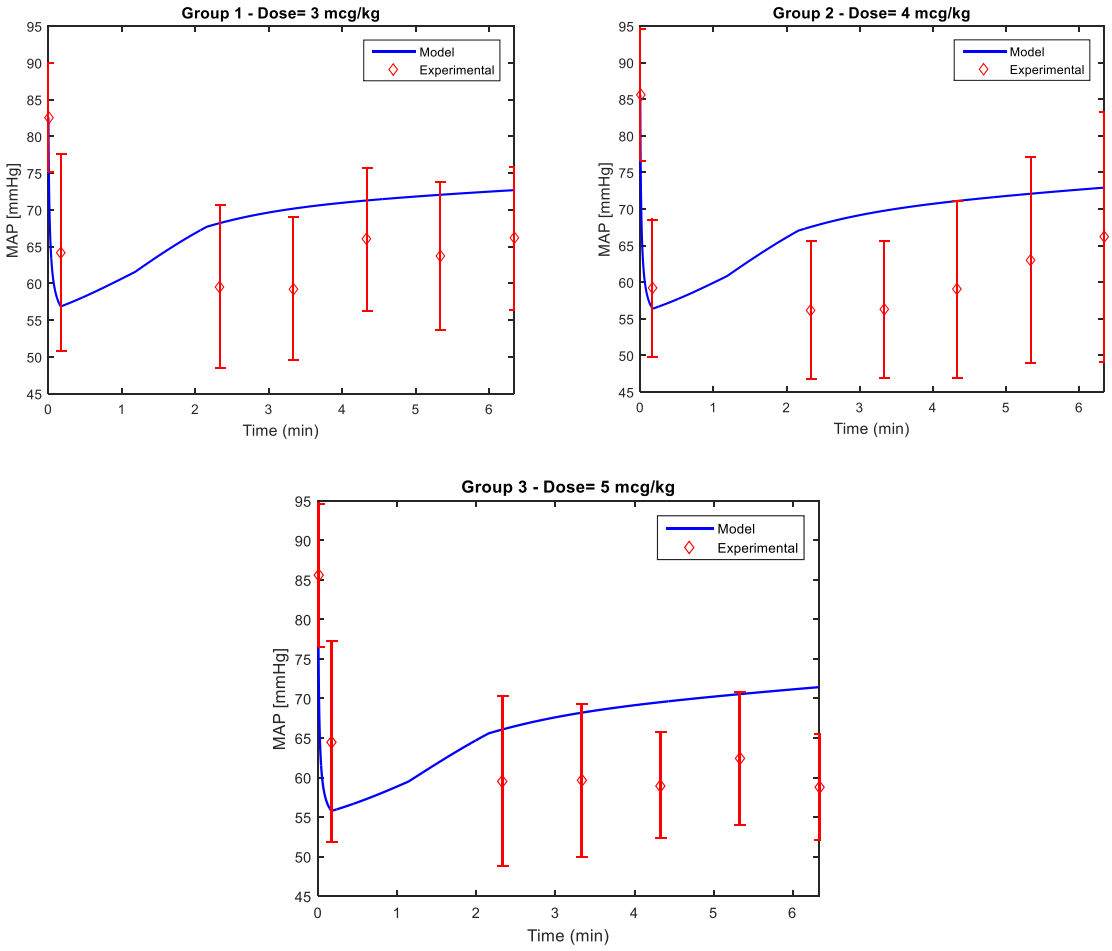

Figure 43 - Comparison between the PD model (blue) and the experimental data (red) of Group 1, 2, and 3 from Alexander et al. (1999).

The model curve belongs to the standard deviation bands for most of the experimental measurements. Compared to the previous cases of study, it is more difficult to detect the stress response to intubation both in the experimental and simulated values (see also Table 29). This may be attributed to the high doses of administered boluses, even though their duration is pretty short, *i.e.* 10 s.

Table 29 - $\Delta E_{Max}\%$ and SAE values for Group 1, 2, and 3 of Alexander et al. (1999).

Group	$\Delta E_{Max}\%$	SAE
1	13.700	6.712
2	19.170	7.933
3	10.000	7.889

3.5.3 Case-study 3: Batra et al. (2004)

Batra *et al.* (2004) investigated the possibility of combining propofol and remifentanil to attenuate the cardiovascular stress response to tracheal intubation in 40 children aged 5-10, who received 2 or 3 µg/kg for 30 s.

Fig. 44 shows the results of the PD model compared to the experimental data. Group 1 and 2 lump the patients according to the administered dose.

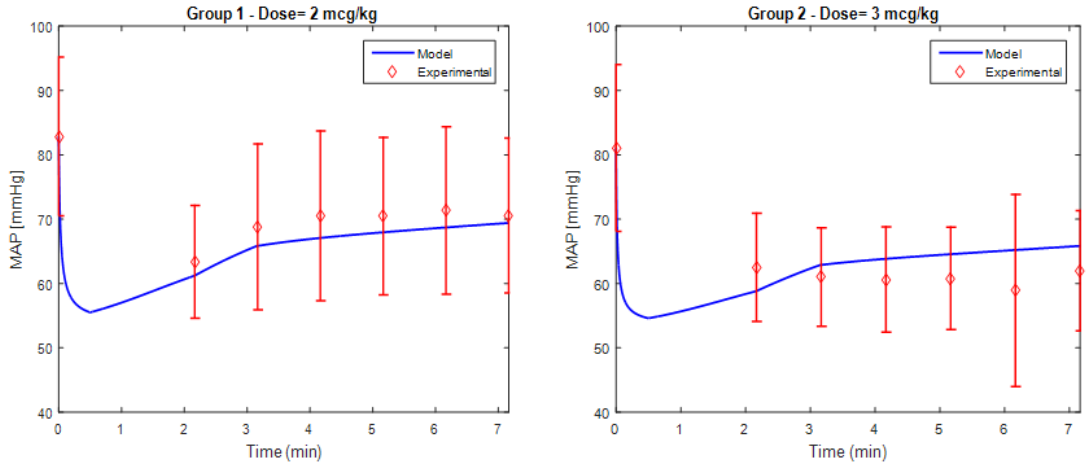

Figure 44 - Comparison between the PD model (blue) and the experimental data (red) of Group 1 and 2 from Batra et al. (2004).

As for Alexander *et al.* (1999), the increase of the blood pressure following intubation is not significant. Again, it is possible to assume that this is due to the high bolus doses, which are in fact out of the clinical dosage range (see Paragraph 1.4). It is worth observing that the simulated curve falls within the standard deviation bands of the experimental data (see also Table 30).

Table 30 - $\Delta E_{Max}\%$ and SAE values for Group 1 and 2 of Batra et al. (2004).

Group	$\Delta E_{Max}\%$	SAE
1	4.340	2.170
2	3.070	3.150

3.5.4 Conclusions

The proposed pharmacodynamic model is able to predict the pharmacological effect of remifentanil in terms of MAP during anesthesia and, in particular, intubation with reasonably good results. Indeed, the maximum error in the prediction of the effect peak is below 20% and the values of the SAE are quite low.

Again, the proposed model should not be used for patients with awake baseline outside the validation range *i.e.* 80-100 mmHg, as it could provide results that significantly deviate from reality.

Both the SAP and MAP models deviate from the experimental data mainly before intubation, which is the phase that immediately follows the induction of anesthesia and therefore the administration of remifentanil. This is an important matter for what will be discussed in Paragraph 3.7.

3.6 Results and discussion – HR model

3.6.1 Case-study 1: Lee et al. (2012)

Paragraph 3.4.1 reports the specific features of the study of Lee *et al*. (2012). Fig. 45 compares the results of the model to the experimental data. Group 1 lumps those, *i.e.* 30 patients, who received remifentanil (see also Table 31).

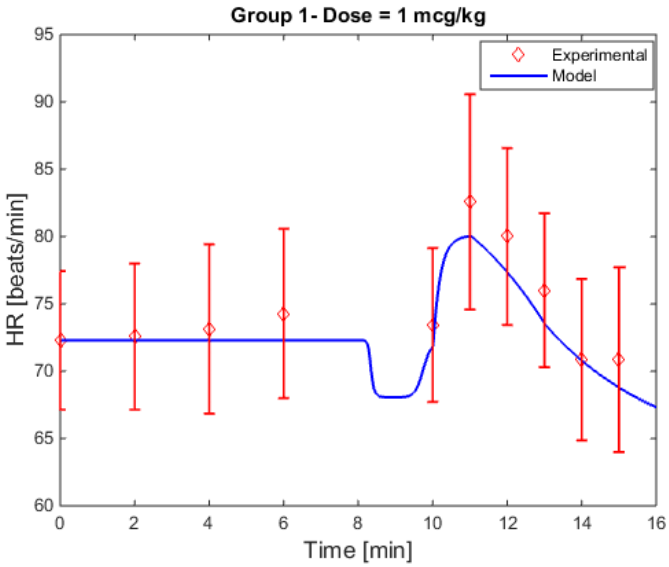

Figure 45 - Comparison between the PD model (blue) and the experimental data (red) of Group 1 of Lee et al. (2012).

Table 31 - $\Delta E_{Max}\%$ and SAE values for Group 1 of Lee et al. (2012).

$\Delta E_{Max}\%$	SAE
3.10	1.45

It is possible to observe that the model gives good results for this case-study, since the values of the performance indexes are low.

3.6.2 Case-study 2: Park et al. (2011)

Paragraph 3.4.3 reported the details of the study of Park *et al*. (2011). Fig. 46 and Table 32 show the results produced by the HR model.

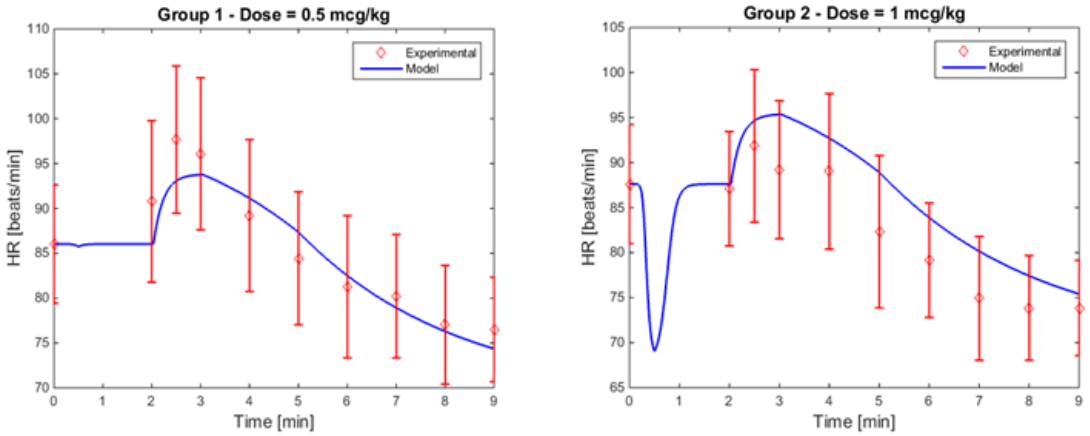

Figure 46 - Comparison between the PD model (blue) and the experimental data (red) of Group 1 and 2 from Park et al. (2011).

Table 32 - $\Delta E_{Max}\%$ and SAE values for Group 1 and 2 of Park et al. (2011).

Group	$\Delta E_{Max}\%$	SAE
1	4.00	2.19
2	3.82	3.48

Also in this case, it is possible to notice that the model is able to predict the HR trend.

3.6.3 Case-study 3: Nora et al. (2007)

Paragraph 3.4.4 reports the specific features of the study of Nora *et al.* (2007). Fig. 47 and Table 33 show the results produced by the HR model.

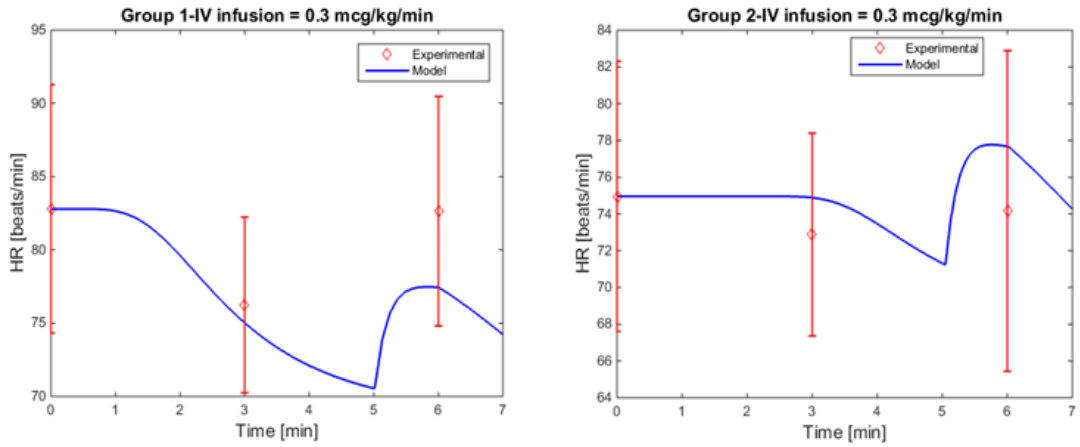

Figure 47 - Comparison between the PD model (blue) and the experimental data (red) from Nora et al. (2007).

Table 33 - $\Delta E_{Max}\%$ and SAE values for Group 1 and 2 of Nora et al. (2007).

Group	$\Delta E_{Max}\%$	SAE
1	1.47	0.19
2	4.87	10.77

The same considerations of case studies 1 and 2 can be extended to this case.

3.6.4 Case-study 4: Hall et al. (2000)

Hall *et al.* (2000) studied the effect of different bolus and infusion regimens on the cardiovascular response to laryngoscopy and orotracheal intubation. Paragraph 3.5.1 reported the main features of that study. Fig. 48 shows the comparison between the model and experimental data.

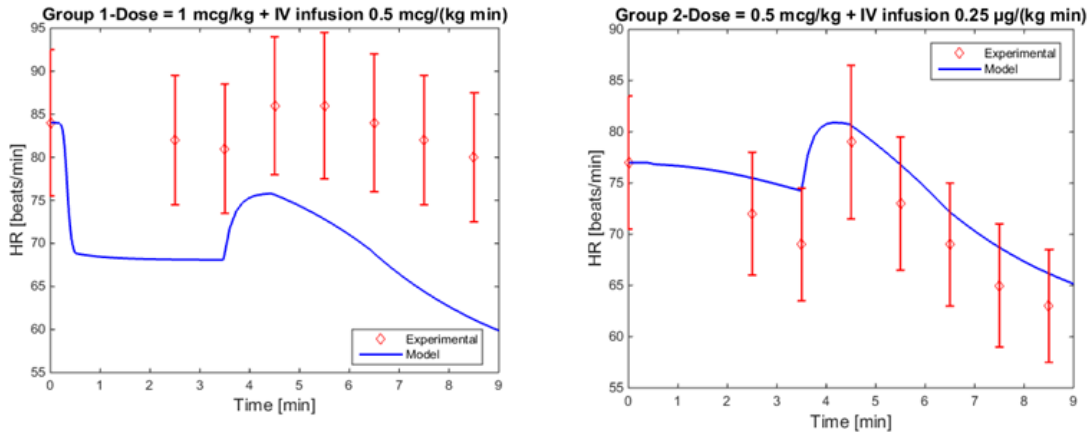

Figure 48 - Comparison between the PD model (blue) and the experimental data (red) of Group 1 and 2 from Hall et al. (2000).

It is evident that the model is able to predict the trend of the experimental data for Group 2, but not for Group 1. This may be related to the fact that the patients of Group 1 received another drug called glycopyrrolate in combination with remifentanil, and this might have had a significant role on their HR.

Table 34 - $\Delta E_{Max}\%$ and SAE values for Group 1 and 2 of Hall et al. (2000).

Group	$\Delta E_{Max}\%$	SAE
1	11.86	12.63
2	2.41	3.03

3.6.5 Case-study 5: Maguire et al. (2001)

Maguire *et al.* (2001) compared the effect of remifentanil and alfentanil on the cardiovascular response to laryngoscopy and tracheal intubation in patients subjected to long-term treatment for hypertension. Forty patients were divided into two groups, who received different analgesics. This work simulated only the remifentanil group. These patients received a bolus of 0.5 µg/kg over 30 s, followed by an intravenous infusion of 0.1 µg/kg/min for the duration of the operation. Fig. 49 shows the results of the model compared to the experimental data, and Table 35 assesses the model quality.

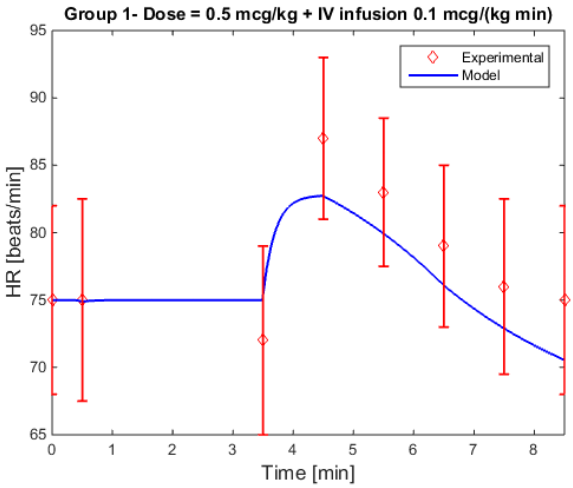

Figure 49 - Comparison between the PD model (blue) and the experimental data (red) of Group1 from Maguire et al. (2001).

Table 35 - $\Delta E_{Max}\%$ and SAE values for Group 1 of Maguire et al. (2001).

$\Delta E_{Max}\%$	SAE
4.91	2.67

3.6.6 Case-study 6: Shajar et al. (1999)

Shajar *et al.* (1999) examined the effect of remifentanil on the hemodynamic response to emergence from anesthesia and tracheal extubation in 20 females. We have assumed that the extubation effect is the same as the intubation from the point of view of stress response. The patients received a bolus of 1 µg/kg over 30 s.

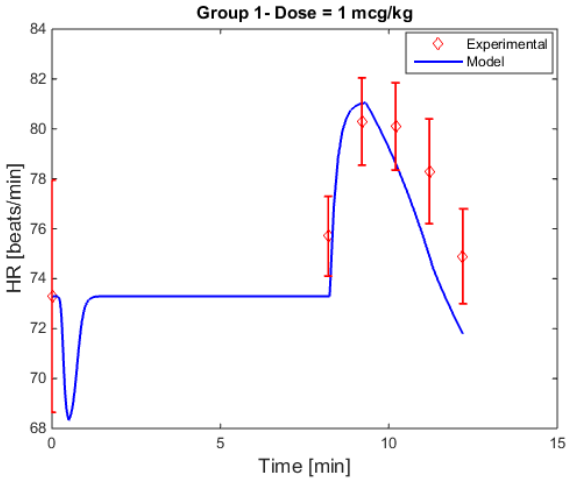

Figure 50 - Comparison between the PD model (blue) and the experimental data (red) of Group 1 from Shajar et al. (1999).

Table 36 - $\Delta E_{Max}\%$ and SAE values for Group 1 of of Shajar et al. (1999).

$\Delta E_{Max}\%$	SAE
0.94	1.85

3.6.7 Conclusions

Analyzing the case studies, it is possible to claim that the proposed PD model is able to predict the evolution of heart rate during anesthesia for laryngoscopy and endotracheal intubation. In fact, the values of SAE and $\Delta E_{Max}\%$ are lower than 11 and 5% respectively, except for the first group of the study of Hall *et al.* (2000), for which a viable explanation was provided.

It is worth reminding that we neglected few measures before intubation for all the analyzed studies (because of the presence of an *emotional* peak in the experimental HR trend). In fact, it is possible to notice that after the drug administration and before the intubation, there is a decrease of SAP and MAP effect, which is not present in HR simulations. This means that the lack of measured values before intubation may affect the parameters identification procedure and alter the dependence of the effect from the drug concentration. However, it is interesting to notice that the model is able to

predict the pharmacological effect of remifentanil on HR in case of different dose regimens.

3.7 Limitations of the PD model

As mentioned above, the deviation of the predicted hemodynamic effects from the measured values is particularly evident before intubation. For instance, Fig. 51 shows the results of the MAP simulation for Groups 1 and 2 in Hall *et al.* (2000), with a focus on that phase, which occurs at 3.5 min.

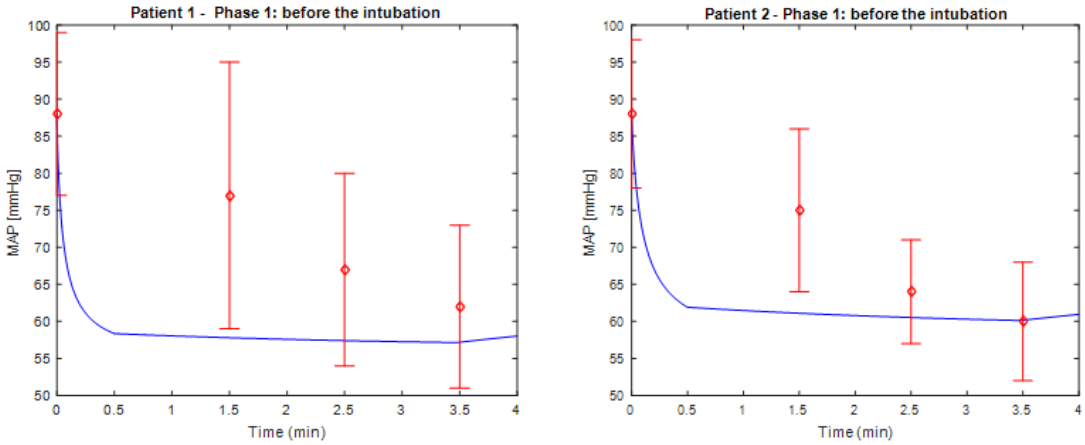

Figure 51 - Anticipation of the model in the prediction of the effect respect to the experimental data. Experimental MAP (red) of Group 1 and 2 from Hall et al. (2000) study.

It is worth observing that for both groups there is an anticipation in the MAP decrease due to the administration of remifentanil.

This phase is the one that immediately follows the induction of anesthesia by the administration of the reference drug. No stress response is evident because intubation has not been performed yet, and as in most cases a bolus is administered, the drug effect is more important in this phase. The reason why intubation is not performed immediately after the anesthesia induction is that although the plasma concentration of the drug reaches a peak within few minutes from the administration (*i.e.* 1.5 min in case of remifentanil), there is a delay between the time of the peak and the time at which the patient reaches unconsciousness. This is the time required for the distribution of the drug from the plasma to the tissues and, in this particular case, to the brain.

The proposed pharmacodynamic model links the pharmacologic effect in terms of MAP, SAP, and HR to the plasma concentration of the drug. This means that conventional pharmacodynamic models are not able to incorporate this delay (*i.e.* a time delay according to the process control terminology) and therefore there will be an anticipation of the simulated drug effects respect to ones recorded experimentally. Remifentanil is a rapidly equilibrating drug (see also Paragraph 1.4). Consequently, the fact that the model does not take into account such time delay is still acceptable.

However, a model that aims at correctly predicting the pharmacological effect of a drug should be able to incorporate such a time delay. This is possible by introducing a virtual compartment called 'Effect-site compartment', which leads to the development of a combined pharmacokinetic-pharmacodynamic model. The features and role of this compartment will be widely discussed in Paragraph 4.1, and the deployment of a 6P PK-PD model is the main object of Chapter 4.

4. A COMBINED PK-PD MODEL

4.1 Combined models and effect-site compartment

Between the '60s and the beginning of '70s of last century, a few authors (Levy (1964); Wagner (1968); Gibaldi (1971); Gibaldi and Levy (1972)) proposed some relations to account for the interaction between drugs pharmacokinetics and pharmacological effect. In fact, they observed that in several cases, the magnitude and the effect onset/offset were related to the drug concentration-time profile in the human body. However, it was also noticed that in some other cases, the pharmacological effect of the drug lagged behind the concentration in the plasma. This observation induced to think that there was no relation between the effect and the concentration of the drug in the plasma. The solution was found in the '80s by Sheiner and co-workers (Sheiner *et al.* (1979); Holford and Sheiner (1982)) grounded on the original idea of Segre (1968) who proposed using a hypothetical effect-site compartment to account for the delay (Meibohm and Derendorf, 1997). Since then, pharmacokinetic-pharmacodynamic (PK-PD) models have evolved and are today an essential tool in pharmacology (Leil and Bertz, (2014); Leil and Ermakov, (2015)).

PK-PD models are in fact the integration of pharmacokinetic models and pharmacodynamic models. In pre-clinical studies, PK-PD simulations can be used for instance to interpret toxicokinetic data and extrapolate results from animals to humans via allometric scaling (provided that the PK model is physiologically based). In clinical testing, PK-PD simulations can be used for the optimization of the dose, its administration, and the interpretation of the dose-response relation. In fact, PK-PD models are not meant to describe phenomena but rather to predict distinct situations. This is why they are particularly effective in testing multiple dosing schemes and/or different routes of administration, escalating-dose studies, and exploring the effect of interaction among drugs. It is easy to see the great potential that these combined models can have throughout the phases of drugs R&D.

For some drugs, the previously mentioned delay between plasma concentration and effect produces a hysteresis in the effect- plasma concentration plots. This delay is due to the time required for the distribution of the drug to the site of action and can be taken into account by considering the addition of a virtual compartment called 'effect-site compartment', which represents the drug site of action. In general, the drug concentration in the action site cannot be measured. First, because it is usually inaccessible, at least in humans, as it would be invasive. Secondly, even if it was possible to take tissue samples, the drug concentration in the microscopic environment of the receptive molecules would not be the same as the concentration approximately measured in, for instance, ground brain or cerebrospinal fluid (CSF). Another quite

challenging issue would be dynamically sampling those tissues to follow their pharmacokinetics. This is why the effect-site strategy is recommended.

Fig. 52 shows how the effect-site compartment allows linking/connecting the PK and PD models.

Figure 52 - Schematic representation of a combined PK-PD model. The effect-site compartment connects the PK model to the PD model.

Mathematically, the effect-site compartment calls for the addition of a differential equation to the 6P PK model (Paragraph 2.2):

$$\frac{dC_e(t)}{dt} = k_{e0} \cdot C_p - \ k_{e0} \cdot C_e \tag{58}$$

Where k_{e0} [min^{-1}] is a first-order distribution rate constant (Hull *et al.* (1978); Egan *et al.* (1996); Dershwitz *et al.* (1996); Standing *et al.* (2010); Felmlee *et al.* (2012)), analogous to a first-order kinetic constant, C_p [ng/mL] is the plasma concentration, C_e [ng/mL] is the effect-site compartment concentration.

k_{e0} quantifies the delay between the plasma concentration and the effect-site compartment concentration (Fig. 53). This topic is discussed in more details in Paragraph 4.2. It is necessary to compute a different k_{e0} value for each pharmacological effect that is modeled (see Paragraph 4.3-4.4-4.5). Furthermore, the value is identified with a specific set of experimental data, but will be valid for any treatment or dose.

The effect will depend on the effect-site concentration derived from Equation 58 and not on the drug concentration in the plasma. By doing so, it is possible to introduce the above-mentioned delay between the plasma concentration and the resulting effect on specific organs/tissues.

Equations (59-61) describe the dynamic evolution of MAP and SAP:

$$E_1 = E_0 - |E_{max} - E_0| \cdot \frac{{C_e}^{\gamma}}{{C_e}^{\gamma} + {EC_{50}}^{\gamma}} \tag{59}$$

$$E_2 = E_0 - |E_{max} - E_0| \cdot \frac{{C_e}^{\gamma}}{{C_e}^{\gamma} + {EC_{50}}^{\gamma}} + Delta \cdot K_p \cdot \left(1 - e^{-\frac{t - t_{int}}{\tau_1}}\right) \tag{60}$$

$$E_3 = E_0 - |E_{max} - E_0| \cdot \frac{C_e^{\gamma}}{EC_{50}^{\gamma} + C_e^{\gamma}} + Delta \cdot K_p \cdot \left(1 - e^{-\frac{t-t_{int}}{\tau 1}}\right) - Gamma \cdot K_p \cdot \left(1 - e^{\frac{t-t_{max}}{2\tau_1}}\right) \quad (61)$$

Equations (62-65) describe the dynamic evolution of HR:

$$E_1 = E_0 - |E_{max} - E_0| \cdot \frac{{C_e}^{\gamma}}{{C_e}^{\gamma} + {EC_{50}}^{\gamma}} \quad (62)$$

$$E_2 = E_0 - |E_{max} - E_0| \cdot \frac{C_e^{\gamma}}{EC_{50}^{\gamma} + C_e^{\gamma}} + Delta \cdot K_p \cdot \left(1 - e^{-\frac{t-t_{int}}{\tau_1}}\right) \quad (63)$$

$$E_3 = E_0 - |E_{max} - E_0| \cdot \frac{C_e^{\gamma}}{EC_{50}^{\gamma} + C_e^{\gamma}} + Delta \cdot K_p \cdot \left(1 - e^{-\frac{t-t_{int}}{\tau_1}}\right) + Delta \cdot K_p \cdot \left(1 - e^{\frac{t-t_{max}}{\tau_2}}\right) \quad (64)$$

$$E_4 = E_0 - |E_{max} - E_0| \cdot \frac{C_e^{\gamma}}{EC_{50}^{\gamma} + C_e^{\gamma}} + Delta \cdot K_p \cdot \left(1 - e^{-\frac{t-t_{int}}{\tau_1}}\right) + Delta \cdot K_p \cdot \left(1 - e^{\frac{t-t_{max}}{\tau_2}}\right) + \frac{E_0 - E_{0,opt}}{E_0} \cdot E_{0,opt} \cdot \left(1 - e^{-\frac{t-t_{end}}{\tau_2}}\right) \quad (65)$$

It would be intuitive to think of the brain as the effect-site compartment for an opioid. However, Piacevoli *et al.* (2015) investigated this subject by using brain microdialysis over nine patients scheduled for elective intracranial surgery for cerebral neoplasia and found no correlation between plasma concentration and cerebral extracellular fluid/cerebrospinal fluid concentration. Therefore, consistently with the majority of the authors, they concluded that the effect-site compartment *"has to be considered a virtual compartment",* with no relation to a real organ or tissue.

It is in fact important to underline that the addition of the effect-site compartment does not affect the pharmacokinetics of the drug in the human body.

4.2 Evaluation of the distribution rate constant k_{e0}

As previously mentioned, the delay between plasma concentration and pharmacological effect results in the formation of a hysteresis loop in the effect- plasma concentration plot (Fig. 53).

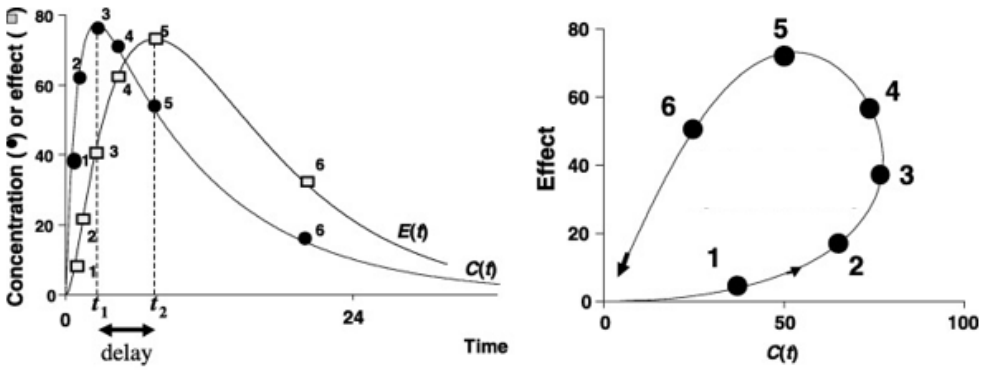

Figure 53 - On the left, dynamic evolution of the plasma concentration and the effect in time. It is possible to detect a delay between the peak concentration and the peak effect. On the right, the hysteresis loop between the effect and the plasma concentration, due to the fact that blood is only the mechanism of transport, not the site of action. (Taken from Toutain and Lees, 2005).

This hysteresis is in fact the clinical manifestation that the plasma is not the site of action of the drug, which means that the hysteresis loop in the effect-plasma concentration plot has a physiological meaning. On the other hand, the hysteresis that can be detected in the effect-effect site concentration plot for initial values of the k_{e0}, has no physiological meaning. Actually, in this plot there should not be any hysteresis because the effect-site compartment represents the site of action, which means that the drug concentration peak in this compartment should correspond to the effect peak. In fact, in the reality no delay is present between the drug peak concentration in the site of action and the clinical manifestation of the pharmacological effect.

The "hysteresis loop minimization" technique (Egan *et a*l., 1996) comes from these considerations.

The hysteresis between effect-site concentration and effect can be collapsed by varying the value of k_{e0}, so that the peak in the site of action physically corresponds to the peak of the pharmacological effect of the drug. The predicted effect can be obtained from the PD models developed, in terms of HR, SAP, and MAP. The error between the predicted and measured effect is calculated as follows:

$$Error = \sum_{i=1}^{N_s}\sum_{j=1}^{N_p}\sum_{l=1}^{N_m}\left(\frac{\left|Effect_{i,j,l}^{exp} - Effect_{i,j,l}^{mod}\right|}{N_m}\right) \quad (66)$$

Where N_s is the number of studies, N_p the number of patients of the *k-th* case-study, and N_m the number of measured values of the effect.

The optimal value of k_{e0} solves the following "hysteresis loop minimization" problem:

$$\underset{k_{e0}}{\text{Min}} \sum_{i=1}^{N_s} \sum_{j=1}^{N_p} \sum_{l=1}^{N_m} \left(\frac{\left| Effect_{i,j,l}^{exp} - Effect_{i,j,l}^{mod} \right|}{N_m} \right) \tag{67}$$

Fig. 54 shows the evolution of the concentration of remifentanil in the plasma and in the effect-site compartment. Demographic data to obtain the profiles come from Thompson *et al* (1998), who administered a single bolus of 1 µg/kg over 30 s followed by an infusion of 0.5 µg/kg/min for the procedure duration, with the aim of studying the response to orotracheal intubation on a group of ten patients. This plot was obtained after finding the optimal value of k_{e0}, based on the "hysteresis loop minimization technique" and refers to Group 1 that lumps the ten patients of the study.

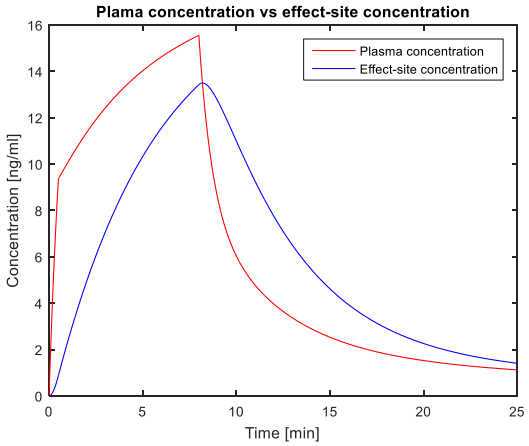

Figure 54 - Comparison between the simulated concentration-time profiles in the plasma (red) and effect-site (blue) compartment.

Fig. 54 shows that not only there is a delay in the peaks, even if rather small, but also the main difference between the profiles is in the velocity of the increment (*i.e.* their derivatives). In fact, the effect-site concentration increases less steeply compared to the plasma concentration profile of the reference drug.

It is worth noticing that at the beginning the derivative of the profile of the effect-site concentration is null. This happens because the first term in Equation 58 is near zero in the first moments that follow the remifentanil administration, while the second term is null because the distribution process to the effect-site compartment has not begun. This null-derivative behavior is typical of second order systems in Process Control. Fig. 54 shows that the profile of the effect-site concentration is analogous to the behavior of two interacting first order systems (*e.g.*, two interacting tanks).

For the sake of clarity, we underline that the plasma concentration curve presents two sharp corners. The first occurs 30 s after the beginning of the dose administration and corresponds to the change of the drug administration way (*i.e.* from bolus injection to

continuous infusion). The second occurs after 8 min and corresponds to the end of remifentanil infusion.

4.3 Application to SAP

The initial value estimate for k_{e0} was chosen according to graphical data analysis and it is equal to 0.5. Fig. 55 shows the results of the optimization procedure.

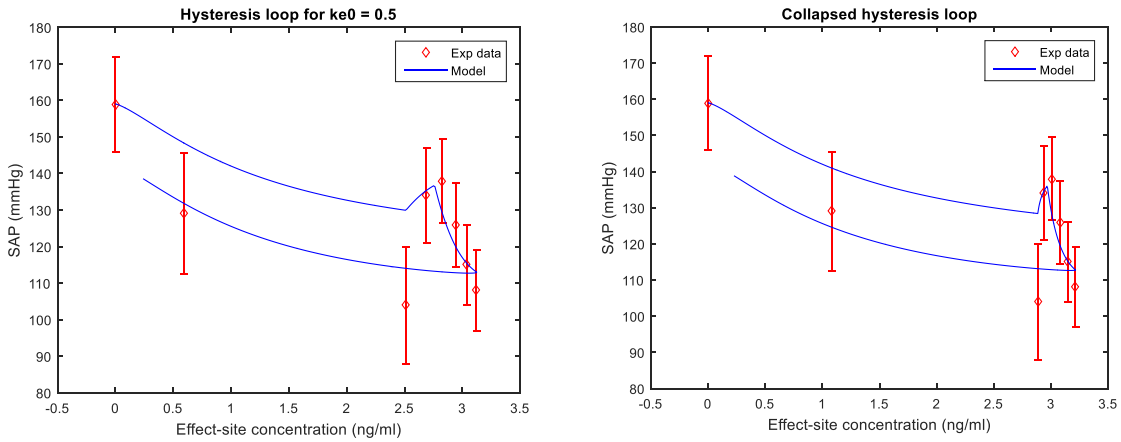

Figure 55 - The left figure shows the hysteresis loop before the optimization procedure. The right figure shows the collapsed hysteresis loop after the optimization procedure. Experimental data (red) from Maguire et al. (2001).

On the left, it is possible to see the hysteresis loop between SAP and concentration in the effect-site for k_{e0} equal to the initial estimate while on the right the final, collapsed hysteresis loop. It is possible to observe that the initial value was a good estimate, as the loop is already rather collapsed. It is more difficult to detect the loop in the case of these experimental data because of the presence of the stress response to intubation, which can be misleading. Again, the experimental data come from Maguire *et al.* (2001).

The optimal value of k_{e0} is 0.9994. This value is consistent with the fact that remifentanil is a rapidly equilibrating drug (Chapter 1).

Subsections 4.3.1, 4.3.2, 4.3.3 compare the results of the PD model to the results of our combined 6P PK-PD model, by analyzing the case studies already discussed in Chapter 3.

4.3.1 Case-study 1: Lee et al. (2012)

Fig. 56 shows the results of the PD model compared to the results of the 6P PK-PD model in simulating the measured SAP of group 1 from Lee *et al.* (2012).

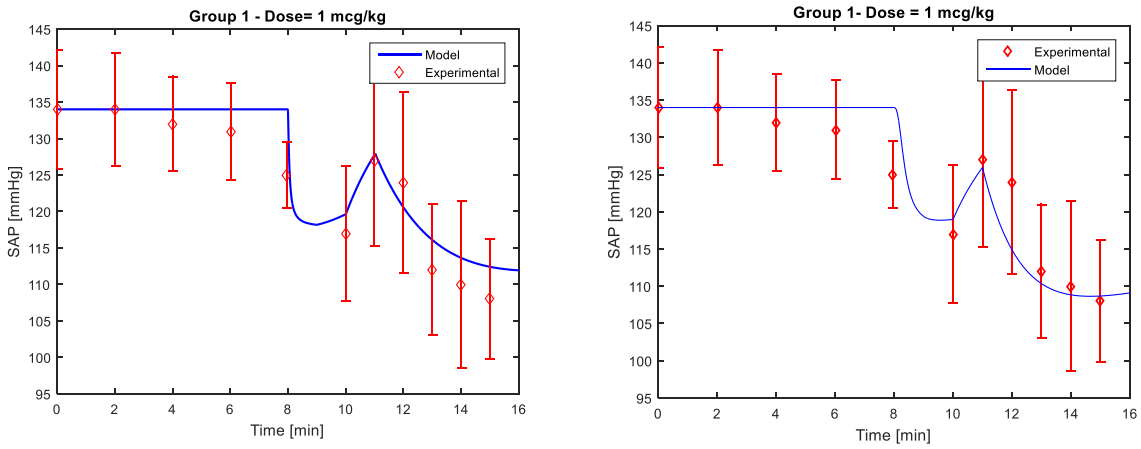

Figure 56 - On the left, the results of the PD model. On the right, the results of the combined 6P PK-PD model. Experimental data come from Lee et al. (2012). The administered dose was 1 µg/kg as a single bolus over 1 min.

It is possible to observe that the precision of the model is still acceptable, even if a worsening of the performance indexes can be noticed (see Table 37). The difference between the PD and 6P PK-PD curves can be highlighted immediately after the administration, which occurs at time 8 min. In fact, the drop in the SAP due to the administration of the opioid is not so steep for the 6P PK-PD model as the one produced by the PD model. The 6P PK-PD simulation is smoother and therefore more realistic. As in Chapters 2 and 3, specific performance indexes were evaluated to verify the reliability of the combined PK-PD model: $\Delta E_{Max}\%$ and SAE (see Table 37).

Table 37 - Values of the performance indexes for Lee et al. (2012). Left column, values for PD model. Right column, values for 6P PK-PD model.

Performance index	*PD Model*	*6P PK-PD Model*
$\Delta E_{Max}\%$	0.72	0.83
SAE	2.995	2.70

4.3.2 Case-study 2: O'Hare et al. (1999)

Fig. 57 shows the results of the PD model compared to the results of the 6P PK-PD model in simulating the measured SAP of three groups from O'Hare *et al.* (1999).

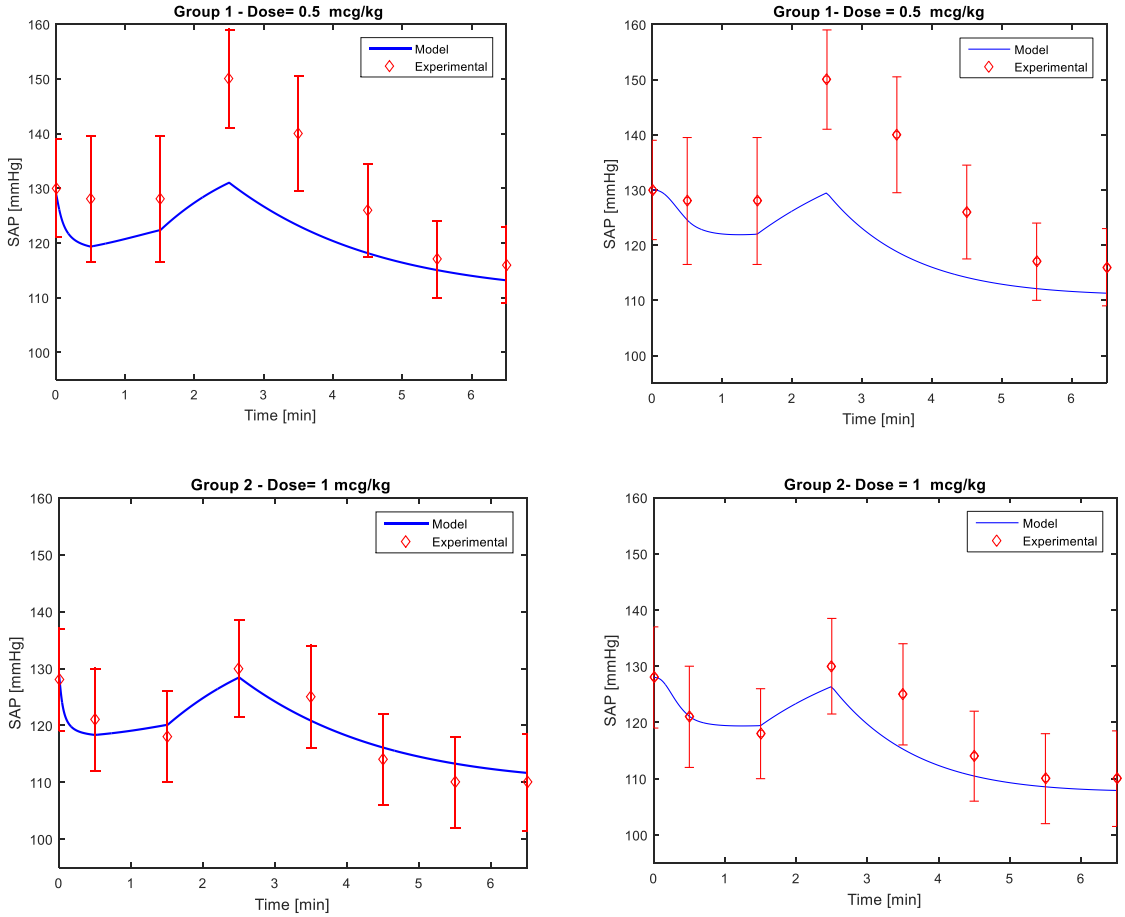

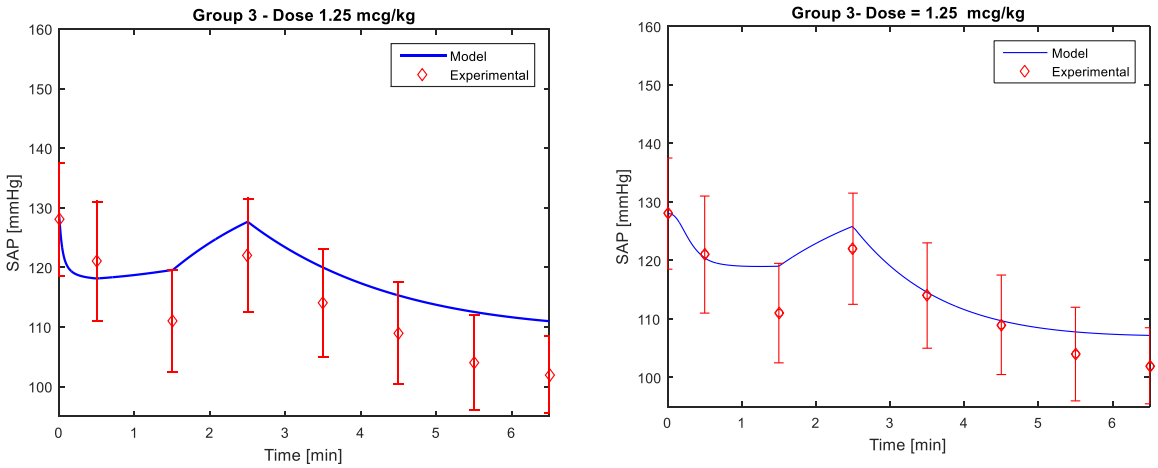

Figure 57 - The left portion shows the results of the PD model. The right portion shows the results of the combined model. Experimental data come from O' Hare et al. (1999). The patients were divided in three groups and received increasing doses as single bolus over 30 s.

The same considerations discussed for case-study 1 are valid. In fact, the minimum effect of the combined model curve, which is due to the administration of the drug, does not exactly correspond to the peak concentration of the drug. It is possible to observe that both models show rather bad results in simulating Group 1, the one who was administered with the lowest dose.

Table 38 lists the values of $\Delta E_{Max}\%$ and SAE.

Table 38 - Values of the performance indexes for O'Hare et al. (1999). Left column, values for PD model. Right column, values for 6P PK-PD model.

Performance index	*Group*	*PD model*	*6P PK-PD model*
$\Delta E_{Max}\%$	1	12.65	13.70
	2	1.20	2.80
	3	4.30	3.10
SAE	1	7.98	9.09
	2	2.32	2.77
	3	5.98	2.81

4.3.3 Case-study 3: Park et al. (2011)

Fig. 58 shows the results of the PD model compared to the results of the 6P PK-PD model in simulating the measured SAP of Groups 1 and 2 from Park *et al.* (2011).

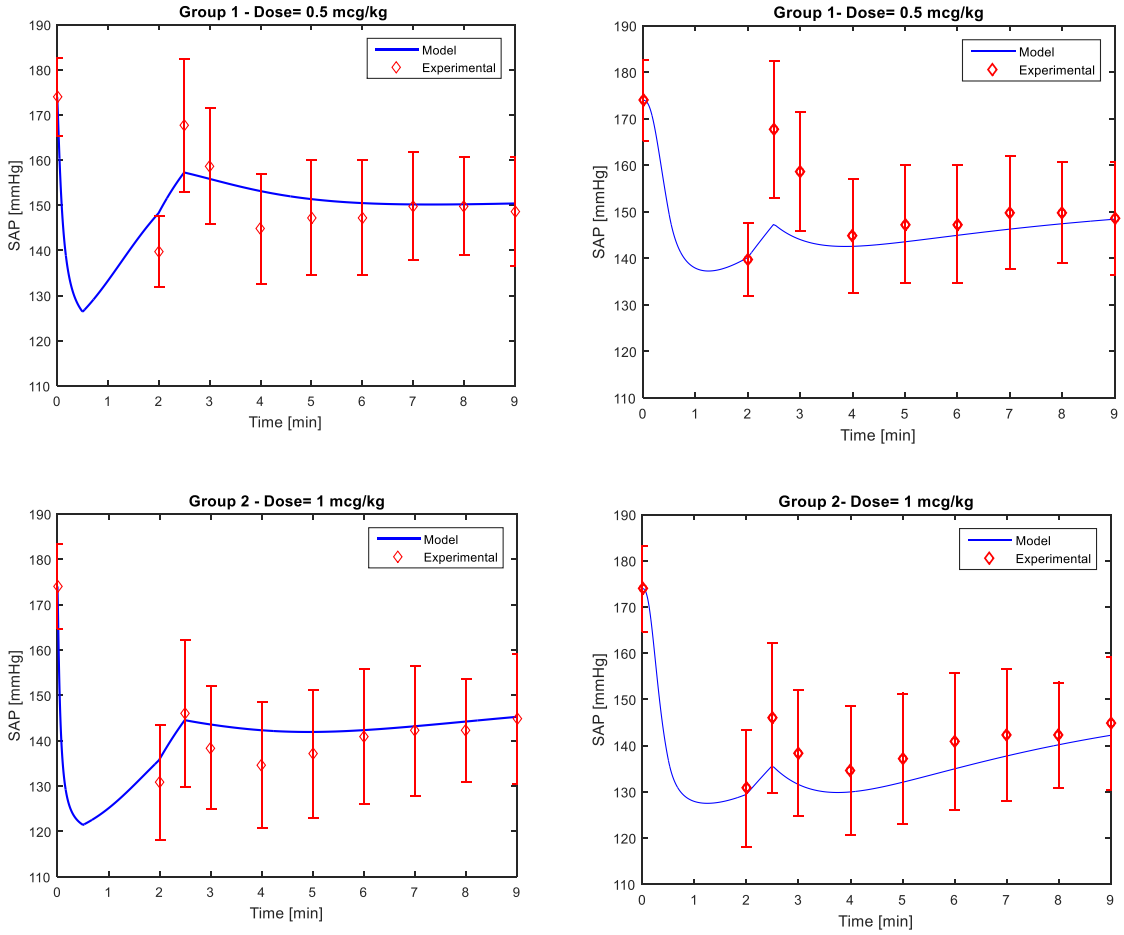

Figure 58 - The left portion shows the results of the PD model. The right portion shows the results of the combined model. Experimental data from Park et al. (2011). The patients were divided in two groups and received two different doses as single bolus over 30 s.

Even if the 6P PK-PD model curves follow the trends of experimental data and are pretty near to the central value of the standard deviation band, for the majority of the measured concentrations, the model fails to reproduce the peak of the stress response to intubation of Group 1. However, the error in the representation of the peak is still acceptable (lower than 15%, as reported in Table 39). The SAE values are actually lower for the PD model but the difference is not numerically significant (see Table 39).

Table 39 - Values of the performance indexes for Park et al. (2011). Left column, values for PD model. Right column, values for 6P PK-PD model.

Performance index	*Group*	*PD Model*	*6P PK-PD Model*
$\Delta E_{Max}\%$	1	6.17	12.15
	2	1.02	7.19
SAE	1	4.02	5.01
	2	2.92	4.34

4.3.4 Case-study 4: Nora et al. (2007)

Fig. 59 shows the results of the PD model compared to the results of the 6P PK-PD model in simulating the measured SAP of Groups 1 and 2 from Nora *et al.* (2007). These two groups received the same dose, but the infusion started at different times (*i.e.* 0 min and 2 min, respectively).

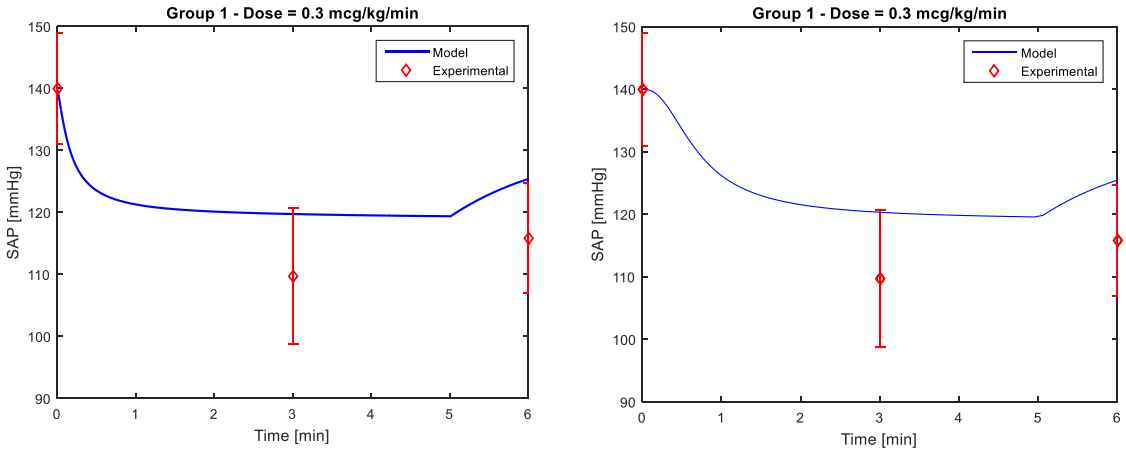

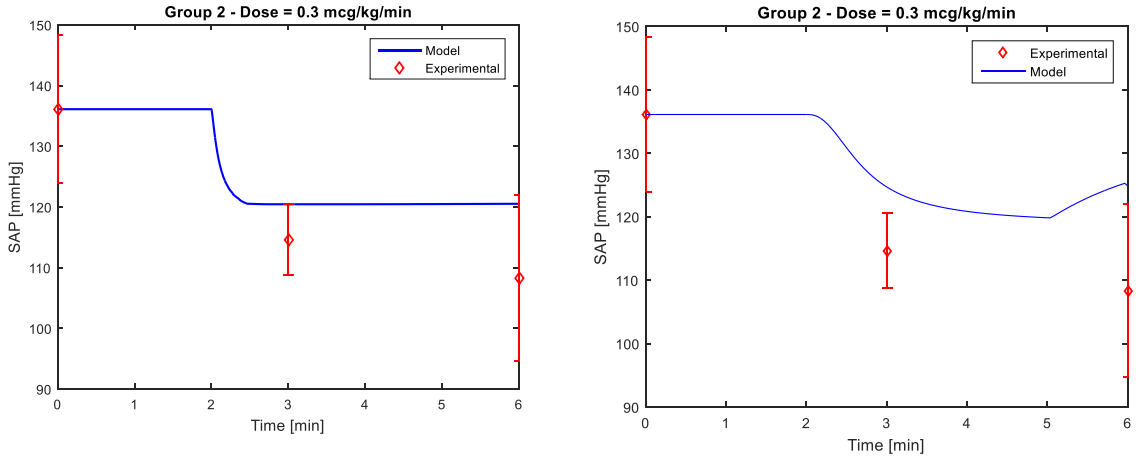

Figure 59 - The left portion shows the results of the PD model. The right portion shows the results of the combined model. Experimental data come from Nora et al. (2007). The difference between the groups is the time at which the remifentanil administration start

The results are similar, even if there appears to be a worsening in the ability of prediction of the SAP of Group 2 in case of the PK-PD model (see Table 40).

Table 40 - Values of the performance indexes for Nora et al. (2007). Left column, values for PD model. Right column, values for 6P PK-PD model.

Performance index	*Group*	*PD Model*	*6P PK-PD Model*
$\Delta E_{Max}\%$	1	8.31	8.34
	2	10.34	9.28
SAE	1	7.99	6.74
	2	6.53	8.86

4.3.5 Conclusions

With reference to the SAP simulation, in some case studies the performance indexes are better for the PD model than for the combined 6P PK-PD model. However, the instantaneous drop of the SAP when simulated by the PD model clearly does not correspond to reality. For this reason, the use of such a model for purposes of finding the optimal dose or comparing different dose regimens may lead to wrong conclusions. Still, it is possible to claim that the combined 6P PK-PD model is able to represent the SAP after administration of remifentanil, because the values of SAE are low (lower than 10) and the values of $\Delta E_{max}\%$ are lower than 10% except for three cases in which $\Delta E_{max}\%$ is higher than 10% but lower than 15%.

It is worth stressing that for all the case-studies (Paragraph 4.3, 4.4, and 4.5) at the end of the simulation the SAP curve tends to values within the normality range of the effect, *i.e.* 90-140 mmHg.

4.4 Application to MAP

The initial estimate for k_{e0} was chosen according to graphical data analysis and it is equal to 0.5. Fig. 60 shows the results of the optimization procedure. On the left, it is possible to see the hysteresis loop between MAP and concentration in the effect-site for k_{e0} equal to the initial estimate. On the right, the final and collapsed hysteresis loop. It is possible to observe that the initial value was a good estimate, as the loop is already pretty collapsed. Again, the experimental data are from Thompson *et al*. (1998).

The value for which the error is minimized is k_{e0} = 0.33. This value is consistent with the fact that remifentanil is a rapidly equilibrating drug.

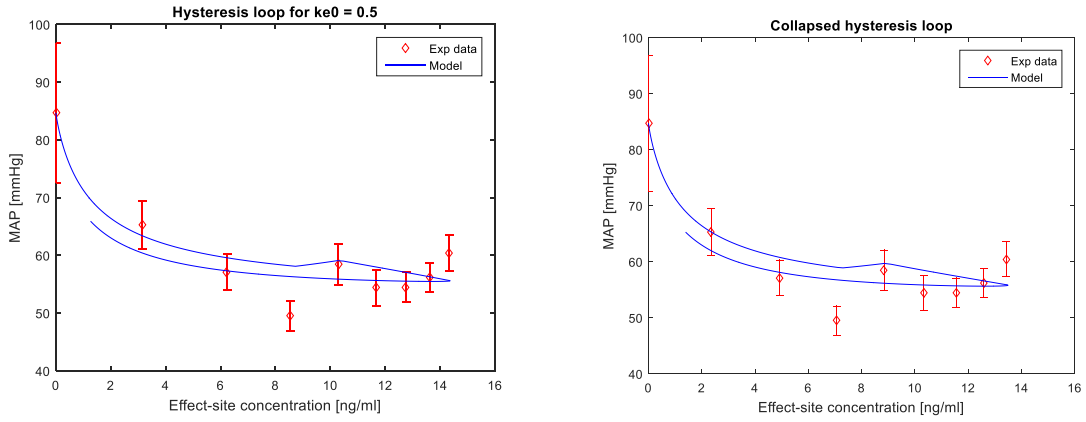

Figure 60 - The left figure shows the hysteresis loop before the optimization procedure. The right figure shows the collapsed hysteresis loop after the optimization procedure. Experimental data come from Thompson et al. (1998).

The case studies discussed in Chapter 3 will now be used to compare the PD and 6P PK-PD models.

4.4.1 Case-study 1: Hall et al. (2000)

Fig. 61 shows the comparison of MAP simulations between the PD and 6P PK-PD models. Experimental values for Groups 1 and 2 come from Hall *et al.* (2000).

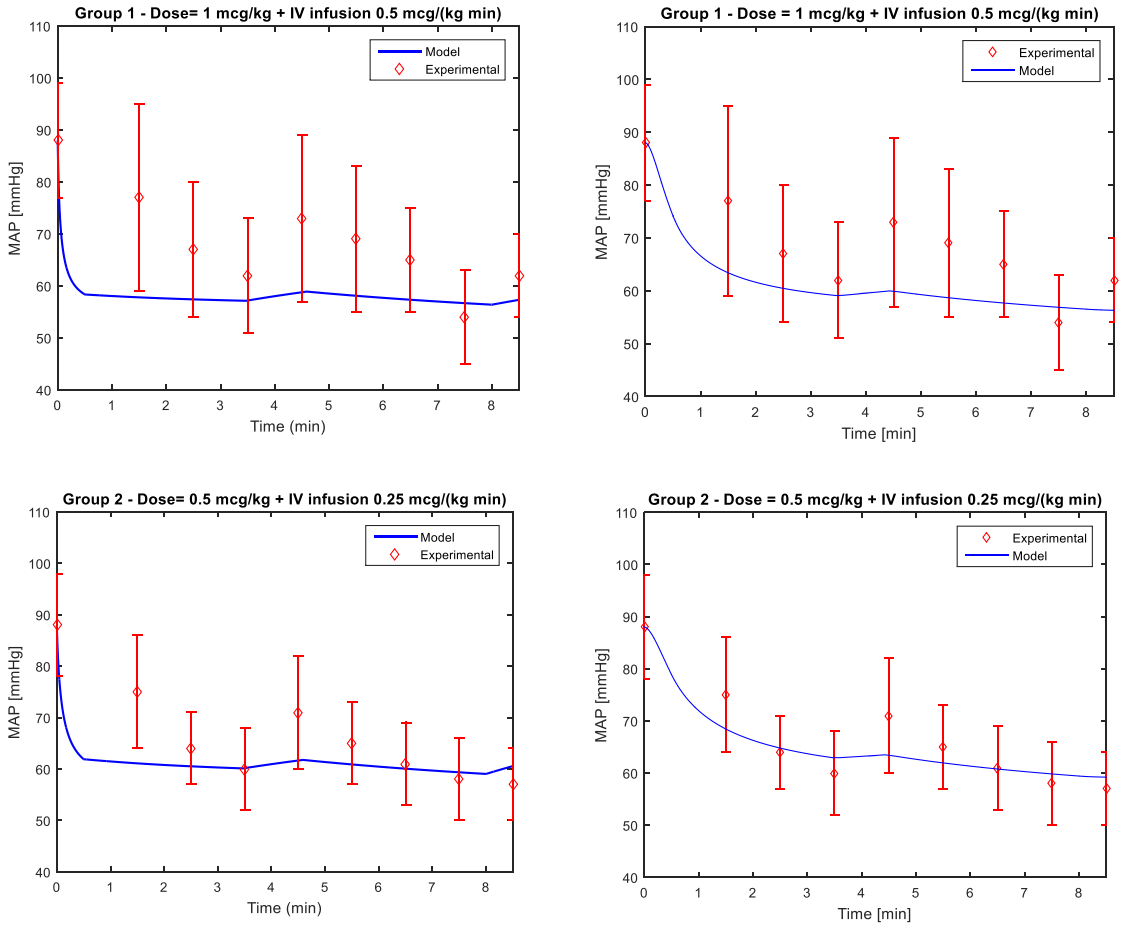

Figure 60 - The left portion shows the results of the PD model. The right portion shows the results of the combined model. Experimental data (red) from Hall et al. (2000). The patients were divided in two groups and received two different doses as single bolus for 30 s followed by an IV infusion.

This case-study allows highlighting the difference in the first phase, the one following the administration of remifentanil, as three blood samples were taken before intubation. In fact, in case of 6P PK-PD model, the simulation curve falls within the standard deviation bands for all the experimental data, differently from the curve

derived from the PD model. Moreover, the performance indexes show an improvement of the combined 6P PK-PD model (see Table 41).

Table 41 - Values of the performance indexes for Hall et al. *(2000). Left column, values for PD model. Right column, values for 6P PK-PD model.*

Performance index	*Group*	*PD Model*	*6P PK-PD Model*
$\Delta E_{Max}\%$	1	19.30	17.85
	2	13.00	10.60
SAE	1	8.19	6.93
	2	4.095	2.80

4.4.2 Case-study 2: Alexander et al. (1999)

Fig. 62 shows the results of the PD model compared to the results of the 6P PK-PD model in simulating the measured MAP of Groups 1, 2, and 3 from Alexander *et al.* (1999).

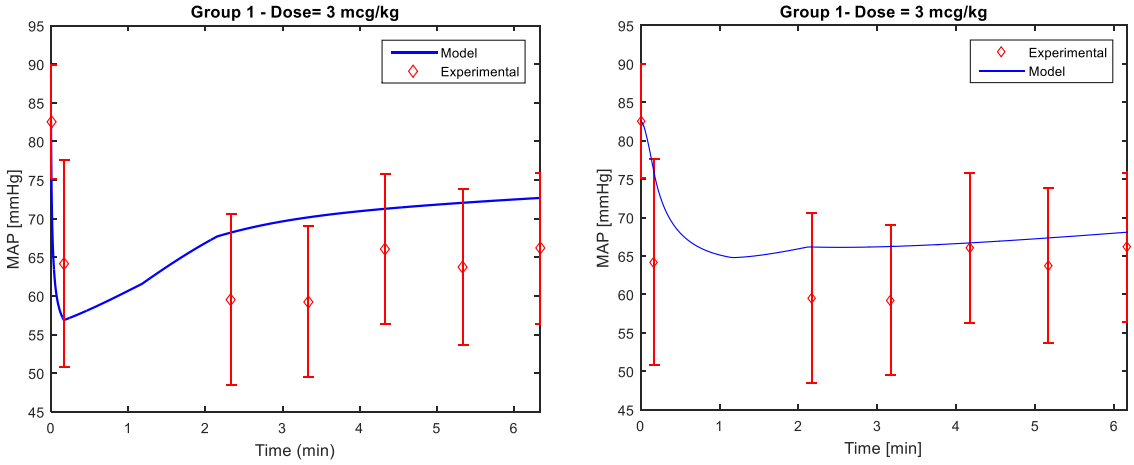

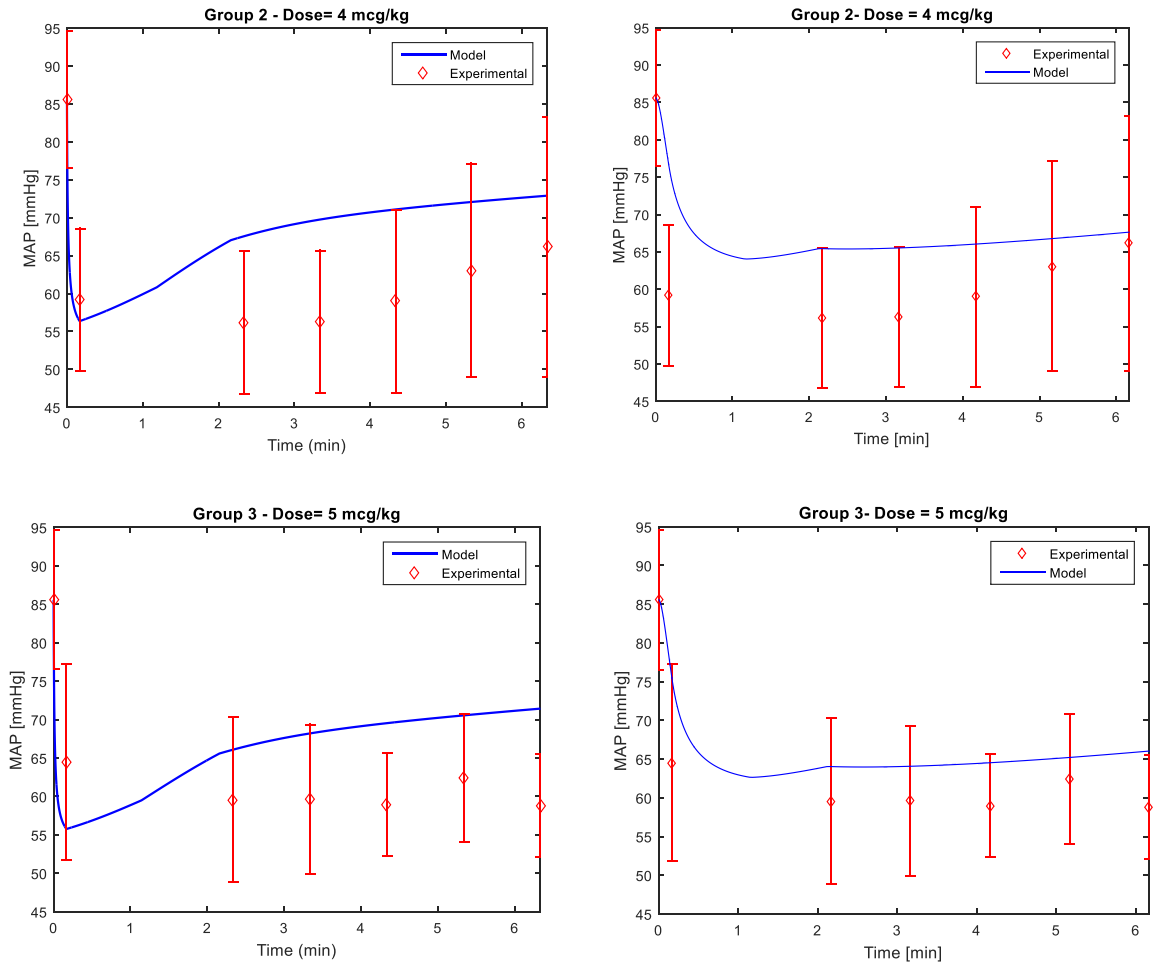

Figure 61 - The left portion shows the results of the PD model. The right portion shows the results of the combined model. Experimental data come from Alexander et al. (1999). The patients were divided into three groups and received three different doses as single bolus for 10 s.

Again, it is possible to observe that there is an improvement of the combined model in describing the MAP of the patients from Alexander *et al*. (1999) study. In fact, the combined 6P PK-PD model does not overestimate the experimental data as the PD model. The performance indexes reflect this improvement (see Table 42).

Table 42 - Values of the performance indexes for Alexander et al. (1999). Left column, values for PD model. Right column, values for 6P PK-PD model.

Performance index	*Group*	*PD Model*	*6P PK-PD Model*
$\Delta E_{Max}\%$	1	13.70	11.10
	2	19.17	16.40
	3	10.00	7.50
SAE	1	6.71	4.52
	2	7.93	6.92
	3	7.89	5.07

4.4.3 Case-study 3: Batra et al. (2004)

Fig. 63 shows the results of the PD model compared to the results of the 6P PK-PD model in simulating the measured MAP of Group 1 and 2 from Batra *et al.* (2004).

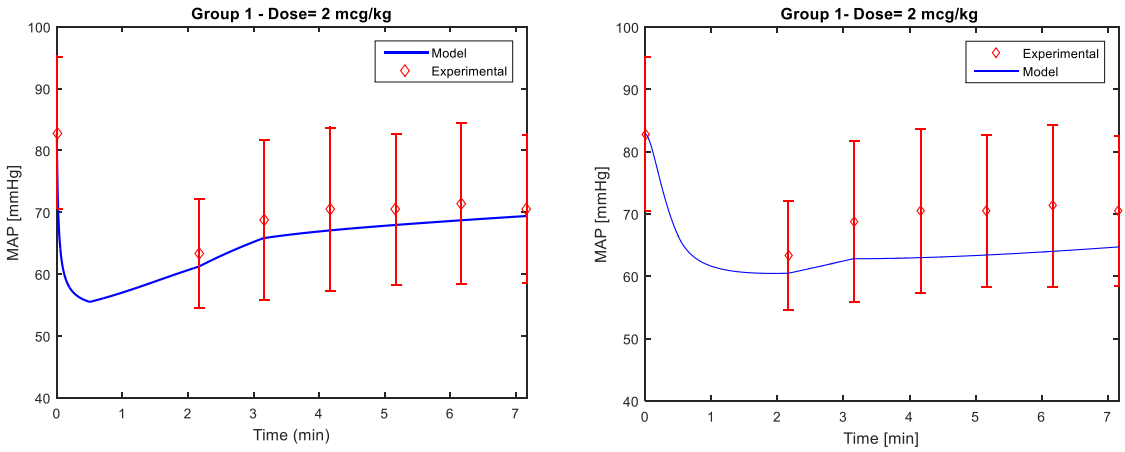

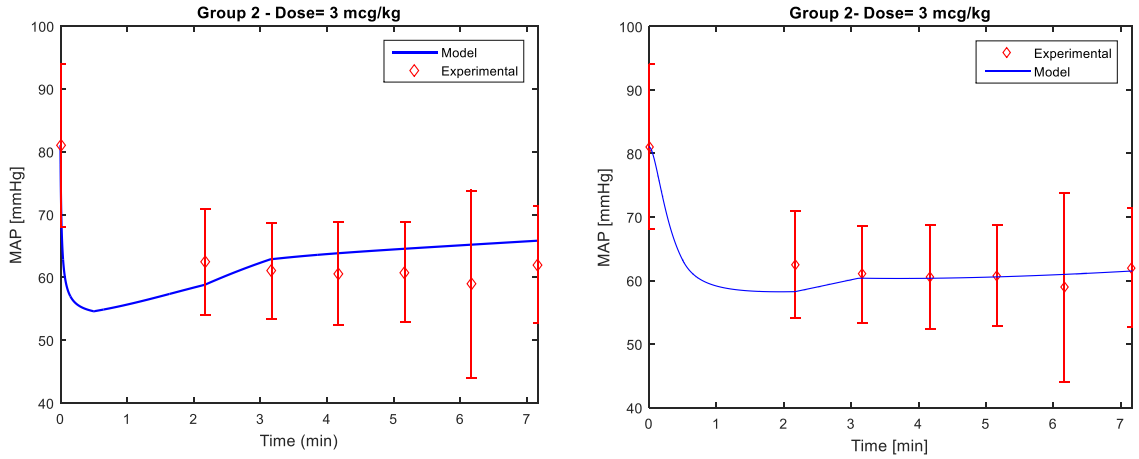

Figure 62 - The left portion shows the results of the PD model. The right portion shows the results of the combined model. Experimental data come from Batra et al. (2004). The patients were divided into two Groups and received two different doses as single bolus for 30 s.

The combined 6P PK-PD model provides satisfactory results, even if there is a worsening in the prediction of the peak effect of the first group of patients (see Table 43). However, the model curve still falls within the standard deviation bands of the experimental remifentanil concentrations, and gives a better prediction of the experimental MAP of Group 2.

Table 43 - Values of the performance indexes for Batra et al. (2004). Left column, values for PD model. Right column, values for 6P PK-PD model.

Performance index	*Group*	*PD Model*	*6P PK-PD Model*
$\Delta E_{Max}\%$	1	4.34	8.70
	2	3.07	1.08
SAE	1	2.17	5.22
	2	3.15	1.13

4.4.4 Conclusions

In most cases, the performance indexes for the MAP simulations showed an improvement of the combined model compared to the PD model, with the additional advantage of the realistic representation of the period that follows the remifentanil administration. It is also worth remarking that the values of $\Delta E_{max}\%$ are lower than 20%, and the values of SAE are lower than 10. Again, the simulation curve of both

models tends to normal values of the effect at the end of the procedure (*i.e.* 70<MAP<105 mmHg).

4.5 Application to HR

The initial value of k_{e0} is 0.5, according to the analysis of the experimental data. The case studies used to find the optimal k_{e0} are the same used to find the PD parameters, *i.e.* Engelhard *et al.* (2004) and O'Hare *et al*. (1999). Fig. 64 shows the results of the optimization procedure for the study of O'Hare *et al.* (1999).

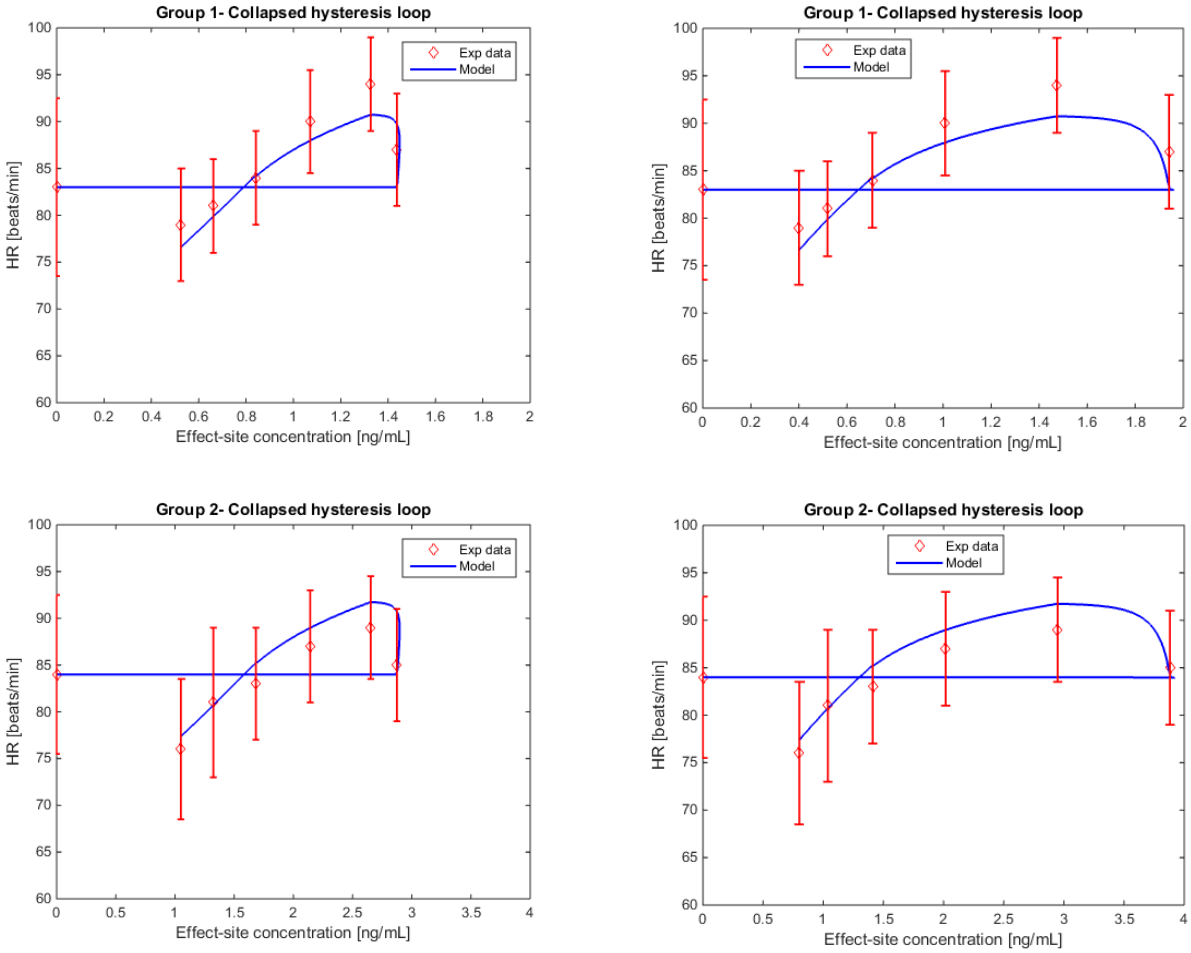

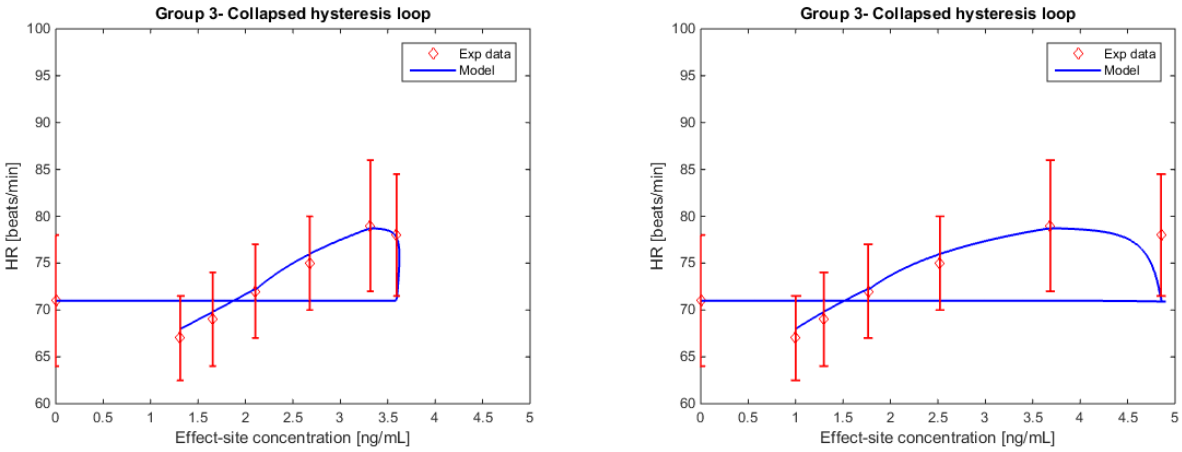

Figure 63 - The left portion shows the hysteresis loop before the optimization procedure. The right portion shows the collapsed hysteresis loop after the optimization procedure. Experimental data (red) from O'Hare et al. (1999).

On the left of Fig. 64, it is possible to observe the hysteresis loop for k_{e0} equal to the initial estimate, while the right side shows the final and collapsed hysteresis loop between HR and the drug concentration in the effect-site. It is possible to observe that the initial value of k_{e0} is a good estimate, as the hysteresis loop is not so evident.

The optimal value for k_{e0} is 0.861. This value is consistent with the fact that remifentanil is a rapidly equilibrating drug.

It is now possible to analyze the results of the combined model for HR and compare them to the results of the PD model. Subsections 4.5.1-4.5.6 report and analyze the cases of studies presented in Chapter 3.

4.5.1 Case-study 1: Lee et al. (2012)

Fig. 65 reports the results of the PD and combined 6P PK-PD models, compared to the experimental data of Lee *et al.* (2012).

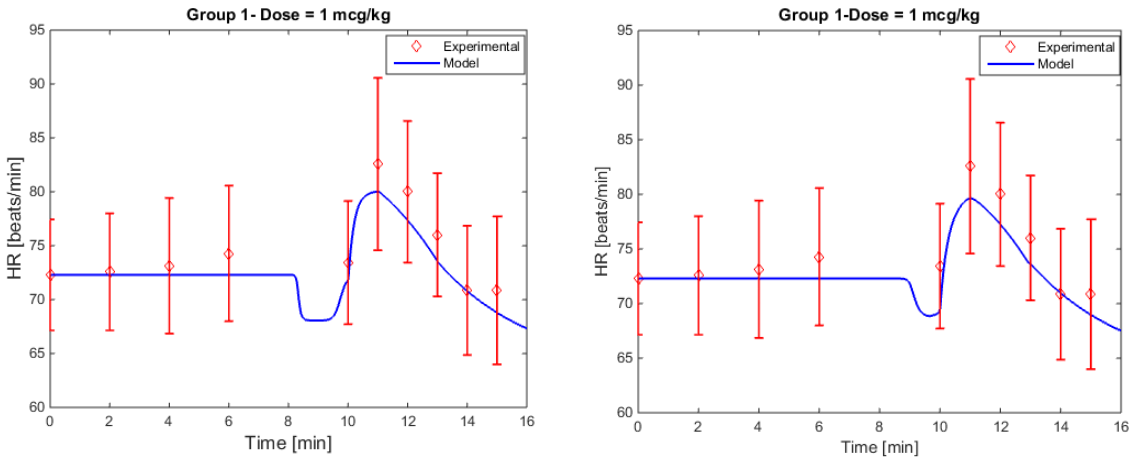

Figure 64 - On the left, the results of the PD model. On the right, the results of the combined model. Experimental data (red) from Lee et al. (2012). The patients received a single bolus over 1 min.

It is worth observing that there is a difference in the first tract. The decrement that occurs after the drug administration is smoother and more realistic in the combined model respect to the PD model, where the decrement is steep.

Table 44 lists the values of the performance indexes.

Table 44 - Values of the performance indexes for Lee et al. (2012). Left column, values for PD model. Right column, values for 6P PK-PD model.

Performance index	*PD Model*	*6P PK-PD Model*
$\Delta E_{Max}\%$	3.08	3.51
SAE	1.45	1.71

4.5.2 Case-study 2: Park et al. (2011)

Fig. 66 reports the results for the PD and combined 6P PK-PD model, compared to the experimental data of Park *et al.* (2011).

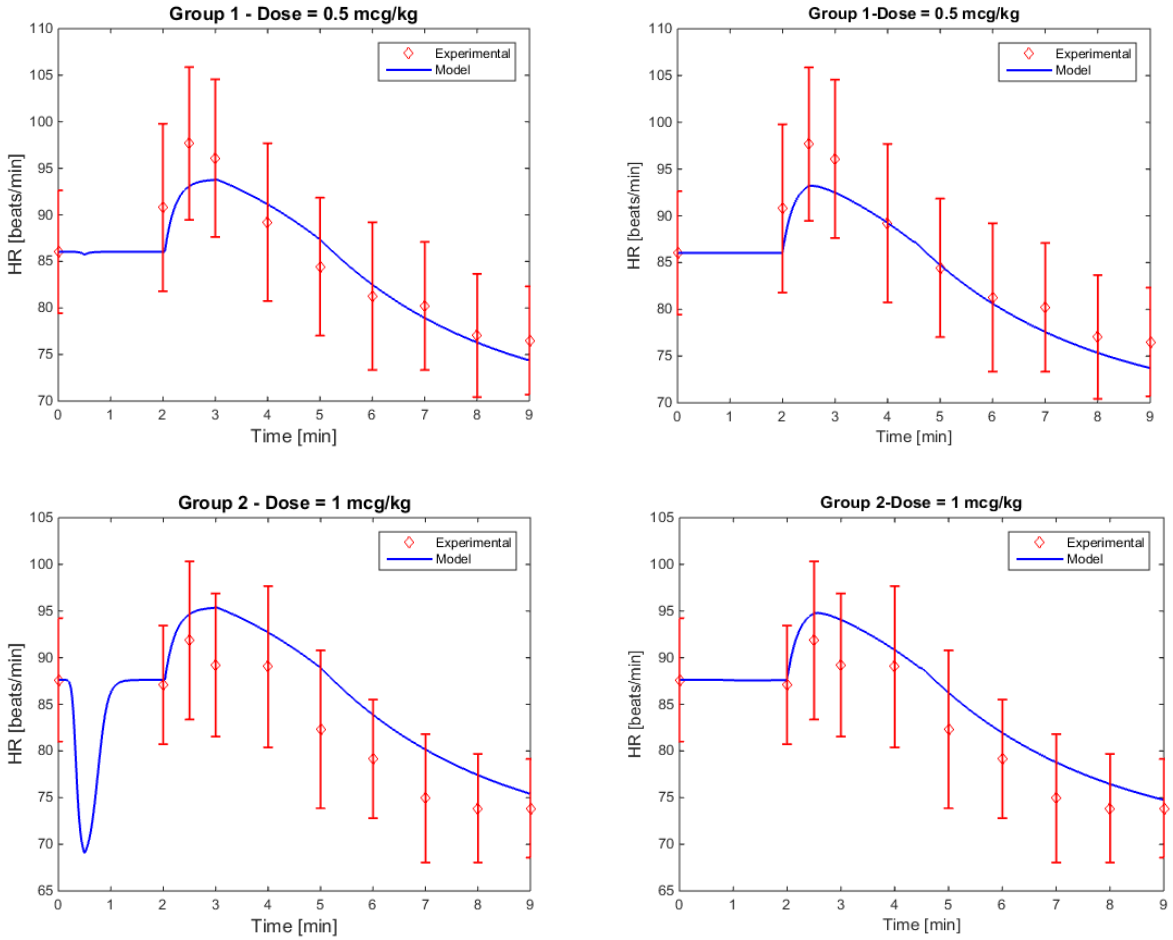

Figure 65 - The left portion shows the results of the PD model. The right portion shows the results of the combined model. Experimental data (red) from Park et al. (2011). The patients were divided in two groups and received two different doses as single bolus for 30 s.

Again, it is possible to observe a difference in the first tract, in particular for Group 2, who received a higher dose. The PD model curve presents an evident decrement of the effect after the drug administration, which disappears in the combined 6P PK-PD model. This is caused by the delay that is introduced by the effect-site compartment.

Table 45 - Values of the performance indexes for Park et al. (2011). Left column, values for PD model. Right column, values for 6P PK-PD model.

Performance index	*Patient*	*PD Model*	*6P PK-PD Model*
$\Delta E_{Max}\%$	1	4.00	4.58
	2	3.82	3.19
SAE	1	2.19	2.08
	2	3.48	2.44

4.5.3 Case-study 3: Nora et al. (2007)

Fig. 67 reports the results for the PD and combined 6P PK-PD model, compared to the experimental data of Nora *et al.* (2007).

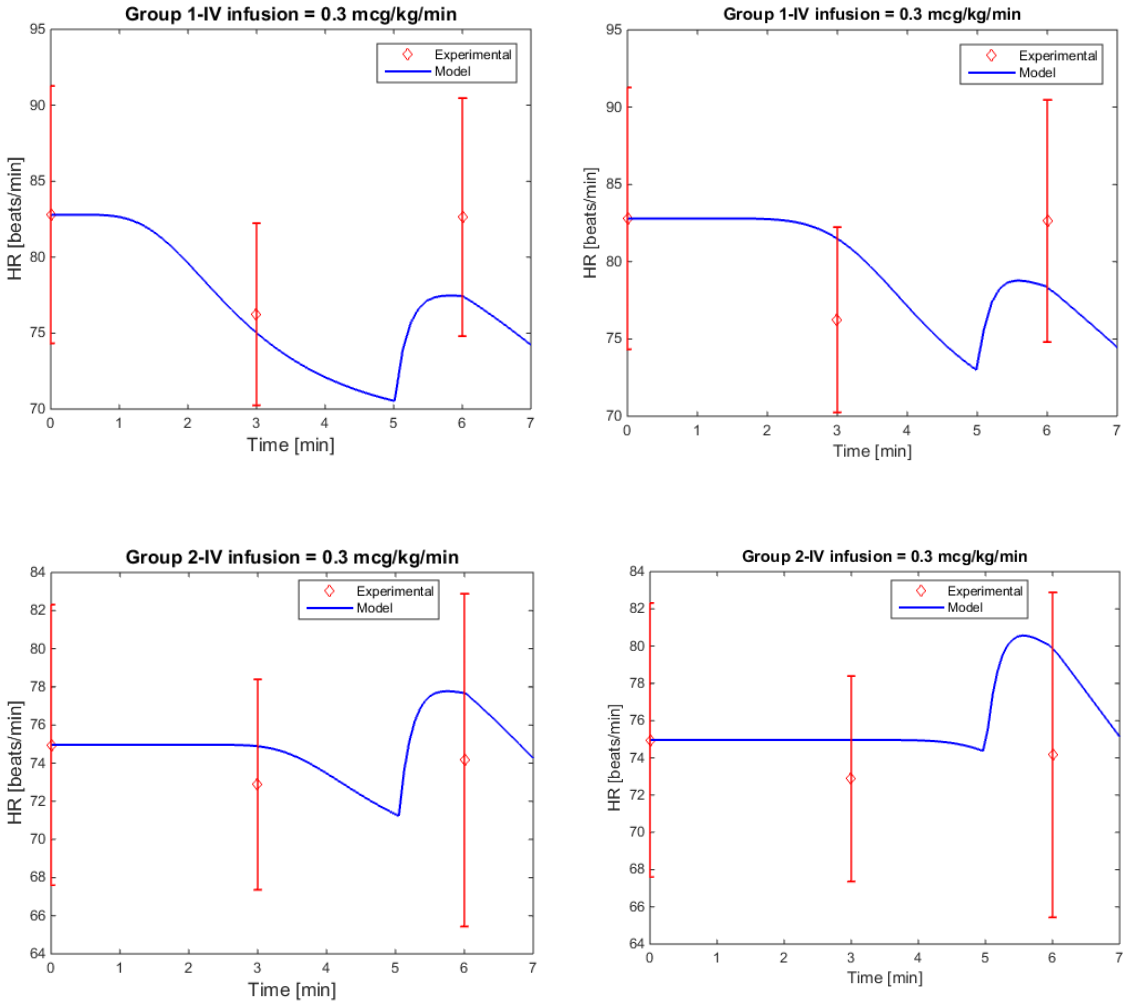

Figure 66 - The left portion shows the results of the PD model. The right portion shows the results of the combined model. Experimental data from Nora et al. (2007). The difference between the groups is the time at which the remifentanil administration starts. The IV infusion starts at time 0 for Group 1 and after 2 min for Group 2.

Again, it is possible to observe a variation of the first tract, where there is an evident delay in the decrease of the effect.

Table 46 - Values of the performance indexes for Nora et al. (2007). Left column, values for PD model. Right column, values for 6P PK-PD model.

Performance index	*Patient*	*PD Model*	*6P PK-PD Model*
$\Delta E_{Max}\%$	1	1.47	4.66
	2	4.87	8.64
SAE	1	2.14	3.19
	2	1.84	2.60

4.5.4 Case-study 4: Hall et al. (2000)

Fig. 68 reports the results for the PD and the combined model, compared to the experimental data of Hall *et al.* (2000).

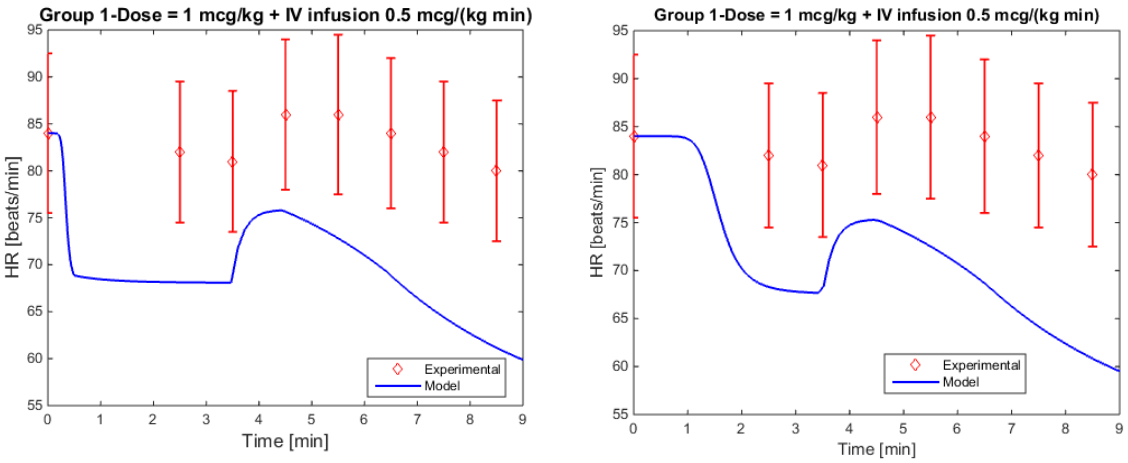

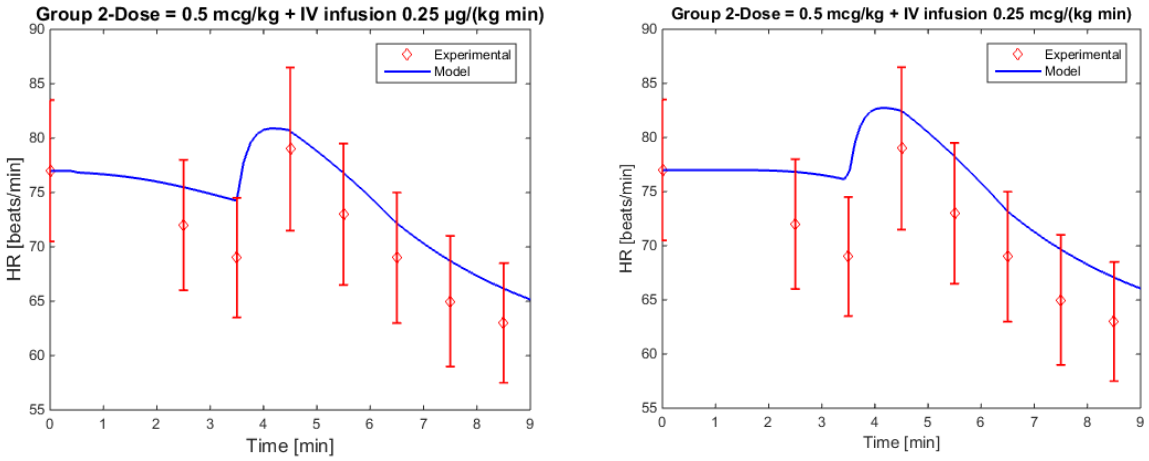

Figure 67 - The left portion shows the results of the PD model. The right portion shows the results of the combined model. Experimental data (red) from Hall et al. (2000). The patients were divided into two groups and received two different doses as single bolus for 30 s followed by IV infusion.

In this case, as in the other ones, it is possible to notice a less steep and longer decrease of the combined 6P PK-PD model simulated effect after the beginning of the drug administration. Both models underestimate the experimental HR of Group 1 (see also Chapter 3).

Table 47 - Values of the performance indexes for Hall et al. (2000). Left column, values for PD model. Right column, values for 6P PK-PD model.

Performance index	*Patient*	*PD Model*	*6P PK-PD Model*
$\Delta E_{Max}\%$	1	11.87	12.46
	2	2.40	4.72
SAE	1	12.63	12.88
	2	3.04	4.26

4.5.5 Case-study 5: Maguire et al. (2001)

Fig. 69 reports the results for the PD and combined 6P PK-PD model, compared to the experimental data of Maguire *et al.* (2001).

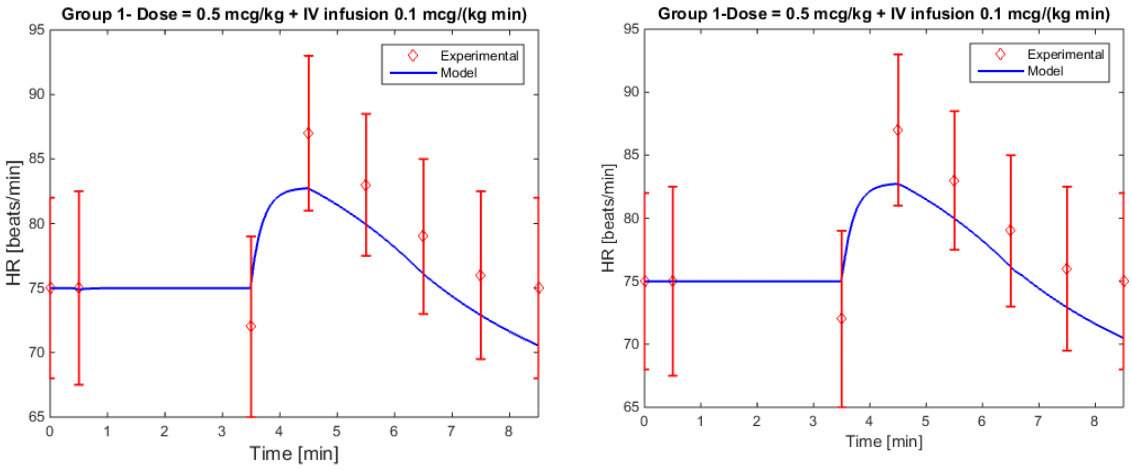

Figure 68 - The left portion shows the results of the PD model. The right portion shows the results of the combined model. Experimental data (red) from Maguire et al. (2001). The patients received a single bolus for 30 s followed by IV infusion.

In this case, there are almost no differences between the models. This may be related to the fact that the administered doses are lower than in the other studies and that the HR dependence from the drug concentration is altered by the presence of an emotional peak (see Paragraph 3.3 for details).

Table 48 - Values of the performance indexes for Maguire et al. (2001). Left column, values for PD model. Right column, values for 6P PK-PD model.

Performance index	*PD Model*	*6P PK-PD Model*
$\Delta E_{Max}\%$	*4.90*	*4.91*
SAE	*2.67*	*2.53*

4.5.6 Case-study 6: Shajar et al. (1999)

Fig. 70 reports the results for the PD and combined 6P PK-PD model, compared to the experimental data of Shajar *et al.* (1999).

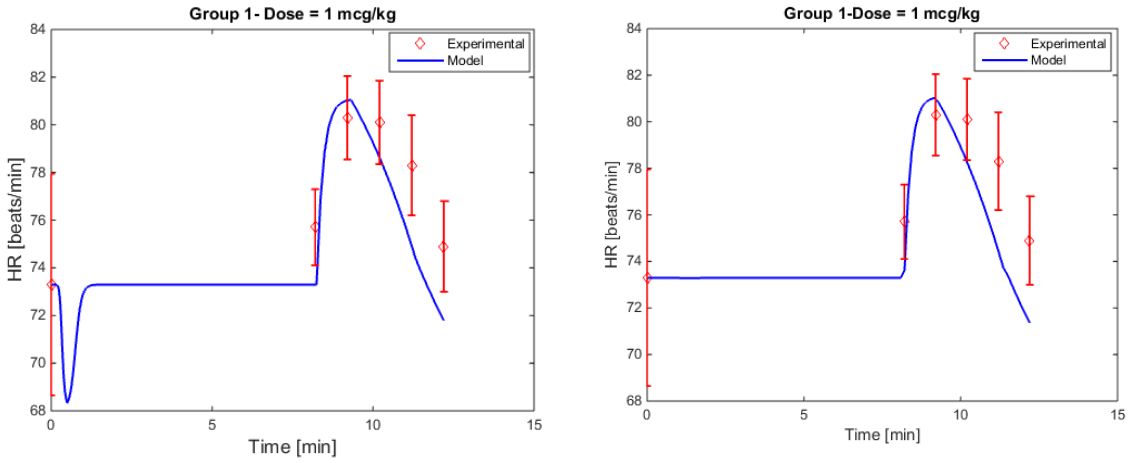

Figure 69 - The left side shows the results of the PD model. The right side shows the results of the combined 6P PK-PD model. Experimental data (red) from Shajar et al. (1999). The patients received a single bolus for 30 s.

The models difference in the first tract is evident. In the PD curve there is a significant decrease of the effect after the drug administration that conversely is not present in the combined 6P PK-PD model. As previously explained, this occurs because of the introduction of the delay between the drug concentration and the effect.

Table 49 - Values of the performance indexes for Shajar et al. (1999). Left column, values for PD model. Right column, values for 6P PK-PD model.

Performance index	*PD Model*	*6P PK-PD Model*
$\Delta E_{Max}\%$	0.94	0.89
SAE	1.85	1.78

4.5.7 Conclusions

The advantages observed in Paragraphs 4.3 and 4.4, which derived from the introduction of the effect-site compartment (*e.g.*, better description of the first tract of the experimental trend) are less evident in case of HR simulations, because the experimental data do not decrease after the drug administration, due to an emotional response (see Chapter 2).

However, it should be underlined that in a number of case studies the performance indexes are better for the 6P PK-PD model, respect to those obtained by the PD model. In the remaining case studies, the values of these indexes are rather low and comparable between the models. In general, all the $\Delta E_{max}\%$ values are lower than 15% and all the SAE values are less than 10. Moreover, as already underlined, the 6P PK-PD

model features a better representation of reality, by introducing a delay between the plasma concentration peak and the maximum produced effect.

4.6 Effect of the variation of dose and dose regimen

Once the combined 6P PK-PD model is validated, it is interesting to investigate its application for the comparison of different doses and/or dose regimens.

In fact, the problem of finding the optimal dose is an open issue in anesthesia, because the effect of the drug must be strong enough to control and attenuate the response to intubation but at the same time typical adverse effects of opioids (*e.g.*, hypotension, bradycardia) must be prevented. From this point of view, the phase that immediately follows the administration of remifentanil is critical.

First, we decided to simulate and compare the pharmacological effect of three bolus doses administrated over 1 min. In the following simulations, intubation is performed at 1.5 min.

Table 50 reports body mass and gender of the simulated patients and selected dose. Fig. 71 shows the results of the simulations.

Table 50 - Demographic data of the simulated patients and administered bolus doses.

Patient	*Body mass [kg]*	*Gender*	*Dose [µg/kg]*
1	72	M	0.5
2	84	M	1.0
3	87	M	1.5

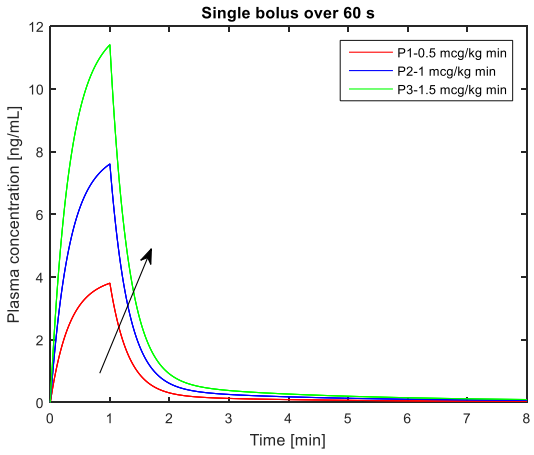

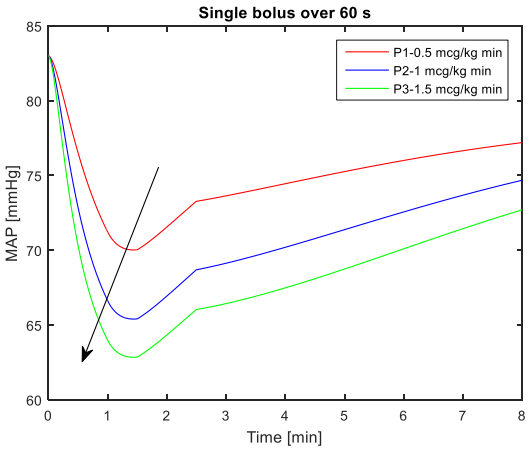

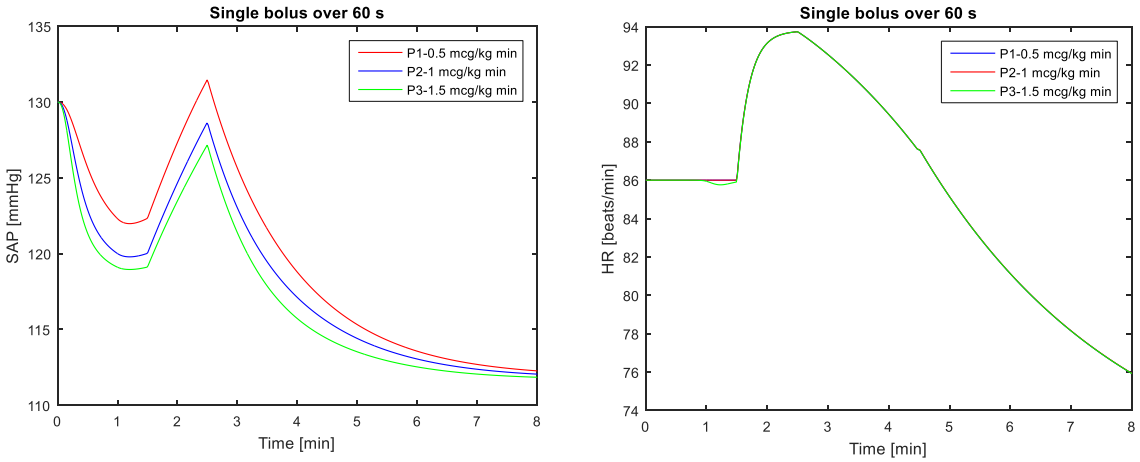

Figure 70 - Plasma concentration evolution in time and hemodynamic effects resulting from the administration of three different bolus doses. The arrow shows the direction of increasing dose.

As expected, the highest dose produces the strongest effect. In fact, the lowest value of SAP, MAP, and HR are reached for a bolus dose of 1.5 µg/kg. The lowest hemodynamic values fall still within the normal range in case of SAP, MAP, and HR (SAP > 90 mmHg, MAP > 70 mmHg, HR > 60 beats/min). According to these simulation curves, only the bolus dose equal to 0.5 µg/kg allows having all the three hemodynamic effects considered inside the normality range and avoiding potential hypotension. The bolus dose equal to 1 µg/kg results in the MAP reaching the value of 65, which is slightly below the recommended lower value of 70 mmHg.

Some authors claim that MAP is the most reliable measure of arterial pressure, because SAP and DAP provide different results if measured with different monitoring methods, while MAP values remain similar even if measured with different methods (McGhee and Bridges, 2002).

In Fig. 71, HR seems not to change with the dose. Actually, there is a small variation (see also the detail of Fig. 72), which is related to the limitations of the HR model, which were already discussed in Chapter 3.

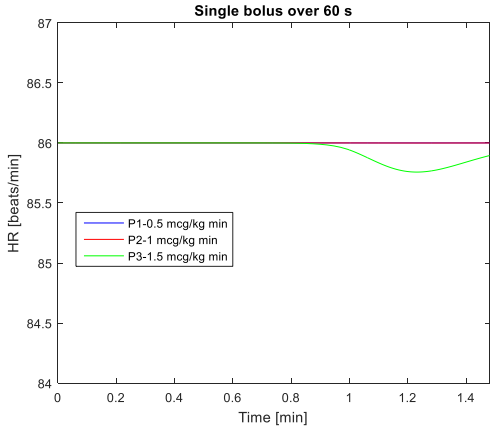

Figure 71 - HR evolution in time in the phase that immediately follows remifentanil administration.

Secondly, we decided to simulate and compare the pharmacologic effect of four infusion doses, administrated for 10 min.

The simulations refer to four male/female patients, whose body mass is reported in Table 51. Intubation is performed 3 min after the start of the remifentanil administration. Fig. 73 shows the results of the simulations.

Table 51 - Demographic data of the simulated patients and administered infusion doses.

Patient	*Body mass [kg]*	*Gender*	*Dose [µg/kg]*
1	82	M	0.1
2	60.0	F	0.2
3	75	M	0.4
4	63.0	F	0.8

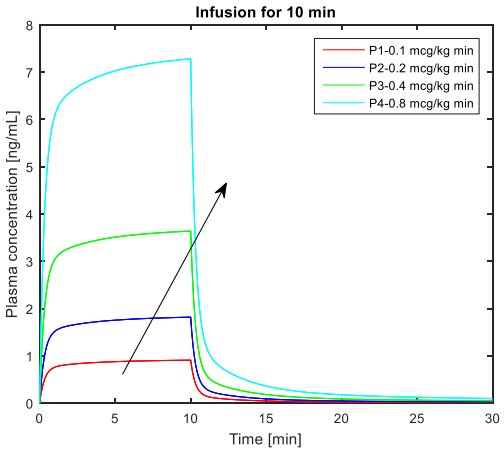

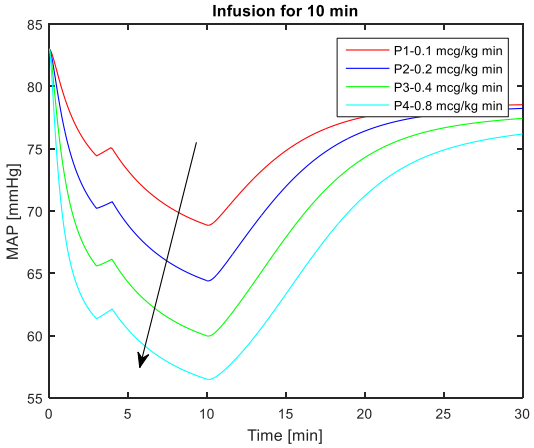

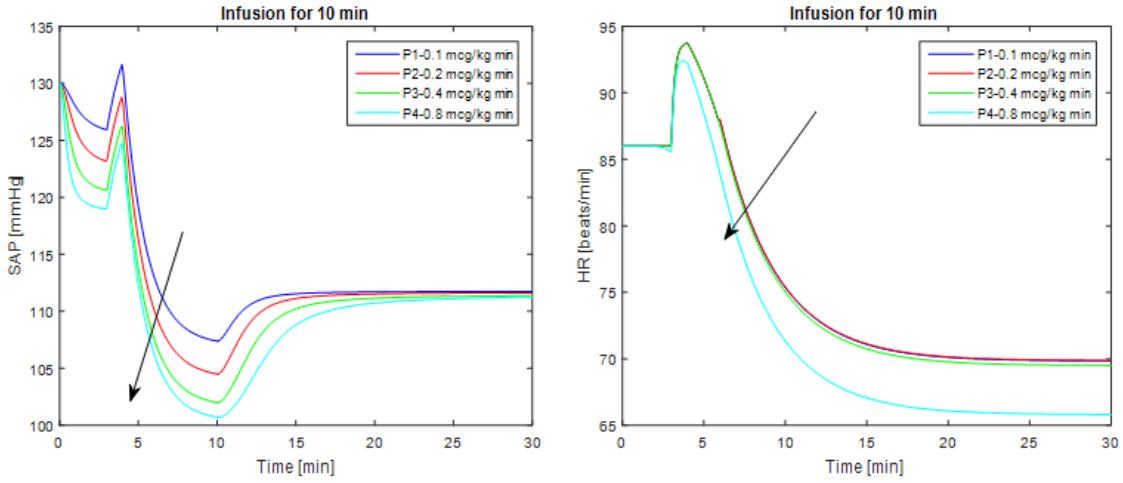

Figure 72 - Plasma concentration evolution in time and hemodynamic effects resulting from the administration of four different doses as IV infusion. The arrow shows the direction of increasing dose.

Again, the obtained results show the valuable features of the combined 6P PK-PD model for the optimal identification of the dose (regimen). According to Fig. 73, the first two doses are so small that they cannot produce a significant pharmacologic effect. On the contrary, the two higher doses are quite effective. The highest leads to a MAP of almost 55 mmHg, which is significantly below the recommend lower value (*i.e.* 70), even if the SAP is still within the "normality" range. The simulation of different infusion doses allows detecting a difference in the HR evolution, which was not available in the previous three different boluses. Fig. 74 focuses on the phase preceding intubation. Only the highest dose produces a limited HR decrease. Again, this is related to the limitations of this model (Chapter 3).

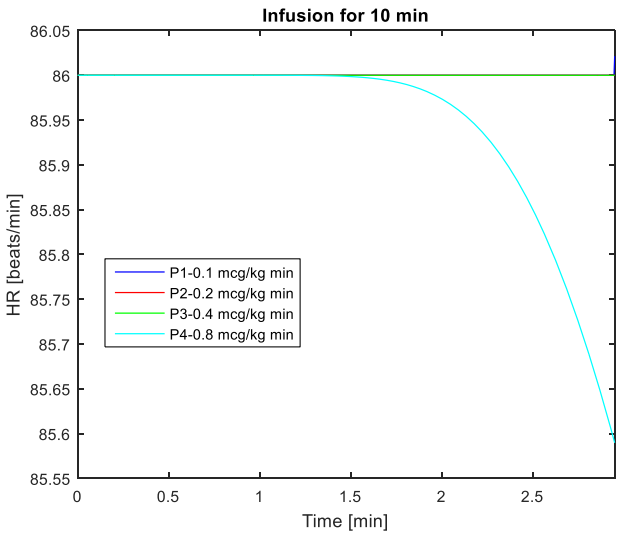

Figure 73 - HR evolution in time in the phase that immediately follows remifentanil administration.

Finally, the combination of bolus and infusion was simulated for two patients of body mass and gender reported in Table 52. In the simulation, a single bolus was administered for 30 s, followed by an infusion for 8 min. Fig. 75 shows the results of these simulations.

Table 52 - Demographic data of the simulated patients and administered doses.

Patient	*Body mass [kg]*	*Gender*	*Bolus [µg/kg]*	*Infusion [µg/kg/min]*
1	80	M	1	0.50
2	65.9	F	0.5	0.25

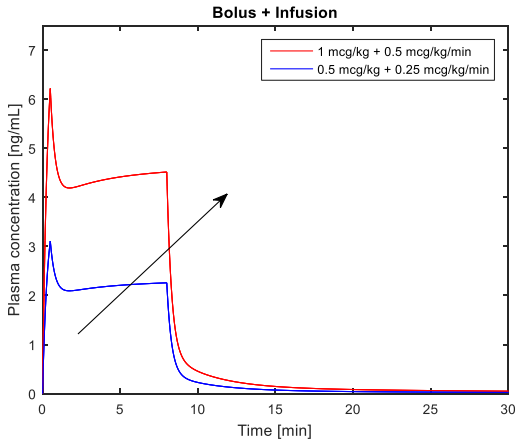

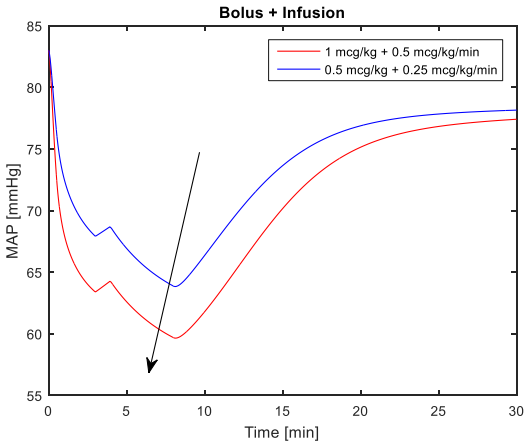

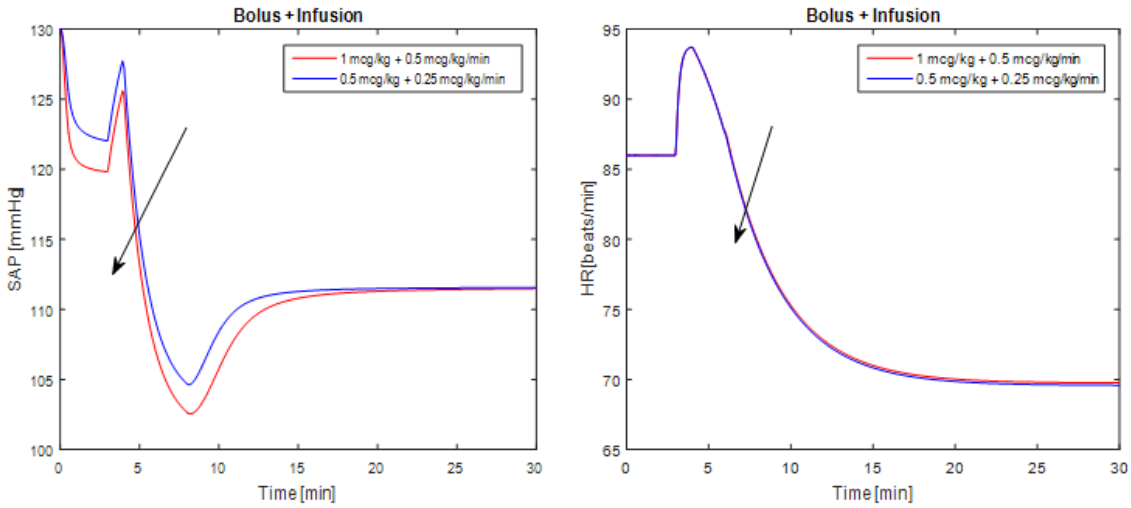

Figure 74 - Plasma concentration evolution in time and hemodynamic effects resulting from the administration of three different bolus doses. The arrow shows the direction of increasing dose.

Again, MAP seems to be the most sensible measure and effect. Both combinations lead to light hypotension, while SAP and HR remain in the normality range (SAP>90 mmHg, HR>60 beats/min). The two administered doses appear to affect HR in the same way (as shown in the bottom right diagram of Fig. 75).

4.7 Influence of gender and body mass

One of the main issues of pharmacokinetic-pharmacodynamic modeling is the inter-individual variability. In order to increase the level of individualization of the model, a different way to calculate the blood volume was considered. Nadler's formulae depend not only on the body mass but also on the height of the patient (Neyrinck and Vrielink, 2014). The constants of the formula depend on the gender of the patient.

$$V_{b\,Male} = 0.3669 \cdot h^3 + 0.03219 \cdot m + 0.6041 \tag{68}$$

$$V_{b\,Female} = 0.3561 \cdot h^3 + 0.03308 \cdot m + 0.1833 \tag{69}$$

Where h is the height [m] and m the body mass [kg]. The blood volume (V_b) is measured in liters. Once calculated, it is possible to derive the plasma volume as follows:

$$V_p = V_b \cdot \frac{100 - hematocrit}{100} \tag{70}$$

$Hematocrit$ is the percentage volume of blood cells (erythrocytes) in blood. It is normally between 40.7% and 50.3% in men and between 36.1% and 44.3% in women (U.S. National Library of Medicine). Averaged values were used for the following calculations: 45% for men and 41% for women. The remaining parameters of the 6P PK model were determined as discussed in Paragraph 2.2.

Now that the model has moved a step forward in the direction of personalization, it is interesting to investigate the influence of the gender on the pharmacokinetics and pharmacodynamics of the drug of interest. According to the literature, we expect that gender affects neither the concentration-time profile nor the pharmacological effects of remifentanil (Minto *et al.*, 1997).

Table 53 lists the demographic data of the two simulated patients. For the sake of simplicity, the administration of two single boluses of 1 µg/kg over 60 s is considered.

Table 53 - Demographic data of the simulated patients.

Patient	*Gender*	*Body mass [kg]*	*Height [m]*
1	M	80	1.80
2	F	50	1.60

The difference between the peak concentrations is 6%, which is in practice rather low. This difference is not clinically significant in terms of effect: in fact, the difference in the maximum effect (MAP and SAP) of the drug is lower: respectively, 0.5% and 0.08%, which are negligible. The gender difference is higher for the HR, because it is 3.3% but still rather moderate (see also Fig. 76).

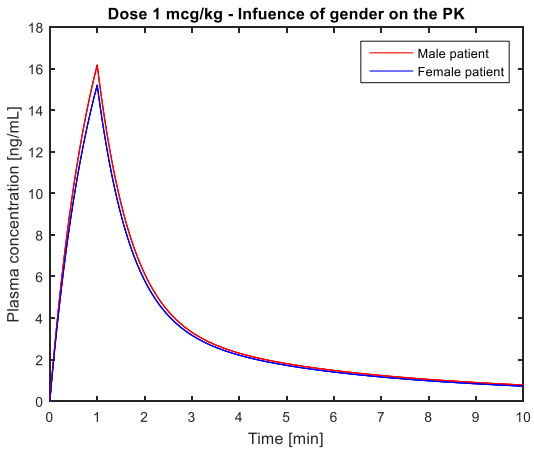

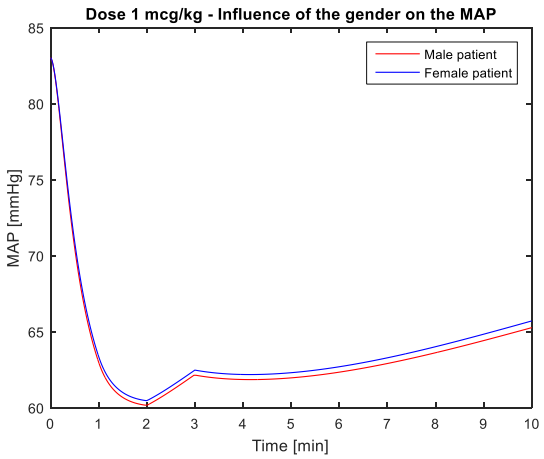

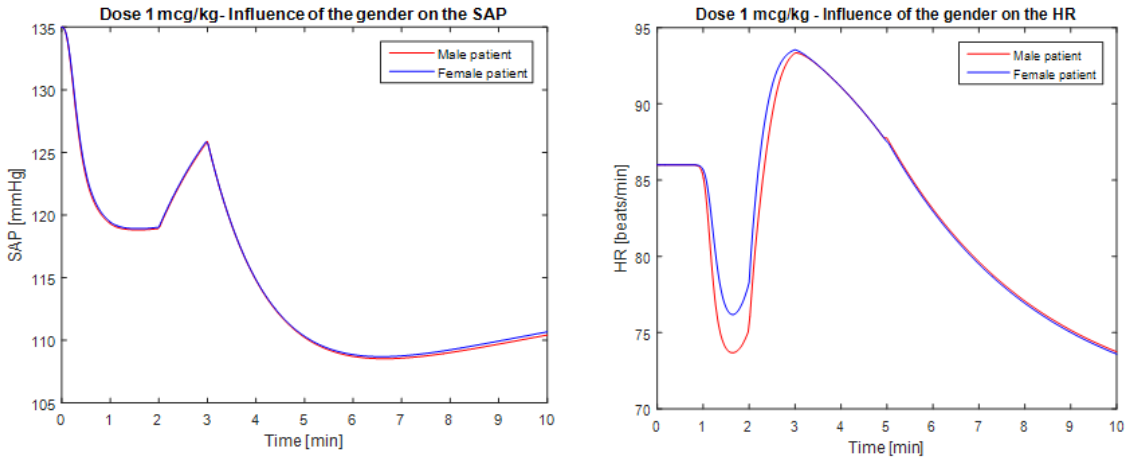

Figure 75 - Comparison between PK and PD of a male patient (red) and a female patient (blue) to investigate the influence of the gender.

It is possible to state that our results are consistent with the literature findings, that is to say that remifentanil pharmacokinetics and pharmacodynamics are gender independent.

It is now interesting to investigate the influence of body mass and, in particular, understand if the model can be used to study the pharmacokinetics and pharmacodynamics of remifentanil in obese patients.

Obesity is today a serious problem in the most developed countries and affects all age groups. The consequences of obesity on health are cardiovascular, respiratory, metabolism, and osteoarticular diseases, which have led to an increasing number of obese patients that are annually subject to surgical procedures. Since obesity also affects the pharmacokinetics and pharmacodynamics of drugs, it is clear that, in this respect, anesthesiologists have to confront with difficult challenges (Domi and Laho, 2012).

In 1998, World Health Organization (WHO) introduced a new and more precise classification (see Table 55) based on the body mass index (BMI), which is calculated as follows:

$$BMI = \frac{body\ mass}{height^2} \tag{71}$$

The body mass is expressed in [kg], while the height in [m]. Since Nadler's formulae present a strong dependence on height and body mass (Equation (68-69)), we expect

that they are indirectly dependent on the BMI, and make the model be more sensitive to mass difference.

Table 54 - Classification of the condition, depending on the BMI. Taken from Domi and Laho (2012).

Condition	*BMI [kg/m^2]*
Underweight	≤18.5
Normal weight	≥18.5-24.9
Overweight	≥25-29.9
Obesity	≥30
Morbid obesity	≥35
Supermorbid obesity	≥55

Egan *et al.* (1998) investigated the pharmacokinetics of remifentanil by comparing a group of lean patients with a group of obese patients. The following simulations were produced using the demographic data of Egan *et al.* (1998) (see Table 55). The patients were administered with a bolus dose over 60 s. The doses in µg are assigned as a function of the body mass so to have 7.5 µg/kg for each patient. In the simulation, intubation is performed at 1.5 min.

Table 55 - Demographic data and BMI of the simulated patients. Last column, administered doses.

Patient	*Body mass [kg]*	*Height [m]*	*BMI [kg/m^2]*	*BMI condition*	*Gender*	*Dose [µg]*
1	57	1.73	19.045	Normal	F	435
2	70	1.9	19.391	Normal	M	550
3	49	1.65	17.998	Underweight	F	340
4	82	1.83	24.486	Normal	M	600
5	136	1.8	41.975	Obese	M	1020
6	123	1.7	42.561	Obese	F	920
7	140	1.83	41.805	Obese	M	1050

Fig. 77 shows differences in the patients' pharmacokinetics, depending on their body mass.

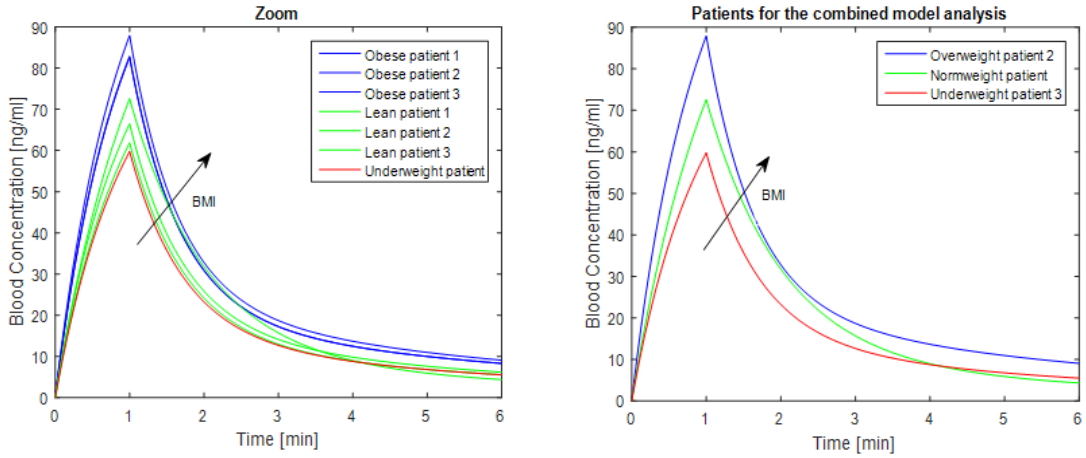

Figure 76 - Concentration-time profile for patients with increasing body weight. On the right, we focus on the two patients with the most extreme conditions and one normweight patient.

For the sake of clarity, we underline that Fig. 77 shows the dynamic evolution of remifentanil concentration in blood and not in plasma only for better readability, since 7 curves, one for each patient, are represented.

There is a difference of approximately 26% between the peak concentration of the most obese patient and the normweight patient, and of approximately 47% between the peak concentration of the most obese patient and the one of the underweight patient.

It is worth observing that at the beginning the drug accumulation in plasma is higher for the obese patients, while once the equilibrium between absorption and elimination (*i.e.* the peak concentration has been reached), the velocity of elimination of the obese patients appears to be equal or superior to the one of the lean/underweight patients. In fact, the blue curve and the green curve touch.

A plausible explanation is related to the fact that under normal conditions, fat tissues are scarcely perfused by blood. In fact, 5% of the total cardiac output is normally directed to fat tissues, 22% to lean tissues (lean body tissue comprises several essential parts, *e.g.*, organs, bones, muscles, tendons, and ligaments), and 73% to the rest of tissues/organs (GUWS Medical). In obese patients, the percentage that is destined to fat and lean tissues is even lower. This can explain the apparent drug accumulation in plasma.

However, once the peak concentration has been reached and elimination has started prevailing, the velocity of elimination might be higher because in absolute terms obese

patients have higher amounts of fat and lean tissues respect to normweight patients, which are the most important sites of elimination of remifentanil (Navapurkar *et al.*, 1998).

Table 56 lists the patients' Lean Body Mass (LBM). LBM is in fact an indicator of the body composition in terms of lean tissues and can be calculated through the James formulae that depend on gender, height, and body mass (Mettler and Mitchell, 2010).

$$LBM_{Male} = 0.3281 \cdot m + 0.33929 \cdot h - 29.52336 \quad (72)$$

$$LBM_{Female} = 0.29569 \cdot m + 0.41813 \cdot h - 43.2933 \quad (73)$$

Table 56 lists the LBM of the simulated patients, associated with the BMI.

Table 56 - LBM and BMI of the simulated patients.

Patient	*BMI [kg/m²]*	*BMI condition*	*LBM [-]*
1	19.045	Normal	45.89
2	19.391	Normal	56.84
3	17.998	Underweight	40.18
4	24.486	Normal	57.47
5	41.975	Obese	76.16
6	42.561	Obese	64.15
7	41.805	Obese	74.62

It is also important to underline that our results on the pharmacokinetics are consistent with Egan *et al.* (1998) results.

One of the main advantages of 6P PK models compared to classical PK models is the possibility to obtain the concentration-time profile of the study drug not only in the plasma but also in some organs and tissues of the human body, depending on the complexity and number of compartments of the 6P PK model.

More on the comparison between 6P PK and classical PK models will be discussed in Chapter 5.

Consistently with what was previously explained, as the percentage of the cardiac output destined to the poorly perfused tissues is lower for the obese patients, it is

possible that a normweight patient has a higher concentration of the drug in the compartments that lump the poorly perfused tissues, compared to an obese patient.

On the contrary, in other compartments that do not contribute to remifentanil elimination, the concentration of the drug for the obese patient is higher compared to the lean patient (Fig. 78).

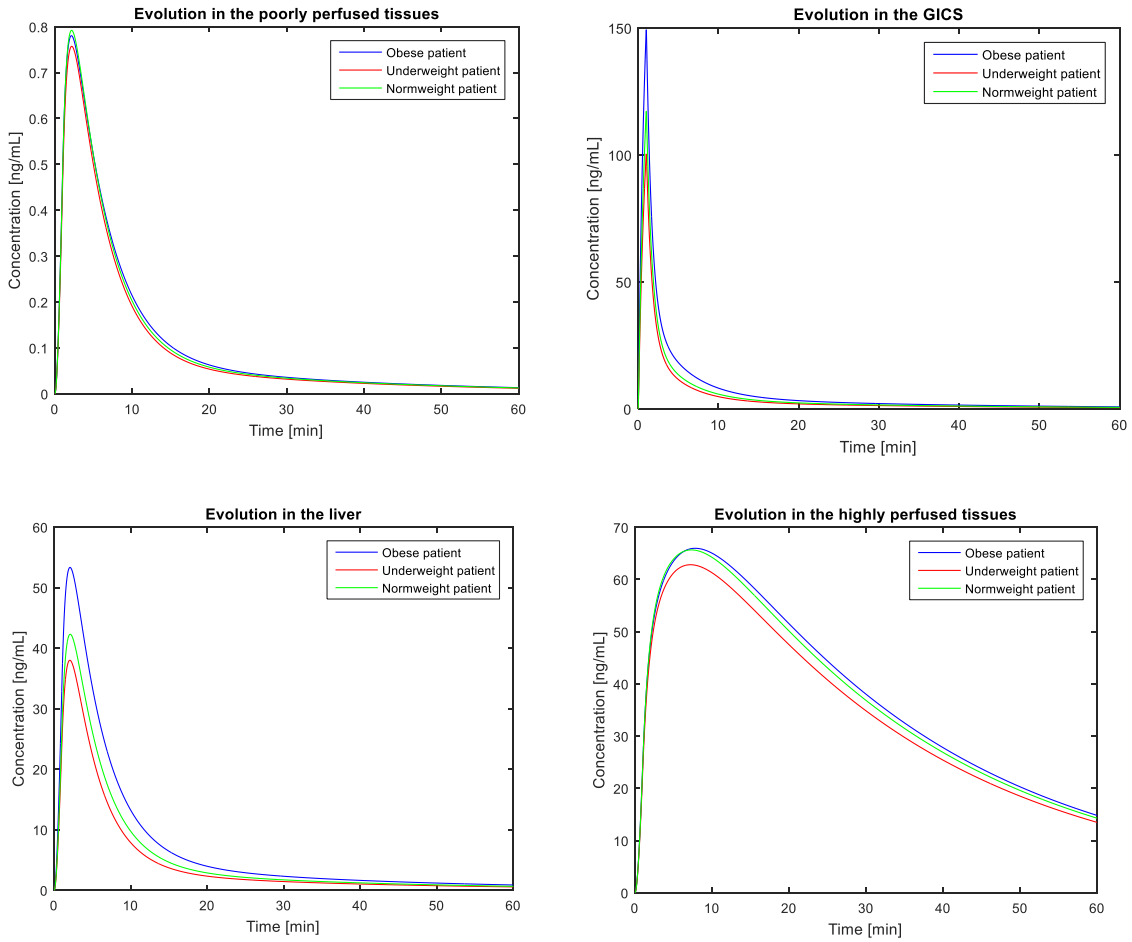

Figure 77 - Concentration-time profile of remifentanil in the poorly perfused tissues, highly perfused organs, liver, and GICS. Comparison of patients with different body weight: obese, normweight and underweight.

It is now interesting to observe the potential pharmacodynamics alterations due to what has been so far discussed. Consistently with the pharmacokinetics, it is possible to observe that the effect of the drug is stronger and faster in the obese patients, for which the lowest values of SAP, MAP, and HR are reached (Fig. 79).

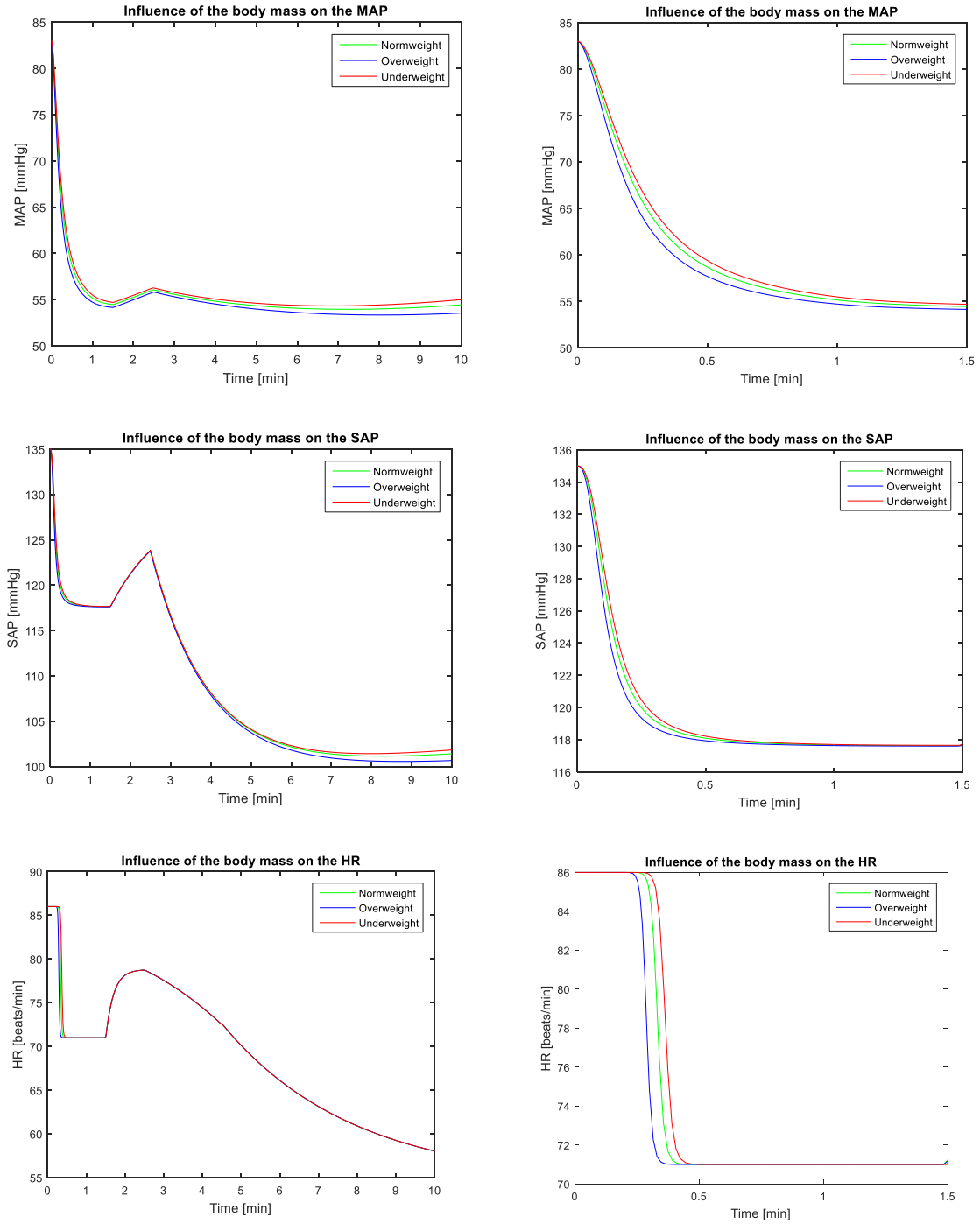

Figure 78 - Influence of the body weight on the hemodynamic effects. The right portion focuses on the phase that follows remifentanil administration. .

5. COMPARISON OF THE THREE-COMPARTMENT PK-PD MODEL AND THE 6P PK-PD MODEL

5.1 Three-compartment model

This thesis proposed, developed, and discussed a combined model to predict both the pharmacokinetics and pharmacodynamics of remifentanil (Chapter 4). In our opinion, it may be interesting to compare our model with the conventional three-compartment model developed by Minto *et al.* (1997). This is the model that nowadays is still used in literature (*i.e.* Drover and Lemmens (1998); Mertens *et al.* (2003); Pitsiu *et al.* (2004)). Since 1997, few modifications were proposed in order to improve the prediction capability of Minto's model. This is the case, for instance, of La Colla and colleagues (2009) who proposed a weight-adjusted height to better describe the PK of morbidly obese patients. They decided to introduce this correction because Minto's model uses the body weight or LBM as coviarate to study the inter- and intra-individual variability among patients (Paragraph 2.1). In the last years, new and more reliable parameters have been introduced in the pharmacokinetic models to have better and more realistic results (*i.e.* BMI) (Miller *et al.*, 2009). Therefore, the work of La Colla *et al.* (2009) is designed to offset this problem. Despite few modifications, like the one exposed, the basic model used in literature remains the one developed by Minto *et al.* (1997). Furthermore, Minto's model is implemented in the target controlled infusion (TCI) pumps employed in anesthesia (Sivasubramaniam S., 2007)**.** TCI pumps are standardized infusion systems for the administration of opioids or propofol and other anesthetics. The operation of this pump is based on *in silico* simulations of a known infusion scheme (Guarracino *et al.*, 2005) that, as previously mentioned, is based on the Minto *et al.* (1997) model for remifentanil. As a consequence, it is interesting to compare this three compartment PK model, widely used in the literature, to our model.

First, this is the proper place where to present the main features of the three-compartment model. Paragraph 2.1 provided a brief presentation of this model. Fig. 80 shows the structure of a three-compartment model.

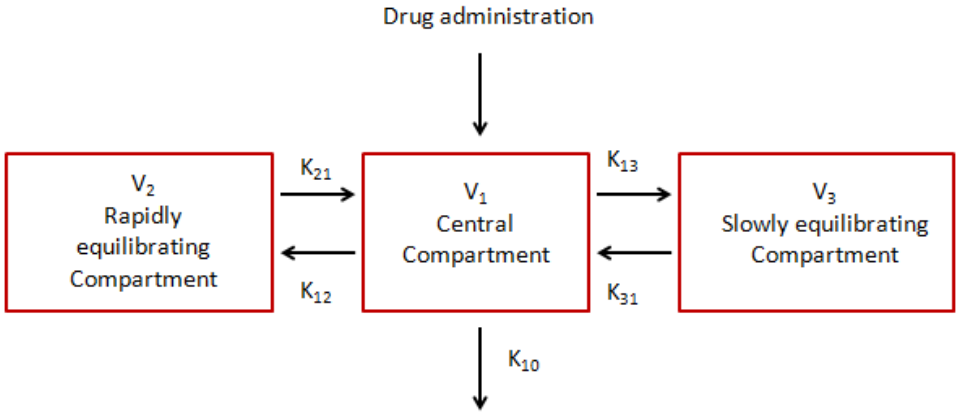

Figure 79 - Structure of the three-compartment model, adapted from Minto et al. (1997).

K_{10}, $K_{12}, K_{13}, K_{21}, K_{31}, K_{13}$ are the rate constants that describe the transport of the drug among the compartments. V_1, V_2, V_3 are parameters that correspond to the volumes of the central compartment and the two peripheral compartments, respectively. The state variables C_1, C_2, C_3 represent the drug concentrations in the central and peripheral compartments. Equations (74-76) describe the pharmacokinetics of remifentanil in the 3-compartment PK model. It is worth observing how Minto's model does not account for any anatomic/physiological features of mammalian body. The two side-compartments, respect to the central one, are just a way of mathematically lumping the information about fast and slow pharmaceutical effects after drugs administration. Also, the elimination path is lumped by the adaptive parameter K_{10}.

$$\frac{dC_1}{dt} = -(K_{10} + K_{12} + K_{13}) \cdot C_1 + \frac{V_2}{V_1} * K_{21} \cdot C_2 + \frac{V_3}{V_1} \cdot K_{31} \cdot C_3 + \frac{IV(t)}{V_1} \quad (74)$$

$$\frac{dC_2}{dt} = \frac{V_1}{V_2} \cdot K_{12} \cdot C_1 - K_{21} \cdot C_2 \quad (75)$$

$$\frac{dC_3}{dt} = \frac{V_1}{V_3} \cdot K_{13} \cdot C_1 - K_{31} \cdot C_3 \quad (76)$$

Table 57 lists the values of the parameters and variables of this model.

Table 57 - Values of the parameters of the 3-compartment PK model for remifentanil, taken from Minto et al. (1997).

Parameter	*Value*	*Unit of measure*
K_{10}	0.494	[min^{-1}]
K_{12}	0.339	[min^{-1}]
K_{13}	0.013	[min^{-1}]
K_{21}	0.188	[min^{-1}]
K_{31}	0.010	[min^{-1}]
V_1	4980	[mL]
V_2	9011	[mL]
V_3	6540	[mL]

5.2 Pharmacokinetic results

Minto *et al.* (1997) model provides a pharmacokinetic prediction for remifentanil. For this reason, first of all we compare the pharmacokinetics resulting from our 6P PK model to the one resulting from the 3-compartment PK model. The aim is to understand if the inclusion of the physiology of the human body in the 6P model provides a more precise and realistic prediction. Paragraphs 5.2.1-5.2.4 report the results of the two models. The considered case studies are the same presented in Chapter 2.

5.2.1 Case-study 1: Egan et al. (1996)

Fig. 81 reports the results of the two models, compared to the experimental data of Egan *et al.* (1996).

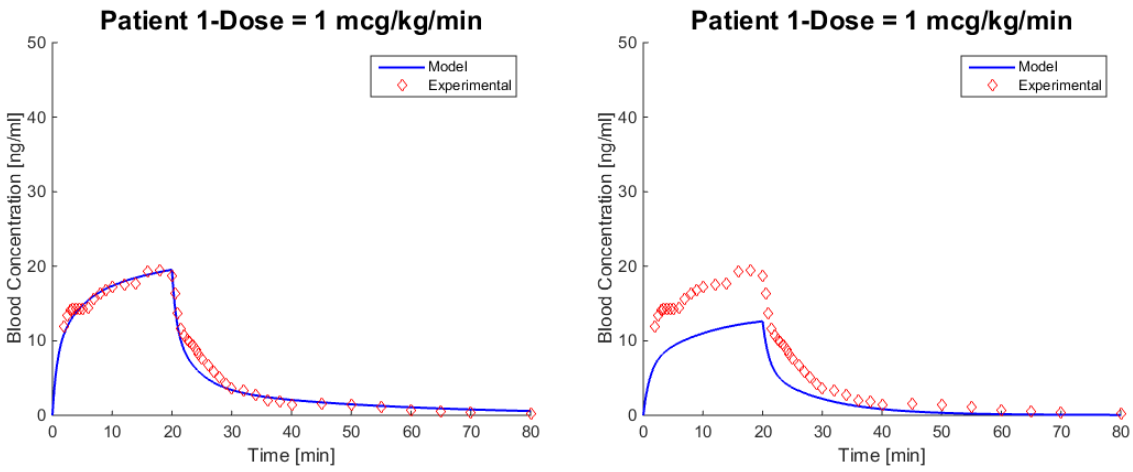

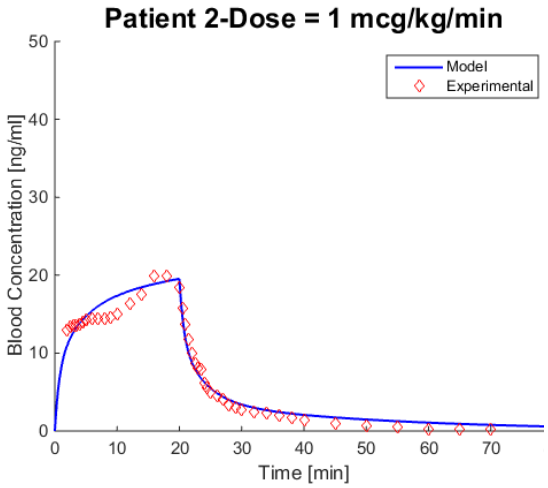
Patient 2-Dose = 1 mcg/kg/min
Model
Experimental
Blood Concentration [ng/ml]
Time [min]

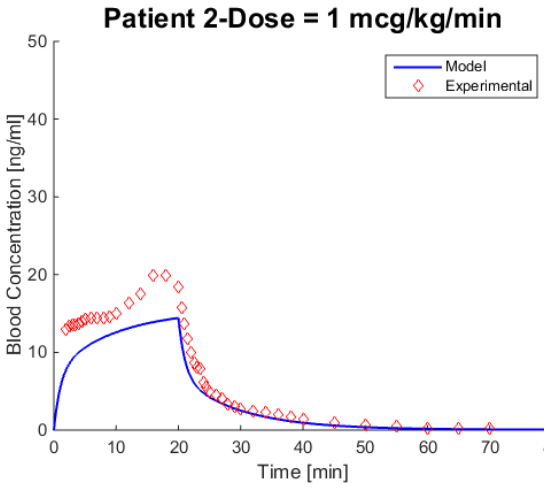
Patient 2-Dose = 1 mcg/kg/min
Model
Experimental
Blood Concentration [ng/ml]
Time [min]

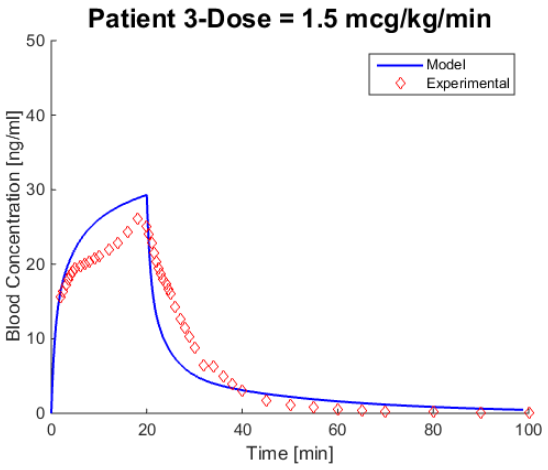
Patient 3-Dose = 1.5 mcg/kg/min
Model
Experimental
Blood Concentration [ng/ml]
Time [min]

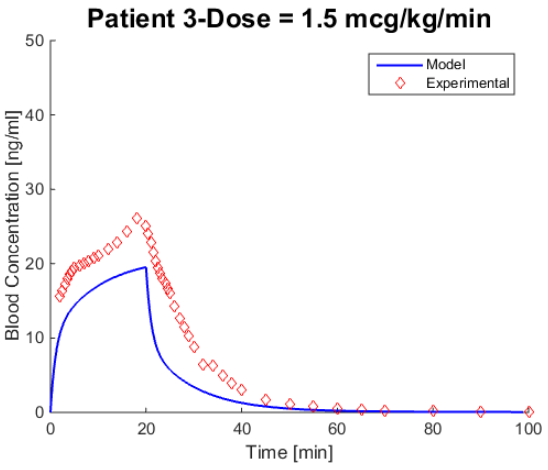
Patient 3-Dose = 1.5 mcg/kg/min
Model
Experimental
Blood Concentration [ng/ml]
Time [min]

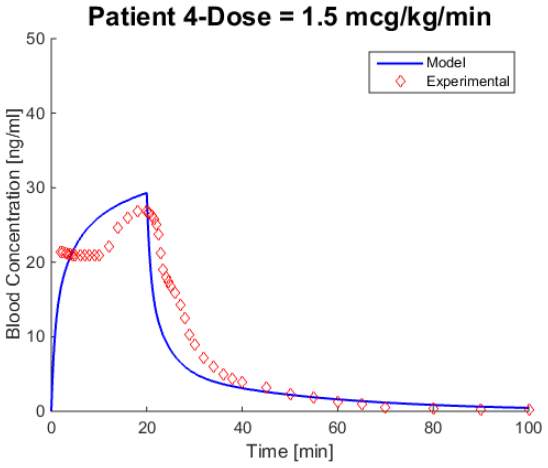
Patient 4-Dose = 1.5 mcg/kg/min
Model
Experimental
Blood Concentration [ng/ml]
Time [min]

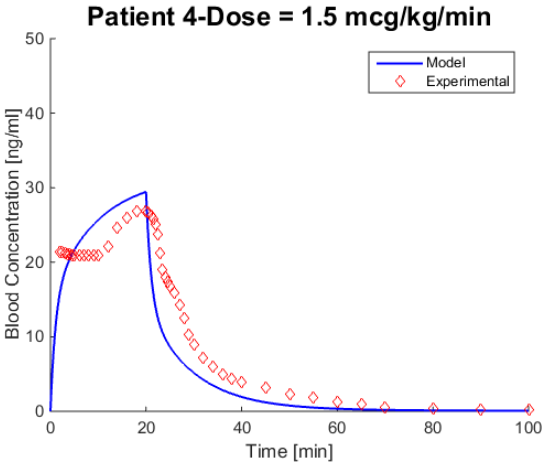
Patient 4-Dose = 1.5 mcg/kg/min
Model
Experimental
Blood Concentration [ng/ml]
Time [min]

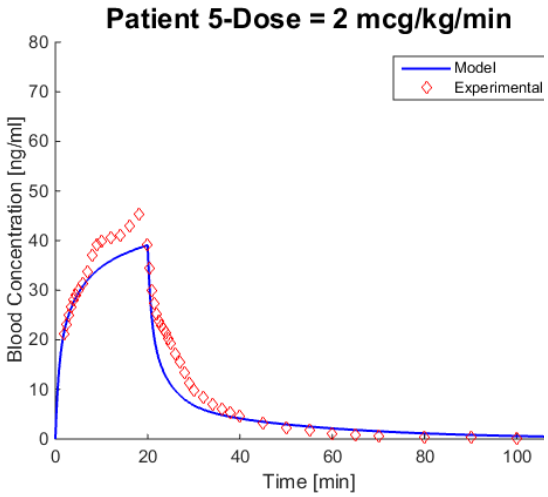
Patient 5-Dose = 2 mcg/kg/min
Model
Experimental
Blood Concentration [ng/ml]
Time [min]

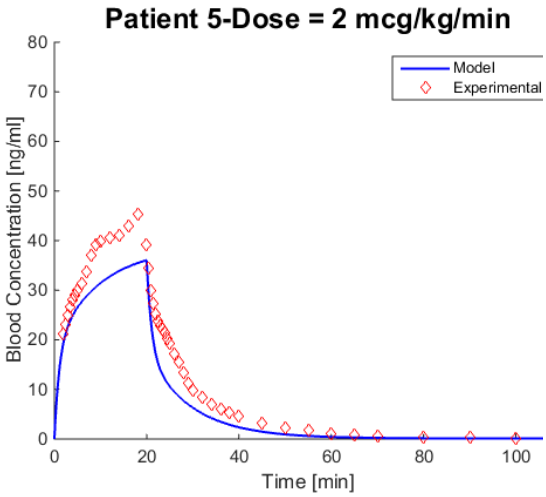
Patient 5-Dose = 2 mcg/kg/min
Model
Experimental
Blood Concentration [ng/ml]
Time [min]

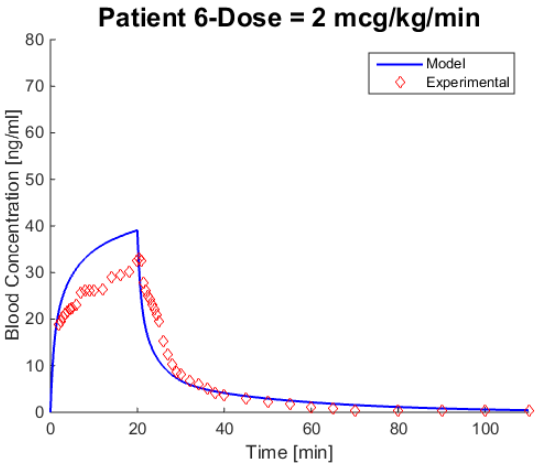
Patient 6-Dose = 2 mcg/kg/min
Model
Experimental
Blood Concentration [ng/ml]
Time [min]

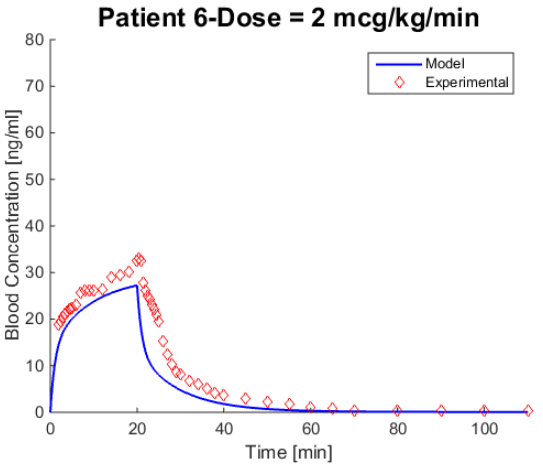
Patient 6-Dose = 2 mcg/kg/min
Model
Experimental
Blood Concentration [ng/ml]
Time [min]

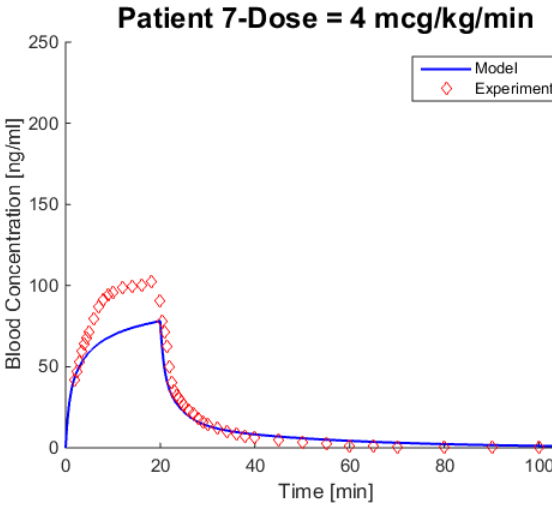
Patient 7-Dose = 4 mcg/kg/min
Model
Experiment
Blood Concentration [ng/ml]
Time [min]

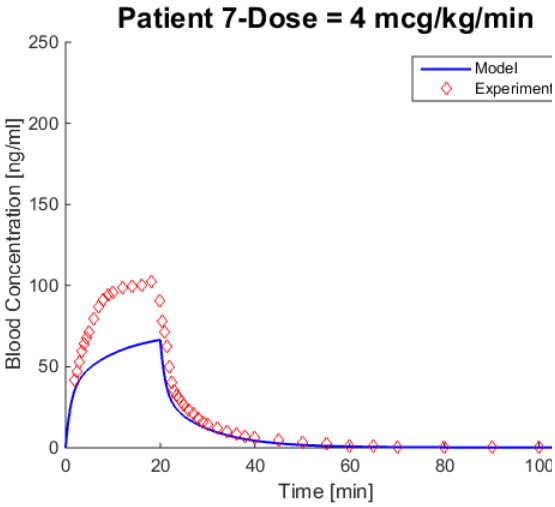
Patient 7-Dose = 4 mcg/kg/min
Model
Experiment
Blood Concentration [ng/ml]
Time [min]

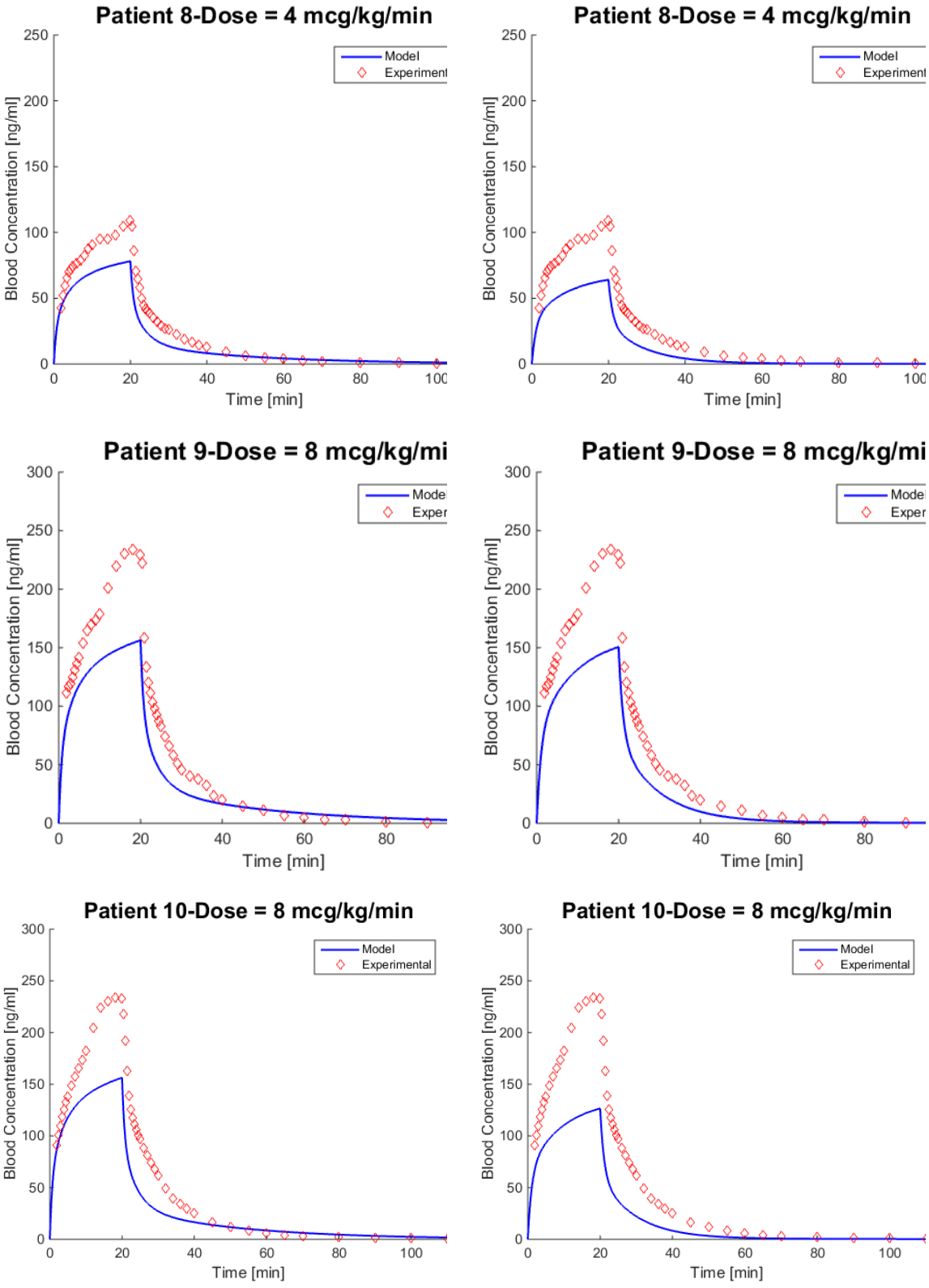

Figure 80 - The left portion shows the results of the 6P model. The right portion shows the results of the 3-compartment PK model of Minto et al., 1997. The experimental data (red) are from Egan et al. (1996).

Some performance indexes were evaluated to compare the two models, *i.e.* $\Delta C_{max}\%$, SAE, and IAE (Equations (24, 27-26), Paragraph 2.4). Tables 58A, 58B, and 58C report the values of such parameters.

Table 58A - Comparison of the $\Delta C_{max}\%$ values between the 6P and Minto's models based on Egan et al. (1996) experimental data.

Patient	Infusion dose [µg/kg/min]	*6P model*	*3-compartment PK model*
1	1	0.36	35.21
2	1	2.06	27.74
3	1.5	11.37	25.82
4	1.5	8.59	9.05
5	2	14.59	21.23
6	2	18.36	17.52
7	4	30.91	41.23
8	4	29.41	41.91
9	8	33.32	35.77
10	8	33.34	46.03

Table 58B - Comparison of the SAE values between the 6P and Minto's models based on Egan et al. (1996) experimental data.

Patient	Infusion dose [µg/kg/min]	*6P model*	*3-compartment PK model*
1	1	0.56	1.95
2	1	0.87	1.50
3	1.5	2.00	2.57
4	1.5	1.53	1.71
5	2	1.54	2.11
6	2	2.39	2.42
7	4	6.30	8.28
8	4	6.38	9.72

9	8	13.60	14.69
10	8	11.46	16.32

Table 58C - Comparison of the IAE values between the 6P and Minto's models based on Egan et al. (1996) experimental data.

Patient	Infusion dose [µg/kg/min]	*6P model*	*3-compartment PK model*
1	1	27.90	100.16
2	1	42.16	76.42
3	1.5	77.59	97.88
4	1.5	83.80	93.38
5	2	99.53	135.66
6	2	135.93	134.60
7	4	330.54	437.78
8	4	414.43	627.24
9	8	839.37	910.48
10	8	432.94	608.82

It is evident that the performance indexes are better for the 6P model for all the patients, but Patient 6 (where there is a rather small advantage of Minto's model as far as $\Delta C_{max}\%$ and IAE are concerned). It has already been underlined that the trend of the experimental data of this patient is unusual.

Eventually, it is possible to claim that the 6P model provides better results than the 3-compartment PK model.

It is worth observing that the simulations of different patients that received the same dose are clearly different in case of Minto's model. On the contrary, they look practically the same in case of the 6P model. The reason is related to the different sensitivity of the models to the patient body mass difference. In fact, this minor sensitivity is an intrinsic feature of the 6P model and this is the reason why in Chapter 4 we have moved towards a higher level of individualization by employing Nadler's formulae (respect to the original 8P model of Abbiati et al., 2016). In fact, Nadler's formulae allowed improving

the degree of individualization of the model, taking into account also the height of the patient (Paragraph 4.7).

5.2.2 Case-study 2: Westmoreland et al. (1993)

Fig. 82 reports the results of the two models, compared to the experimental data of Westmoreland *et al.* (1993).

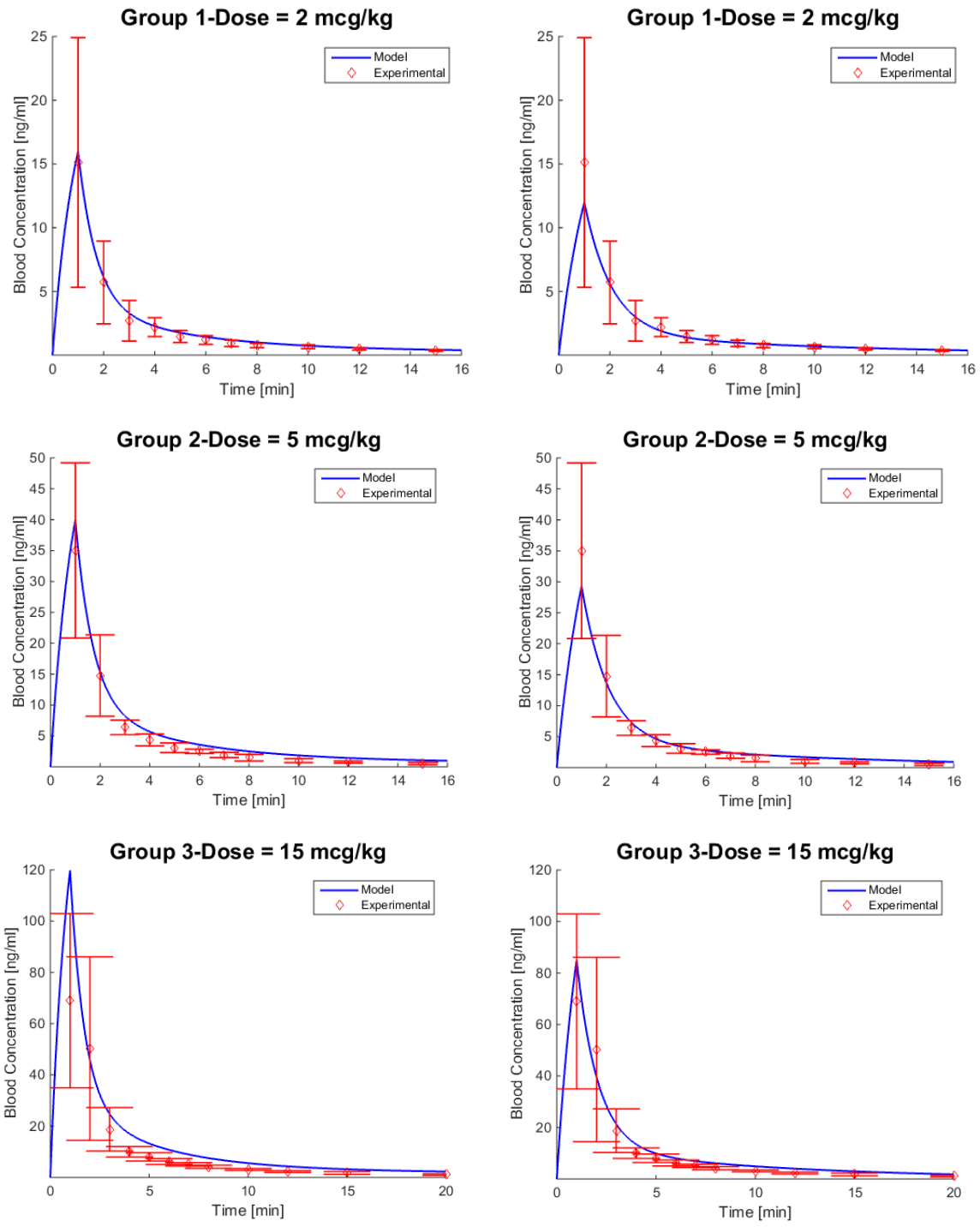

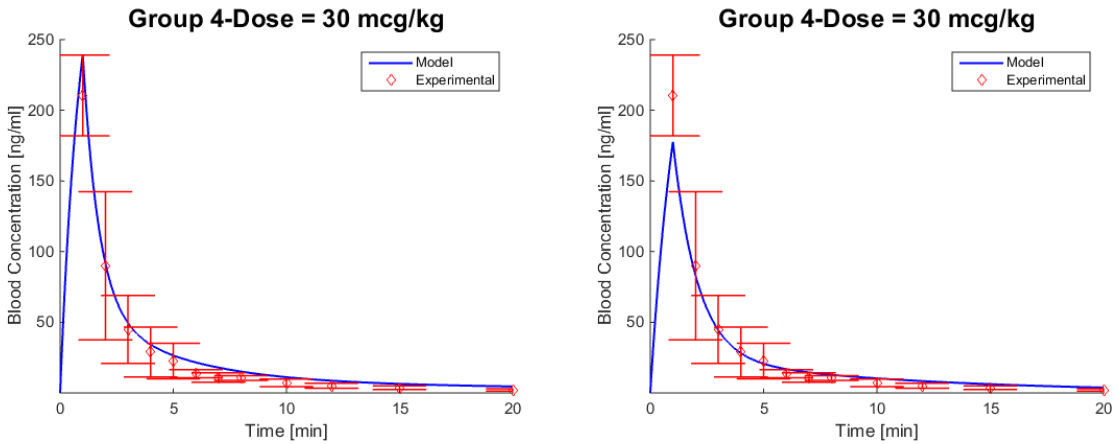

Figure 81 - The left portion shows the results of the 6P model. The right portion shows the results of the 3-compartment PK model of Minto et al., 1997. The experimental data are from Westmoreland et al. (1993).

Tables 59A, 59B, and 59C list the values of the performance indexes.

Table 59A - Comparison of the $\Delta C_{max}\%$ values between the 6P and Minto's models based on Westmoreland et al. (1993) experimental data.

Group	*Bolus dose [µg/ kg]*	*6P model*	*3-compartment PK model*
1	2	5.66	20.72
2	5	14.05	16.32
3	15	73.74	23.21
4	30	13.79	15.62

Table 59B - Comparison of the SAE values between the 6P and Minto's models based on Westmoreland et al. (1993) experimental data.

Group	*Bolus dose [µg/ kg]*	*6P model*	*3-compartment PK model*
1	2	0.240	0.311
2	5	1.033	0.754
3	15	5.308	2.568
4	30	4.622	3.529

Table 59C - Comparison of the IAE values between the 6P and Minto's models based on Westmoreland et al. (1993) experimental data.

Group	Bolus dose [μg/ kg]	6P model	3-compartment PK model
1	2	2.90	2.77
2	5	14.09	9.15
3	15	70.12	38.18
4	30	68.66	47.04

It is possible to notice that the $\Delta C_{max}\%$ values are lower for the 6P model, while SAE and IAE are lower for the 3-compartment PK model. However, IAE and SAE values are not significantly different between the models, but for Patient 3. The specific case of this patient was discussed in Chapter 2.

As underlined in Chapter 2, the 6P model is physiologically based and so even if it seems to produce worse pharmacokinetic predictions (respect to experimental measurements), it is nearer to a realistic representation of the human body. In this case, the 6P model is able to predict the peak of the drug concentration with better results, but it is less able to follow the rest of the trend.

5.2.3 Case-study 3: Pitsiu et al. (2004)

Fig. 83 shows the results for the two models, compared to the experimental data of Pitsiu *et al.* (2004). Patients 1, 2, 3, and 4 represent four single patients.

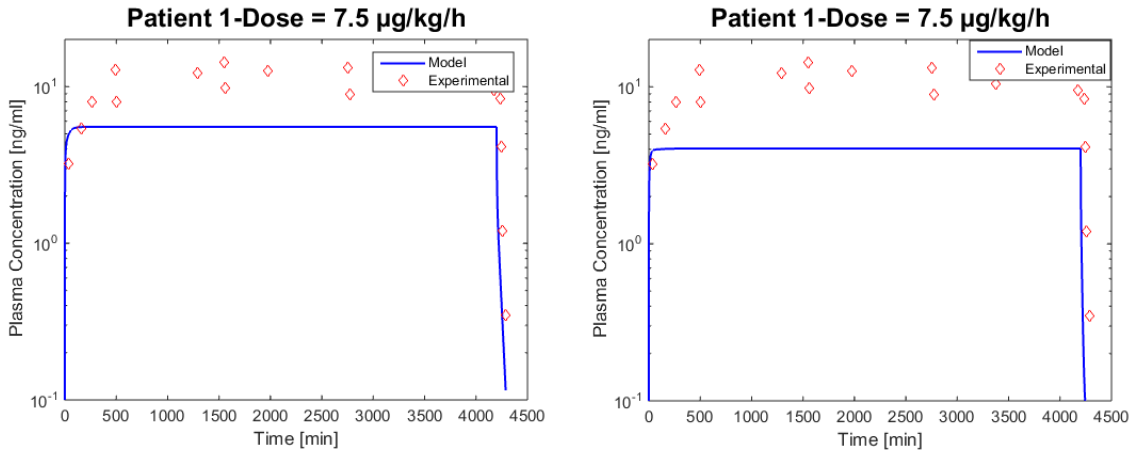

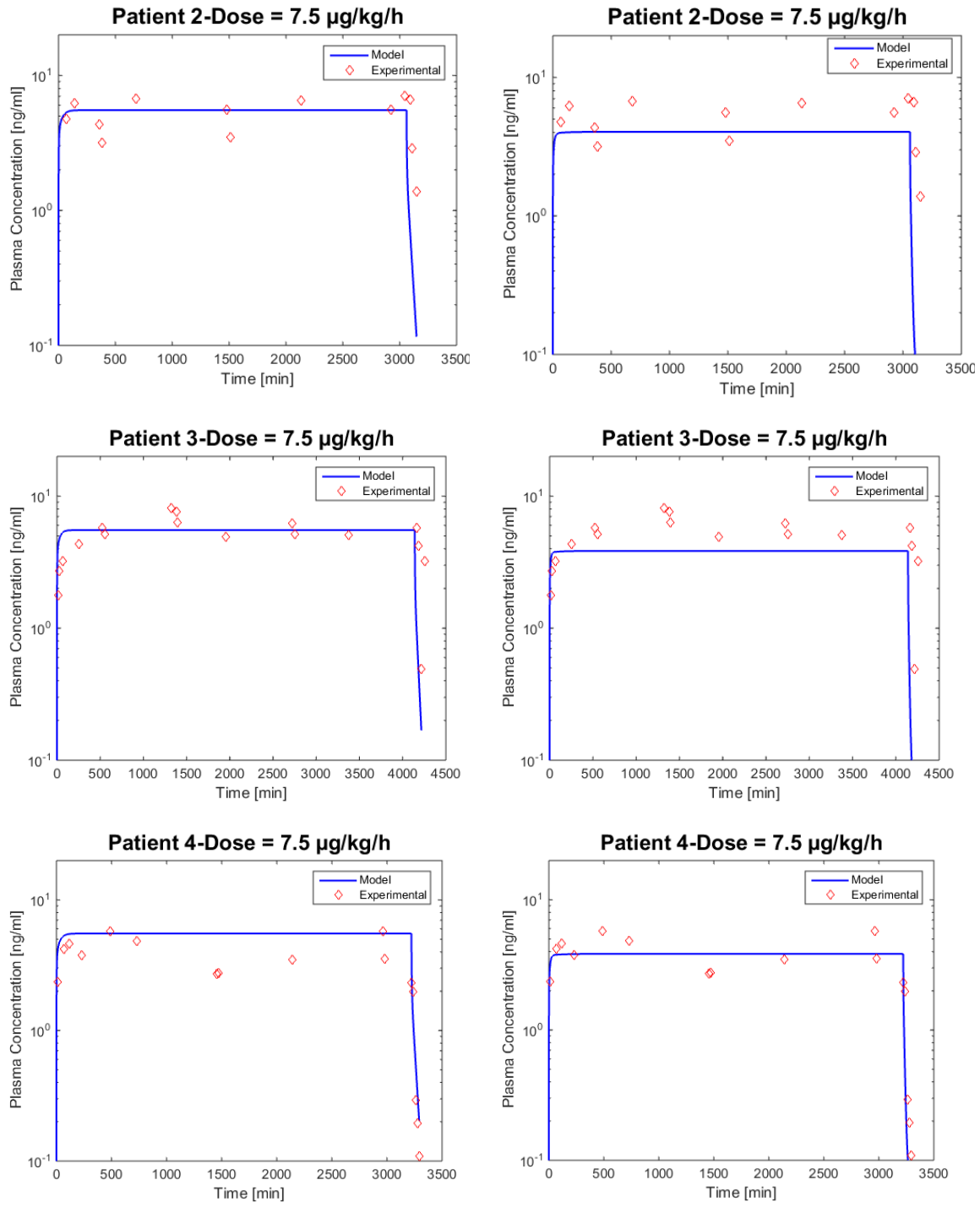

Figure 82 - The left portion shows the results of the 6P model. The right portion shows the results of the 3-compartment PK model of Minto et al., 1997. The considered experimental data (red) are from Pitsiu et al. (2004).

Tables 60A and 60B report the values of the performance indexes. As explained in Chapter 2, in this case it is not interesting to evaluate the $\Delta C_{max}\%$,, therefore only the value of SAE and IAE will be reported.

Table 60A - Comparison of the SAE values between the 6P and Minto's models based on Pitsiu et al. (2004) experimental data.

Patient	Infusion dose [µg/ kg/ h]	6P model	3-compartment PK model
1	7.5	4.308	5.360
2	7.5	1.564	2.037
3	7.5	1.106	2.153
4	7.5	1.301	0.835

Table 60B - Comparison of the IAE values between the 6P and Minto's models based on Pitsiu et al. (2004) experimental data.

Patient	Infusion dose [µg/ kg/h]	6P model	3-compartment PK model
1	7.5	72.31	90.57
2	7.5	19.398	25.44
3	7.5	18.637	35.61
4	7.5	19.812	12.86

In this case too, it is possible to observe that the 6P model provides better results than the 3-compartment PK model.

5.2.4 Case-study 4: Glass et al. (1993)

Fig. 84 reports the results for the two models, compared to the experimental data of Glass *et al.* (1993).

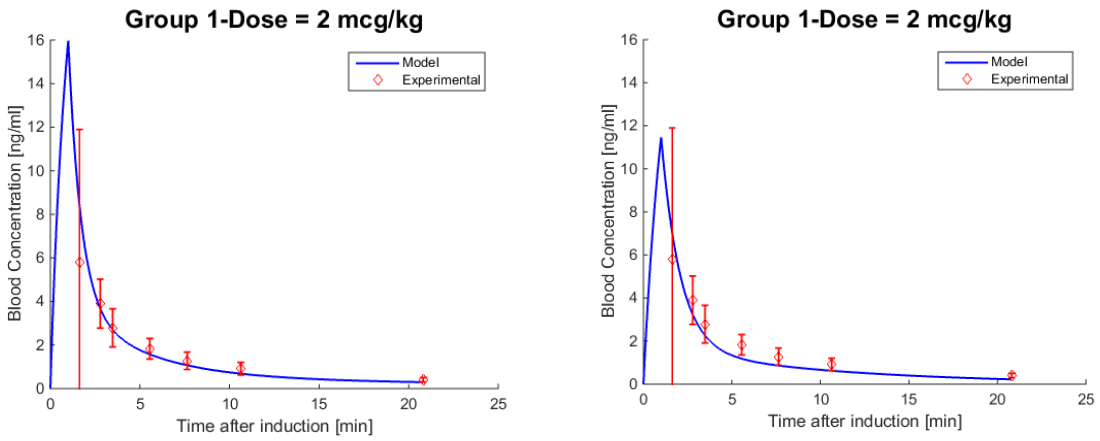

Figure 83 - The left figure shows the results of the 6P model. The right figure shows the results of the 3-compartment PK model of Minto et al., 1997. The experimental data (red) are from Glass et al. (1993).

In this case $\Delta C_{max}\%$ was not evaluated because of the lack of the experimental value of the concentration peak in the paper, therefore only SAE and IAE were evaluated and their values are listed in Table 61.

Table 61 - Comparison of the SAE and IAE values between the 6P and Minto's models based on Glass et al. (1993) experimental data.

Performance index	*Group*	*Bolus dose [μg/ kg]*	*6P model*	*3-compartment PK model*
SAE	1	2	0.201	0.558
IAE	1	2	2.338	3.217

Again, it is possible to observe that 6P model gives better results than the 3-compartment PK model.

5.2.5 Final remarks

Concerning the pharmacokinetics, it is possible to sustain that the 6P model is better than the 3-compartment PK model (Minto *et al.*, 1997) as in most cases the 6P model performance indexes are lower. Moreover, when they are higher, they are pretty similar to the ones of the 3-compartment PK model. As previously underlined, the 6P model has the additional advantage of a physiological base and so it is more realistic than the 3-compartment model, in which the body is approximated with only three compartments.

This confirms that the 6P model gives a better prediction of the pharmacokinetics of remifentanil.

5.3 Pharmacodynamic results

Starting from the pharmacokinetic considerations, it is possible to analyze the pharmacodynamic simulations. Minto did not investigate the pharmacodynamics of remifentanil in terms of cardiovascular effects. For this reason, we built a combined model in which the pharmacokinetic model is the one of Minto et al. (1997), to analyze the influence of that model on the pharmacodynamics. The employed PD models (*i.e.* SAP, MAP, and HR) are the same as those presented in Chapter 3. Specific values for k_{e0} were computed for the three PD models in order to link Minto's PK and PD. Table 62 lists the k_{e0} values and compares them to the k_{e0} values of our PD models (Chapter 4). These values were computed using the same strategy adopted for the combined model that is based on the collapse of the hysteresis loop (see Paragraph 4.2).

Table 62 - Left column, values of k_{e0} for the 6P PK-PD model. Right column, values for the 3-compartment PK-PD model.

PD effect	k_{e0} for 6P PK-PD model	k_{e0} for 3-compartment PK-PD model
SAP	0.9994	0.911
MAP	0.364	0.702
HR	0.861	0.749

It is possible to observe that, only for MAP, the value of k_{e0} changes significantly, while for the other two effects (*i.e.* SAP and HR) the difference is not so evident. Paragraphs 5.3.1-5.3.3 report the results of the 3-compartment PK-PD model, compared to our 6P PK-PD model. The case studies used to compare these two models are the same presented in Chapter 3 and Chapter 4.

5.3.1 Results for SAP

Case-study 1: Lee et al. (2012)

Fig. 85 shows the results of the two models, compared to the experimental data of Lee *et al.* (2012).

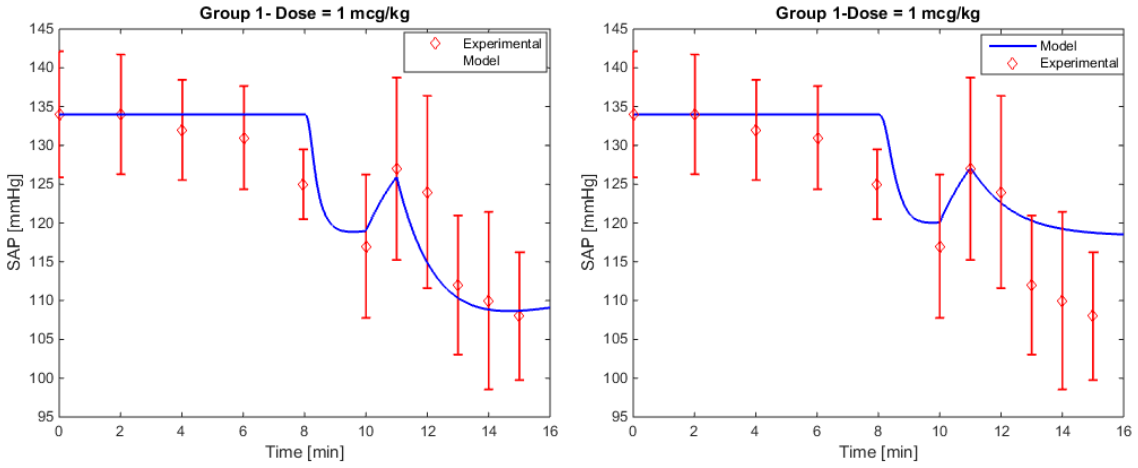

Figure 84 - The left figure shows the results of the 6P PK-PD model. The right figure shows the results of the 3-compartment PK-PD model. The experimental data (red) are from Lee et al. (2012).

As usual, it is possible to evaluate some performance indexes to compare the models and verify their reliability (Equations (51-52), Paragraph 3.4). Table 63 lists $\Delta E_{max}\%$ and SAE values.

Table 63 - Comparison of $\Delta E_{max}\%$ and SAE values for SAP between the 6P PK-PD and Minto's PK-PD models based on Lee et al. (2012) experimental data.

Performance index	*Group*	*6P PK-PD model*	*3-compartment PK-PD model*
$\Delta E_{max}\%$	1	8.30	5.17
SAE	1	2.70	4.26

In this case, it is possible to notice that the 3-compartment PK-PD model is able to predict better only the effect response to laryngoscopy. In fact, considering the rest of the trend, it is evident that the 6P PK-PD model produces better results. This is shown by the values of the performance indexes: the $\Delta E_{max}\%$ is lower for the 3-compartment PK-PD model, while the value of SAE is lower for our model. The difference between the models is particularly evident in the last tract, where the effect tends to return to its normal value. In fact, in this tract the 6P PK-PD model has a similar trend respect to the experimental data, while the 3-compartment PK-PD model does not almost fall within the error bars.

Case-study 2: Park et al. (2011)

Fig. 86 shows the results of the two models, compared to the experimental data of Park *et al.* (2011).

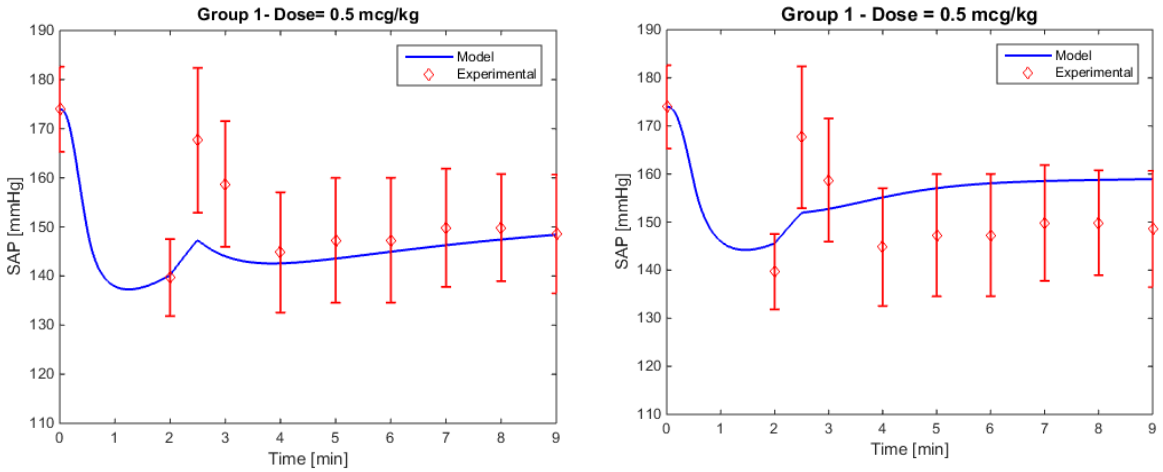

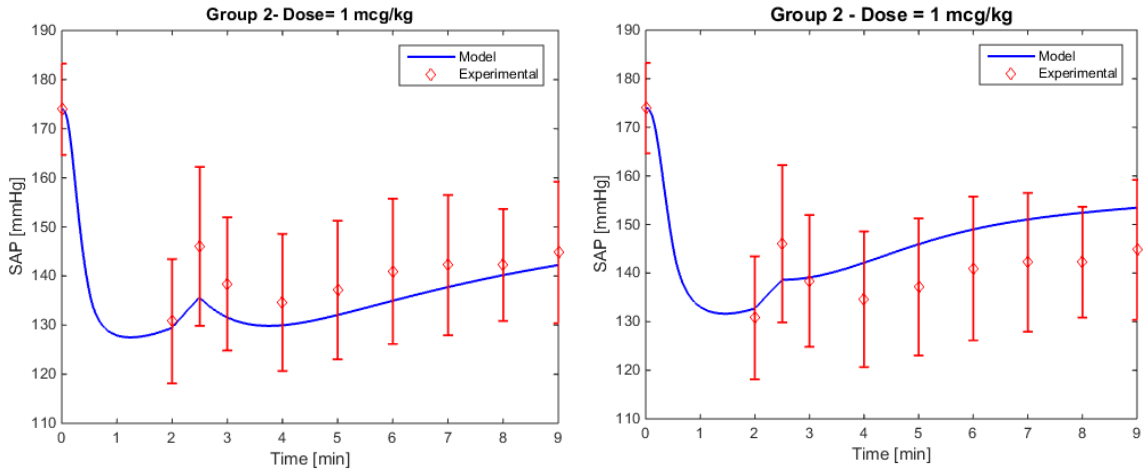

Figure 85 - The left portion shows the results of the 6P PK-PD model. The right portion shows the results of 3-compartment PK-PD model. The experimental data (red) are from Park et al. (2011).

Tables 64A and 64B report the values of the performance indexes.

Table 64A - Comparison of the $\Delta E_{max}\%$ values between the 6P PK-PD and Minto's PK-PD SAP models based on Park et al. (2011) experimental data.

Group	*6P PK-PD model*	*3-compartment PK-PD model*
1	12.15	9.44
2	7.19	5.07

Table 64B - Comparison of the SAE values between the 6P PK-PD and Minto's PK-PD SAP models based on Park et al. (2011) experimental data.

Group	*6P PK-PD model*	*3-compartment PK-PD model*
1	5.01	8.65
2	4.34	6.22

The results of this case-study are similar to the previous one and the considerations made there can be extended to this case-study.

Case-study 3: O'Hare et al. (1999)

Fig. 87 reports the results of the two models, compared to the experimental data of O'Hare *et al.* (1999).

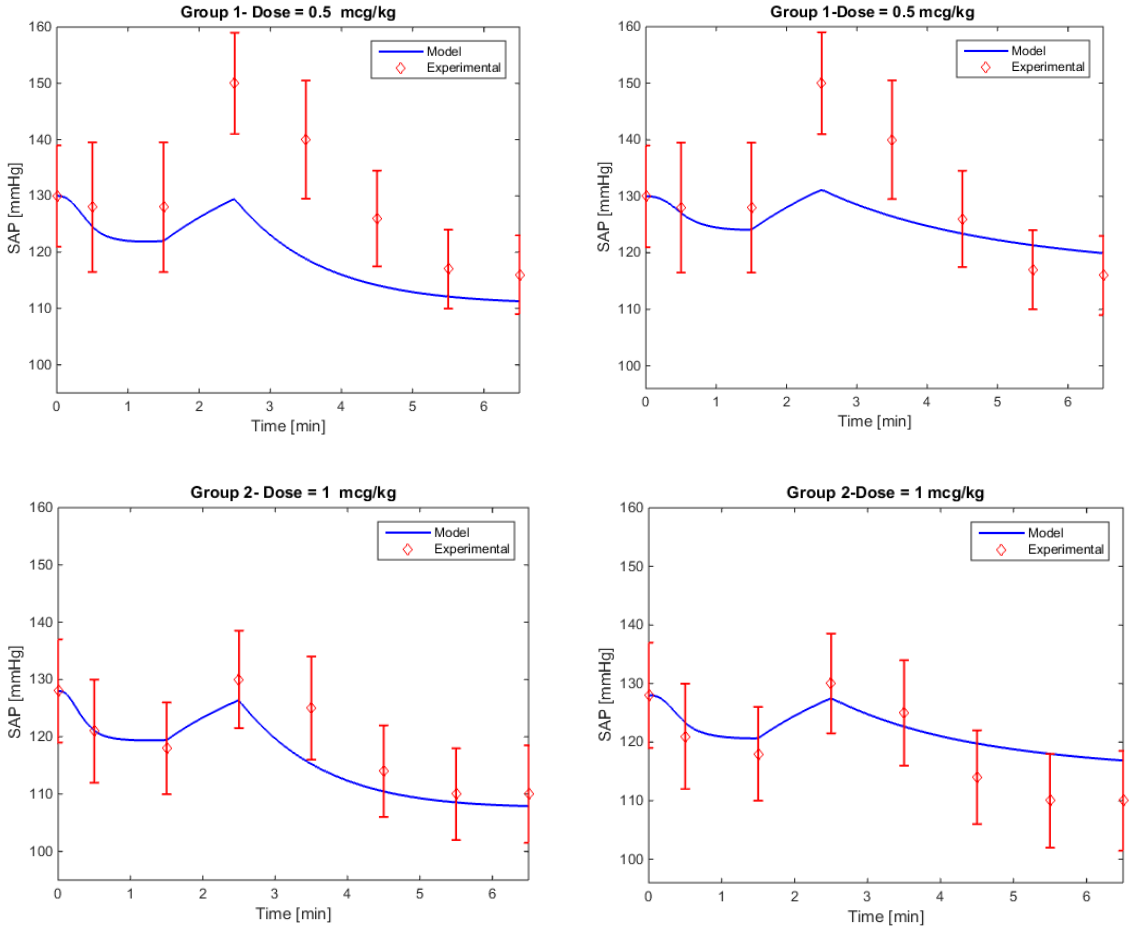

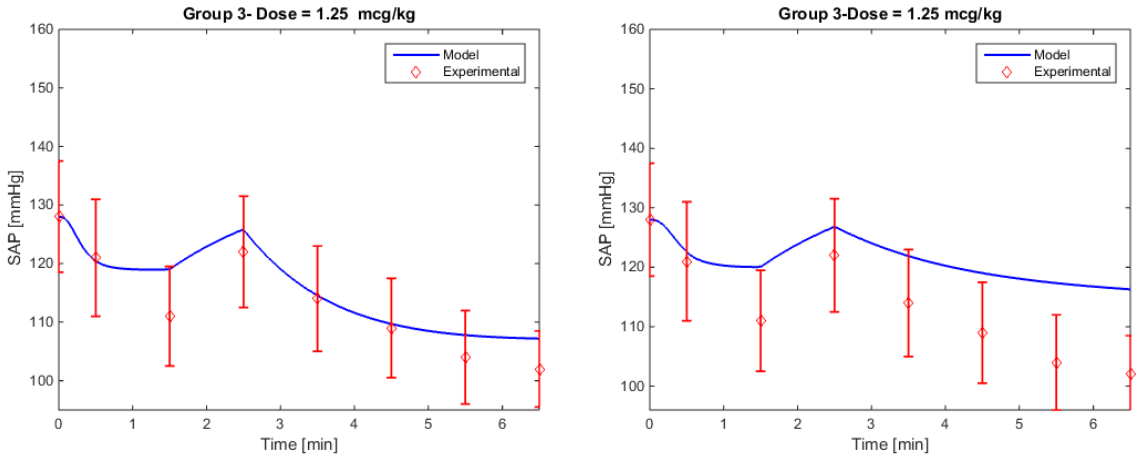

Figure 86 - The left portion shows the results of the 6P PK-PD model. The right portion shows the results of the 3-compartment PK-PD model. The experimental data (red) are from O'Hare et al. (1999).

Tables 65A and 65B list the values of the performance indexes.

Table 65A - Comparison of the $\Delta E_{max}\%$ values between the 6P PK-PD and Minto's PK-PD SAP models based on O'Hare et al. (1999) experimental data.

Group	*6P PK-PD model*	*3-compartment PK-PD model*
1	13.70	12.62
2	2.81	1.98
3	3.11	3.94

Table 65B - Comparison of the SAE values between the 6P PK-PD and Minto's PK-PD SAP models based on O'Hare et al. (1999) experimental data.

Group	*6P PK-PD model*	*3-compartment PK-PD model*
1	9.09	6.03
2	2.77	3.82
3	2.81	7.62

Again, it is possible to make similar considerations to the previous case studies. In fact, the values of $\Delta E_{max}\%$ are lower for the 3-compartment PK-PD model, while the values of SAE are lower for our model.

Conclusions

In general, the values of $\Delta E_{max}\%$ are lower for the 3-compartment PK-PD model, while the values of SAE are lower for the 6P PK-PD model. The 3-compartment PK-PD model is more precise in the prediction of the peak effect, while the 6P PK-PD model provides better results throughout the simulated trend. However, the values of the performance indexes are not significantly different. Therefore, the difference in the pharmacokinetics does not reflect significantly into clinical differences in the pharmacodynamics, at least in terms of SAP. As previously discussed, the tract in which the difference is more evident is the last one.

Again, it is important to remark that the 6P PK-PD model is a physiologically based model and it provides better pharmacokinetic results respect the 3-compartment PK model (Paragraph 5.2).

5.3.2 Results for MAP

Case-study 1: Alexander et al. (1999)

Fig. 88 reports the results of the two models, compared to the experimental data of Alexander *et al.* (1999).

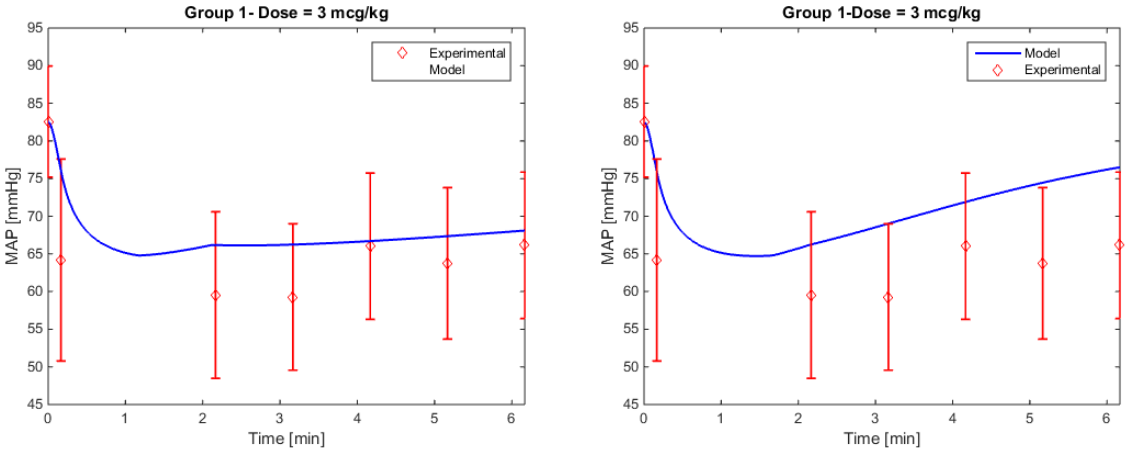

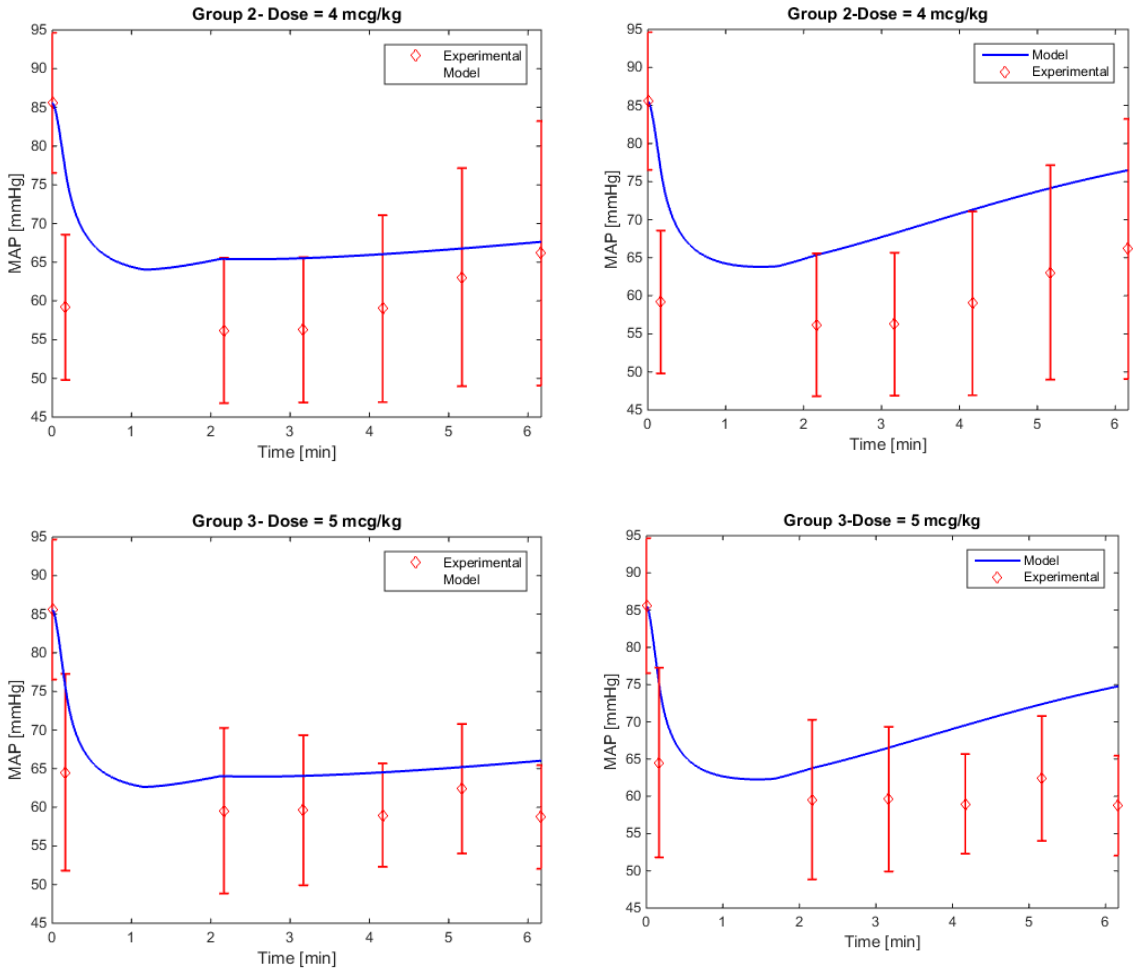

Figure 87 - The left portion shows the results of the 6P PK-PD model. The right portion shows the results of the 3-compartment PK-PD model. The experimental data (red) are from Alexander et al. (1999).

Tables 66A and 66B report the values of the performance indexes.

Table 66A - Comparison of the $\Delta E_{max}\%$ values between the 6P PK-PD and Minto's PK-PD MAP models based on Alexander et al. (1999) experimental data.

Group	*6P PK-PD model*	*3-compartment PK-PD model*
1	11.10	11.20
2	16.40	16.20
3	7.50	7.03

Table 66B - Comparison of the SAE values between the 6P PK-PD and Minto's PK-PD MAP models based on Alexander et al. (1999) experimental data.

Group	*6P PK-PD model*	*3-compartment PK-PD model*
1	6.71	7.87
2	7.93	10.32
3	7.89	8.32

$\Delta E_{max}\%$ values show that the difference between the models is practically negligible. This means that the two models have approximately the same precision in the prediction of the effect peak in this case. The values of SAE are instead lower for the 6P PK-PD model, so that it seems to provide better results than the 3-compartment PK-PD model.

Case-study 2: Hall et al. (2000)

Fig. 89 shows the results of the two models, compared to the experimental data of Hall *et al.* (2000).

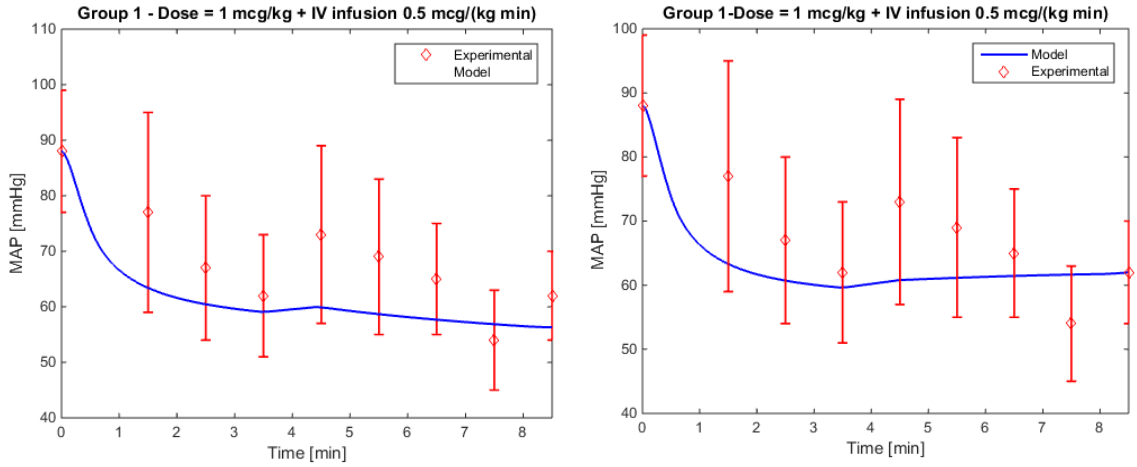

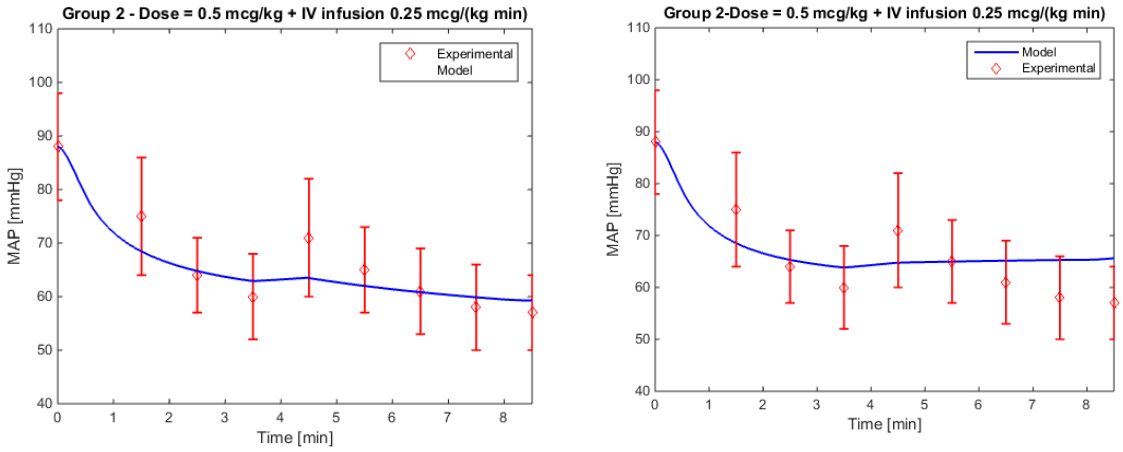

Figure 88 - The left portion shows the results of the 6P PK-PD model. The right portion shows the results of the 3-compartment PK-PD model. The experimental data (red) are from Hall et al. (2000).

Tables 67A and 67B list the values of the performance indexes.

Table 67A - Comparison of the $\Delta E_{max}\%$ values between the 6P PK-PD and Minto's PK-PD MAP models based on Hall et al. (2000) experimental data.

Group	*6P PK-PD model*	*3-compartment PK-PD model*
1	17.85	16.77
2	10.60	8.81

Table 67B - Comparison of the SAE values between the 6P PK-PD and Minto's PK-PD MAP models based on Hall et al. (2000) experimental data.

Group	*6P PK-PD model*	*3-compartment PK-PD model*
1	6.93	5.96
2	2.80	4.22

The $\Delta E_{max}\%$ values are lower for the 3-compartment PK-PD model, but the values of SAE are lower for our model. Therefore, it is possible to make the same considerations as in the previous case.

Case-study 3: Batra et al. (2004)

Fig. 90 shows the results of the two models, compared to the experimental data of Batra *et al.* (2004).

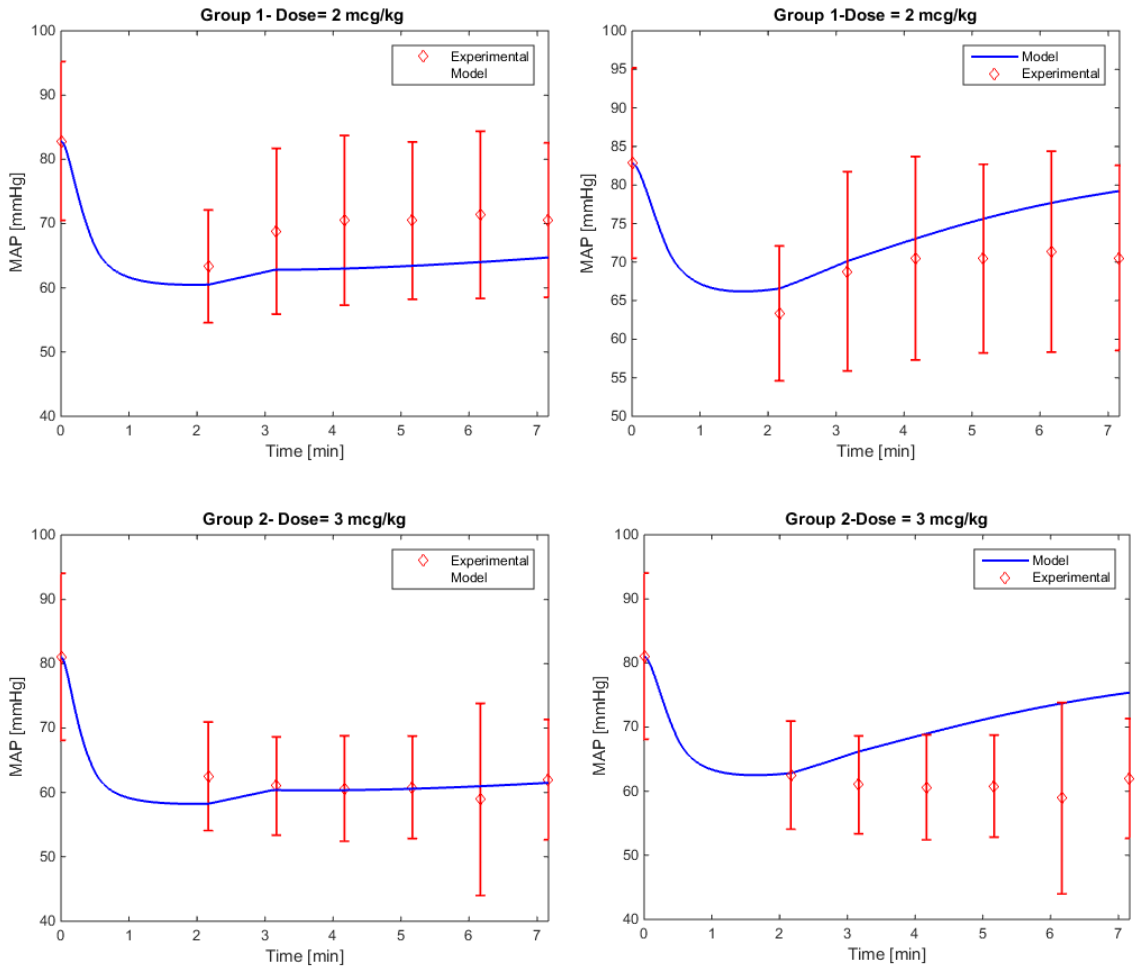

Figure 89 - The left portion shows the results of the 6P PK-PD model. The right portion shows the results of the 3-compartment PK-PD model. The experimental data (red) are from Batra et al. (2004).

Tables 68A and 68B list the values of the performance indexes.

Table 68A - Comparison of the $\Delta E_{max}\%$ values between the 6P PK-PD and Minto's PK-PD MAP models based on Batra et al. (2004) experimental data.

Group	*6P PK-PD model*	*3-compartment PK-PD model*
1	8.70	1.67
2	1.08	8.37

Table 68B - Comparison of the SAE values between the 6P PK-PD and Minto's PK-PD MAP models based on Batra et al. (2004) experimental data.

Group	6P PK-PD model	3-compartment PK-PD model
1	5.22	3.89
2	1.13	7.55

Also in this case the values of the performance indexes are not significantly different.

Conclusions

Previous considerations about SAP can be extended to MAP. In fact, the performance indexes are very similar between the models, without highlighting any particular differences.

As for SAP, the last tract presents more evident differences. The 6P PK-PD model is more reliable in the description of this tract, respect to the 3-compartment PK-PD model.

5.3.3 Results for HR

Case-study 1: Lee et al. (2012)

Fig. 91 shows the results of the two models, compared to the experimental data of Lee *et al.* (2012).

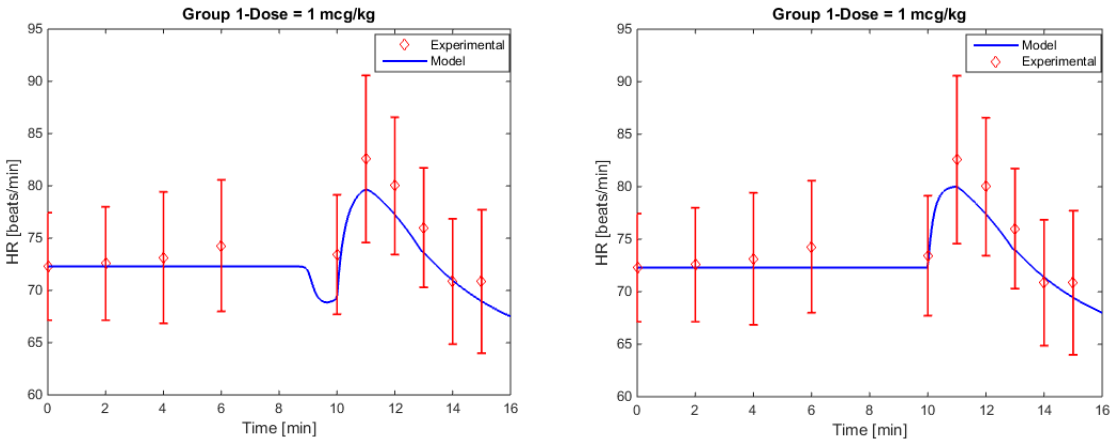

Figure 90 - The left figure shows the results of the 6P PK-PD model. The right figure shows the results of the 3-compartment PK-PD model. The considered experimental data (red) are from Lee et al. (2012).

In this case, it is possible to see that in the 6P PK-PD model there is a decrement after the administration of remifentanil, which occurs 8 min after the beginning of the

measurements, which is on the contrary absent in the 3-compartment PK-PD model. This is related to the difference in the pharmacokinetic prediction.

Table 69 lists the values of the performance indexes.

Table 69 - Comparison of the $\Delta E_{max}\%$ and SAE values between the 6P PK-PD and Minto's PK-PD HR models based on Lee et al. (2012) experimental data.

Performance index	*Group*	*6P PK-PD model*	*3-compartment PK-PD model*
$\Delta E_{max}\%$	1	3.51	3.10
SAE	1	1.71	1.31

Case-study 2: Park et al. (2011)

Fig. 92 reports the results of the two models, compared to the experimental data of Park *et al.* (2011).

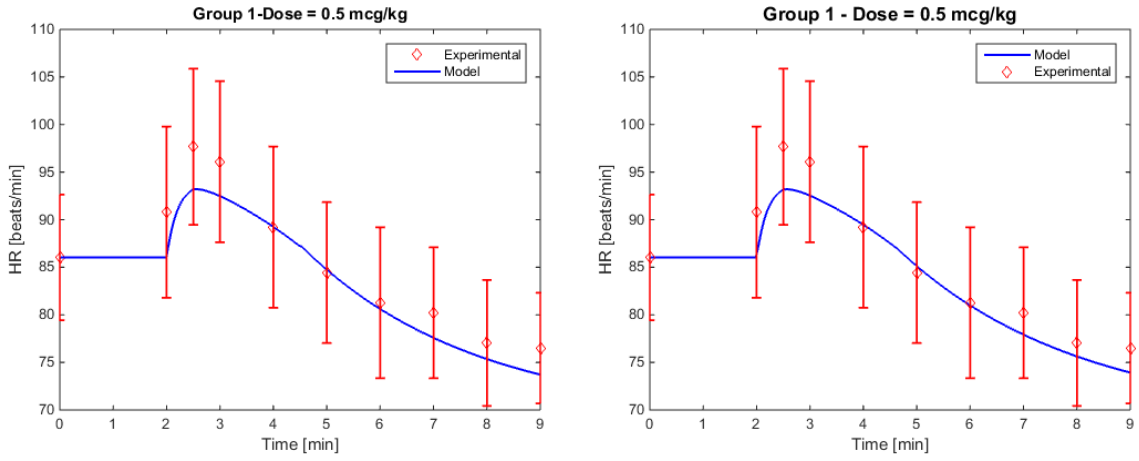

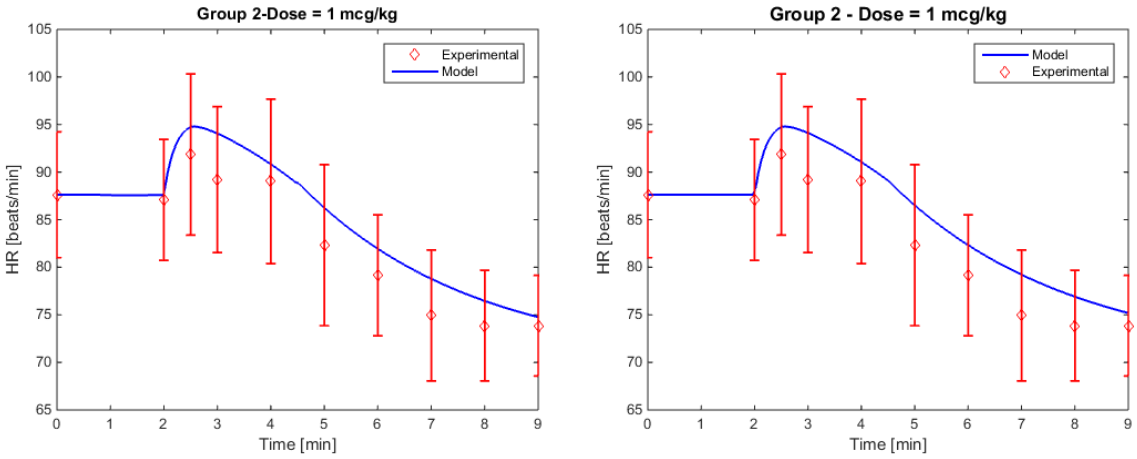

Figure 91 - The left portion shows the results of the 6P PK-PD model. The right portion shows the results of the 3-compartment PK-PD model. The experimental data (red) are from Park et al. (2011).

In this case there are not significant differences, as it is also possible to observe by analyzing the values of the performance indexes listed in Tables 70A and 70B.

Table 70A - Comparison of the $\Delta E_{max}\%$ values between the 6P PK-PD and Minto's PK-PD HR models based on Park et al. (2011) experimental data.

Group	*6P PK-PD model*	*3-compartment PK-PD model*
1	4.58	4.58
2	3.19	3.20

Table 70B - Comparison of the SAE values between the 6P PK-PD and Minto's PK-PD HR models based on Park et al. (2011) experimental data.

Group	*6P PK-PD model*	*3-compartment PK-PD model*
1	2.08	1.87
2	2.44	2.68

Case-study 3: Maguire et al. (2001)

Fig. 93 reports the results of the two models, compared to the experimental data of Maguire *et al.* (2001).

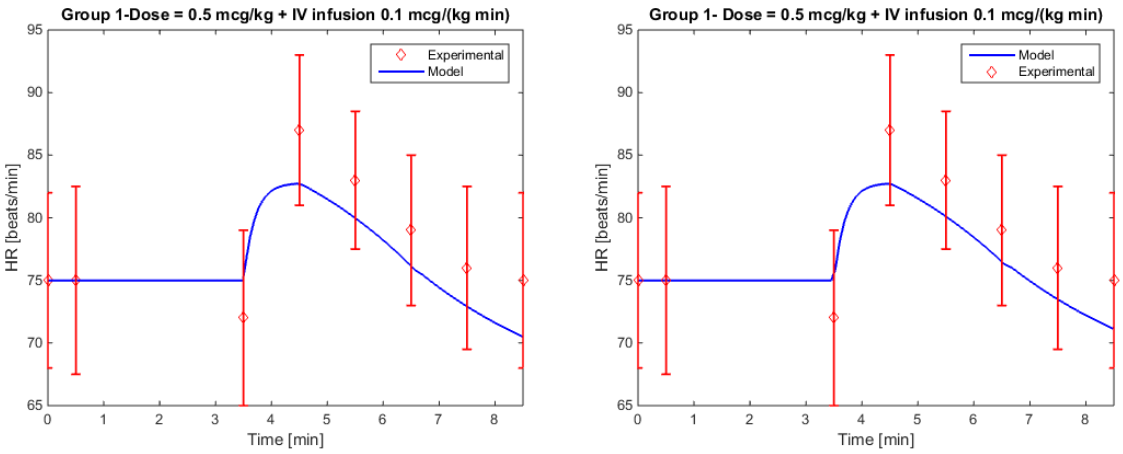

Figure 92 - The left figure shows the results of the 6P PK-PD model. The right figure shows the results of the 3-compartment PK-PD model. The experimental data (red) are from Maguire et al. (2001).

Also in this case, there are not so evident differences between the models. Table 71 reports the values of the performance indexes.

Table 71 - Comparison of the $\Delta E_{max}\%$ and SAE values between the 6P PK-PD and Minto's PK-PD HR models based on Maguire et al. (2001) experimental data.

Performance index	*Group*	*6P PK-PD model*	*3-compartment PK-PD model*
$\Delta E_{max}\%$	1	4.91	4.92
SAE	1	2.53	2.46

Conclusions

In case of HR, the difference between the models is even less evident than for SAP and MAP models.

As previously explained, the HR model may have an altered dependence on the drug concentration because of the presence of the *emotional* peak in the experimental data (see Paragraph 3.6.7). For this reason, a different pharmacokinetic prediction has a lower influence on HR.

5.3.4 Final remarks

The pharmacokinetic differences between the models observed in the previous paragraph are not so evident in case of pharmacodynamic predictions. This may be related to modeling limitations. In fact, in order to build a combined model, it is necessary to add a virtual compartment to account for the delay of the effect respect to the drug plasma concentration. By doing so, the physiological aspects of the 6P model can be diluted and become less evident. In fact, this virtual compartment is linked only to the plasma compartment and since the differences in the pharmacokinetic predictions are not so high, it is possible that such differences not affect significantly the pharmacodynamics. This means that the pharmacokinetic differences showed in Paragraph 5.2 may not be clinically significant in terms of effects.

Finally, it is possible to conclude that the combined model is able to better predict the pharmacokinetics of remifentanil, respect to the 3-compartment PK model. Concerning the pharmacodynamics, the 6P PK-PD model gives moderately better results for SAP and MAP, and approximately equally good results for HR. It could be interesting to verify this fact also for minute ventilation and bispectral index, other measures of the anesthetic state of the patients. However, because of a lack of experimental data in the literature, this is not possible.

6. CONCLUSIONS AND FUTURE DEVELOPMENTS

Aim of this thesis was the development of a pharmacokinetic-pharmacodynamic model for the remifentanil administration in anesthesia. Remifentanil is in fact a very interesting analgesic opioid, mainly due to its rapid onset and offset. A combined PK-PD model would be an efficient tool in the difficult task of providing a balanced analgesia, which is a fundamental aspect of anesthesia.

We adapted the physiologically-based pharmacokinetic (PBPK) model of Abbiati *et al.* (2016) to make it more specific to remifentanil by working on the metabolism/elimination pathways. We obtained an improvement (the 6P model) compared to the original model, by eliminating two of the four elimination pathways (*i.e.* liver and kidneys).

However, this improvement was rather limited in case of high doses (which fall significantly out of the recommended clinical treatments), since both models showed high deviations from the experimental data of Egan *et al.* (1993). In fact, for high doses the model underestimated the experimental data, as if there was an accumulation in the plasma that the model is not able to describe. Therefore, we hypothesized that this accumulation might be related either to variations in the protein binding or an effect of saturation of the enzymes. The 6P model was therefore used to investigate the influence of the administered dose on both the protein binding and the elimination rate, with satisfactory results. Eventually, the model was able to predict the measured blood concentrations in case of both small and high doses, beyond the recommended dose range, with a remarkable precision. However, at present, we are still not able to discriminate the effective real mechanism that occurs at high doses, because of the lack of in-depth biochemistry knowledge and more detailed experimental data. Indeed, it would be quite interesting to integrate our studies with the knowledge of experts in biochemistry and biology.

Finally, the 6P model was modified to include a dependence on the body temperature and was successfully validated with datasets from studies performed during hypothermic cardiopulmonary-bypass (CPB). Unfortunately, the dataset was rather limited because of the specificity of the operation. Again, it would be interesting to verify the accuracy of the model with experimental data from more recent studies.

The development of a pharmacodynamic (PD) model allowed correlating the plasma concentration of remifentanil, which can be derived from the 6P model, to the corresponding hemodynamic effect in terms of SAP, MAP, and HR. However, the PD model was not realistic in the description of the effect, especially in the phase that immediately follows the administration of remifentanil and the induction of anesthesia.

Consequently, a virtual compartment was introduced to deliver a pharmacokinetic-pharmacodynamic model for remifentanil. This combined model allows correlating the dose of remifentanil to its cardiovascular effects: AP and HR.

Because of the lack of experimental data on bispectral index and minute ventilation, we limited our investigations to the hemodynamic effects. However, it would be useful to integrate cardiovascular effects with indexes of the cerebral activity and the respiratory rate, to have a complete view of the anesthetic state of the patient.

One of the main issues of PK-PD modeling is the inter-individual variability. In order to move towards a higher level of personalization of our model, we investigated the influence of gender and body mass employing Nadler's formulae (Neyrinck and Vrielink, 2014) for the evaluation of the blood volume of patients. We found that these formulae allow the model attaining a higher sensitivity to the patient physical characteristics (*i.e.* individual features). Therefore, the model is able to describe the pharmacokinetics and the pharmacodynamics of patients with different gender and anatomical features, such as height and body mass. Starting from these considerations, it may be interesting to substitute the formulae that are currently used for the evaluation of the individualized parameters, with formulae that feature more physical characteristics of the simulated patient (*i.e.* the height, not only the body mass) and are more specific. For instance, it would be possible to scale some formulae that are currently used for animals and apply them to our 6P model. All these recommendations go towards the individualization of prescriptions and medical treatments, which represent the future of medicine (Lesko and Schmidt, 2012).

Another improvement for the 6P model could be the introduction of a coefficient that accounts for sudden blood losses or hemodilution due to transfusions/surgeries. In fact, these two conditions are common during surgery and affect the remifentanil volume of distribution, altering its pharmacokinetics.

In the last part of this work, we have demonstrated that the 6P model can be considered an improvement respect to the classical three-compartment PK model, not only in terms of advantages such as the possibility of studying the evolution of the drug in various organs and tissues, but also of precision in the prediction of the measured blood concentration. The classical three-compartment PK model has been in fact the most widely used PK model for remifentanil (*i.e.* Glass *et al.* (1993); Dershwitz *et al.* (1996); Minto *et al.* (1997); Drover and Lemmens (1998); Egan *et al.* (1996); Mertens *et al.* (2003); Pitsiu *et al.* (2004)).

The most interesting future development of our 6P PK-PD model is in the control of anesthesia. In fact, today the anesthesiologists' greatest challenge is the maintenance of the anesthetic state of the patient, via drug-induced unconsciousness, muscle

relaxation, and analgesia. The related problems are, of course inter- and intra-individual variability, variable time delays, dynamics dependent on the hypnotic agent (the anesthetic), agent and stability issues (Nascu *et al.*, 2015). In recent years, automated drug infusion has been implemented with feedback strategies to control the anesthesia. Most investigators have used feedback control with a classical proportional, integral, and derivative (PID) control scheme (Soltesz *et al.* (2011); Soltesz *et al.* (2012); Moore *et al.* (2014); Van Heusden *et al.* (2014); Zhusubaliyev *et al.* (2015)).

The control of anesthesia for future applications can be studied and implemented according to two different approaches: the first is purely *in silico*, the second is *in vivo*.

Regarding the *in silico* approach, once the combined 6P PK-PD model is validated, it would be interesting to develop *in silico* simulations of a model-based control-loop for anesthesia. Fig. 94 shows a schematization of the final control-loop for the patient's anesthesia.

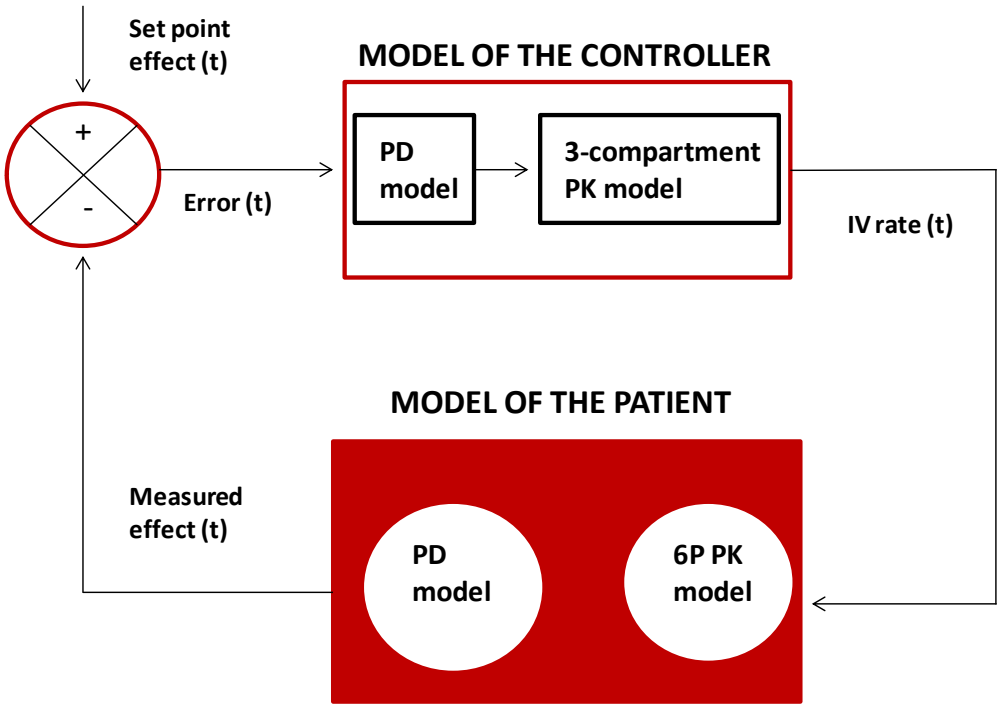

Figure 93 - Schematic representation of the in silico anesthesia control-loop. The set point is a target effect. The MP controller generates a control action as IV infusion rate. The 6P PK-PD model is used to simulate a virtual patient. The classical three-compartment

In the anesthesia control-loop the set point is a target effect ($SAP(t)$, $MAP(t)$, and $HR(t)$) and the control action consists of the intravenous infusion rate of remifentanil.

In terms of scientific fairness, a mismatch between the model that represents reality and the model that embodies the controller features is recommended. In fact, if this did not happen, the control action would be perfect. This is the reason why the 6P PK-PD

model, which is near to the real physiology and anatomy of the human body, might work as the model of the patient, whilst in the controller a robust and fast-simulation three-compartmental PK model might be implemented.

The second level mentioned above is the *in vivo* model-based control (Fig. 95). In this case, the patient is real, and therefore it is not necessary to approximate reality with a model. Therefore, the 6P PK-PD model can now be implemented in the controller. The idea is to design an anesthesia robot for mammals surgeries (*e.g.*, mice, rats, dogs, cats, horses). In fact, the 6P PK-PD model can be easily adapted, with few modifications, for specific mammals.

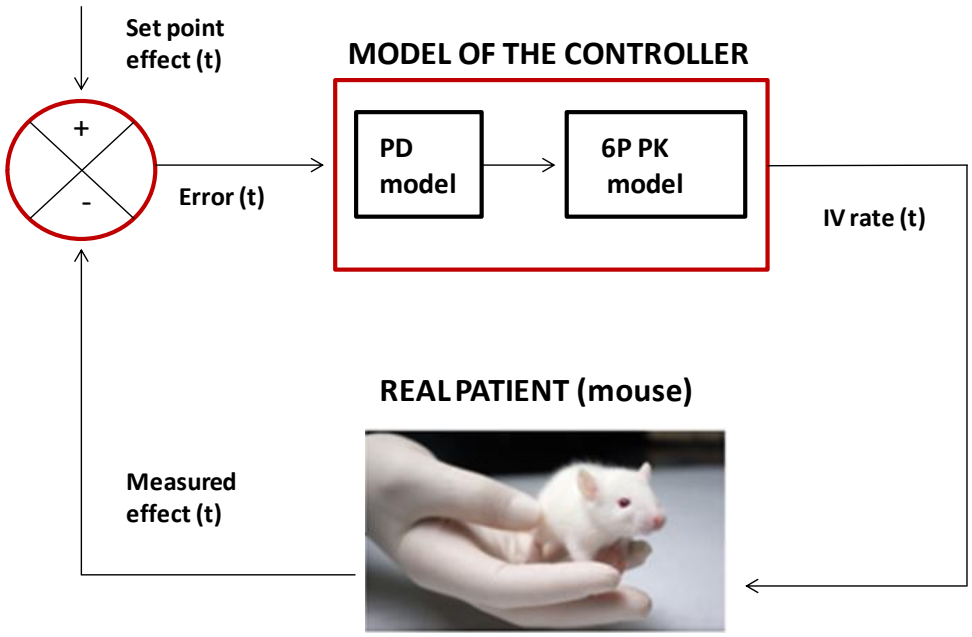

Figure 94 - Schematic representation of the in vivo anesthesia control-loop. The set point is a target effect. The controller generates a control action as IV rate of infusion, employing the 6P PK-PD model. The real patient is represented by a laboratory mouse.

One could object that the 6P PK-PD model is not as fast as the three-compartment model, and this might be a disadvantage from the point of view of the practical application in anesthesia. However, in the practice the infusion rate is not changed that frequently, but only if and whenever the patient manifests any discomfort sign. Therefore, the controller could periodically propose a control action that the anesthesiologist would decide whether or not to approve.

The finish-line of the work would be the Target Control Infusion (TCI) on humans. TCI is operated through a pump (Fig. 96) that nowadays functions according to the pharmacokinetic prediction of the Minto's three-compartment model (Minto *et al.*, 1997).

Figure 95 - TCI pump (Taken from Gopinath et al., 2015).

The anesthesiologist inserts the physical characteristics of the patient in the pump that defines the optimal dose in order to maintain some specific pharmacological effects inside suitable user-defined ranges. The physiologically based 6P model could improve the pharmacokinetic prediction for a specific patient, especially from a perspective of improvement of the level of individualization, and therefore select a more suitable dose.

Bibliography

Abbiati RA, Lamberti G, Grassi M, Trotta F, Manca D, 2016, *Definition and validation of a patient-individualized physiologically-based pharmacokinetic model*, Computer & Chemical Engineering, 48.

Alexander R, Olufolabi AJ, Booth J, El-Moalem HE, Glass PS, 1999 Nov, *Dosing study of remifentanil and propofol for tracheal intubation without the use of muscle relaxants*, Anaesthesia, 54(11), 1037-40.

Al-Hasani R, Bruchas MR, 2011, *Molecular mechanisms of opioid receptor-dependent signaling and behaviour*, Anesthesiology, 115(6), 1363-81.

Amin HM, Sopchak AM, Esposito BF, Henson LG, Batenhorst RL, Fox AW, 1995 July, *Naloxone-induced and spontaneous reversal of depressed ventilatory responses to hypoxia during and after continuous infusion of remifentanil or alfentanil*, J.Pharmacol.Exp.Ther., 274(1), 34-9.

Anderson KB, Poloyac SM, 2013, *Therapeutic hypothermia: implications on drug therapy*, Therapeutic hypothermia in brain injury; p. 131-147.

Batra YK, Al Qattan AR, Ali SS, Qureshi MI, Kuriakose D, Migahed A, 2004 June, *Assessment of tracheal intubating conditions in children using remifentanil and propofol without muscle relaxant,* Paediatr.Anaesth., 14(6), 452-6.

Biljana B, Petrovska, 2012, *Historical review of medicinal plants' usage*, Pharmacogn rev, 6(11), 1-5.

Breen D, Wilmer A, Bodenham A, Bach V, Bonde J, Kessler P, et al., 2014 Feb., *Offset of pharmacodynamic effects and safety of remifentanil in intensive care unit patients with various degrees of renal impairment,* Crit.Care, 8(1), R21-30.

Brown RP, Delp MD, Lindstedt SL, Rhomberg LR, Beliles RP,1997 Jul-Aug, *Physiological parameter values for physiologically based pharmacokinetic models*, Toxicol.Ind.Health, 13(4), 407-84.

Chen J, Gupta AK, Pan J, 1991, *Information criterion and change point problem for regular models,* The indian journal of statics, 68(2), 252-82.

Cowles AL, Borgstedt HH, Gillies AJ, 1971 Nov., *Tissue weights and rates of blood flow in man for the prediction of anesthetic uptake and distribution*, Anesthesiology, 35(5), 523-6.

Dahaba AA, Oettl K, von Klobucar F, Reibnegger G, List WF, 2002 Apr., *End-stage renal failure reduces central clearance and prolongs the elimination half-life of remifentanil*, Can.J.Anaesth., 49(4), 369-74.

Dahaba AA, von Klobucar F, Rehak PH, List WF, 1999 July, *Total intravenous anesthesia with remifentanil, propofol and cisatracurium in end-stage renal failure*, Can.J.Anaesth., 46(7), 696-700.

Davis L, Britten JJ, Morgan M, 1997 Mar., *Cholinesterase. Its significance in anaesthetic practice,* Anaesthesia, 52(3), 244-60.

Davis PJ, Ross A, Stiller RL, Muir K, Mc Yowan FX, 1995, *Pharmacokinetics of remifentanil in anesthetized children 2-12 years of age*, Anesth.Analg.

Davis PJ, Stiller RL, Wilson AS, McGowan FX, Egan TD, Muir KT, 2002 Nov., *In vitro remifentanil metabolism: the effects of whole blood constituents and plasma butyrylcholinesterase*, Anesth.Analg., 95(5), 1305-7

Davis PJ, Wilson AS, Siewers RD, Pigula FA, Landsman IS, 1999 Oct., *The effects of cardiopulmonary bypass on remifentanil kinetics in children undergoing atrial septal defect repair*, Anesth.Analg., 89(4), 904-8.

Dershwitz M, Rosow CE, 1996 May, *The pharmacokinetics and pharmacodynamics of remifentanil in volunteers with severe hepatic or renal dysfunction*, J.Clin.Anesth., 8(3 Suppl), 88S-90S.

Domi R, Laho H, 2012 Oct., *Anesthetic challenges in the obese patient*, J.Anesth., 26(5), 758-65.

Drover DR, Lemmens HJ, 1998 Oct., *Population pharmacodynamics and pharmacokinetics of remifentanil as a supplement to nitrous oxide anesthesia for elective abdominal surgery*, Anesthesiology, 89(4), 869-77.

Egan TD, Huizinga B, Gupta SK, Jaarsma RL, Sperry RJ, Yee JB, et al., 1998 Sept., *Remifentanil pharmacokinetics in obese versus lean patients*, Anesthesiology, 89(3), 562-73.

Egan TD, Lemmens HJ, Fiset P, Hermann DJ, Muir KT, Stanski DR, et al., 1993 Nov., *The pharmacokinetics of the new short-acting opioid remifentanil (GI87084B) in healthy adult male volunteers*, Anesthesiology, 79(5), 881-92.

Egan TD, Minto CF, Hermann DJ, Barr J, Muir KT, Shafer SL, 1996 Apr., *Remifentanil versus alfentanil: comparative pharmacokinetics and pharmacodynamics in healthy adult male volunteers*,Anesthesiology, 84(4), 821-33.

Engelhard K, Reeker W, Kochs E, Werner C, 2004 Apr., *Effect of remifentanil on intracranial pressure and cerebral blood flow velocity in patients with head trauma*, Acta Anaesthesiol.Scand., 48(4), 396-9.

Felmlee MA, Morris ME, Mager DE, 2012, *Mechanism-based pharmacodynamic modeling*, Methods Mol.Biol., 929, 583-600.

Fournier T, Medjoubi-N N, Porquet D, 2000 Oct., *Alpha-1-acid glycoprotein*, Biochim.Biophys.Acta, 1482(1-2), 157-71.

Gibaldi M, Levy G, Hayton H, 1972, *Kinetics of the elimination and neuromuscular blocking effect of d-tubocurarine in man,* Anesthesiology, 36, 213-8.

Gibaldi M, Levy G, Weintraub H, 1971, *Drug distribution and pharmacologic effect*s, Clinical pharmacology and therapeutics, 5, 734-42.

Gillis AM, Yee YG, Kates RE, 1985, *Binding of antiarrhytmic drugs to purified human a1-acid glycoprotein*, Biochemical Pharmacology, 34, 4279-82.

Glass PS, Gan TJ, Howell S, 1999 Oct., *A review of the pharmacokinetics and pharmacodynamics of remifentanil*, Anesth.Analg., 89(4 Suppl), S7-14.

Glass PS, Hardman D, Kamiyama Y, Quill TJ, Marton G, Donn KH, et al., 1993 Nov., *Preliminary pharmacokinetics and pharmacodynamics of an ultra-short-acting opioid: remifentanil (GI87084B),* Anesth.Analg., 77(5), 1031-40.

Gopinath MV, Ravishankar M, Nag K, Kumar VH, Velraj J, Parthasarathy S, 2015 May, *Estimation of effect-site concentration of propofol for laryngeal mask airway insertion using fentanyl or morphine as adjuvant,* Indian J.Anaesth., 59(5), 295-9.

Guarracino F, Lapolla F, Cariello C, Danella A, Doroni L, Baldassarri R, et al., 2005 June, *Target controlled infusion: TCI,* Minerva Anestesiol., 71(6), 335-7.

Guida all'uso dei farmaci sulla base del British national formulary, 2005, Agenzia italiana del farmaco, Roma.

Hall AP, Thompson JP, Leslie NA, Fox AJ, Kumar N, Rowbotham DJ, 2000 Jan., *Comparison of different doses of remifentanil on the cardiovascular response to laryngoscopy and tracheal intubation,* Br.J.Anaesth.,84(1), 100-2.

Hermann DJ, Egan TD, Muir KT, 1999 May, *Influence of arteriovenous sampling on remifentanil pharmacokinetics and pharmacodynamics*, Clin.Pharmacol.Ther., 65(5), 511-8.

Hill SA, 2004, *Pharmacokinetics of drug infusions*, Continuing Education in Anesthesia, Critical Care & Pain, 4.

Hoboken NJ, 2005, *Physiologically based pharmacokinetic modeling: science and applications*, Wiley-Interscience, Chichester: John Wiley distributor

Hoke JF, Shlugman D, Dershwitz M, Michalowski P, Malthouse-Dufore S, Connors PM, et al., 1997 Sept., *Pharmacokinetics and pharmacodynamics of remifentanil in persons with renal failure compared with healthy volunteers*, Anesthesiology, 87(3), 533-41.

Holford NH, Sheiner LB, 1982, *Kinetics of pharmacologic response*, Pharmacol., 16(2), 143-66.

Hull CJ, Van Beem HB, McLeod K, Sibbald A, Watson MJ, 1978 Nov., *A pharmacodynamic model for pancuronium*, Br.J.Anaesth., 50(11), 1113-23.

James MK, Vuong A, Grizzle MK, Schuster SV, Shaffer JE, 1992 Oct., *Hemodynamic effects of GI 87084B, an ultra-short acting mu-opioid analgesic, in anesthetized dogs*, J.Pharmacol.Exp.Ther., 263(1), 84-91.

Jones H, Rowland-Yeo K, 2013 Aug., *Basic concepts in physiologically based pharmacokinetic modeling in drug discovery and development*, CPT Pharmacometrics Syst.Pharmacol.,14, 2:e63.

Kaul HL, Bharti N, 2002, *Monitoring depth of anesthesia*, Indian J. Anaesth., 46(4), 323-32.

Kissin I, 2000 May, *Depth of anesthesia and bispectral index monitoring*, Anesth.Analg., 90(5), 1114-7.

La Colla L, Albertin A, La Colla G, 2009, *Pharmacokinetic model-driven remifentanil administration in the morbidly obese: the 'critical weight' and the 'fictitious height', a possible solution to an unsolved problem?,* Clin.Pharmacokinet., 48(6), 397-8.

Lee JH, Kim H, Kim HT, Kim MH, Cho K, Lim SH, et al., 2012 Aug., *Comparison of dexmedetomidine and remifentanil for attenuation of hemodynamic responses to laryngoscopy and tracheal intubation,* Korean J.Anesthesiol., 63(2), 124-9.

Leil TA, Bertz R, 2014 Nov., *Quantitative Systems Pharmacology can reduce attrition and improve productivity in pharmaceutical research and development*, Front.Pharmacol., 10, 5:247.

Leil TA, Ermakov S, 2015 June, *Editorial: The emerging discipline of quantitative systems pharmacology,* Front.Pharmacol., 30, 6:129.

Lesko L, Schmidt S, 2012, *Individualization of drug therapy: hystory, present state, and opportunities for the future,* Clinical pharmacology and therapeutics, 98, 456-4585.

Levy RP, Cammarn MR, Smith MJ, 1964 Dec 21, *Computer Handling of Ambulatory Clinic Records*, JAMA, 190, 1033-7.

Maguire AM, Kumar N, Parker JL, Rowbotham DJ, Thompson JP, 2001 Jan., *Comparison of effects of remifentanil and alfentanil on cardiovascular response to tracheal intubation in hypertensive patients,* Br.J.Anaesth., 86(1), 90-3.

Manullang J, Egan TD, 1999 Aug., *Remifentanil's effect is not prolonged in a patient with pseudocholinesterase deficiency*, Anesth.Analg., 89(2), 529-30.

McGhee BH, Bridges MEJ, 2002, *Monitoring arterial blood pressure: what you may not know,* Critical care nurse, 22(2), 60-79.

Meibohm B, Derendorf H, 1997, *Basic concepts of phamacokinetic/pharmacodynamic (PK/PD) modeling,* International journal of clinical pharmacology and therapeutics, 35(10), 401-13.

Mertens MJ, Olofsen E, Engbers FH, Burm AG, Bovill JG, Vuyk J, 2003 Aug., *Propofol reduces perioperative remifentanil requirements in a synergistic manner: response surface modeling of perioperative remifentanil-propofol interactions*, Anesthesiology, 99(2), 347-59.

Mettler S, Mitchell N, Tipton KD, 2010 Feb., *Increased protein intake reduces lean body mass loss during weight loss in athletes*, Med.Sci.Sports Exerc., 42(2), 326-37.

Michelsen LG, Holford NH, Lu W, Hoke JF, Hug CC, Bailey JM, 2001 Nov., *The pharmacokinetics of remifentanil in patients undergoing coronary artery bypass grafting with cardiopulmonary bypass,* Anesth.Analg., 93(5), 1100-5.

Miller R, Eriksson L, Fleisher L, Wiener-Kronish J, Young W, 2009, *MIller's anesthesia*, 7th edition ed., Churchill Livingstone, Philadelphia.

Miller-Keane, O'Toole, 2003, *Encyclopedia and dictionary of medicine, nursing, and allied health*, 7th edition ed., Saunder

Minto CF, Schnider TW, Egan TD, Youngs E, Lemmens HJ, Gambus PL, et al.,1997 Jan., *Influence of age and gender on the pharmacokinetics and pharmacodynamics of remifentanil. I. Model development,* Anesthesiology, 86(1), 10-23.

Moore BL, Pyeatt LD, Kulkarni V, Panousis P, Padrez K, Doufas AG, 2014, *Reinforcement learning for closed-loop propofol anesthesia: a study in human volunteers,* Journal of machine research, 15, 655-96.

Nascu I, Krieger A, Ionescu CM, Pistikopoulos EN, 2015 Mar., *Advanced model-based control studies for the induction and maintenance of intravenous anaesthesia*, IEEE Trans.Biomed.Eng., 62(3), 832-41.

Natick MA, 1997, *Technology overview: bispectral index,* Aspect medical systems.

Navapurkar VU, Archer S, Gupta SK, Muir KT, Frazer N, Park GR, 1998 Dec., *Metabolism of remifentanil during liver transplantation,* Br.J.Anaesth., 81(6), 881-6.

Nelson D, Cox M, 1970, *Lehninger Principles of biochemistry*, Worth publisher Inc., U.S.

Neyrinck MM, Vrielink H, 2014, *Calculations in apheresis*, Journal of clinical apheresis

Nora FS, Klipel R, Ayala G, Oliveira Filho GR, 2007 June, *Remifentanil: does the infusion regimen make a difference in the prevention of hemodynamic responses to tracheal intubation*?, Rev.Bras.Anestesiol., 57(3), 247-60.

O'Hare R, McAtamney D, Mirakhur RK, Hughes D, Carabine U, 1999 Feb,. *Bolus dose remifentanil for control of haemodynamic response to tracheal intubation during rapid sequence induction of anaesthesia*, Br.J.Anaesth., 82(2), 283-5.

Park BY, Jeong CW, Jang EA, Kim SJ, Jeong ST, Shin MH, et al*.,* 2011 Jan., *Dose-related attenuation of cardiovascular responses to tracheal intubation by intravenous remifentanil bolus in severe pre-eclamptic patients undergoing Caesarean delivery*, Br.J.Anaesth., 106(1), 82-7.

Petrovska BB, 2012 Jan., *Historical review of medicinal plants' usage*, Pharmacogn Rev., 6(11), 1-5.

Philip BK, Scuderi PE, Chung F, Conahan TJ, Maurer W, Angel JJ, et al., 1997 Mar., *Remifentanil compared with alfentanil for ambulatory surgery using total intravenous anesthesia. The Remifentanil/Alfentanil Outpatient TIVA Group,* Anesth.Analg., 84(3), 515-21.

Piacevoli Q, Del Gaudio A, Mincolelli G, Tonti MP, Wouters G, Mastronardi P, 2015 Mar., *No correlation between remifentanil blood, cerebrospinal fluid and cerebral extracellular fluid levels and TCI prediction: a pharmacokinetic study,* Minerva Anestesiol., 81(3),305-11.

Pitsiu M, Wilmer A, Bodenham A, Breen D, Bach V, Bonde J, et al., 2004 Apr., *Pharmacokinetics of remifentanil and its major metabolite, remifentanil acid, in ICU patients with renal impairment*, Br.J.Anaesth., 92(4), 493-503.

Ponganis KV, Stanski DR, 1985, Pharm. Sci., 74, 57-60.

Russel D, Roysto D, Ree PH, Gupta SK, Kenny GNC, 1997, *Effect of temperature and cardiopulmonary bypass on the pharmacokientics of remifentanil,* British journal of anaesthesia, 79, 456-9.

Sam WJ, Hammer GB, Drover DR,2009 July, *Population pharmacokinetics of remifentanil in infants and children undergoing cardiac surgery*, BMC Anesthesiol., 9(5), 2253-9-5.

Saroj P, Satyanarayana A, Suhasini PS, Chaitanya BK, Kranthi J, 2016, *Comparative study of effect of intravenous magnesium sulphate and intravenous fentanyl in attenuating the hemodymìnamic responses to laryngoscopy and intubation*, Indian J.Anaesth., 3(30), 1360-7

Scannel JW, Blanckley A, Boldon H, Warrington B, 2012, *Diagnosing the decline in pharmaceutical R&D efficiency,* Nat. Rev. Drug Discov., 11, 191-200.

Sebel PS, Hoke JF, Westmoreland C, Hug CC, Muir KT, Szlam F, 1995 May, *Histamine concentrations and hemodynamic responses after remifentanil*, Anesth.Analg., 80(5), 990-3.

Segre G, 1968 Oct., *Kinetics of interaction between drugs and biological systems*, Farmaco Sci., 23(10), 907-18.

Selinger K, Nation RL, Smith GA, 1995, *Enzymatic and chemical hydrolysis of remifentanil*, Anesthesiology.

Shajar MA, Thompson JP, Hall AP, Leslie NA, Fox AJ, 1999 Oct., *Effect of a remifentanil bolus dose on the cardiovascular response to emergence from anaesthesia and tracheal extubation*, Br.J.Anaesth., 83(4), 654-6.

Sheiner L, Stanski D, Vozeh S, Miller R, Han J, 1979, *Simultaneous modeling of pharmacokinetics and pharmacodynamics: application to d-tubocurarine,* Clinical pharmacology and therapeutics, 3, 358-71.

Shribman AJ, Smith G, Achola KJ, 1987 Mar., *Cardiovascular and catecholamine responses to laryngoscopy with and without tracheal intubation*, Br.J.Anaesth., 59(3), 295-9.

Soltesz K, Hahn JO, Dumont GA, Ansermino JM, 2011, *Individualized PID control of depth of anesthesia based on patient model during the induction phase of anesthesia*, IEEE Conference on Decision and Control and European Control Conference, 855-60.

Soltesz K, Van Heusden K, Dumont JA, Hagglund T, Petersen CL, West N, et al., 2012, *Closed-loop anesthesia in children using a PID: a pilot study,* IFAC Conference on Advances in PID Control.

Sorger PK, Allerheiligen SRB, Abernethy DR, Altman RB, Brouwer KLR, Califano A, 2011, *Quantitative and systems pharmacology in the post-genomic era: new approaches to discovering drugs and understanding therapeutic mechanisms*, NIH White Paper.

Standing JF, Hammer GB, Sam WJ, Drover DR, 2010 Jan., *Pharmacokinetic-pharmacodynamic modeling of the hypotensive effect of remifentanil in infants undergoing cranioplasty, Paediatr.Anaesth.,* 20(1), 7-18.

Stiller RL, Davis PJ, McGowan FX, 1995, *In vitro metabolism of remifentanil: the effects of pseudocholinesterase deficiency,* Anesthesiology, 83.

Sultan SS, 2014 Nov., *Patient-controlled sedation with propofol/remifentanil versus propofol/alfentanil for patients undergoing outpatient colonoscopy, a randomized, controlled double-blind study,* Saudi J.Anaesth., 8(Suppl 1), S36-40.

Teorell T, 1937 Sept., *Studies on the Diffusion Effect upon Ionic Distribution: Ii. Experiments on Ionic Accumulation*, J.Gen.Physiol., 21(1), 107-22.

Tesseromatis C, Alevizou A, Tigk E, Kotsiou A, 2011, *Acute-Phase Proteins: Alha-1-Acid Glycoprotein,* Acute Phase Proteins - Regulation and Functions of Acute Phase Proteins, 247-57.

The Merck Manual. 14th ed.: Merck Sharp & Dohme Research Laboratories; 1982.

Thompson JP, Hall AP, Russell J, Cagney B, Rowbotham DJ, 1998 Apr., *Effect of remifentanil on the haemodynamic response to orotracheal intubation,* Br.J.Anaesth., 80(4), 467-9.

Toutain PL, Lees P, 2005, *Integration and modeling of pharmacokinetic and pharmacodynamic data to optimize dosage regimens in veterinary medicine*, Journal of veterinary pharmacology and therapeutics.

Van Heudsen K, West N, Umedaly A, Ansermino JM, Merchant NR, Dumont GA, 2014, *Safety, constraints and anti-windup in closed-loop anesthesia,* IFAC Proceedings Volumes, 47(3), 6569-74.

Vander A, Lucian D, Sherman J, 1998, *Human physiology: the mechanisms of body function*, McGraw-Hill education, Boston.

Wagner JG, 1968, *Kinetics of pharmacologic response*, J.Thor. Biol., 20, 173-201.

Warner DS, Hindman BJ, Todd MM, Sawin PD, Kirchner J, Roland CL, et al., 1996 Aug., *Intracranial pressure and hemodynamic effects of remifentanil versus alfentanil in patients undergoing supratentorial craniotomy*, Anesth.Analg., 83(2), 348-53.

Warner DS, Hindman BJ, Todd MM, Sawin PD, Kirchner J, Roland CL, et al., 1996 Aug., *Intracranial pressure and hemodynamic effects of remifentanil versus alfentanil in patients undergoing supratentorial craniotomy*., Anesth.Analg., 83(2), 348-53.

Westmoreland CL, Hoke JF, Sebel PS, Hug CC, Muir KT, 1993 Nov., *Pharmacokinetics of remifentanil (GI87084B) and its major metabolite (GI90291) in patients undergoing elective inpatient surgery,* Anesthesiology, 79(5), 893-903.

Wilhelm W, Hammadeh ME, White PF, Georg T, Fleser R, Biedler A, 2002 Feb., *General anesthesia versus monitored anesthesia care with remifentanil for assisted reproductive technologies: effect on pregnancy rate*, J.Clin.Anesth., 14(1), 1-5.

Williams LR, Leggett RW, 1989 Aug., *Reference values for resting blood flow to organs of man,* Clin.Phys.Physiol.Meas., 10(3), 187-217.

Wong AKL, Hsia JC, 1983, *Biochem. Cell. Bio*., p. 1114-1116.

Wuesten R, Van Aken H, Glass PS, Buerkle H, 2001 Feb., *Assessment of depth of anesthesia and postoperative respiratory recovery after remifentanil- versus alfentanil-based total intravenous anesthesia in patients undergoing ear-nose-throat surgery*, Anesthesiology, 94(2), 211-7.

Xue SF, Zhang GH, Sun HY, Li CW, Li P, Sun HT, et al., 2006, *Blood pressure and heart rate changes during intubation: comparison of direct laryngoscopy and a fibreoptic method*, Anesthesia, 61, 444-8.

Zhusubaliyev ZT, Medvedev A, Margarida M, 2015, *Bifurcation analysis of PID-controlled neuromuscular blockade in closed-loop anesthesia,* Journal of process control, 152-63.

Ringraziamenti

Desideriamo ringraziare il prof. Davide Manca per averci permesso di lavorare su un argomento così particolare, e soprattutto per averci fatto da guida lungo questo percorso e dato continuamente nuovi spunti, rendendo il lavoro interessante e stimolante.

Ringraziamo inoltre l'Ing. Roberto Abbiati per la pazienza e la disponibilità dimostrate nonostante la distanza, e l'Ing. Valentina Depetri per l'aiuto.